NUMERICAL STUDIES--
PACIFIC MARINE ENVIRONMENTAL LABORATORY

by

J. A. Galt, J. E. Overland,
C. H. Pease, and R. J. Stewart

U.S. Department of Commerce
National Oceanic and Atmospheric Administration
Environmental Research Laboratories
Pacific Marine Environmental Laboratory
3711 15th Avenue N.E.
Seattle, Washington 98105

Final Report
Outer Continental Shelf Environmental Assessment. Program
Research Unit 140

September 1978

(Minor Revisions, November 1984)

TABLE OF CONTENTS

TABLE OF CONTENTS (continued)

PREFACE

Numerical studies have been a part of OCSEAP research since the program began in July of 1974. During the four and one-quarter years of funding for research unit #140, a number of research projects have been undertaken in support of the overall goal of describing the surface transport processes for specific OCS regions. These studies have been carried out by a number of different investigators and have been coordinated with many other studies and agencies. In particular, the numerical studies have been strongly influenced by the observational oceanographic field programs and by data collected by the Spilled Oil Research Team of OCSEAP. Related pollutant trajectory work has been carried out by the Marine Ecosystems Analysis Program, by NOAA Marine Services studies, and by PMEL base funded research. In addition to developing specific products associated with numerical descriptions of transport phenomena, research group members have taken an active role in the planning, coordination and information transfer for the larger-scope physical oceanographic studies being carried out by OCSEAP. For example, during the fifty-one months of the project to date, group members have traveled over seventy times on business directly related to oil trajectory research. About one-fourth of this travel was for overall program planning. Another fourth was for research planning and for coordination with other OCSEAP investigators. Four different times the group has presented data at OCSEAP physical oceanography principal investigators' meetings (which we originally instigated). On eleven different occasions group members have presented briefings of research results (three times to NOAA senior management, five times directly to BLM or DOI personnel - including the transfer of computer algorithms for use in their assessment models, and three

times to national advisory boards). Group personnel have taken part in seven or more different observational field programs and have described their research results to the Juneau Project Office at seven different briefings.

Research results from group members have also been presented at six national meetings and at three special workshops, with the contributions being published for four of these.

Papers by group members relating to oil trajectory analysis are represented by the following:

Regional Meteorological Model for Mountainous Coastal Regions, PMEL Technical Report (in press), J. Overland, M. Hitchman and Y.-J. Han.

Comments on "Numerical Simulation of Cold Easterly Circulation Over the Canadian Western Plains Using a Mesoscale Boundary Layer Model", Boundary Layer Meteorology, 1978 (14): 433-434, J. Overland.

Tankers in U.S. Waters, (1977), Oceanus 20(4), Robert J. Stewart.

Bayesian Hypothesis Tests of Sampling Function Form, Robert J. Stewart (submitted to JASA for publication).

Estimating Tanker Spill Risks in U.S. Waters, Proceedings of the 1978 Joint Statistical Meeting, San Diego, Calif., Robert J. Stewart.

Estimating Oil Spill Risks for Offshore Development, Proceedings of the 1978 Joint Statistical Meetings, San Diego, Calif. Robert J. Stewart.

Physical Oceanography and Dynamics of the NE Gulf of Alaska, Proceedings AINA Conference, Anchorage, 16-17 October, 1975, J.A. Galt and Thomas T. Royer.

The Use of a Diagnostic Circulation Model for Oil Trajectory Analysis, EPA/API/USCG Oil Spill Conference, New Orleans, March 7-11, J.A. Galt and Carol H. Pease. (1977)

Circulation Studies on the Alaska Continental Shelf Off the Copper River Delta, NOAA/ERL Technical Report, March 1976, J.A. Galt.

Investigation of Physical Processes, J.A. Galt, The AMOCO CADIZ Oil Spill, NOAA/ERL Report, Wilmot N. Hess, Editor. (1978)

A Numerical Investigation of the Bering Sea Circulation Using a Linear Homogeneous Model; NOAA Draft Technical Report, Y. J. Han and J.A. Galt.

Development of a Simplified Diagnostic Model for the Interpretation of Oceanographic Data, NOAA Technical Report ERL 399-PMEL-25, 1975, J.A. Galt.

A Finite Element Solution Technique for a Diagnostic Shelf Circulation Model, NOAA/ERL/PMEL Technical Report (submitted) G. Watabayashi and J.A. Galt.

A Linear Decomposition of a Diagnostic Shelf Circulation Model and Discussion of Alternate Boundary Condition Formulations, NOAA/ERL/PMEL Technical Report (submitted), J.A. Galt and G. Watabayashi.

A Synoptic Climatology for Surface Winds Along the Southern Coast of Alaska, NOAA/ERL.PMEL (Draft Tech Report), J.E. Overland and T.R. Hiester.

Since some of these papers are still in draft form, and thus not generally available, they have been included as appendices to this report. This collection covers selected aspects of the spill trajectory investigations that have been carried out by the Numerical Studies group. A more complete coverage of their activities carried out under RU#140 is

contained in the annual reports of the last four years.

The first of these, "Physical Oceanography Contribution to the First Annual Report" by J.A. Galt (July, 1975), was an attempt to collect the contributions of D. Barrick (WPL), D. Halpern (PMEL), s. Hayes (PMEL), R.M. Reynolds (PMEL), T. Royer (IMS) and J. Schumacher (PMEL) to produce an initial synthesis from the NEGOA area, concentrating on a description of regional dynamic processes.

The next annual report, "Numerical Studies of Alaska Region" RU#140, 146, 149, 31 (June 1976) by J.A. Galt, describes the conceptual design of a general oil spill trajectory model, a stochastic dispersion experiment based on NEGOA winds, the ice problem in the Beaufort Sea, initial diagnostic model experiments for NEGOA, and some results from preliminary modeling studies in the Bering Sea. A study of the circulation off the Copper River and a bibliography of sea ice papers were also included as part of that report.

The third annual report by J.A. Galt, J.E. Overland, C.S. Smyth, Y. J. Han and C.H. Pease (June 1977) describes a conceptual advanced trajectory model, a series of trajectory modeling experiments run for the NEGOA area, initial diagnostic model studies of the Kodiak region, an investigation of the use of small scale planetary boundary layer models to predict surface wind patterns, additional results from modeling studies of the Bering Sea circulation, and an analysis of computer requirements for a trajectory graphics system.

The fourth annual report "Alaska Numerical Modeling" by J.A. Galt, J.E. Overland, R.J. Stewart, C.H. Pease and M. Hitchman (May 1978), described the continuing analysis of the diagnostic circulation model, concentrating on the formal decomposition of the linear model equations. In addition,

available data sets for running NEGOA trajectory analysis studies were identified, and strategies for forming environmental libraries were described. That report also discussed weather typing experiments being carried out for the Alaska region.

The four years of numerical studies that have been carried out have seen the development of a consistent and balanced approach for the study of pollutant trajectories. This approach combines both theoretical work and empirical data so that the underlying dynamics responsible for particular physical response can be clearly identified. It is now possible to assemble the various components and to carry out a serious analysis of regional trajectories for an OCS region. The following report is a demonstration of the techniques developed in RU#140 applied to the investigation of. trajectories in the Northeast Gulf of Alaska.

In addition to the principal authors of this report significant support was given by other Numerical Studies personnel: Clifford Fridlind, Gary Torgrimson, Debra Payton, Curtis Mobley, Jon Nestor and Y. J. Han. Contract help was received from Thomas R. Hiester and Betty-Ann Morse. Students also contributed to individual sections, including Eric Raisters, Glen Watabayashi, Matthew Hitchman, John DeVault, Rita Chin and Mark Bjornson. We would also like to acknowledge help from Carl Pearson (Coastal Physics, PMEL) in the preparation of field data for model input.

1. Introduction

The following report documents a series of studies that have been carried out as part of OCSEAP, RU #140. This research represents a multi-year effort that has been carried out by scientists in the Numerical Studies group at the Pacific Marine Environmental Laboratory of NOAA/ERL. The general subject addressed by OCSEAP Research Unit #140 is best described as numerical, or computer oriented, techniques for the interpolation and synthesis of environmental data to present a composite analysis of pollutant trajectories. In carrying out this work many different approaches have been used. Fundamental research in meteorology, oceanography, statistics and computer science have all played a part. Additional use has been made of empirical data sets made available through the continous efforts of other OCSEAP investigators and their predecessors. In all of these component studies underlying dynamic principles have been identified. Formal solutions have been combined with observational information in such a way as to yield optimum coverage of expected environmental situations. It has been felt that this approach offers the best opportunity, using regional information, to obtain a consistent and conceptually balanced bases for trajectory analysis.

As with any research, not all of the proposed paths lead directly to the objectives. Thus some of the studies carried out during this project do not see their way into the final synthesis. Also to be considered is that alternate dynamic formulations are often considered while zeroing in on a useful regional representation. The final procedures and combinations of dynamics and data will be chosen from the available techniques so as to focus on the immediate area of concern. The following chapters of this report are a detailed case study of pollutant trajectory analysis for a specific region, the Northeast Gulf of Alaska.

Among the processes that are likely to control the movement and spreading of spilled oil, some of the first thought to come into play are due to the wind. The wind actually enters the problem in several distinct ways. The wind generates a local surface wind drift, which advects any floating pollutants. In addition the local wind transfers momentum to floating oil indirectly through wave and stress interactions. Although neither one of these local wind effects is completely understood, the net movement of the oil can be reasonably well parametrized in terms of the wind. The wind also enters the trajectory problem through the regional forcing of the shelf circulation. Here the wind across the shelf sets up the sea surface slope, creating a pressure gradient that drives the flow. To fulfill these requirements for both regional wind patterns and for detailed local wind vectors, a meteorological study of the NEGOA region was carried out and is described in the second section of this report. In developing these NEGOA wind patterns a number of techniques were applied to various data sets, with the results converging towards the development of a single set of patterns capable of representing all the meteorological situations that could be expected for the region.

Starting with large scale pressure data, as represented on synoptic weather maps, an investigation was carried out to identify the dominant weather types. This was done subjectively by a visual comparison of a large number of daily maps. Upon completing this phase of the study, the results were compared to previous subjective typing studies that had been carried out for the entire Alaska region. Then objective typing techniques were considered, with the eventual choice of pattern correlation methods over other methods of pattern recognition (empirical orthogonal functions and factor analysis) primarily because of time constraints.

Small scale local wind patterns have been investigated by concentrating on the processes that modify the larger scale synoptic patterns in the planetary boundary layer and in coastal regions. Included in these studies were the results of one- and two-dimensional boundary layer models, as well as the results of observational studies of coastal winds. The final wind patterns chosen to represent the NEGOA region are based on the large synoptic patterns (types), with local wind vectors derived by the careful subjective application of the information obtained from the boundary layer studies.

After establishing the required characterizations of the representative wind patterns for NEGOA, the determination of regional current patterns can be made. Currents enter into the pollutant trajectory problem as a process that simply advects floating material. The description of the regional currents must include considerations of the bathymetry, stratification and major dynamic forcing. To include these effects, a diagnostic shelf circulation model has been used. This model assumes that the currents are a combination of geostrophic and Ekman flows. The density field, bottom topography, and winds are the independent variables; the model solves for the sea surface elevation.

The application of the diagnostic model is greatly simplified by the decomposition of the resulting flow into density-driven and wind-driven components. This procedure and its application to the NEGOA region are described in section three of this report. The partitioning of the model dynamics makes it possible to easily identify the regional response associated with each of the individual forcing mechanisms. A bathystrophic balance between the regional winds and the sea surface set-up is assumed and with this assumption it is possible to derive

regional current patterns corresponding to each of the climatological wind patterns described in Section Two. This approach insures that the currents have two very important characteristics. First that they are directly related to the large scale climatological forcing, for which long historical records are available. And second, that when used in conjunction with the wind patterns in a pollutant trajectory analysis, the appropriate wind-current correlations for the region are preserved. The correct representation of these correlations is essential for obtaining realistic trajectory statistics for regional assessment investigations.

The pollutant trajectory model used in the study of the NEGOA region is a series of algorithms which incorporates the regional wind, current and geography information into appropriate parameterizations. The model predicts the sequential displacements of a floating mass of hydrocarbons, and presents the results in a suitable graphical format. The algorithms require various time series records for the specific periods of time for which investigations are desired. These records contain a progression of climate types, as well as wind and current data, from single keying (or scaling) stations. Conceptually, all of the wind, current and time series data can be thought of as a regional environmental library which the trajectory algorithms must access. The actual numerical development of this library, with a description of file structure and data packing strategy, is described in the fourth section of this report.

Both the wind pattern and current pattern information have been developed in terms which describe the flow only in a relative sense. To obtain the absolute winds or currents it is first necessary to identify the pattern that most closely represents the synoptic situation. Then

the observed winds from a station within the model region are used to scale the entire wind pattern; the currents are scaled by the square of the wind speed, consistent with the bathystrophic assumptions used in the diagnostic model decomposition. This procedure yields a consistent series of wind and current data for every location within the model domain and reflects the appropriate climatology as well as the smaller scale region dynamics. What is not included in these pattern keying strategies is the higher frequency variations (which are unresolved by the 12 hour weather maps). Such time dependent scales of motion are not dynamically represented in either the wind or current model studies, and their effects must be modeled as uncertainties, or pseudo-random displacements. The higher frequency information from wind and current records is compared with model predictions, and the deviations are taken as a measure of uncertainty. The details of this keying strategy application and the statistics of the observed residual winds and currents are examined in section five of this report.

The sixth section of the report documents examples of pollutant trajectory investigations. Two specific time periods are considered: summer, 1974 and winter, 1975. These are presented as examples of the model and library concept and make no attempt to present a statistical assessment. The components are complete and such a study could be carried out with the existing meteorological data. The analysis incorporates all of the system components described in the previous sections of the report. The examples use climate pattern sequencing from weather maps during the period in question, with the definition of local winds and currents corresponding to the synoptic situation scaled by observations at Middleton Island, High frequency variations in the observed records,

which are not explicitly included in the model formulation are incorporated into the trajectory algorithms and give a realistic estimate of composite uncertainty in the analysis.

The final section in the report presents conclusions and recommendations based on the numerical studies carried out in RU #140 and in the NEGOA study.

2.0 NEGOA Wind Fields

2.1 Introduction

This section describes a synoptic climatology to estimate surface winds over NEGOA for trajectory calculations coupled with the ability to provide frequency of occurrence information from the meteorological record. It is an abbreviated version of the appended draft technical report (Overland and Hiester, 1978). A synoptic climatology is a collection of generalized quasi-steady states of the atmosphere which are frequently observed or a continuum of states along particular storm tracks. Weather types aim to maintain the range of synoptic variability while grouping daily weather maps which have the same basic meteorological structure but slightly different locations or intensities. A synoptic climatology differs from calculation of means in that it specifies specific type "patterns, such as a high or low pressure center, which could occur on any given day rather than forming an average over several possibly different sequential daily maps.

It should be recalled that atmospheric modes are continuous in time and that synoptic systems differ in size and intensity throughout their individual life cycle and from one storm to the next.' Given the assumption that classification is possible, our approach regards patterns of weather circulation as implicit functions of the static sea level pressure distribution (Barry, 1972). It differs from a kinematic approach in which synoptic weather maps are classified in terms of principal storm tracks. The former approach is most appropriate in regions where a proportion of features form and/or decay in situ or are persistent. Since the Gulf of Alaska is often the decay center for storms in the Pacific, the static approach is taken as a working hypothesis. Western Europe and the East

Coast of the United States are examples where a kinematic approach would be more appropriate.

There are two approaches to map typing which can be referred to as objective (or at least automated) and subjective. Objective typing can be considered a pattern recognition problem involving digitized weather maps. Such techniques are generally based upon principal component analysis, factor analysis and their close relatives (Kendall and Stuart, 1972), or pattern correlation techniques (Lund, 1963). General objective techniques are being investigated as a companion study to the research reported here. The subjective approach involves assigning daily weather maps into different categories by a synoptic meteorologist. A rationale for subjective typing is that in order for patterns to be successful the underlying meteorological processes leading to these patterns should be recognizable.

Six subjectively derived weather types have been established for the Northeast Gulf of Alaska (NEGOA) - Kodiak Island region, which are subdivided into twelve subtypes. These six patterns were derived from combining and modifying patterns from two previous studies by Sorkina (1963) and Putnins (196.6), subjective analysis of fall 1977- summer 1978 sea level pressure charts from the National Meteorological Center, and post modification of patterns based upon daily typing of candidate patterns. Post analysis indicated the necessity of including subtypes. Subtypes within a type contain the same general distribution of features and meteorological basis but represent slight variations in locations of features which cause changes in the orientation of the geostrophic wind at the central location of the NEGOA coastline.

The digitized sea level pressure grids for the northern hemisphere produced by the National Meteorological Center (Jenne, 1975) are an additional

source for this study. These fields are available for 1968-1975. Each subjective subtype was digitized on the same mesh as the Meteorological Center grid for twenty-four common points. A daily map may then be quickly typed by computing its correlation with each of the subjective types. Such a procedure forms the basis for percent coverage and transition probability calculations for various types.

The second approach to typing considered in this report consists of applying the pattern correlation technique (Lund, 1963) to the digitized daily weather maps. The pattern correlation technique consists of forming the correlation of each day with all the other days during the year. The days with the highest number of correlations greater than a prescribed cutoff value with type A are removed and the procedure is repeated to find type B; the analysis is continued until the data are exhausted. This procedure is applied to NEGOA as an independent check on the subjective typing.

The relations of the surface wind fields over coastal waters of Alaska to geostrophic winds are complicated by coastal blocking, extensive air mass modification and mesoscale features induced by coastal topography. The available density of station data does not provide the resolution of the spatial variation of the wind field over the water for input to trajectory calculations. As an alternative we have developed local wind fields on a 7½ minute latitude by 15 minute longitude grid which are the assumed local winds that occur with each synoptic scale subtype. These local patterns use a single point planetary boundary layer model proposed by Cardone (1969) to compute surface stress from the geostrophic wind, including corrections for thermal influence, and modify the near shore wind field based upon the field program of Reynolds, et al. (1978).

2.2 The Six Surface Weather Type Patterns

The six types represented by twelve subtype patterns as described in the attached draft technical report are summarized by Table 2-1. All 22 of Putnins' patterns can be incorporated into these slightly more general patterns, and most of the 77-78 surface maps subjectively resemble one or another of the twelve subtypes.

To determine pattern frequencies automated sea level pressure analyses over the northern hemisphere produced at the National Meteorological Center (NMC) were obtained for 1968-1975. A subset of 24 grid points was extracted from each 12 hour map for the NEGOA region. Each subjective subtype was also digitized to provide sea level pressure values at each of the 24 grid point locations. The correlation was then computed between each map and the twelve subtypes to determine the pattern for each 12 hour weather map:

$$r_{it} = \sum_{m=1}^{24} \left(P_{imptm} \right) \left(\sum_{m=1}^{24} P_{im}^2 \sum_{m=1}^{24} P_{tm}^2 \right)^{-\frac{1}{2}}$$

where P_{im} and P_{tm} represent the deviation of pressures from the map average for date i and type t at grid pointy. The weather type with the largest correlation is assigned to that map. The magnitude of the correlation is recorded along with the type.

The percent of occurrence of each type by year and season are listed in Table 2.2 and graphed in Figure 2-1. The Aleutian low (pattern 2.0) is dominant in all seasons. Pattern 3.0 (high in the interior of Alaska) is confirmed as a winter pattern and the east Pacific high pressure as a summer pattern. Lows to the north (pattern 4) peak in summer and lows to the southeast (pattern 6) peak in winter. The same tables also list

TABLE 2.1

Type	Description	Sorkina Type	Putnins Type	Dominant Season
I	Low in Gulf of Alaska	4C	A′, A_1, G, H	Winter
II	Aleutian Low	5b	A, C, E, A_c	Winter, Spring, Fall
111	High pressure in Alaskan Interior	6a	D, B, D	Winter
IV	Low pressure center over Central Alaska	la	A″, A_3, F	Summer
v	Pacific Anticyclone	lb, 5a	A‴, A_2, E′, E'_1	Summer
VI	Stagnating low off of Queen Charlotte Islands	7a	D′, E″, El, F_1	Spring, Fall

TABLE 2.2

TRANSITIONS FROM INITIAL TYPE TO FOLLOWING TYPE

Based on 12 Hourly Analyses 1968-1974

	Initial Type	% Occurrence of Initial Type	% of Initial Type Followed by Following Type					
								6
YEAR	1	16	47	17	6	13	2	15
	2	31	12	71	6	7	3	1
	3	9	14	15	56	1	1	13
	4	18	8	11	~0	60	16	5
	5	12	~0	24	1	15	59	1
	6	14	15	3	9	8	3	62
WINTER	1	23	57	15	6	6	1	15
	2	26	13	71	8	6	1	1
	3	19	10	10	70	~0	1	9
	4	7	19"	14	1	42	13	11
	5	4	0	29	5	14	52	0
	6	21	14	2	9	4	1	70
SPRING	1	16	43	17	6	16	1	17
	2	37	11	73	6	7	2	1
	3	8	16	21	47	o	0	16
	4	16	8	14	1	54	16	7
	5	9	0	35	2	10	52	1
	6	14	16	4	8	10	4	58
SUMMER	1	8	34	20	4	27	5	10
	2	30	8	68	5	9	8	2
	3	3	27	20	29	2	7	15
	4	26	4	7	0	67	20	2
	5	27	~0	19	o	12	68	1
	6	6	14	7	4	15	7	52
FALL	1	18	45	18	6	14	1	16
	2	30	15	68	6	8	2	1
	3	8	16	18	43	3	1	19
	4	22	9	12	~0	60	13	6
	5	7	1	27	0	34	37	1
	6	15	15	2	10	9	3	61

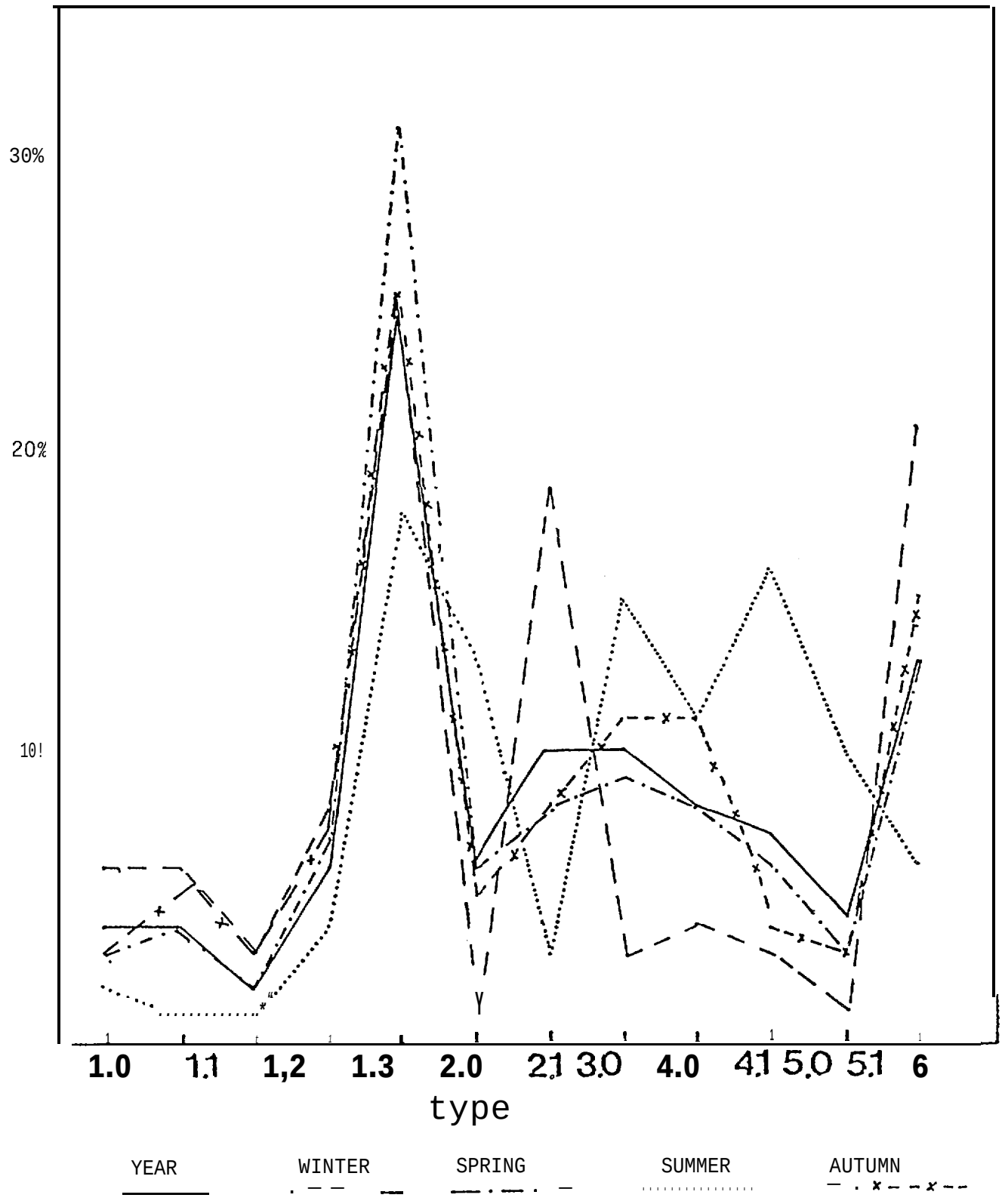

F gure 2-1. Percentage of occurrence of synoptic weather *type* by season.

transition probabilities. The large diagonal components, many over 50% are an indication of persistence of each pattern.

Figure 2-2 plots the percentage of days from the 1968-1973 record which could be typed by at least one of the patterns at a given threshold value of the correlation coefficient. Approximately 75% of the record can be typed by subjective patterns with a correlation of 0.7 or better. The figure also shows results for types generated by the pattern correlation technique applied to 1974 data. The final curve is typing the 1968-1973 data against ten daily maps drawn at random from 1974.

2.3 Local Wind Fields for NEGOA

This section discusses the generation of local wind fields from surface pressure pattern types described in section 2. For use in the oil spill trajectory calculations all local wind speeds within a pattern will be scaled against an anemometer record. Therefore, the primary aim is to produce wind fields showing local direction and relative magnitude. Computation began by computing gradient wind speeds and directions from the patterns on a uniform set of grid points over the localized area. The grid consisted of 800 boxes; each box was 7½ minutes in latitude by 15 minutes in longitude. At 60°N the boxes were 13.89 km on a side.

We assumed a thermal structure for the marine planetary boundary layer (PBL) so that the baroclinicity of the PBL was consistent with an ideal storm structure and climatology. Isotherms were drawn to reproduce the climatological large scale temperature gradient from the OCSEAP atlas (Brower, 1977) and then distorted to be consistent with storm structure packing the isotherms in frontal zones. Actual fronts were not created so as not to over-specify the generalized storm. From the isotherms, the magnitude and direction (relative to the surface geostrophic wind)

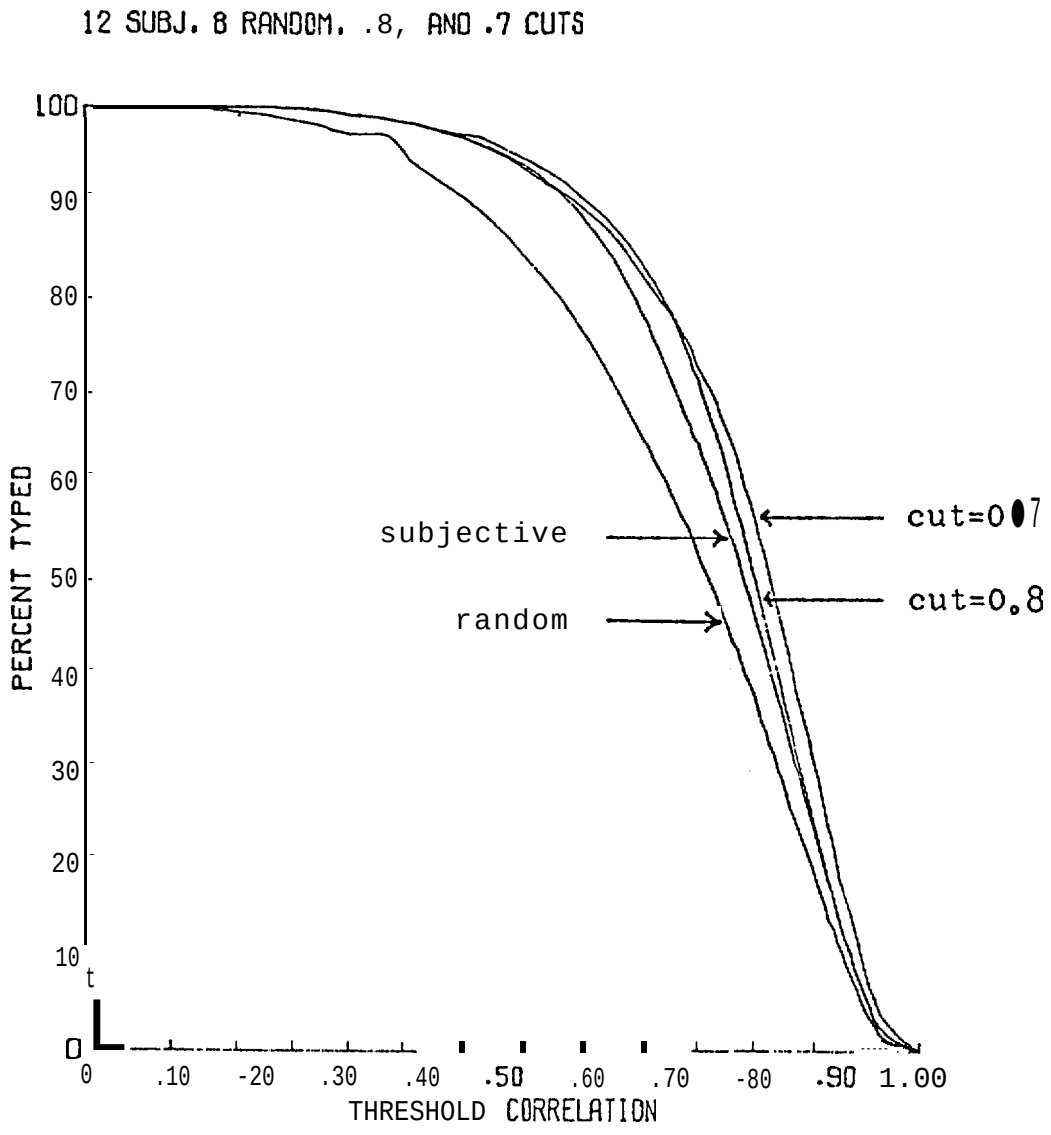

Figure 2-2. Percentage of 12 hour NMC pressure fields typed by the subjective approach, the two pattern correlation types and the average of eight sets of ten maps drawn at random from the NMC data set for 1974.

of the baroclinic field (thermal wind) were determined. The distribution of air-sea temperature difference was also assumed "for each pattern, also drawing on idealized storm structure and climatology.

Cardone's (1969) Ekman layer model was used to provide the friction velocity u_* and cross isobar flow angle a. The inputs required are the gradient wind speed, G, the magnitude of the PBL horizontal temperature gradient, $\nabla\overline{T}$, the angle between the surface gesotrophic wind and the thermal wind, η, and the air-sea temperature difference $\Delta\theta$.

Surface stress was converted to a neutral stratification 10 m surface layer wind speed. Only constant drag coefficients or drift factors should be used with these winds as wind speed and stability corrections are already included.

By comparing the baroclinic, stability dependent 10 m wind field with a wind field based on a constant $u_*/G = 0.025$ for pattern type 1.0, the effects of stability and baroclinicity are about 15%.

Within 50 - 100 km of the coast where Cardone's model is inappropriate, primary guidance was taken from actual measurements and descriptions of coastal processes reported in the draft NOAA Technical Report, "Coastal Meteorology in the Gulf of Alaska, Icy Bay to Yakutat Bay" (Reynolds, Hiester, Macklin, 1978). That report dealt only with the Icy Bay to Yakutat coastline but the following principles of that area were applied to the remainder of the NEGOA coastline.

Planetary boundary layer air piles up against the sides of coastal mountains when the incident winds are obliquely onshore. A pressure gradient forms normal to the coastline which establishes longshore geostrophic flow. This orographic forcing is part of the reason the low pressure systems stagnate in the Gulf of Alaska. The length scale

of the seaward extent that the deviation from the incident geostrophic flow is discernible is poorly understood. The length scale probably depends on the angle between the initial geostrophic flow and the coast, and the speed of an impinging pressure system. There are indications that the length scale may sometimes exceed 100 km.

Near the surface and nearshore, the winds are not in geostrophic balance and blow at an angle to the coastline. Within 20 km of the coast, the winds can have an offshore katabatic component due to drainage of denser air from the mountain valleys and glaciers. This is an almost permanent feature in winter but occurs mainly at night in the summer. Winds nearshore also respond to the coastal discontinuity in frictional drag creating an offshore wind component when there are longshore easterlies in NEGOA and an onshore component for longshore westerlies.

Figure 2-3 shows the wind speed and direction measured from an aircraft in a line directly offshore of the Malaspina Glacier. Nearshore winds were blowing from the NNE, slightly offshore and out of Yakutat Bay, while 50 km offshore, the winds were from the SE. Where the offshore and the onshore winds merged, the flow accelerated and formed a coastal jet 10 to 30 km offshore and parallel to the shore. That was the best example measured, but we believe the jet is a frequently occurring feature. The sensitivity of the jet to variations in meteorological parameters remains unknown.

In winter the winds nearshore are persistently offshore but in summer the drainage winds are weak and easily overcome by an onshore push. There is a deceleration as the shore is approached. Data from EB-70, EB-43, and an anemometer at Pt. Riou (on the shore at the western tip of the Malaspina Glacier) were used to scale these decelerations.

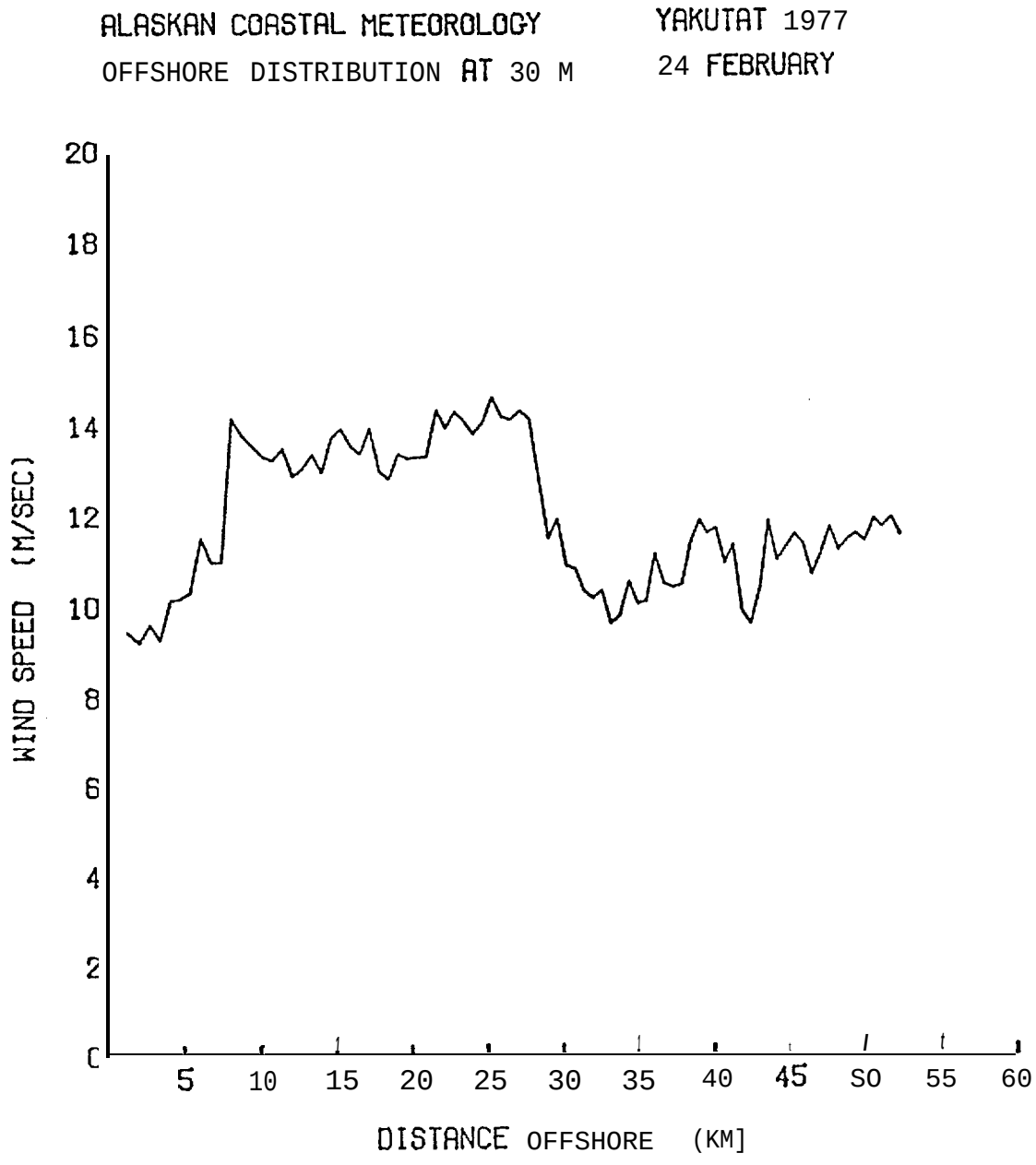

Figure 2-3(a). Wind speed as a function of offshore distance

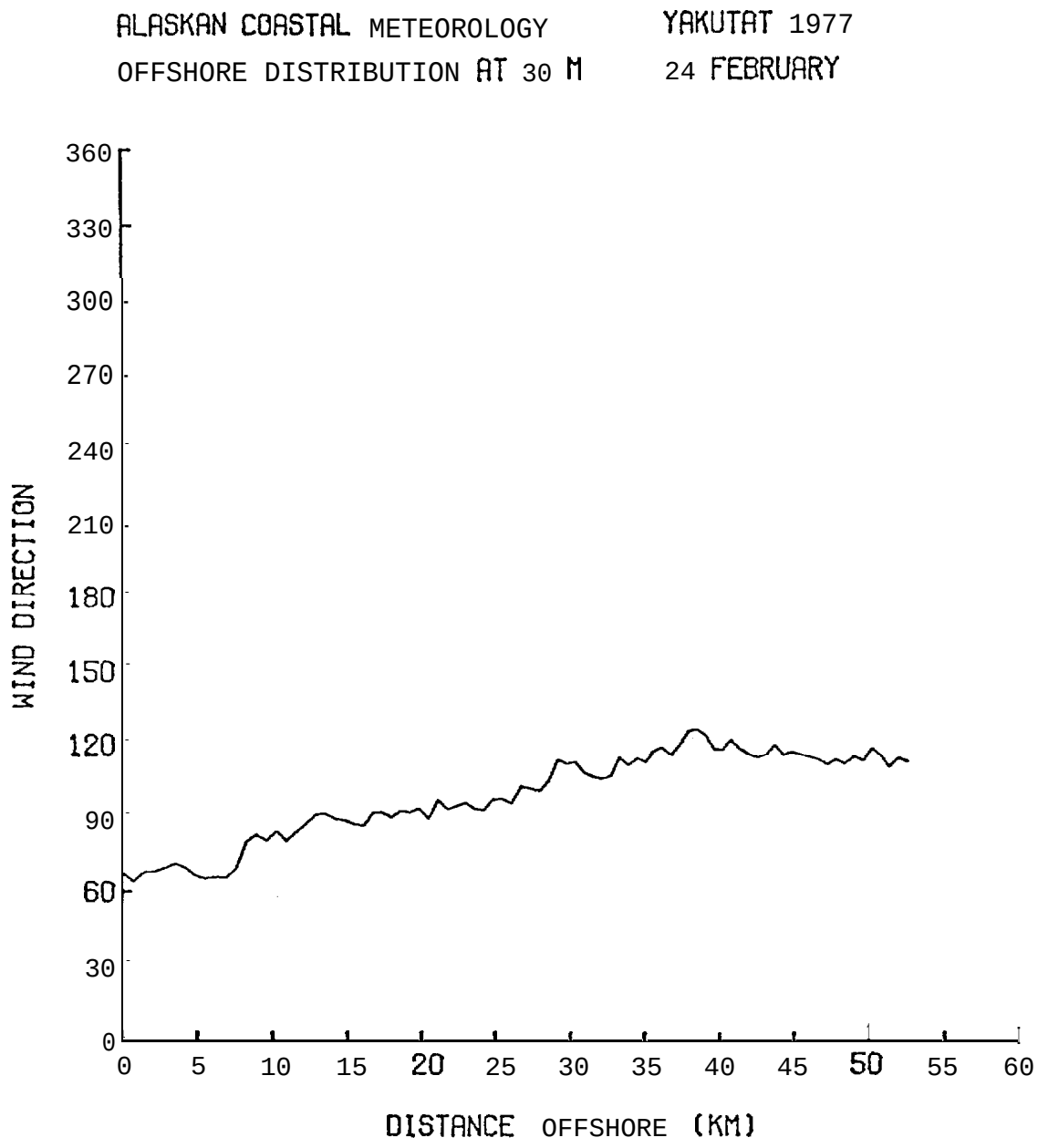

Figure 2-3(b). Direction of the 30 meter wind as a function of offshore direction.

After using the above principles to modify the coastal winds, the wind fields were smoothed. A nine point smoother was used on all grid boxes that were at least one box away from the shore.

Finally, the divergence at each grid point was computed for every wind field. The contours of the divergence field (x 10^5) for type 1.0 are shown in figure 2-4. The values at the coastline cannot be taken too literally as the wind vectors only represent the over water wind. The figure provides confidence in the overall method. There is convergence (of sensible magnitude) at the center of the storm, divergence behind the cold front, and convergence just off the coast where onshore flow meets katabatic flow.

Thirteen velocity fields for the synoptic subtypes described in section 2 are shown at the end of this section as figures A through M. The length of each arrow is a measure of the relative wind speed, and each arrow points downwind.

Synoptic pattern 1 represents a low pressure system contained within the Gulf of Alaska by coastal mountains. This pattern was broken down into four subtypes corresponding to four positions of the storm center as it migrates through the Gulf. Figure 2D is the vector plot for type 1.3 with the storm center at 57°N and 152°W, just east of Kodiak Island. The topographical forcing of the boundary layer is not yet strong so the flow near shore, in the mid to western portions of our grid is onshore, Near the shoreline and at the surface (not necessarily repesentative of the entire depth of the PBL) there is offshore katabatic flow. Fed by surrounding tributaries, the drainage flow is deeper in the estuaries such as Yakutat Bay and hence dominates the wind fields in those regions. Whenever flow encounters land it decelerates and turns toward lower pressure.

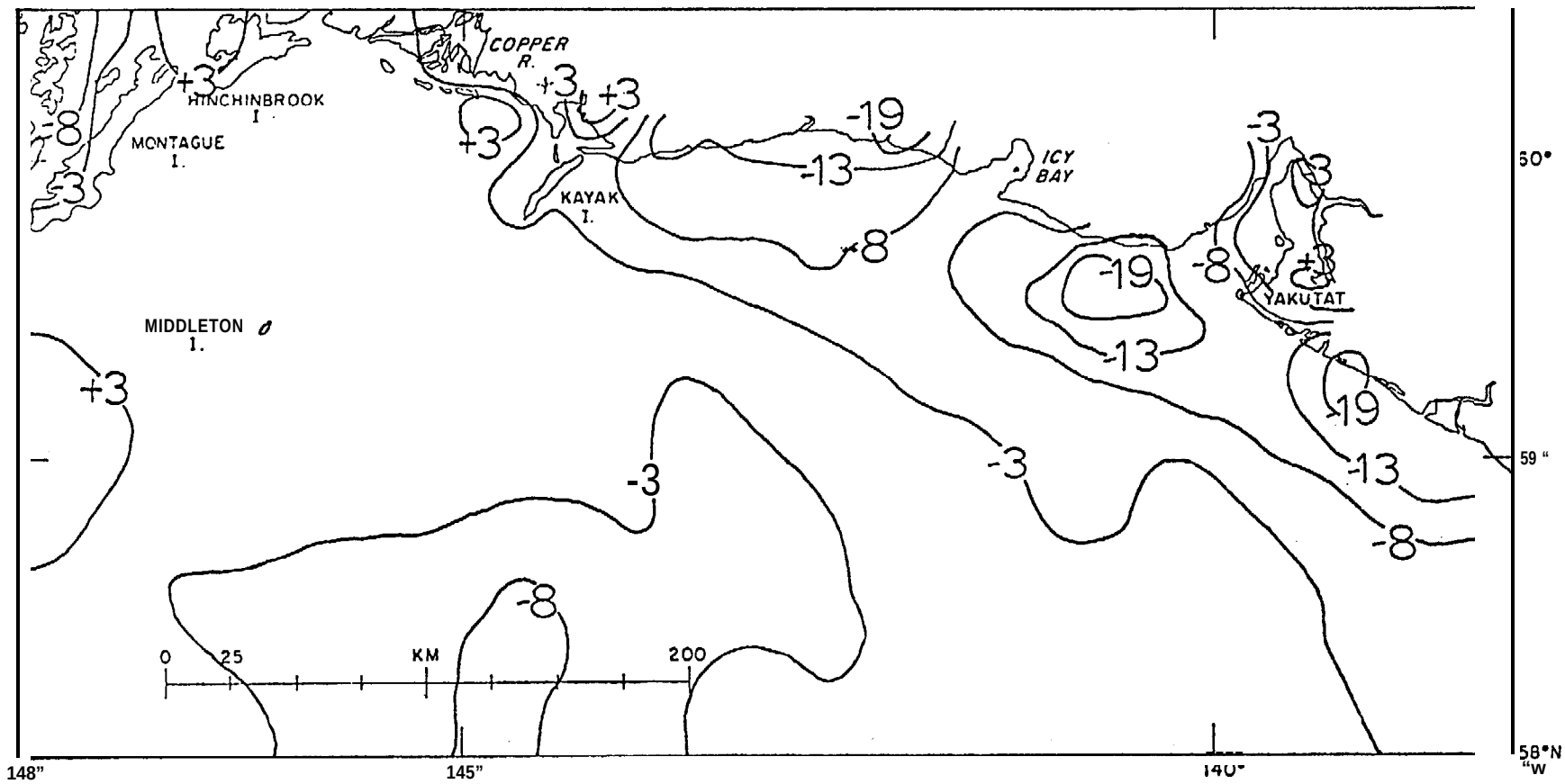

Figure 2-4. Divergence field calculated from the local wind field for type 1,0.

For example, the winds that blow across Kayak Island are retarded and deflected to the south. The air accelerates around the southern tip of the island to rejoin undisturbed flow on the lee side. The winds are also generally slowed by the landforms at the entrances to the Copper River Delta and Prince William Sound, however some passes channel and accelerate the flow.

Figure 2B is the wind field for type 1.1 when the storm is centered at about 50°N, 148°W. The considerations are similar to those documented for type 1.3.

The archetype for this series, type 1.0, is shown in figure 2A. As the storm moves eastward into this position the orographic forcing of the PBL becomes strong, especially in the Yakutat to Kayak Island region. There the offshore flow (katabatically, frictionally and topographically forced) meets the onshore flow and the two form an alongshore jet. The winds blowing offshore in the western portion of the grid accelcrate from their nearshore speeds up to their open ocean speeds, causing some divergence there,

Figure 2C shows the wind field for type 1.2. The storm is at it's eastern extreme; at about 58°N, 141°W. The alongshore jet is mostly east of our grid region but is visible entering the region at the eastern border. The jet quickly dissipates in the difluent region in the northwest quadrant of the storm.

Type 2 represents an Aleutian low. The local wind field is shown in figure 2E. There is also an alongshore jet for this type. Since the flow in the eastern part of the grid is roughly alongshore, there is no alongshore acceleration there. The jet forms between Icy Bay and Kayak Island where the geostrophic flow is more directly onshore. The confluence at the mouth of the Yakutat Bay and the deceleration windward

of Kayak Island cause those areas to be convergence centers. There is relief behind Kayak Island where the winds turn northward to almost be in geostrophic-frictional balance before encountering the drainage winds in the Copper River area. The winds are slowed by the land masses in the Cape Hinchinbrook region, but are not blocked by them. Figure 2F represents an autumn case of type 2.1 with a remanant of high pressure to the east.

We have split the synoptic type 3 into two cases. Type 3.0 (figure 2G) is the usual case where the anticyclone over the Yukon dominates the NEGOA area. This is typically a time of clear skies. Radiational cooling of the land surfaces causes katabatic flow, especially off of the Bering, Malaspina, and Hubbard Glaciers. East of Yakutat, the winds accelerate offshore making it a region of divergence. From Yakutat Bay to Kayak Island there is convergence of katabatic and alongshore winds. West of the Bering Glacier is another region of divergence. The winds blowing from the Copper River delta hit Hinchinbrook and Montague Islands quite obliquely, so we show the air blowing roughly parallel to those shores and around the islands to the south rather than making the more energy consuming trip over the tops as in the previously described types. The eastern shores of these islands are, therefore, in a covergent region.

Type 3.1 (figure 2H) allows for the reported cases of very strong (50 to 100 knots) winds near shore along the NEGOA coast. The surface pressure pattern is virtually indistinguishable from that of type 3.0. The air northeast of the coastal mountains is very cold throughout a very deep layer; i.e., the 1000-500 mb thickness is less northeast of the mountains than in the Gulf. When the reservoir of cold air gets deep enough, the cold air spills through the mountain passes like water

over a dam. The low temperature is somewhat maintained (against adiabatic warming during descent) by flow over the radiationally cooled icefields. Large velocities build up as the air drains out of the prominent valleys. We have allowed strong winds to blow out of the Alsek River Valley, Yakutat Bay, Icy Bay, off the Bering Glacier, and from the Copper River Valley.

The Icy Bay winds are strongest and actually blow off the Malaspina Glacier just east of Icy Bay. Guidance for this location came from a preliminary meteorological model run (Overlandlet al. 1977). We assumed the core of strong winds would totally mix with the ambient air about 100 km downstream of the shore. Most cores turn to the right as they mix with the ambient flow. The Bering Glacier and Copper River winds meet and mutually interfere.

Synoptic pattern 4 is a summertime case when a large low pressure system over central Alaska dominates with the Pacific high retreating to the south. It is also observed if the Aleutian low (type 2) drifts north. In the local wind fields (figure 21 and 2J) we weaken the katabatic flow off the ice (the land surfaces may be warmer than the ocean), and the land-sea frictional differences encourage onshore flow. The winds also blow up estuaries, unlike previously described cases.

Synoptic pattern 5 represents the predominant summer case of the Pacific anticyclone. The local wind fields, shown in figure 2Kand 21 were treated similarly to type 4. There is some topographical forcing, however, as the isobars are slightly packed on the eastern side of the high. The central area of the high is divergent with the onshore flow at the coast being convergent.

Synoptic type 6 represents the low pressure center west of the Queen Charlotte Islands. Frequently this low stagnates and fills in place,

but it also may move NNW into the Gulf of Alaska and become type 1.2. The local wind field (figure 2M) is divergent over most of the NEGOA grid. Guidance in scaling the small horizontal variations for this pattern was taken from aircraft measurements made under similar synoptic conditions, reported in the Reynolds et al. report.

2.4 Weather Typing for the Trajectory Calculations

July-August 1974 and February-March 1975 are the two periods for the sample trajectory calculations. The hand drawn sea level pressure analyses from the National Meteorological Center were visually typed every twelve hours through these periods (Table 2.3 and 2.4).

Figure 2-5 shows the direction of the local wind (meteorological) at Middleton Island for each weather type as inferred from figures 2A - 2M. For comparison the anemometer record at Middleton Island during the sample periods was stratified by synoptic type. Vector mean winds were then computed within each type and plotted for the winter period on figure 2-5 and for the summer period in figure 2-6. A similar plot for winds at EB-33 in winter is shown in figure 2-7. A discussion of wind residuals as compared to Middleton Island and EB-33 winds is presented in section 5.

(SUMMER)

Table 2.3

SUBJECTIVE TYPING

AY	TIME (GMT)	TYPE
	JULY, 1974	
1	00	1.3
1	12	1.3
2	00	4.1
2	12	2.1
3	00	4.1
3	12	4.0
4	00	5.0
4	12	5.1
5	00	5.1
5	12	1.1
6	00	1.1
6	12	5.1
7	00	5.1
7	12	5.0
8	00	5.1
8	12	5.0
9	00	5.1
9	12	5.1
0	00	5.1
0	12	1.1
1	00	1.1
1	12	1.3
2	00	1.1
2	12	1.1
3	00	2.1
3	12	2.0
4	00	4.0
4	12	5.1
5	00	5.1
5	12	5.1
6	00	4.0
6	12	5.1
7	00	4.1
7	12	5.1
8	00	5.0
8	12	4.0
9	00	4.0
9	12	2.1
0	00	2.1
0	12	2.0
1	00	2.0
1	12	1.3
2	00	1.3
2	12	1.1
23	00	1.3
23	12	2.1
24	00	1.1
24	12	4.0
25	00	4.0
25	12	1.1
26	00	5.0
26	12	5.1
27	00	5.1
27	12	5.1
28	00	5.0
28	12	5.0
29	00	4.0
29	12	5.0
30	00	5.1
30	12	5.1
31	00	5.1
31	12	4.0
	AUGUST, 1974	
1	00	3.0
1	12	2.0
2	00	1.3
2	12	1.3
3	00	1.1
3	12	1.1
4	00	1.1
4	12	6.0
5	00	5.0
5	12	4.0
6	00	2.1
6	12	2.1
7	00	2.1
7	12	1.3
8	00	1.1
8	12	4.0
9	00	5.0
9	12	5.0
10	00	5.0
10	12	5.1
11	00	5.1
11	12	5.1
12	00	5.1
12	12	5.1
13	00	5.1
13	12	5.1
14	00	5.1
14	12	5.1
15	00	5.1
15	12	5.1
16	00	5.1
16	12	5.0
17	00	5.1
17	12	5.1
18	00	1.0
18	12	4.1
19	00	5.1
19	12	5.1
20	00	4.1
20	12	1.1
21	00	4.1
21	12	4.0
22	00	4.0
22	12	4.0
23	00	1.1
23	12	4.1
24	00	4.1
24	12	5.0
25	00	1.3
25	12	1.3
26	00	1.0
26	12	4.0
27	00	2.1
27	12	2.0
28	00	2.1
28	12	2.1
29	00	2.1
29	12	2.1
30	00	2.1
30	12	2.1
31	00	5.1
31	12	4.0

Table 2.4 (WINTER)

SUBJECTIVE TYPING

DAY	TIME (GMT)	TYPE	DAY	TIME (GMT)	TYPE	DAY	TIME (GMT)	TYPE
FEBRUARY, 1975								
1	00	6.0	23	00	2.0	16	00	3.0
1	12	6.0	23	12	5.0	16	12	1.3
2	00	6.0	24	00	4.0	17	00	1.3
2	12	6.0	24	12	2.1	17	12	6.0
3	00	6.0	25	00	1.3	18	00	6.0
3	12	6.0	25	12	2.0	18	12	6.0
4	00	6.0	26	00	1.3	19	00	6.0
4	12	5.1	26	12	2.0	19	12	1.0
5	00	5.1	27	00	4.0	20	00	5.0
5	12	5.1	27	12	2.1	20	12	4.0
6	00	3.0	28	00	5.0	21	00	2.1
6	12	6.0	28	12	5.0	21	12	4.0
7	00	6.0	MARCH, 1975			22	00	4.1
7	12	1.2				22	12	1.2
8	00	2.0	1	00	6.0	23	00	1.1
8	12	2.0	1	12	6.0	23	12	1.1
9	00	4.1	2	00	5.1	24	00	1.1
9	12	6.0	2	12	3.0	24	12	4.0
0	00	6.0	3	00	6.0	25	00	4.1
0	12	6.0	3	12	5.0	25	12	4.1
1	00	6.0	4	00	2.1	26	00	1.3
1	12	1.0	4	12	2.0	26	12	1.3
2	00	1.0	5	00	1.3	27	00	2.0
2	12	1.0	5	12	1.0	27	12	2.0
3	00	1.1	6	00	1.0	28	00	2.0
3	12	1.1	6	12	1.2	28	12	3.0
4	00	1.1	7	00	6.0	29	00	2.0
14	12	2.0	7	12	6.0	29	12	4.1
15	00	4.0	8	00	5.1	30	00	5.1
5	12	4.0	8	12	1.2	30	12	5.0
6	00	5.0	9	00	1.0	31	00	1.3
6	12	2.0	9	12	2.0	31	12	5.0
7	00	1.3	10	00	3.0			
7	12	4.0	10	12	2.0			
8	00	2.0	11	00	2.0			
8	12	2.1	11	12	4.0			
9	00	2.0	12	00	5.0			
9	12	4.1	12	12	2.0			
20	00	4.0	13	00	3.0			
20	12	4.1	13	12	2.0			
21	00	2.0	14	00	1.3			
21	12	2.0	14	12	1.2			
22	00	2.0	15	00	1.3			
22	12	4.0	15	12	1.1			

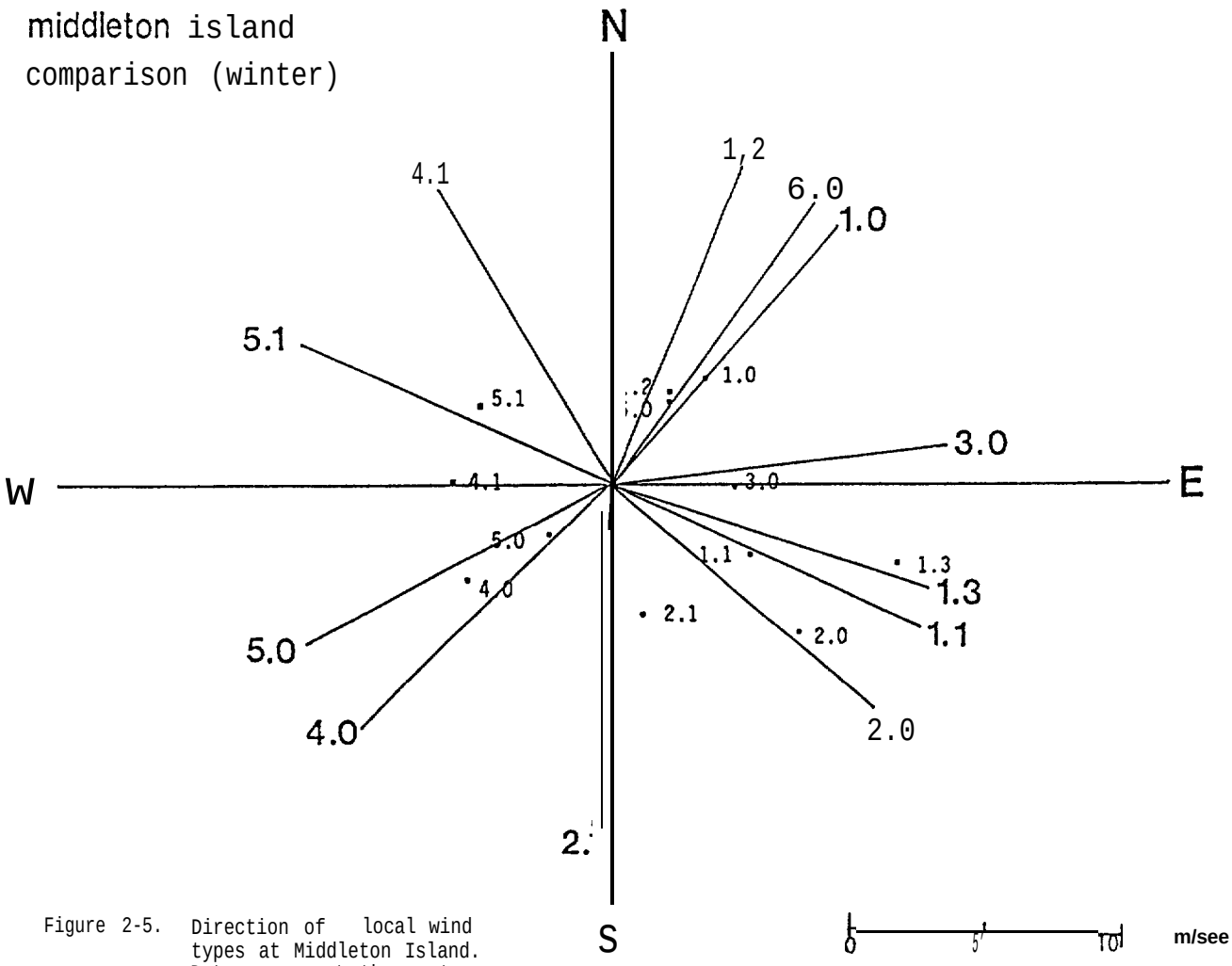

Figure 2-5. Direction of local wind types at Middleton Island. Dots represent the vector mean observed wind at Middleton stratified by subtypes for the February-March 1975 period.

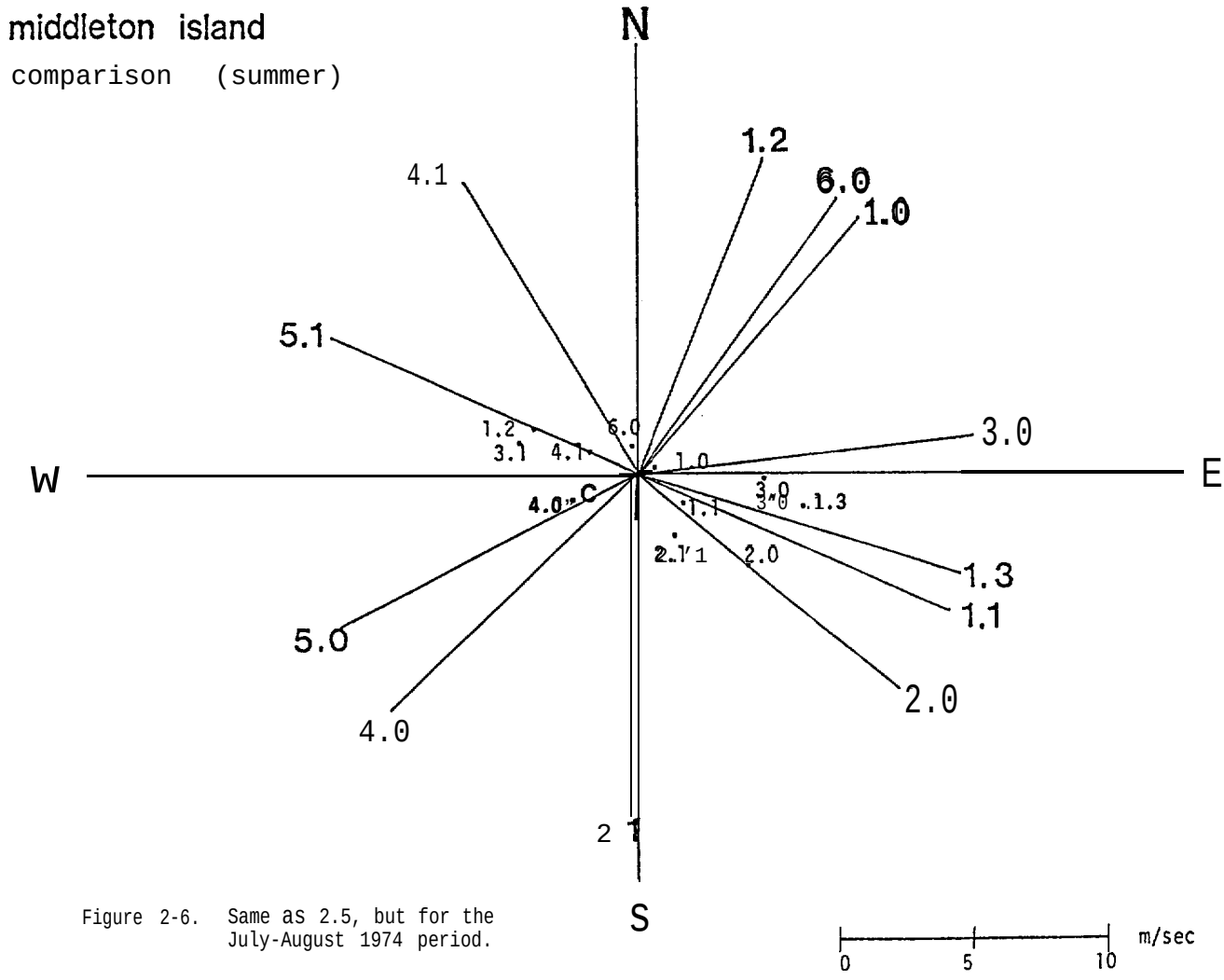

Figure 2-6. Same as 2.5, but for the July-August 1974 period.

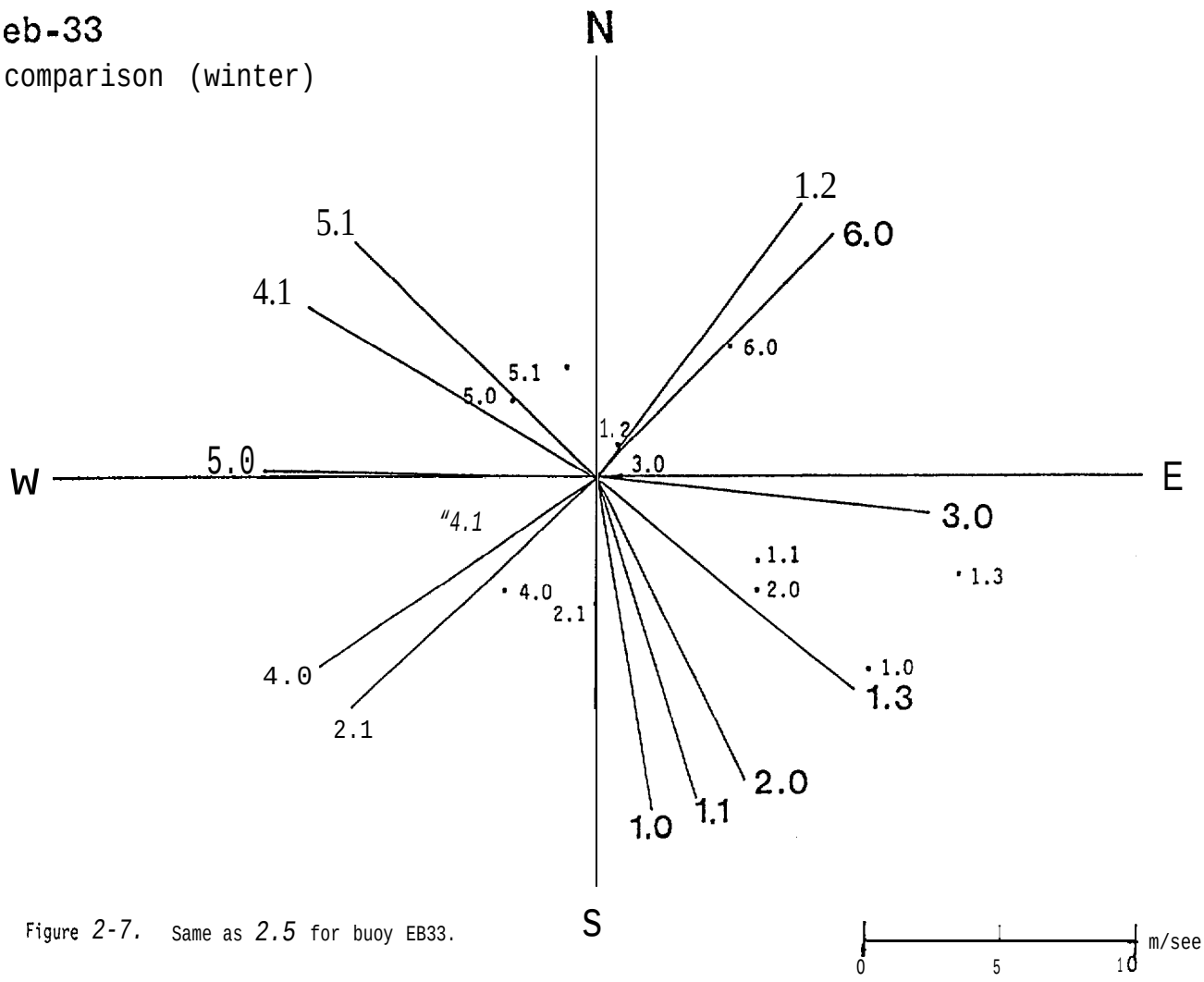

Figure 2-7. Same as 2.5 for buoy EB33.

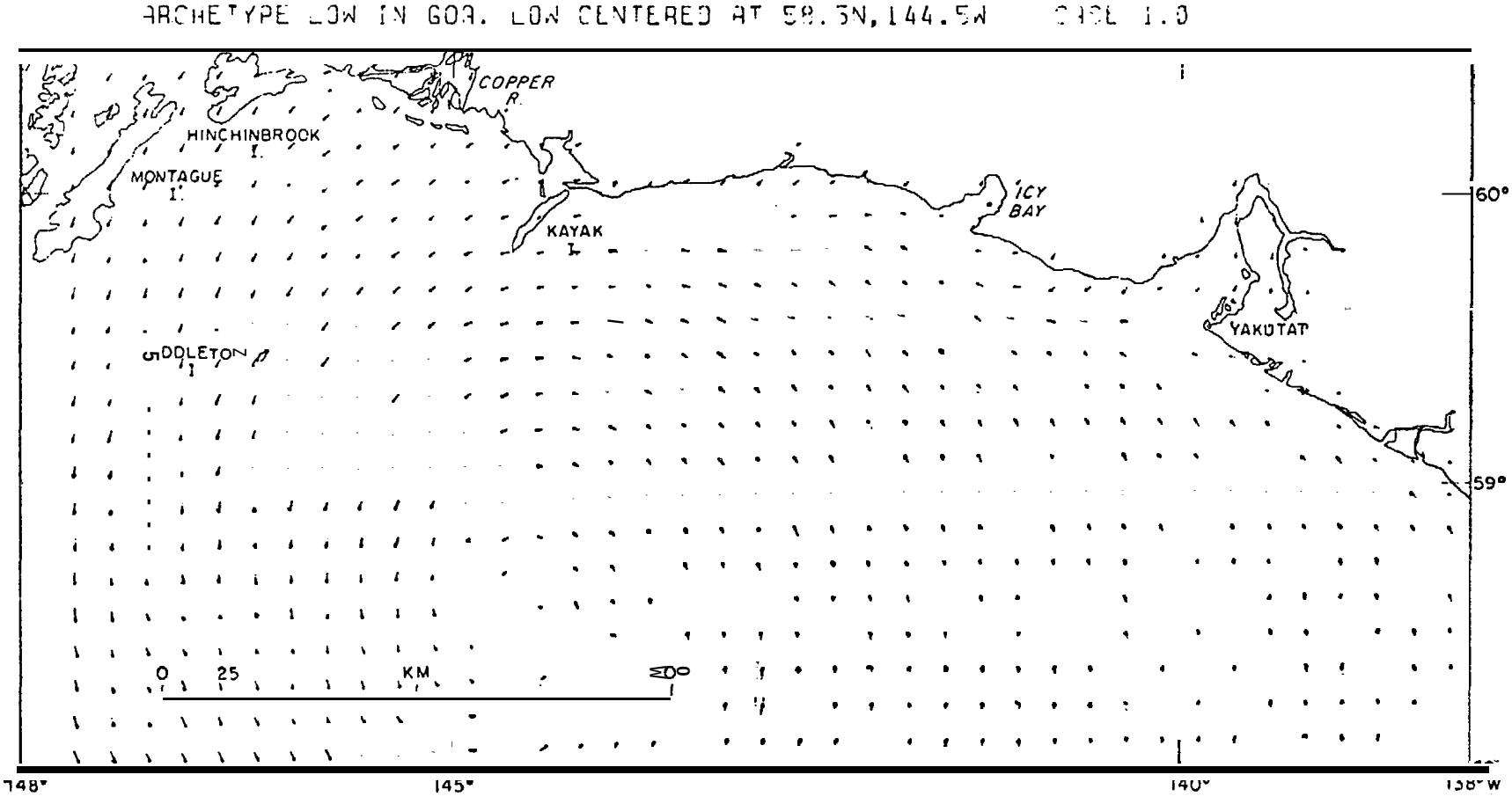
ARCHETYPE LOW IN GOA. LOW CENTERED AT 58.3N, 144.5W
COPPER R.
HINCHINBROOK I.
MONTAGUE I.
KAYAK I.
ICY BAY
YAKUTAT
GIDDLETON I.
60°
59°
0 25 KM 100
148°
145°
140°
138°W

Figure 2A

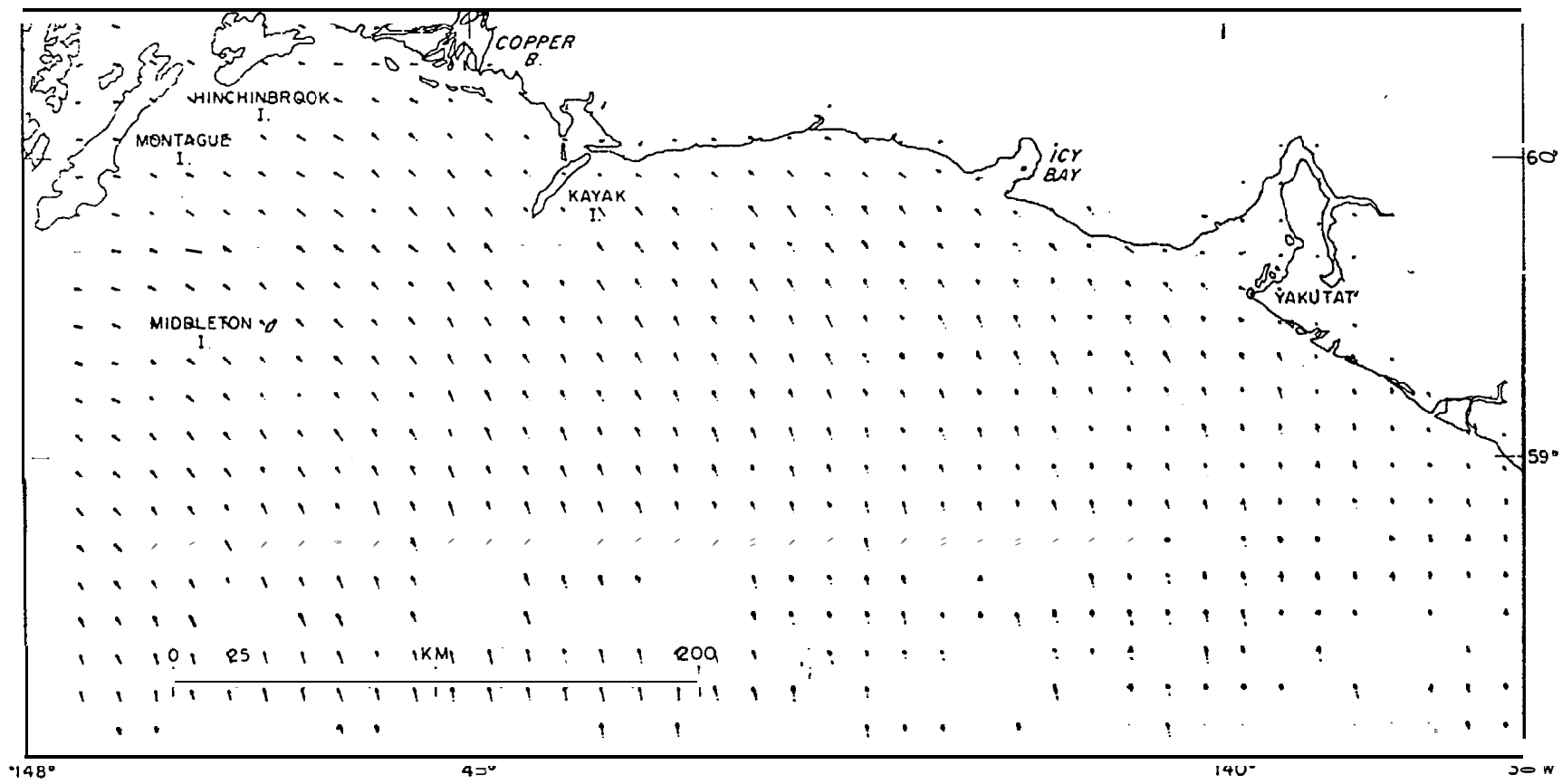
LOW IN GOA. CENTERED AT 50N, 148W
CASE 1.
COPPER R.
HINCHINBROOK I.
MONTAGUE I.
KAYAK I.
ICY BAY
YAKUTAT
MIDDLETON I
60°
59°
0 25 KM 200
148°
140°

Figure 2B

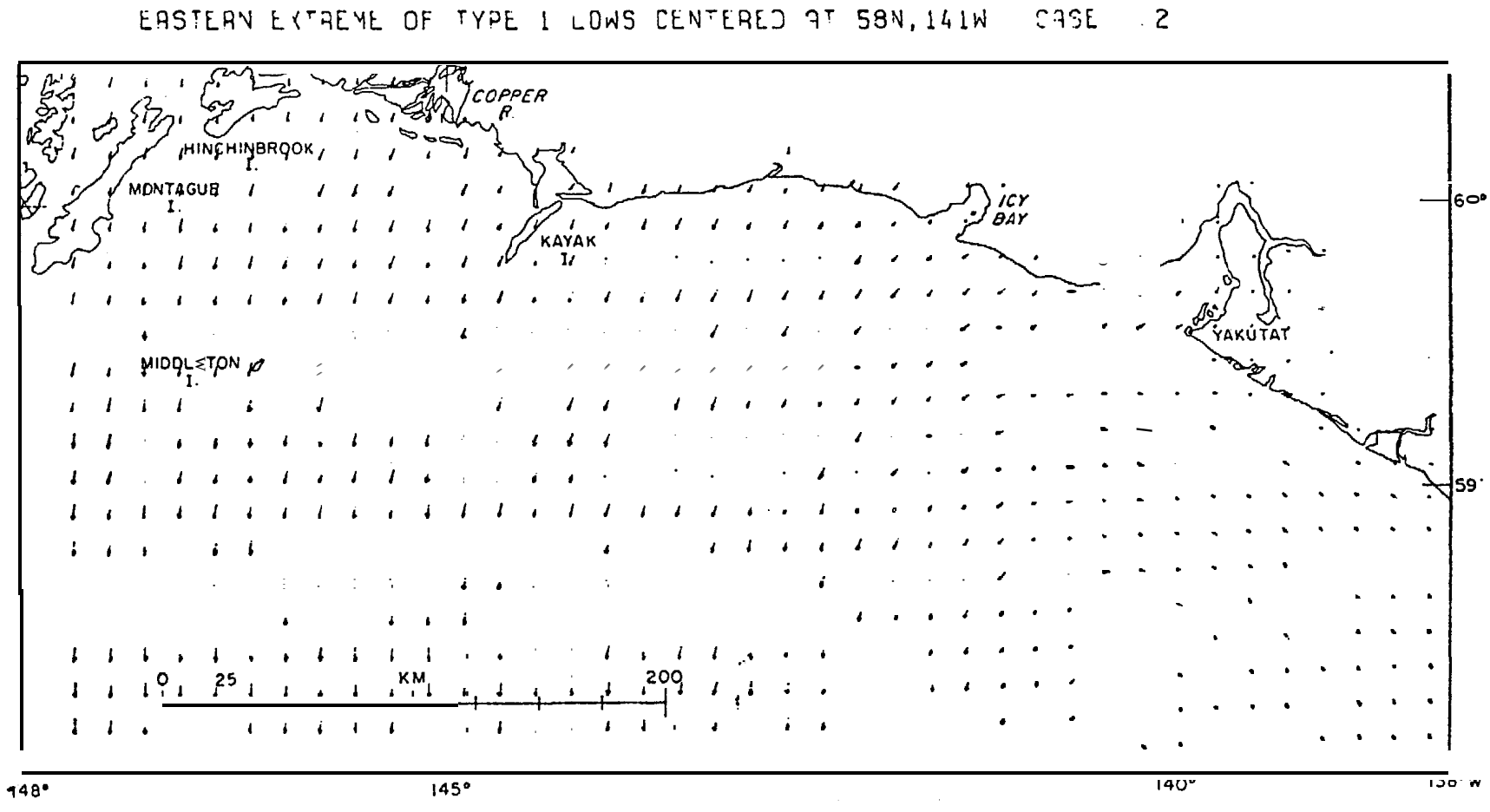
EASTERN EXTREME OF TYPE I LOWS CENTERED AT 58N, 141W CASE 2
COPPER R.
HINCHINBROOK I.
MONTAGUE I.
KAYAK I.
ICY BAY
YAKUTAT
MIDDLETON I.
0 25 KM 200
60°
59°
148°
145°
140°

Figure 2C

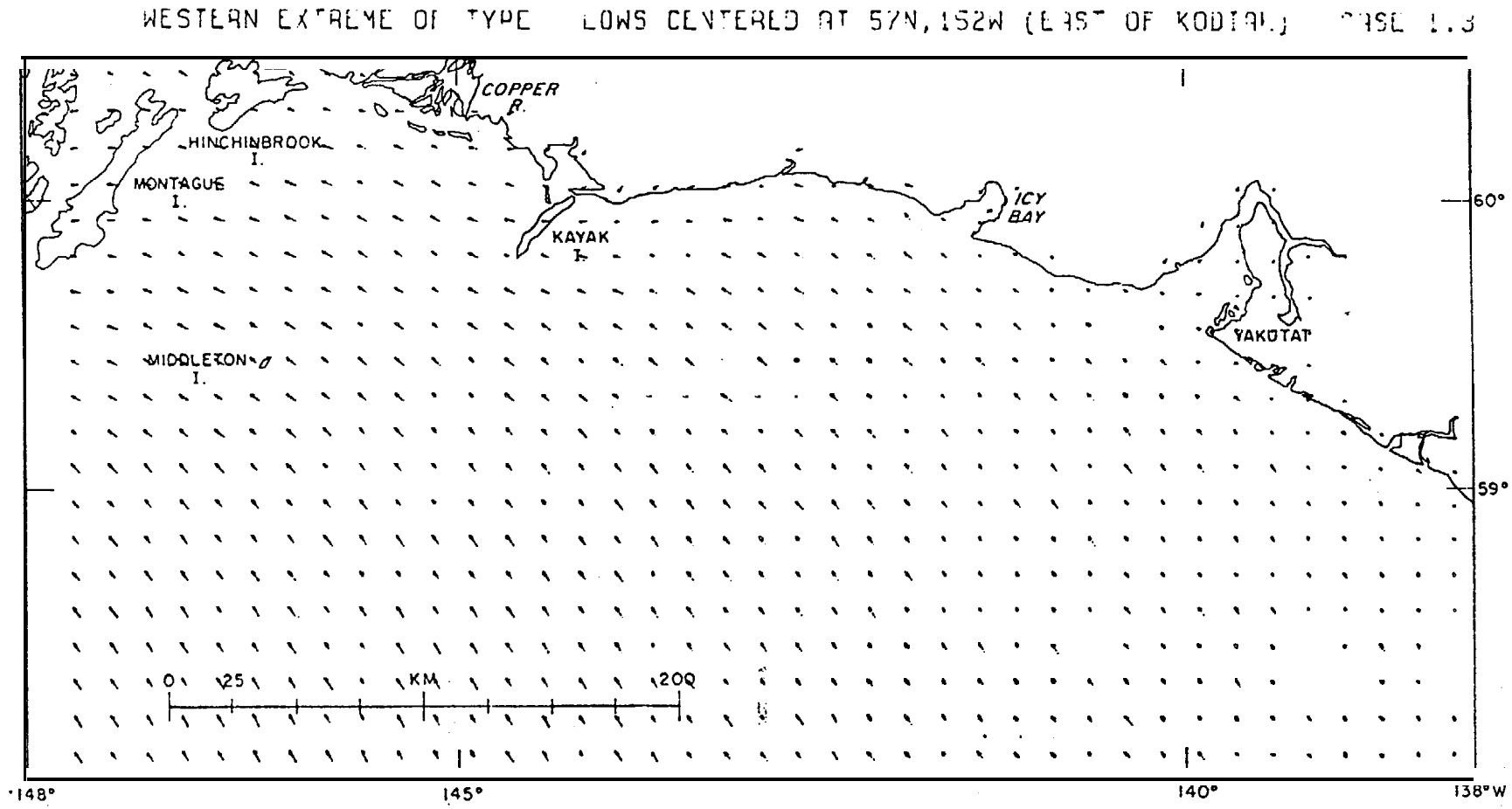
WESTERN EXTREME OF TYPE LOWS CENTERED AT 57N, 152W (EAST OF KODIAK)
COPPER R.
HINCHINBROOK I.
MONTAGUE I.
KAYAK I.
ICY BAY
YAKUTAT
MIDDLETON I.
0 25 KM 200
60°
59°
148°
145°
140°
138°W

Figure 2D

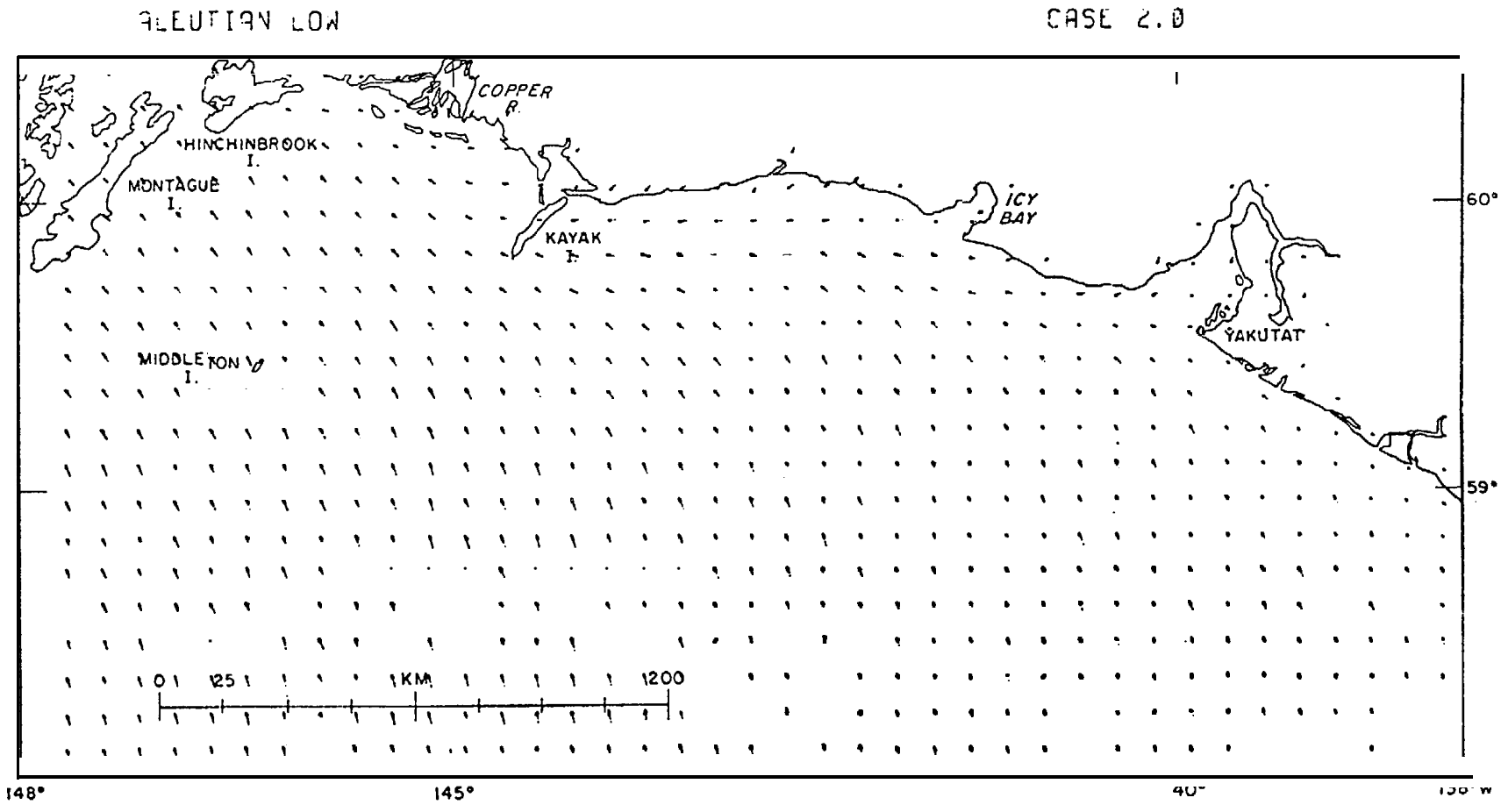
ALEUTIAN LOW
CASE 2.0
COPPER R.
HINCHINBROOK I.
MONTAGUE I.
KAYAK I.
ICY BAY
YAKUTAT
MIDDLETON I.
60°
59°
0 125 1KM 1200
148°
145°
40°

Figure 2E

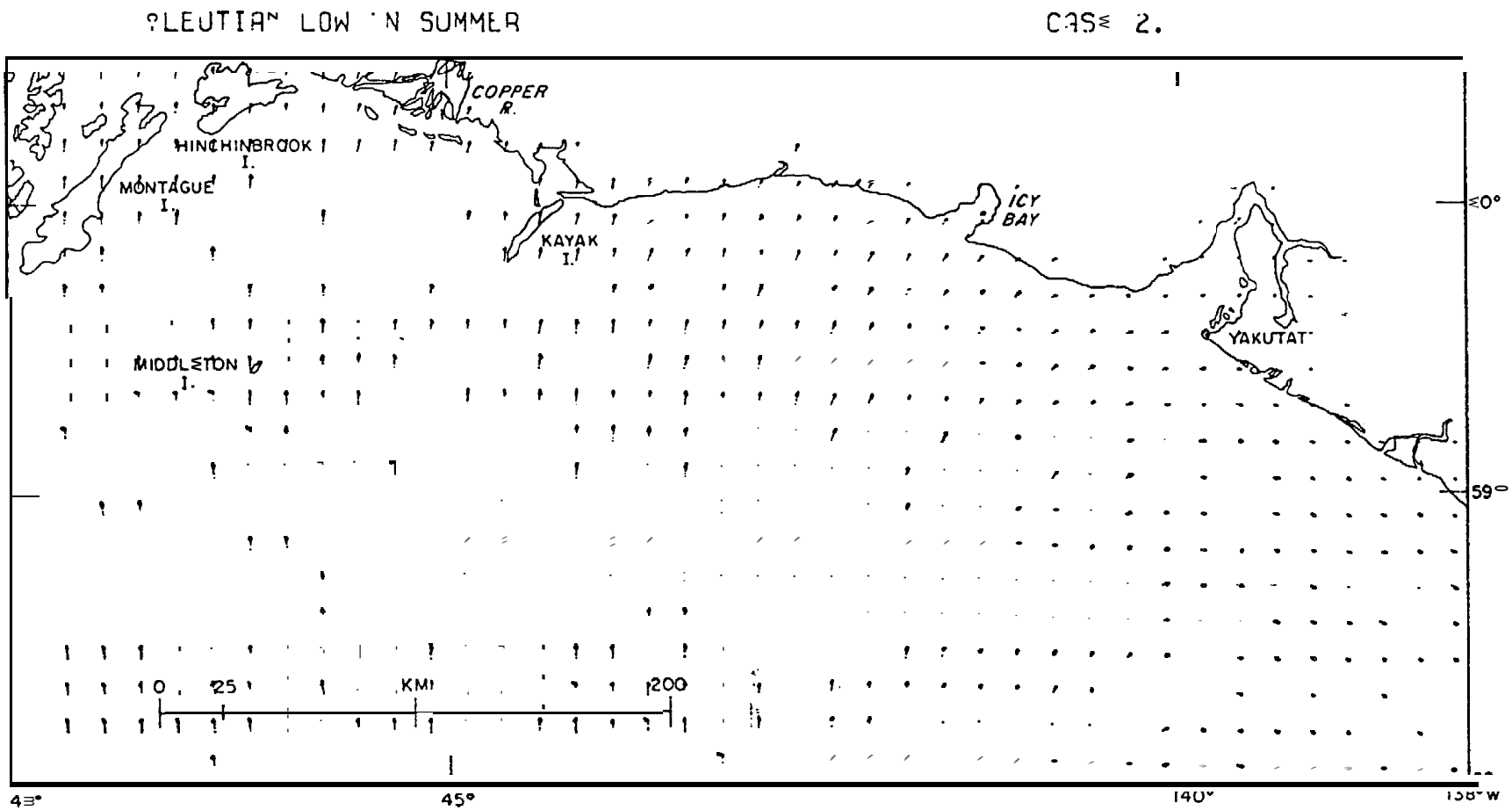
ALEUTIAN LOW IN SUMMER
CASE 2.
COPPER R.
HINCHINBROOK I.
MONTAGUE I.
KAYAK I.
ICY BAY
YAKUTAT
MIDDLETON I.
60°
59°
10
25
KM
200
43°
45°
140°
138° W

Figure 2F

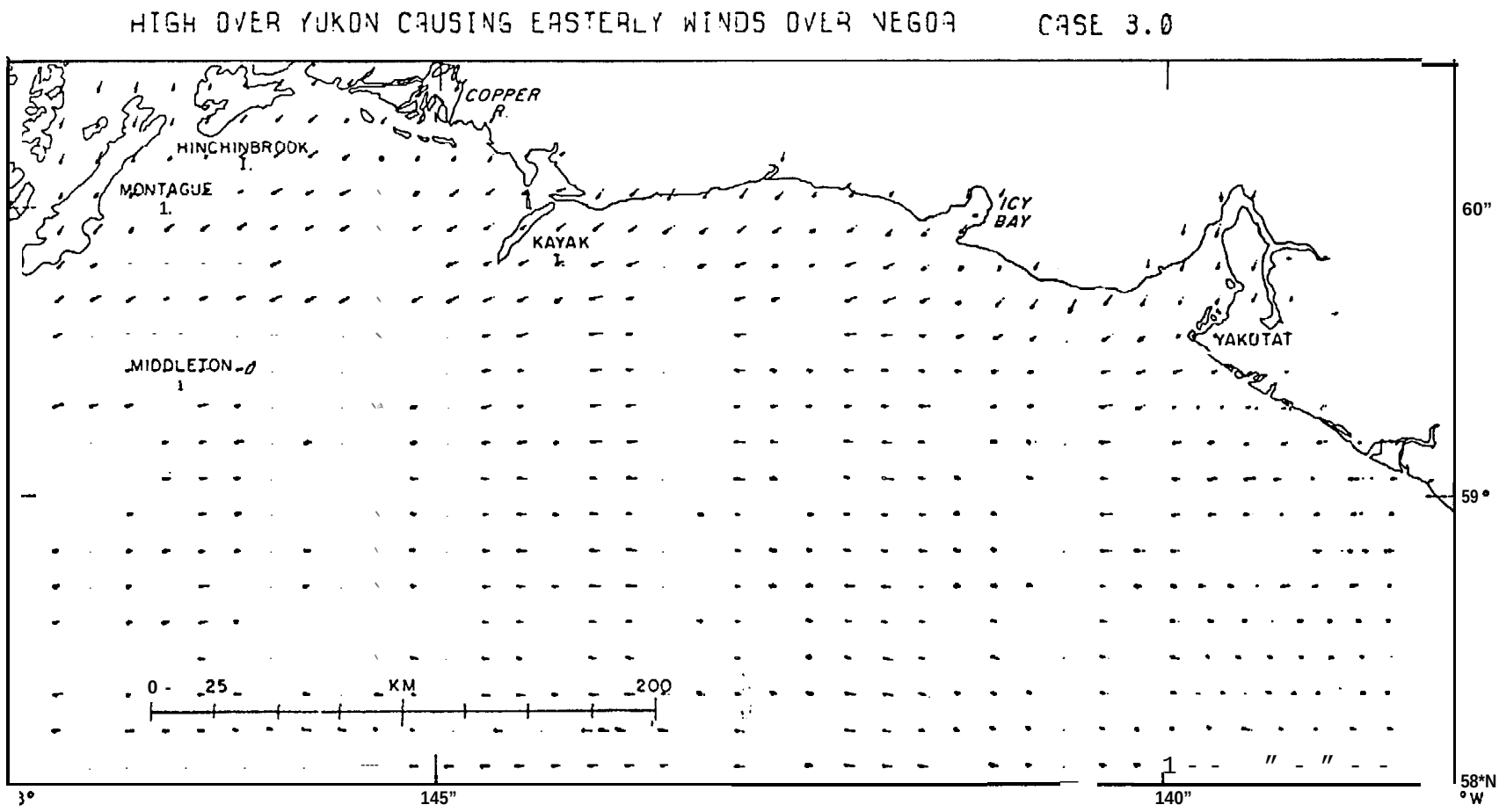
HIGH OVER YUKON CAUSING EASTERLY WINDS OVER NEGOA CASE 3.0
COPPER R.
HINCHINBROOK I.
MONTAGUE I.
KAYAK I.
ICY BAY
YAKUTAT
MIDDLETON I
0 - 25 - KM - 200
60"
59°
58°N
145"
140"

Figure 2G

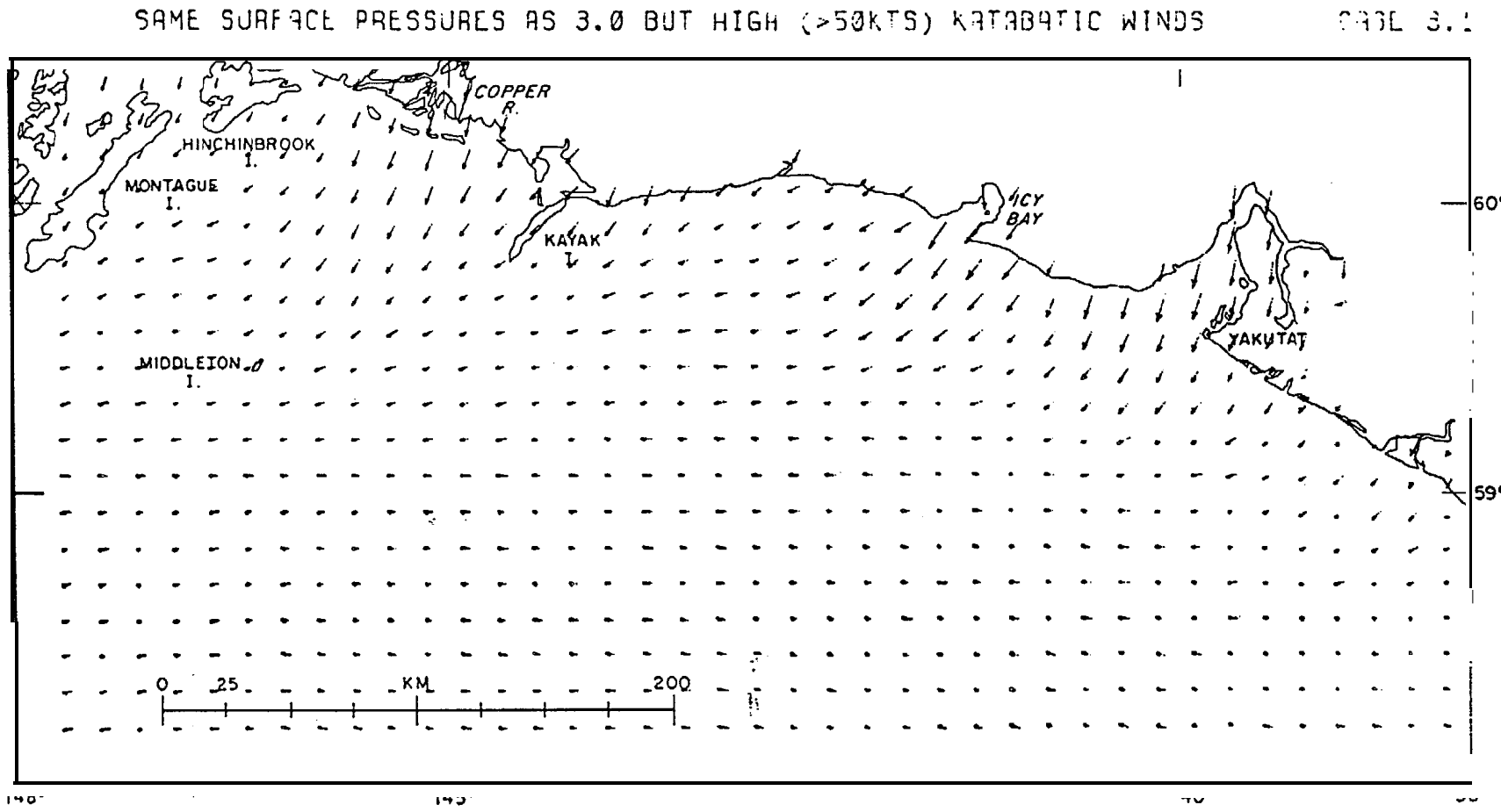
SAME SURFACE PRESSURES AS 3.0 BUT HIGH (>50KTS) KATABATIC WINDS
COPPER R.
HINCHINBROOK I.
MONTAGUE I.
KAYAK I.
ICY BAY
YAKUTAT
MIDDLETON I.
60°
59°
0 25 KM 200

Figure 2H

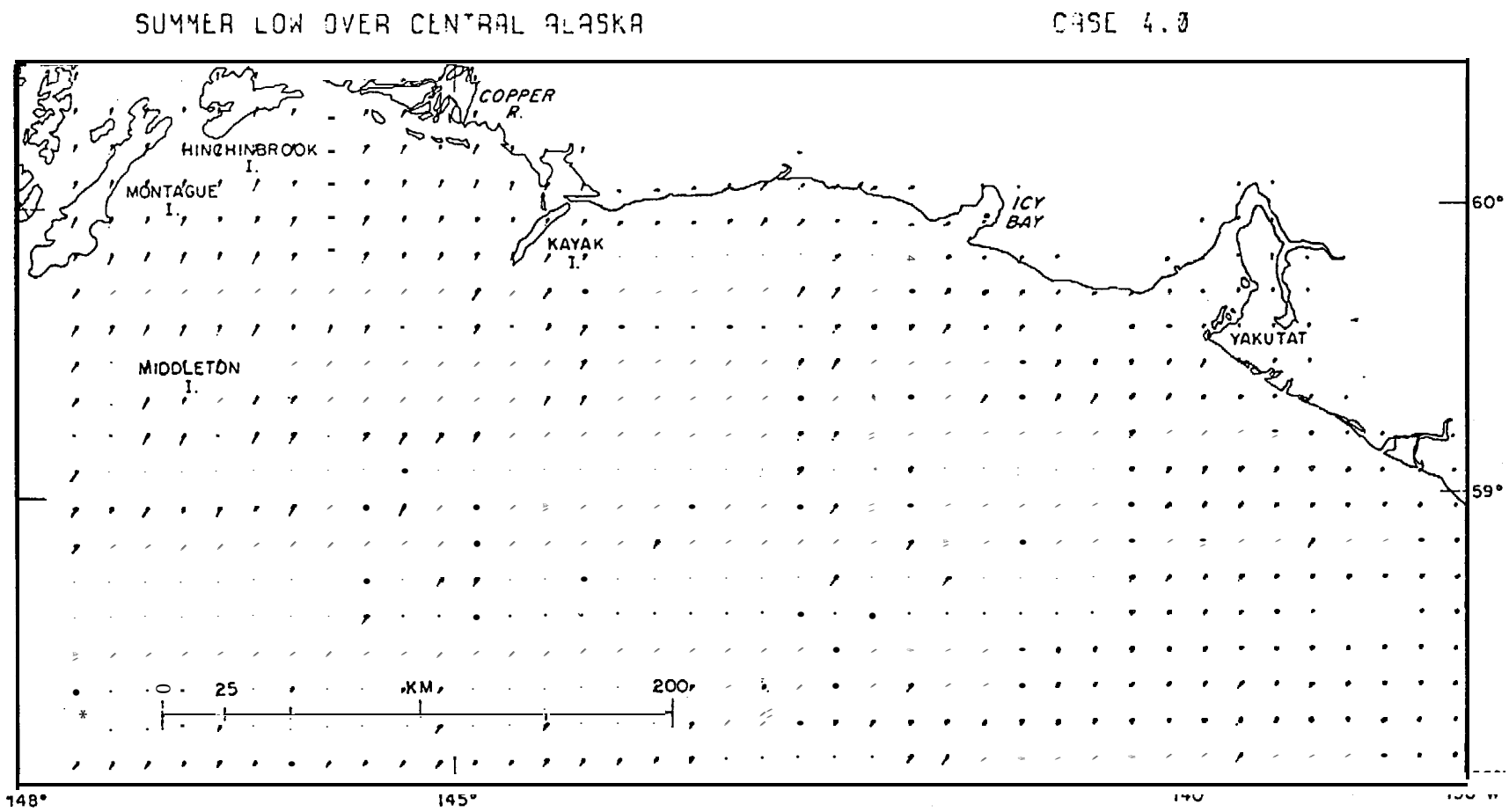
SUMMER LOW OVER CENTRAL ALASKA
CASE 4.0
COPPER R.
HINCHINBROOK I.
MONTAGUE I.
KAYAK I.
ICY BAY
YAKUTAT
MIDDLETON I.
60°
59°
0 25 KM 200
148°
145°

Figure 2I

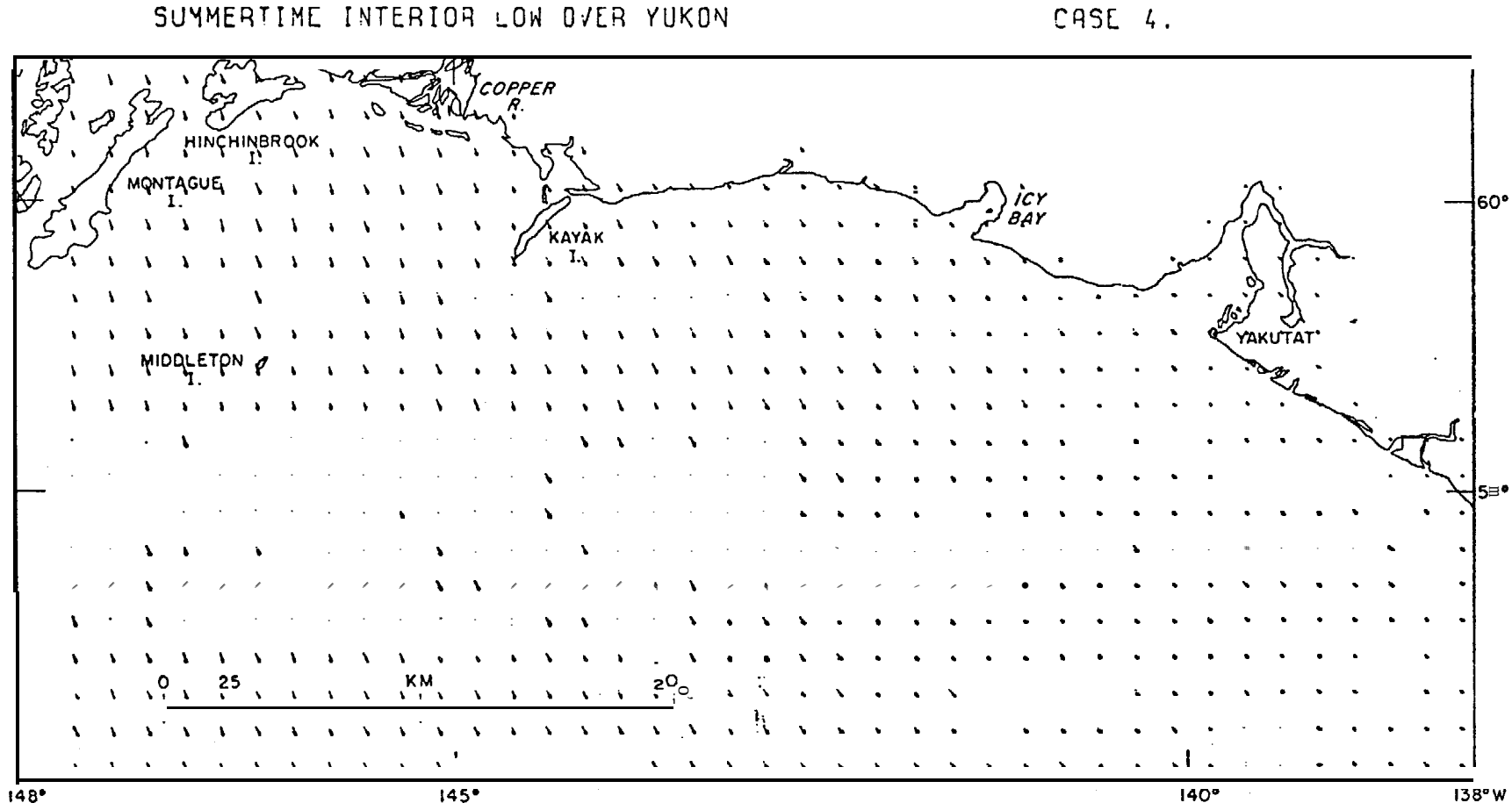
SUMMERTIME INTERIOR LOW OVER YUKON
CASE 4.
COPPER R.
HINCHINBROOK I.
MONTAGUE I.
KAYAK I.
ICY BAY
YAKUTAT
MIDDLETON I.
0 25 KM 200
60°
148°
145°
140°
138°W

Figure 2J

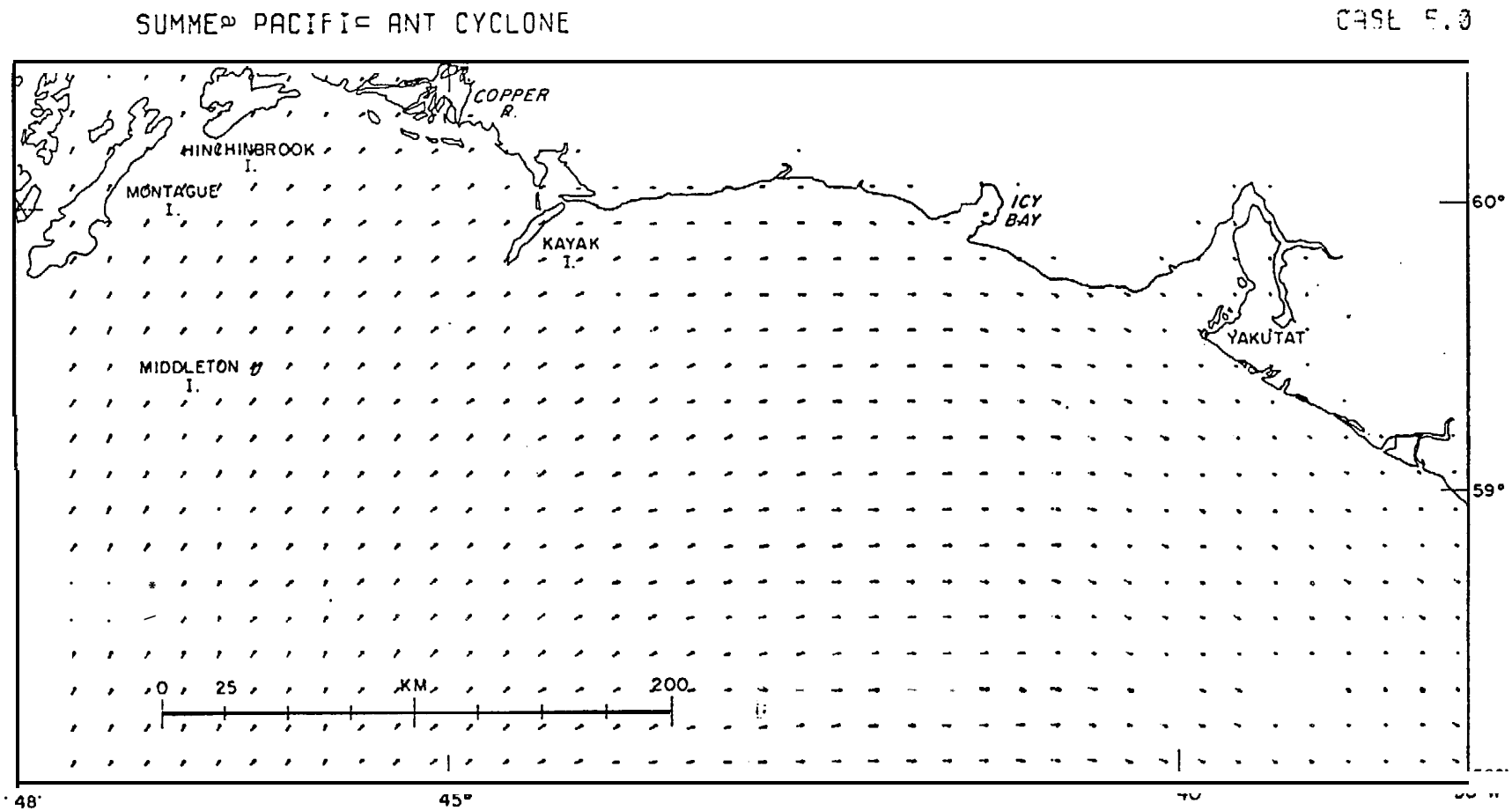
SUMMER PACIFIC ANT CYCLONE
CASE 5.0
COPPER R.
HINCHINBROOK I.
MONTAGUE I.
KAYAK I.
ICY BAY
YAKUTAT
MIDDLETON I.
60°
59°
0 25 KM 200
48°
45°

Figure 2K

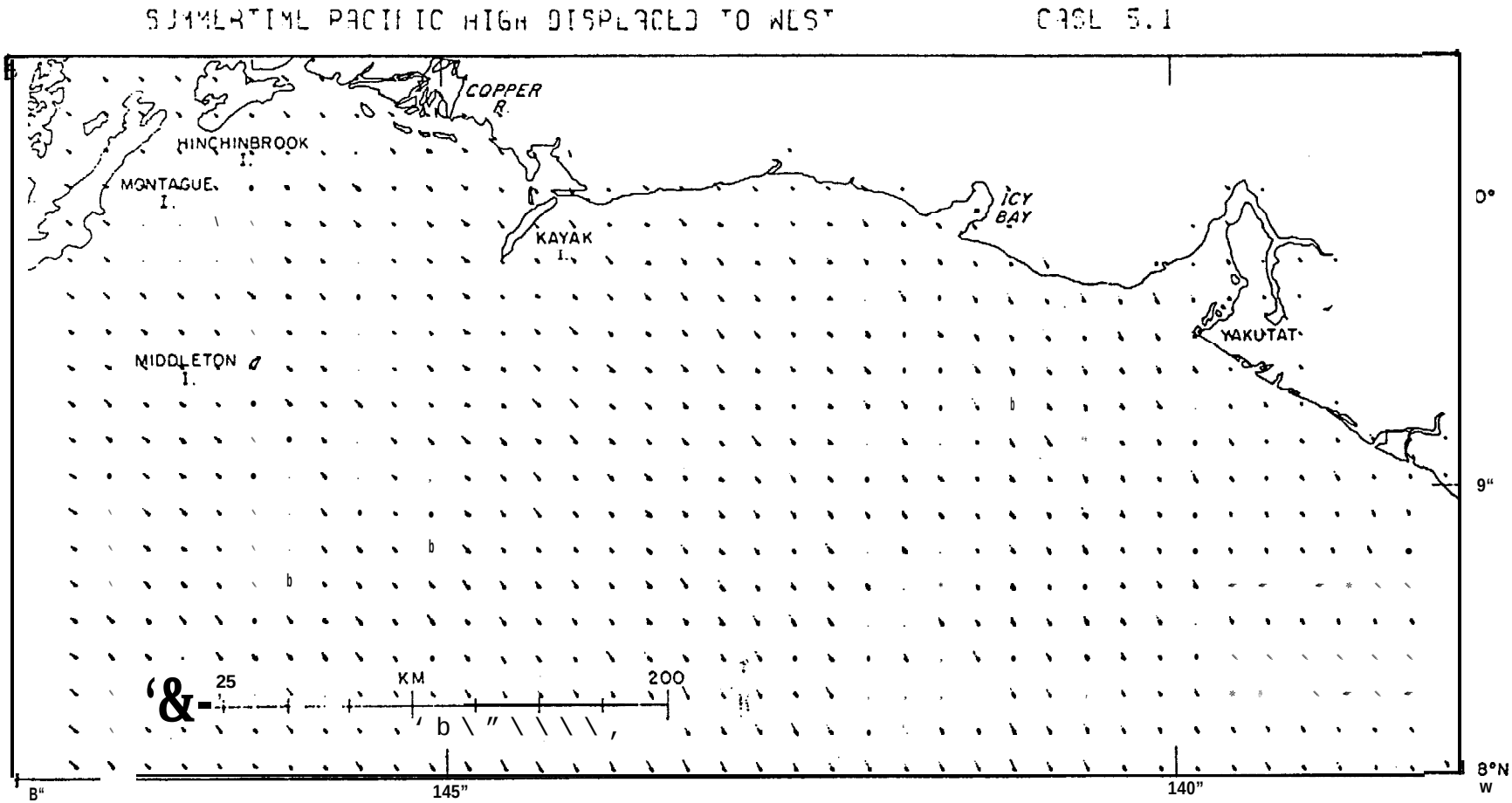
SUMMERTIME PACIFIC HIGH DISPLACED TO WEST
CASE 5.1
COPPER R.
HINCHINBROOK I.
MONTAGUE I.
KAYAK I.
ICY BAY
YAKUTAT
MIDDLETON I.
25
KM
200
145"
140"
8°N
W
9"
0°

Figure 2L

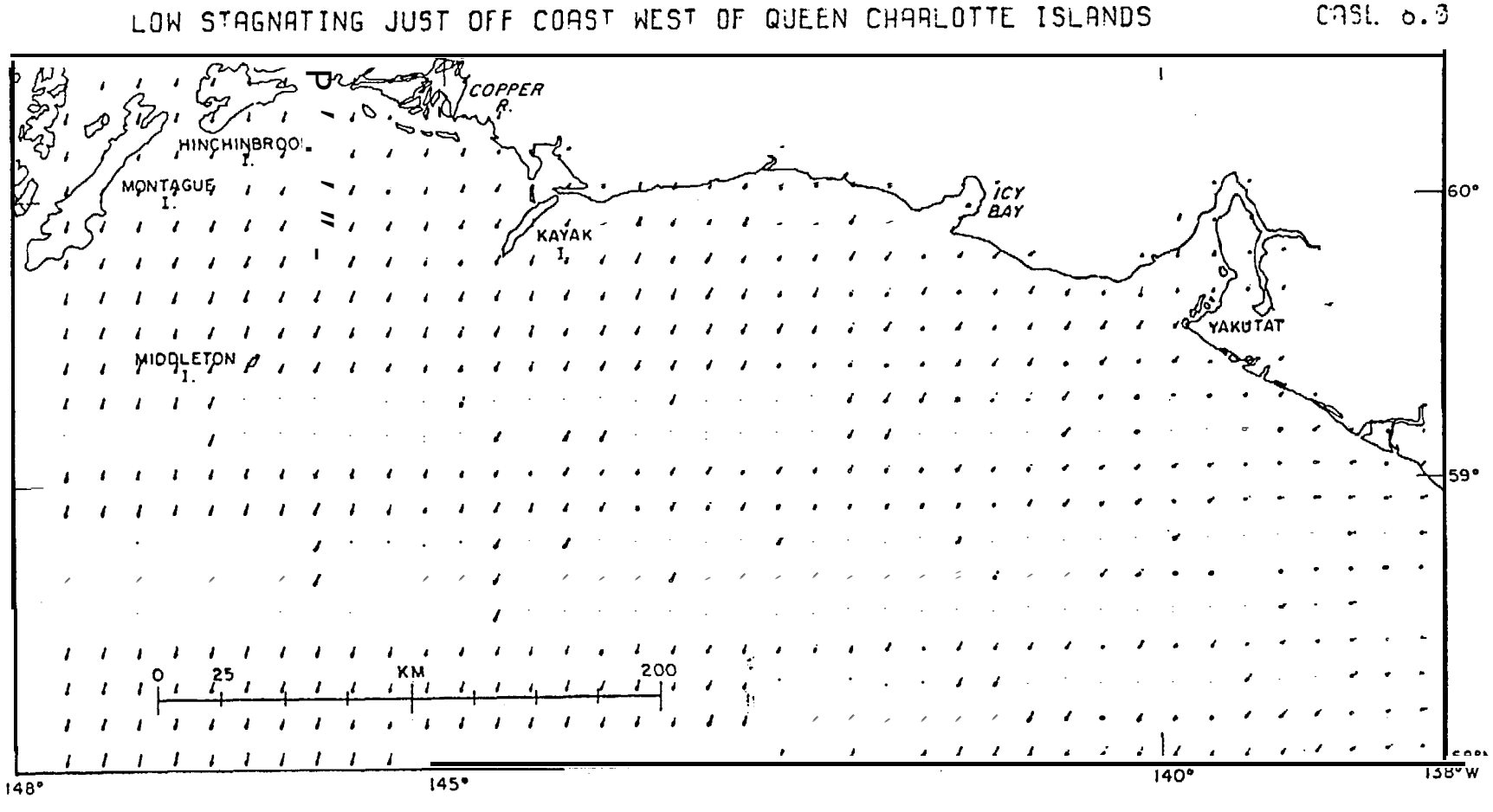
LOW STAGNATING JUST OFF COAST WEST OF QUEEN CHARLOTTE ISLANDS
CASE 6.3
COPPER R.
HINCHINBROOK I.
MONTAGUE I.
KAYAK I.
ICY BAY
YAKUTAT
MIDDLETON I.
0 25 KM 200
60°
59°
148°
145°
140°
138°W

Figure 2M

Barry, R.G. and A.H. Perry (1973): Synoptic Climatology, Methods and Application. London: Methuen & Co. 553 pp.

Brewer, W.A.Jr., H.F. Diaz, A.S. Prechtel, H.W. Searby and J.L. Wise. (1977): Climatic Atlas of the Outer Continental Shelf waters and coastal regions of Alaska: Vol. 1, Gulf of Alaska, National Climate Center, Environmental Data Service, NOAA, Ashville, N.C. 439 pp.

Cardone, V.J. (1969): Specification of the wind distribution in the marine boundary layer for wave forecasting. Report GSL TR69-1 New York University School of Engineering Science, 131 pp.

Jenne, R.L. (1975): Data sets for meteorological research. NCAR Tech Note NCAR-TN/1A, 194 pp.

Kendall, M.G. and A. Stewart (1975): The Advanced Theory of Statistics, vol. 3. New York, N.Y., Hafner Press, 585 pp.

Lund, I.A. (1963): Map pattern classification by statistical methods. J. Appl. Meteor. 2, p 56-65.

Overland, J.E. and Thomas R. Hiester (1978): A Synoptic Climatology for Surface Winds Along the Southern Coast of Alaska. NOAA/ERL/PMEL, Tech. Report (draft).

Overland, J.E., M.H. Hitchman and Y.-J. Han (1978): A Regional Surface Wind Model for Mountainous Coastal Areas PMEL/ERL/NOAA Technical Report (in press).

Putnins, P. (1966): The sequence of baric pressure patterns over Alaska. Studies on the meteorology of Alaska 1st Interim Report, Washington D. C., Environmental Data Service, ESSA, 57 pp.

Reynolds, R.M., T.R. Hiester and S.A. Macklin (1978): Coastal Meteorology of the Gulf of Alaska Icy Bay to Yakutat Bay. PMEL/ERL/NOAA Tech. Report (In press).

Sorkina, A.I. (1963): Tipy atmosfernoi tsirkuliatsii, Israel Program for Scientific Translations, Jerusalem, 247 pp.

3.0 Analysis of Northeast Gulf of Alaska Current Patterns

3.1 Introduction

The Northeast Gulf of Alaska (NEGOA) area is situated in the northern bight of the Gulf of Alaska, with the present area of interest centered on the continental shelf between Yakutat and Montague Island (figure 3-1). The shelf topography is quite complex with many small and intermediate scale features (5-50 km). On a large scale the shelf is relatively narrow east of Kayak Island and comparatively broad west of that point. The shelf break as indicated by the 100 fa. contour (figure 3-1) is irregular and gives the shelf domain a very complex shape. The coastal morphology is dominated by mountains, and the weather patterns and coastal winds show evidence of significant orographic influence. For many years this region saw very little in the way of systematic oceanographic studies, but with the advent of potential offshore gas and oil development a series of studies was initiated. These have included the repeated mapping of state variables with CTD or STD cruises, moored current meter deployments, Lagrangian drifter studies, installation of bottom mounted pressure gauges, coastal meteorological studies, and the placement of large weather buoys within the study area.

Early studies have shown the relationship of the NEGOA area to the larger scale current of the Gulf of Alaska (Favorite, et al. 1976). More detailed studies of the shelf circulation proper were presented by Galt (1976) and regional hydrology has been discussed by Royer (1975), Galt and Royer (1975), and Royer (1978). The relationship between the bottom pressure distribution across the shelf off Icy Bay and the local currents has been investigated by Hayes and Schumacher (1976) and Hayes (1979).

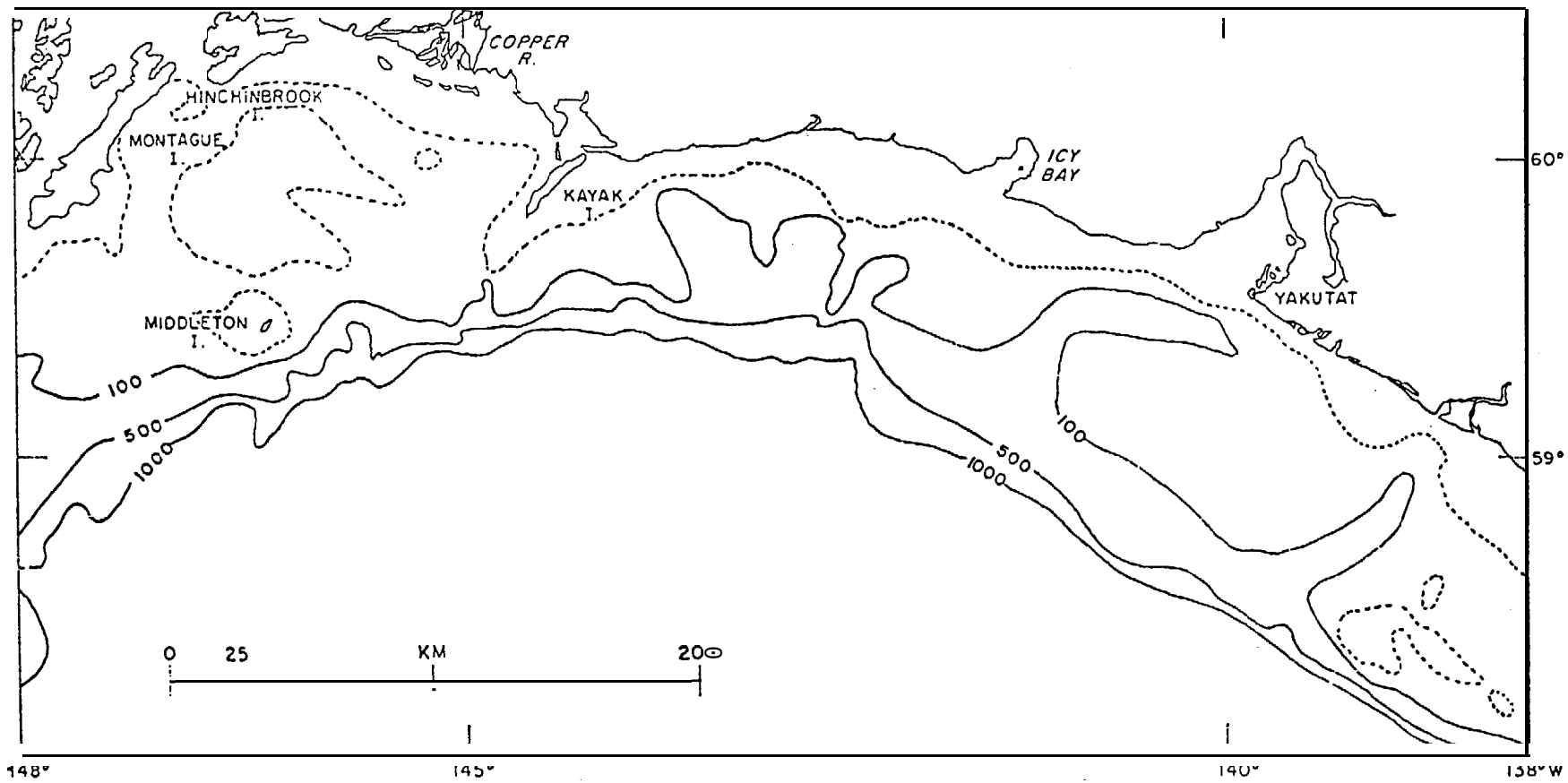

Figure 3-1. Northeast Gulf of Alaska study area. Depth contours shown in fathoms. Dotted contour represents 50 fathom curve.

The Lagrangian current measurements from drogue studies have been described by Royer, et al. (1978). In addition to these recent oceanographic studies, the regional meteorology has also come under scrutiny. The coastal region has been investigated by Reynolds, et al. (1978) with particular attention being directed towards the description of the nearshore wind regime. Starting with earlier work by Putnins (1966), Overland and Hiester (1977) extended the climatology for the Gulf of Alaska with weather typing studies concentrating on the definition of a set of inclusive patterns for the synoptic scale pressure field and their relationship to the regional wind fields.

All in all a great deal of new information has become available about the NEGOA region within the last few years, and it is now possible to qualitatively describe many of the features of the general flow. In addition a number of dynamic processes have been identified and in some cases can be quantitatively documented. The off shelf region is under the continuing influence of the general Gulf of Alaska circulation, and its baroclinic signature is clearly evident over the continental slope and shelf break. Coastal run-off and precipitation also induce baroclinic fields that are clearly seen to influence the near shore region over the shelf. Over the shelf proper the regional winds set up a barotropic response which has a much shorter adjustment period than is evident in the internal density field and in the resulting density driven currents. In all cases the irregular bathymetry appears to have a significant effect by channeling the flow.

Despite our greatly improved documentation of the Northeast Gulf of Alaska region and the contributions that many of the authors have made, there are still some significant gaps in the overall understandings

of regional dynamic processes and in the description of the currents. The object of this study is to address one particular facet of this problem: the spatial distribution of the surface currents. Most of the oceanographic information that has been gathered for NEGOA has been Eulerian in nature, giving dense temporal coverage at a single location. The regional studies have, for the most part, concentrated on the definition of dynamic processes and not on the delineation of flow patterns. Two exceptions were the Lagrangian drifter experiments (Royer, et al. 1978) and the numerical trajectory experiments (Galt, 1976), but these were limited in coverage.

In this report a more general approach to the study of Northeast Gulf of Alaska current patterns is attempted using a numerical circulation model. The model is a finite element diagnostic formulation developed by Galt (1975). The details of the numerical techniques and program for the model solution are described by Watabayashi and Galt (1978). The dynamic partitioning of the model and recommended strategies for its use, along with an example, are presented by Galt and Watabayashi (1978). The model dynamics are a simple linear combination of geostrophic and Ekman currents formulated for an arbitrarily shaped continental shelf region. The geostrophic flow is made up of both barotropic and baroclinic (internal and external) modes, and the Ekman dynamics leads to the inclusion of both upper and lower frictional boundary layers.

The dynamics included in this formulation has been the subject of many studies in the past. The problem for homogeneous water and enclosed basins was first addressed by Welander (1956). More recent studies for simplified geometries have been carried out by Pedlosky (1974) and Csanady (1978). Pedlosky's work introduces the possibility of coastal boundary layers subject to a more complex dynamics than is represented by the

simple formulation considered in this study. For regions that are dominated by these side wall boundary layers one may expect the present results to be deficient. Scale analysis suggests that the influence of these layers is confined to within a few tens of kilometers of the coast, and by implication there is a corresponding band in which the solutions may be considered incomplete. A finite difference formulation of a diagnostic model for shelf circulation has been developed by Hsueh and Peng (1978). Their results are applicable to relatively simple shelf configurations for which the dynamic influence of depth variations is limited to one dimension, normal to the coast line. In addition, however, these authors do present a section discussing the time dependent form of the equations, where the terms responsible for shelf waves are scaled.

In this work it will be assumed that the steady state form of the diagnostic model equations is valid. This implies a number of things. To start with the density field, which is specified by a set of hydrographic cruises, is assumed to give synoptic distributions which can be considered fixed for time periods on the order of a month. This assumption is amenable to test, both in the NEGOA data and through related diagnostic model studies carried out by Harm (1978). In general it seems that the baroclinic shears are well represented by the fields for periods of a week or so and can be considered as representative, but not correct in detail, for longer periods. The barotropic wind set-up response of the region is also assumed to be in steady state balance, but not necessarily the same for all time. This brings in the second set of assumptions about the modeled current patterns. The adjustment of the barotropic response to the regional wind patterns (sea surface set-up) is assumed to be continuous. This means two things. First of all the flow is quasi-geostrophic

at all times (except within the Ekman layers). And second, the adjustment process is smooth enough so that energetic shelf waves are not generated. This second assumption is somewhat more restrictive than the first. An examination of smoothed current meter records (Galt, 1976) from the NEGOA region show directional oscillations around the mean flow that may well be related to shelf wave phenomena. These oscillations are not represented by the diagnostic model formulation, but they do not appear to dominate the flow. And to the extent that they are linear, the oscillations will not even interact with the dominant and most energetic patterns that the model does represent.

The following sections will present the diagnostic model analysis of Northeast Gulf of Alaska current patterns subject to the caveats that (1) only time scales in excess of what are needed for quasi-geostrophic assumptions are considered, (2) shelf waves are not represented, (3) baroclinic shears may not be correct in detail beyond a few weeks of the time they were observed, and (4) within the immediate vicinity of the shoreline additional side wall boundary layers may contribute significant components to the flow.

3.2 Model Decomposition

In this section the linear decomposition of the diagnostic model equations will be briefly reviewed, and the relationship of these component flows to the input data and assumptions will be outlined. A more detailed description of the linear aspects of model formulation and the rationale for this partitioning are presented by Galt and Watabayashi (1978).

The basic governing equation for the diagnostic model describes the dependent variable, the surface elevation as follows:

$$N_2\nabla^2\xi - J(\xi,d) + N_1N_2\nabla^2\alpha - N_1J(\alpha,d) - k\cdot\nabla\times\tau = 0 \qquad (3\text{-}1)$$

where

ξ = surface elevation

d = depth

α = the integral of the density from the bottom to the surface

$k \cdot \nabla x \tau$ = curl of the surface wind stress

N_1 = stratification parameter

N_2 = bottom friction parameter

All of the terms in this vorticity equation are scaled and nondimensional, The first term represents the vorticity stretching caused by the barotropic mode, (depth independent) flow created by pressure forces related to variations in the sea surface elevation driving a bottom Ekman layer. The second term represents the interaction of the barotropic flow with the bottom and describes the vorticity stretching caused by the flow crossing isobaths. The third term represents vorticity stretching of the baroclinic mode evaluated at the bottom (flow created by the pressure forces related to the internal mass distribution) driving a bottom Ekman layer. The forth term represents the vorticity induced by the joint baroclinic and bathymetric interaction and is seen to relate to the stretching caused by the baroclinic component of the flow crossing isobaths. The last term is the curl of the wind stress, or the vorticity added by the wind.

To solve this equation it may be noted that the system is linear, so that a decomposition is possible. Doing this, the following two problems can be considered:

$$N_2 \nabla^2 \xi_1 - J(\xi,d) - k \cdot \nabla x \tau = 0 \qquad (3\text{-}2)$$

and

$$N_2 \nabla^2 \xi_2 - J(\xi_2,d) + (N_1 N_2 \nabla^2 \alpha - N_1 J(\alpha,d)) = 0 \qquad (3\text{-}3)$$

The total solution is just the sum of these two component solutions, i.e.

$$\xi = \xi_1 + \xi_2 \qquad (3\text{-}4)$$

The problem defined by the first of these equations will be referred to as the wind set-up component. The problem defined by the second equation will be referred to as the density driven component.

Turning first to the wind set-up component of the flow, it is necessary to define appropriate boundary conditions and to apply the finite element solution technique described by Watabayashi and Galt (1978). To develop these boundary conditions for the NEGOA area a number of assumptions is made.

As a point of departure the curl of the wind stress will be considered negligible for the region. This is done for two reasons, first, that the actual data available on regional wind stress curl on this scale is practically nil (Bakun, 1973), and second, that the direct local set-up of the cross shelf sea surface slope by along-shore winds is the dominant wind forcing. To parametrize the relationship between the wind and the cross shelf component of the sea surface slope, a bathystrophic balance will be hypothesized. This assumes that the along-shore component of the wind stress is locally balanced by the along-shore component of the water stress, and that the normal component of the sea surface gradient is in geostrophic balance with the along-shore current. For the linear stress law hypothesized by the Ekman dynamics this is represented by

$$\frac{\partial \xi}{\partial n} = c(w)^2 \cos(\theta_s) , \qquad (3\text{-}5)$$

i.e., the sea surface slope normal to the coast is proportional to the square of the wind speed times the cosine of the angle between the wind and the coastline.

With this suggested balance it now remains to specify how this relationship is to be applied as boundary conditions. We know that the sea surface slope imposed at the boundary does not extend seaward indefinitely, but is confined to the shelf area. As a first approximation it will be assumed that the forced component of the slope is uniform for a band extending from the coast to the vicinity of the shelf break. Along the coast line a zero transport normal to the coast is imposed and along any open cross shelf boundaries the differential equation is applied right up to the boundary without additional constraints (the so called finite element method natural boundary conditions). For a more detailed discussion refer to Galt and Watabayashi (1978). Thus the wind set-up forcing is envisioned as a simple linear profile where the sea surface is undisturbed in deep water, but slopes up or down uniformly across the shelf (with the slope proportional to the along-shore wind speed squared), as if hinged at the shelf break. Such a response has been suggested for other areas in the past (Beardsley and Butman, 1974), In specific studies of the NEGOA area, Hayes (1979) suggested that such a linear cross shelf hinge profile accounts for a major segment of the variance observed in the bottom pressure measurements.

The question of where to apply this hinge profile to drive the wind set-up response of the model requires careful thought. Obviously the wind acts as a continuum along the coast line, and at any coastal boundary point we could impose a uniform slope through a line of stations leading away from the shore. Solving the model with this single imposed hinge profile will give the regional response to this type forcing. To combine a number of these is straightforward, since it is possible to consider any single hinge profile as the Green's function response to an imposed

bathystrophic profile at that point.

For example, suppose that

$R(x, Y, S_o)$

is the model response to a unit amplitude hinge imposed on the coastline at point So, and that

$W(s)$

is the distribution of alongshore wind specified along the coastline, with S being simply distance along the coast. Then the total wind set-up response will be the superposition

$$\xi_1(x, y) = \int_{\text{coast}} C\, R(x, y, S)\, W(s)^2 \cos(\theta_s) ds \qquad (3\text{-}6)$$

For the present NEGOA study the numerical approximation to this integral formulation will be made with six simple hinge modes, each of which is seen to influence specific segments of the shelf domain.

It should be pointed out that the Green's function formulation outlined here does not result in a composite pattern that has a uniform cross shelf profile everywhere. Instead each cross shelf profile is influenced by its neighbors, taking into account alongshore variations in the wind, bathymetry, and model dynamics.

A final point to consider with the wind set-up response is that alternate strategies are possible for determining the relative hinge weights in the composite patterns. For example, if sea surface elevations were available at n locations along the coast, the Green's function integral could easily be inverted to solve for the coefficients associated with n independent hinge modes, whose composite would satisfy the observed coastal distribution, consistent with the model dynamics.

It is now possible to consider the second partition of the diagnostic mode, the density driven response. This is represented by equation (3-3). In this equation it can be seen that the density distribution acts as forcing through two terms: the baroclinic bottom Ekman layer, and the joint baroclinic - bathymetric interaction. Both of these can be seen to induce vorticity to the barotropic flow either through cross isobath flow or through stretching of the water column. This ξ_2 component of the sea surface displacement (barotropic mode) can be thought of as required by the fact that any given density driven flow will in general result in some stretching of the water column through these bottom interactions. In the presence of this stretching some barotropic adjustment is required to satisfy model dynamic constraints, even in the absence of wind set-up or forcing.

An examination of equation (3-3) shows that

$$\xi_2 + N_1\alpha^* = \text{constant} \qquad (3\text{-}8)$$

is a solution for the interior of the domain, where a* is the pressure deviation defined for any region as

$$a(X, y, Z) = a'(Z) + \alpha^*(x, y)$$

The solution given by (3-8) has a number of characteristics of interest. Galt and Watabayashi (1978) have shown that this solution corresponds to a minimum potential energy of the sea surface distribution ξ_2 that is consistent with the model dynamics over an extended open shelf domain. This minimum barotropic mode forced by the density field has the physical significance that for an unforced region, with a fixed density distribution, one would expect the sea surface to relax, or set-down, as much as possible,

consistent with the dynamic vorticity constraints. It can also be seen that (3-8) yields a solution which gives a terrain following level of no motion because the baroclinic and barotropic flow just cancel out at the bottom over the entire domain. This then is a natural extension of the level of no motion concepts that are routinely applied in deep water off of the shelf. Thus the minimum potential energy barotropic mode can also be seen to represent the minimum bathymetric interaction mode. It should also be noted that (3-8) is the only possible invisid solution to equation (3-3), and that as such it is the only possible unforced, steady state solution that could be expected.

For the NEGOA region we expect a number of patterns which are linear superpositions of the following responses: (1) wind set-up responses, which are determined by the wind pattern *only* (and thus are independent of the density distribution and are valid for all seasons), and (2) density driven responses (one response for each density distribution), which yield a minimum barotropic mode.

3.3 Wind Set-up Response Patterns

The wind set-up response for the NEGOA area will be given by the solution to equation (3-2). This will be composed of a number of hinge modes. Each of these will assume a bathystrophic balance over a single across shelf profile. The coastal boundary will be subject to a no net transport condition, and off shore in deep water the surface elevation remains unperturbed. A high resolution grid with approximately two hundred vertices covers the shelf region between Yakutat and Seward (figure 3-2) giving increased resolution of the complex bathymetric features. Within the area of particular interest between Yakutat and Montague Island six individual hinge modes are investigated (figure 3-2). These have been

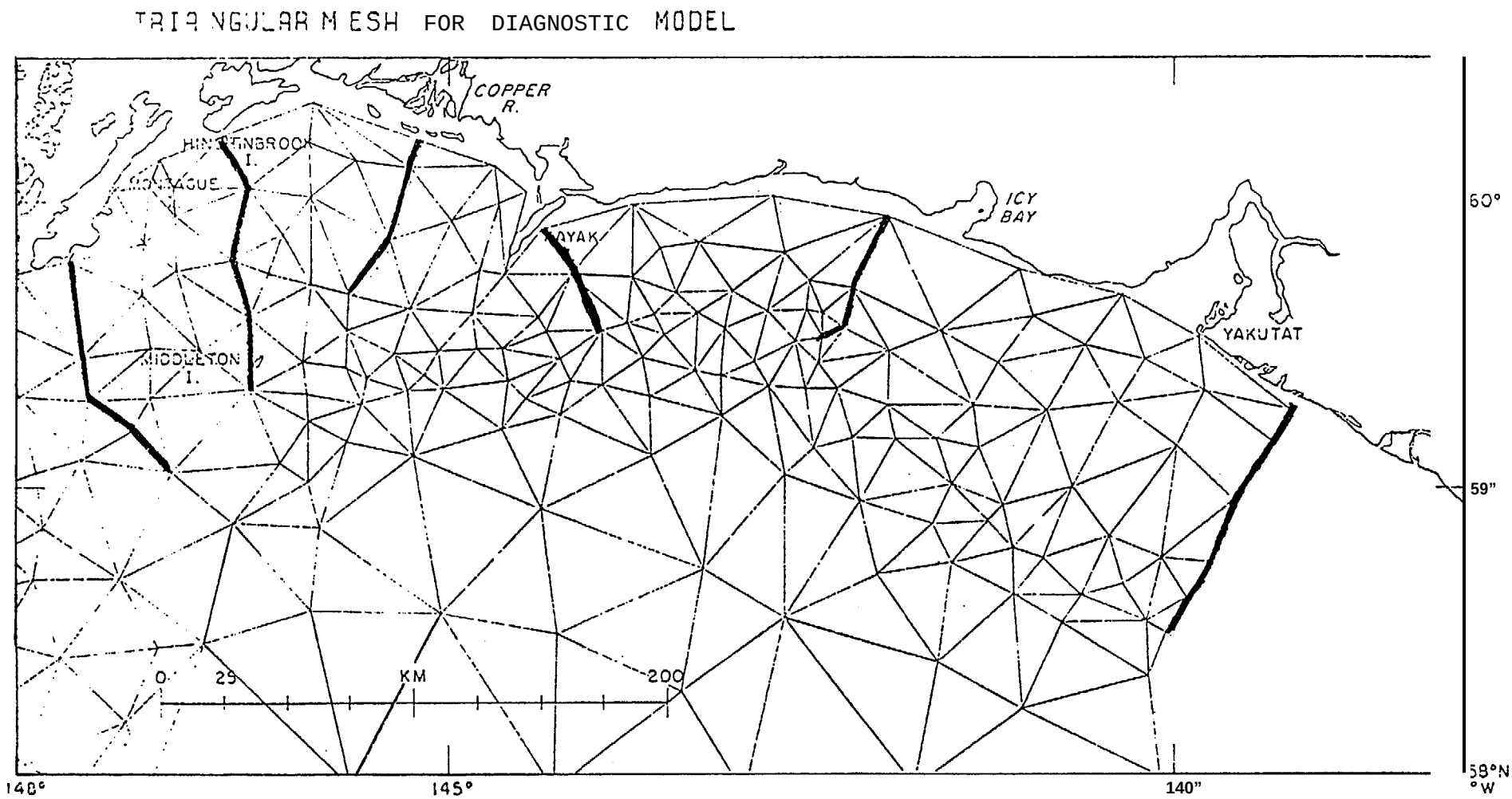

Figure 3-2. Triangle mesh used for Northeast Gulf of Alaska wind set-up study. Heavy lines represent positions of bathystrophically balanced hinge modes.

chosen in such a way as to obtain a fundamental set that cover the domain. They are not unique and alternate choices are certainly possible. Nonetheless, these suitably cover the region of interest and do not show excessive overlap, so each can be considered to represent the local influence of coastal winds. Actual scale analysis and the rationale for choosing various hinge configurations are discussed in Galt and Watabayashi (1978). The six hinge response modes for the area of interest are shown in figures (3-3) through (3-8). These six patterns give the independent degrees of freedom that comprise the wind set-up for this section of shelf. The magnitudes associated with these patterns are arbitrary; only the relative spatial distributions associated with the set-up hinges are shown. The vector arrows in these figures have been transformed from the finite element triangular domain onto a regular cartesian grid for ease in interpretation and in subsequent computer library storage.

For any particular distribution of surface winds the six basic hinge modes described above are combined to give the composite wind set-up corresponding to that wind pattern distribution. The basic wind patterns that will be considered are those that have been obtained from the NEGOA meteorological analysis carried out by Overland and Hiester (1978). Their research, based on climate typing techniques and local analysis, has identified six dominant weather types, with a total of thirteen patterns including sub-types.

For each of these patterns the relative weight factors for the various hinges are obtained from the square of the wind (scaled to the value at Middleton Island, since the wind patterns are also arbitrary) at each hinge point times the cosine of the angle between the local wind vector and the coastline. In evaluating these relative weighting factors, the

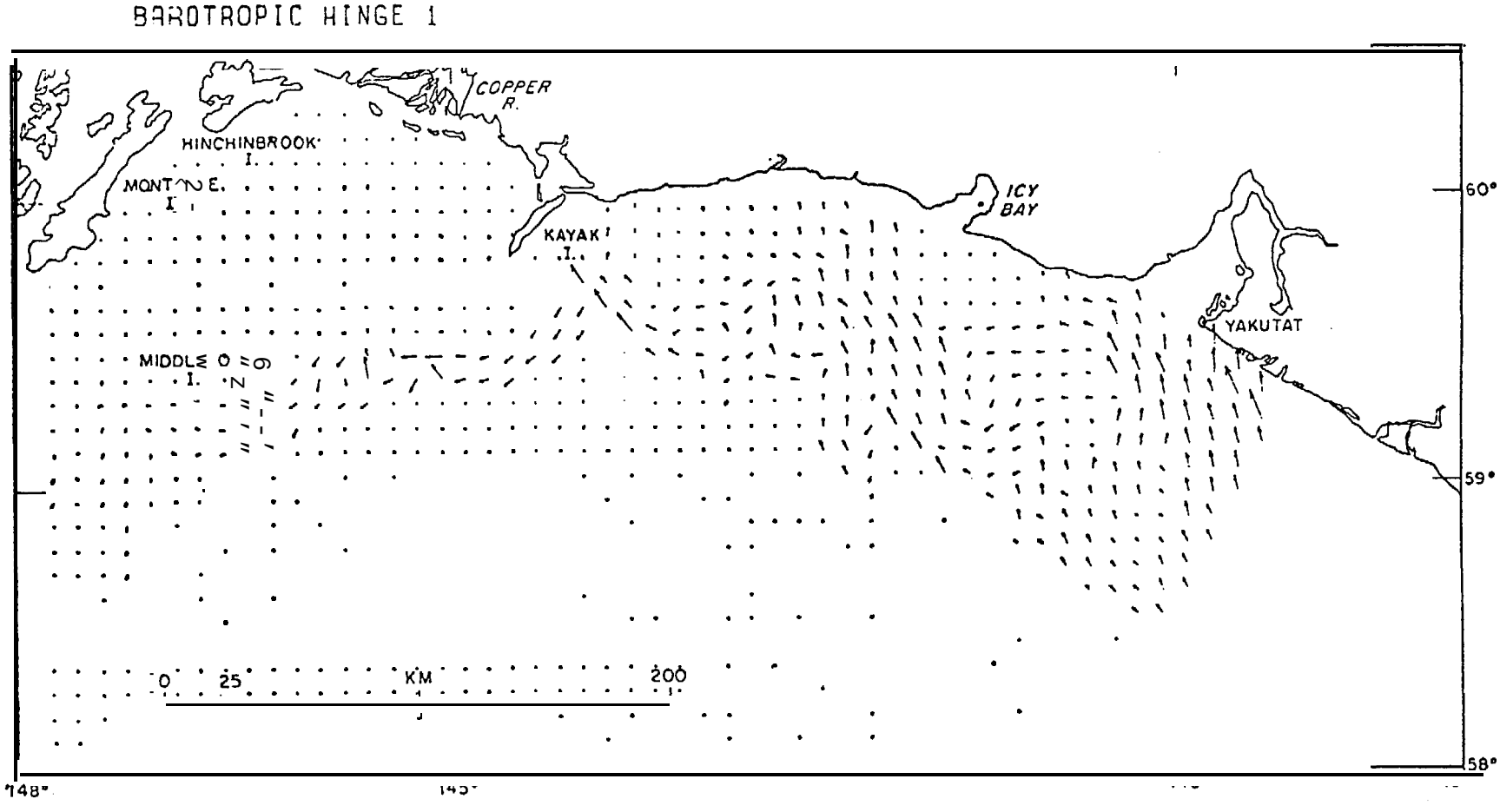

Figure 3-3. Bathystrophic wind set-up, or hinge mode one (Yakutat).

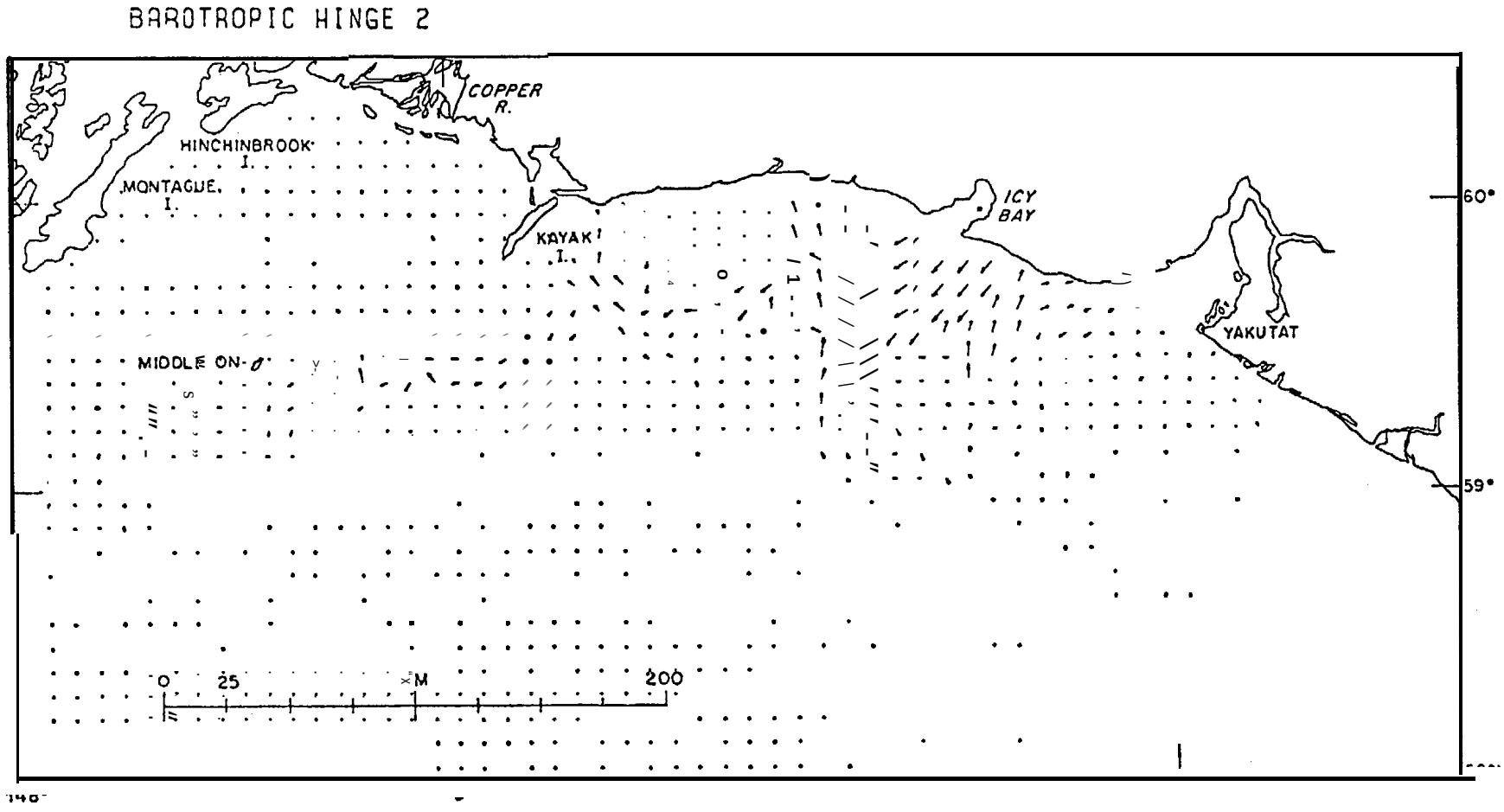

Figure 3-4. Bathystrophic wind set-up, or hinge mode two (Icy Bay).

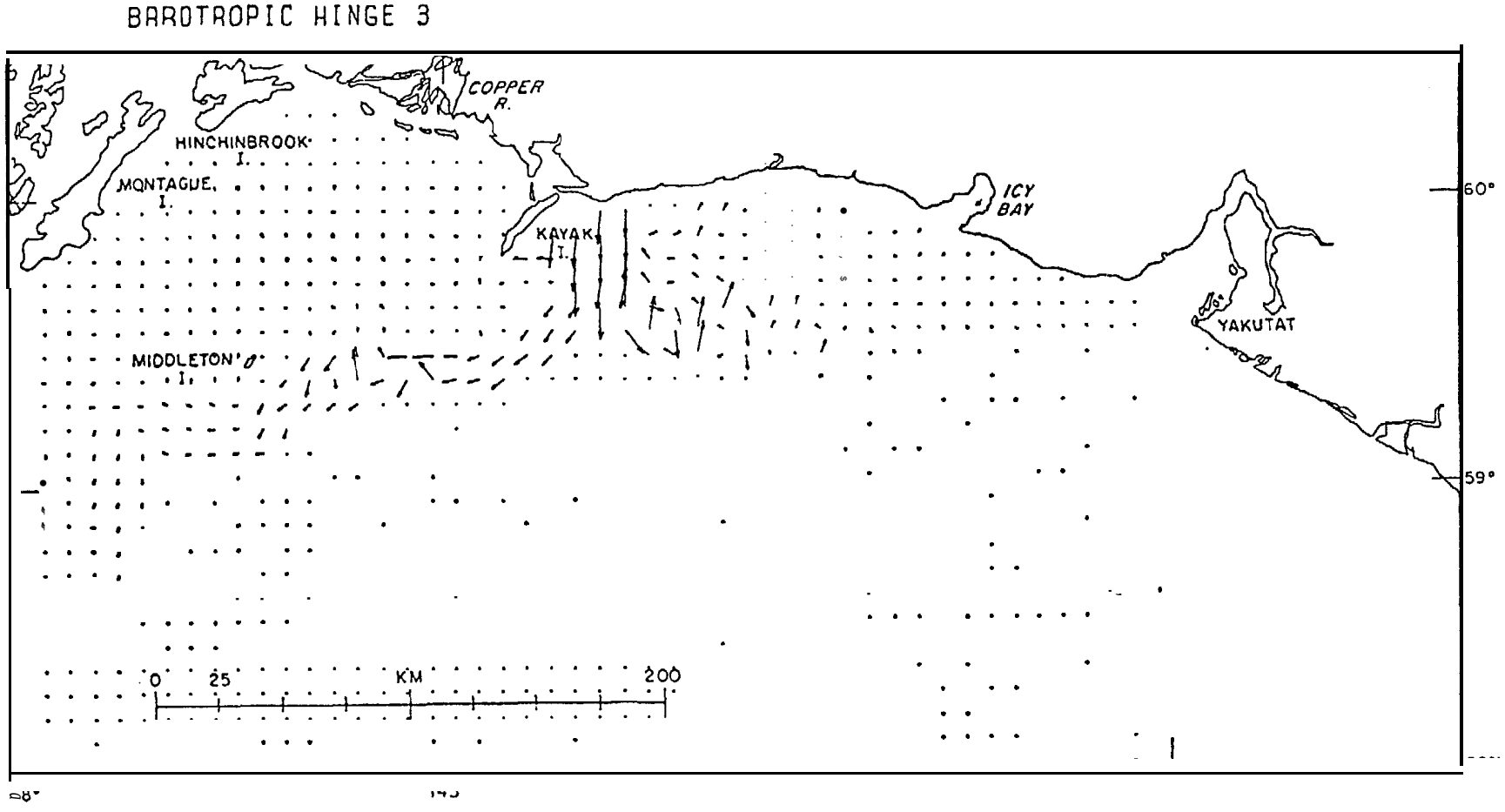

Figure 3-5. Bathystrophic wind set-up, or hinge mode three (Kayak Island).

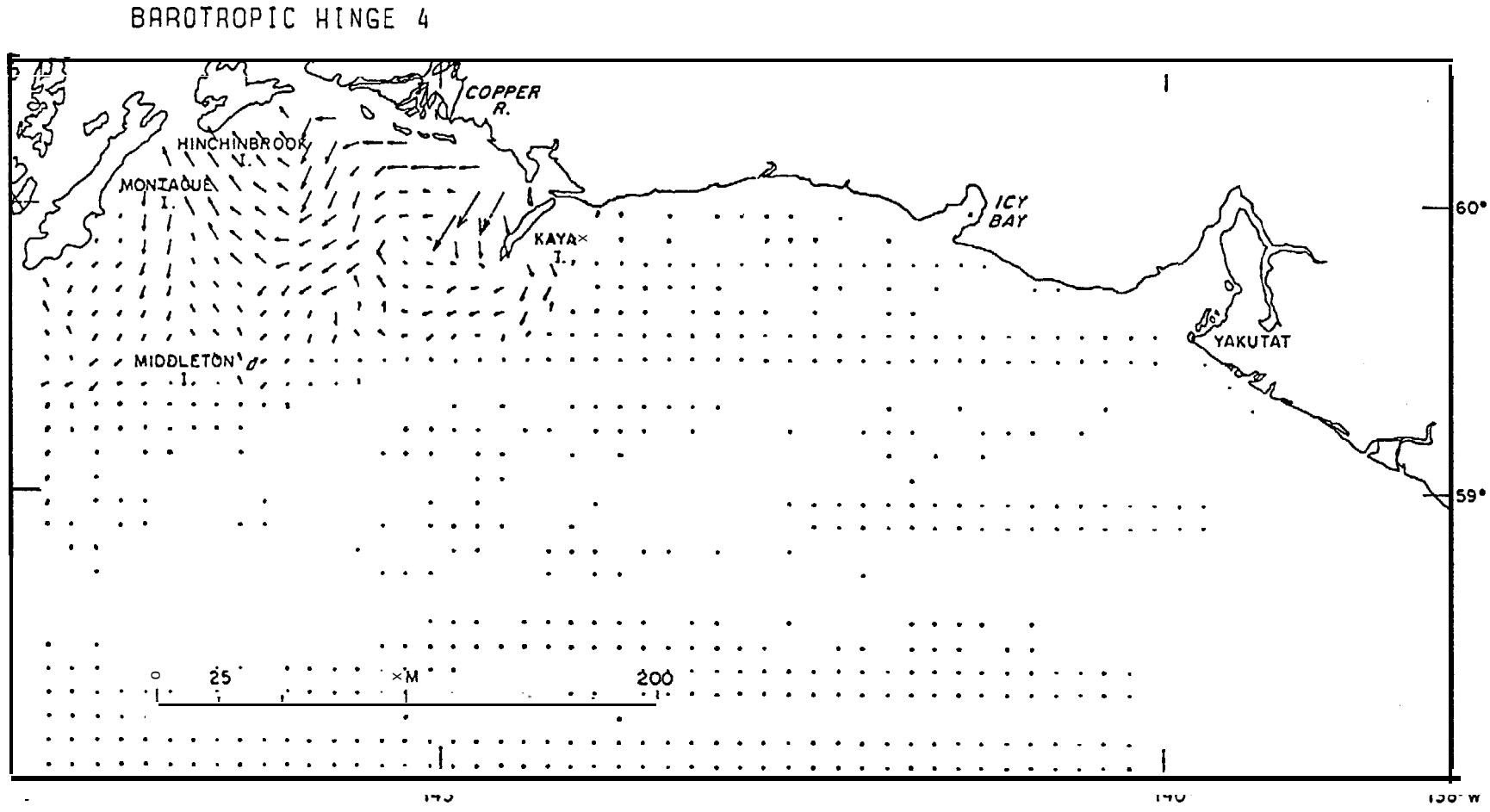

Figure 3-6. Bathystrophic wind set-up, or hinge mode four (Copper River).

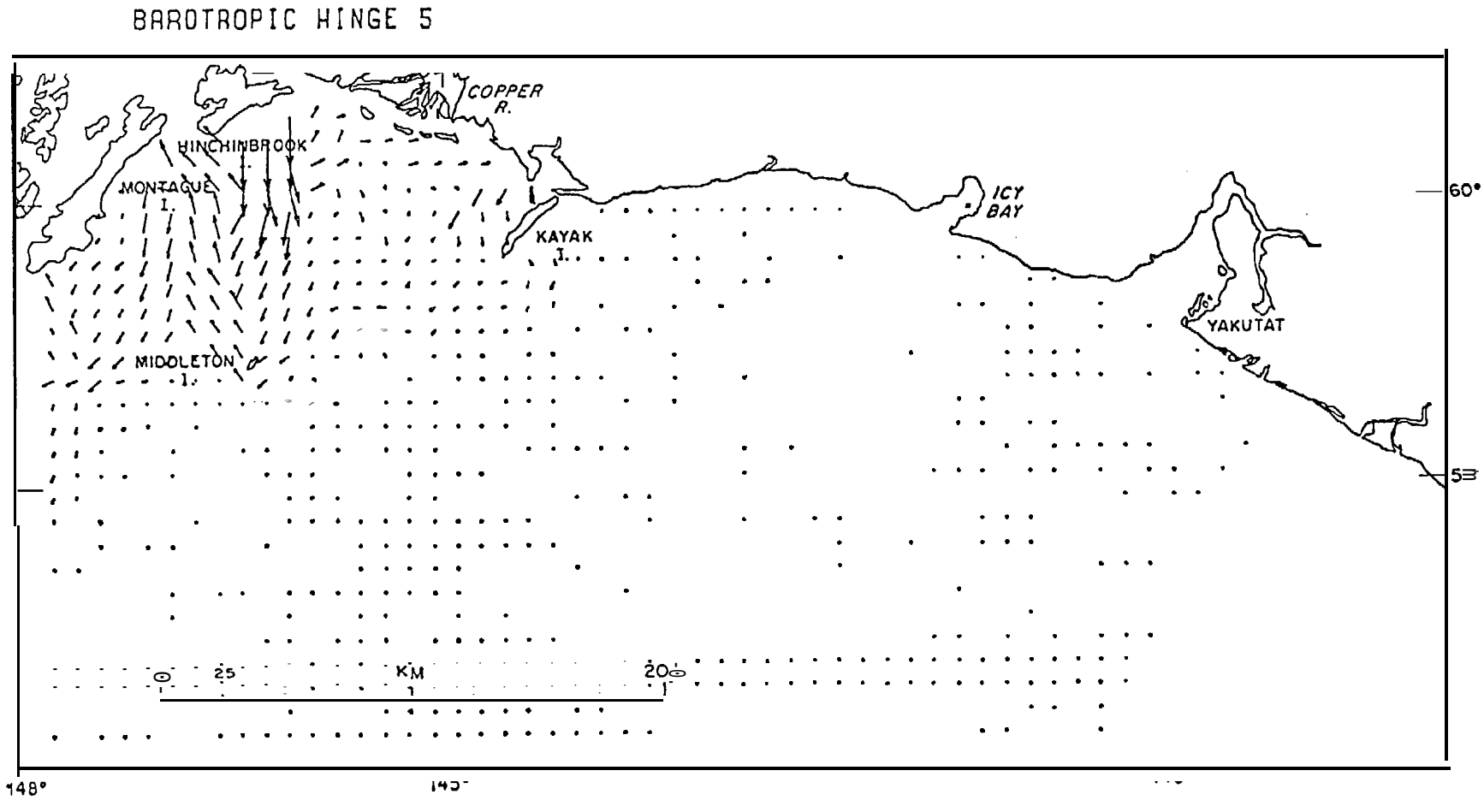

igure 3-7. Bathystrophic wind set-up, or h nge mode five (Hinch nbrook Island

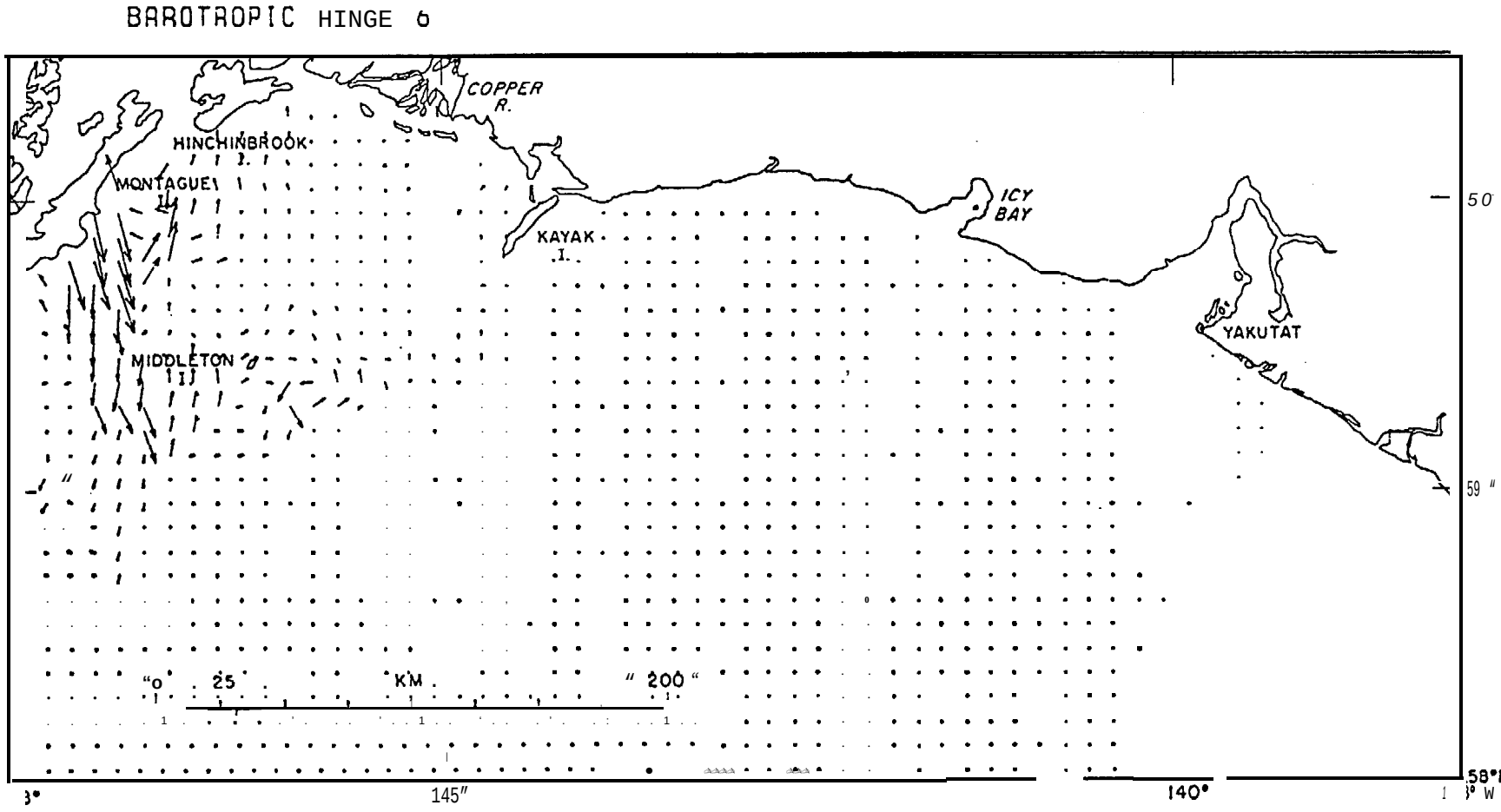

Figure 3-8. Bathystrophi c wind set-up, or hinge mode six (Montague Island).

vector winds were averaged over the inner shelf region of individual hinges, in order to get winds which were more representative than the actual coastal value. Table 3-1 gives the relative weighting factors for the thirteen patterns described by Overland and Hiester (1978).

The coefficients from Table 3-1 are used to form linear combinations of the basic patterns for each of the wind patterns. The resulting current patterns are shown in figures (3-9) through (3-21). Once again the magnitudes of these current patterns are arbitrary, with the vector arrows only giving relative pattern information. Assuming that the bathystrophic assumptions are correct, the magnitudes for the currents associated with these patterns should be scaled as proportional to the square of the wind speed at Middleton Island.

The first four current patterns, figures (3-9) through (3-12), correspond to weather patterns dominated by low pressure systems situated in the Gulf of Alaska. The first of these (wind pattern 1.0) can be thought of as the prototype. The currents are seen to move generally east to west across the shelf. The effects of bathymetric influence on the currents are evident. The deep segment of the shelf off of Yakutat shows reduced current magnitudes with the general tendency for the flow to follow isobaths. The complex topography on the shelf to the west of Icy Bay also is clearly reflected in the current directions. The general tendency for enhanced flow along the shelf break is also clear. The large submarine canyon that cuts across the shelf break east of Middleton Island causes a meander in the shelf break flow with the potential for the formation of an eddy associated with this topographic feature. Other regions of enhanced flow are seen in the lee of Kayak Island and are associated with the sea valley leading into Prince William Sound between Hinchinbrook and Montague Island. The second wind pattern (1.1)

TABLE 3-1

RELATIVE AMPLITUDES FOR THE FUNDAMENTAL HINGE MODES CORRESPONDING TO THE WIND PATTERNS DESCRIBED BY OVERLAND AND HIESTER (1978)

Wind Pattern	Hinge Coefficients					
	1	2	3	4	5	6
1.0	.77	1.73	.76	.74	.88	.93
1.1	.78	1.27	.42	1.00	.59	.94
1.2	.63	.24	.55	.13	.29	.55
1.3	.43	.69	.41	.67	,73	.60
2.0	.55	.94	.91	.81	.64	.71
2.1	.65	.39	.64	-.20	.39	.42
3.0	.74	.66	1.15	.77	.79	.80
3.1	.50	2.05	1.59	.39	.79	.79
4.0	-.05	-.51	-.55	-.27	-.75	-.80
4.1	-.67	-1.07	.41	.89	.22	.19
5.0	-.97	-.80	-.77	-.50	-.94	-.85
5.1	-1.28	-.98	-.49	-.70	-.92	-.65
6.0	.24	.31	.60	.28	.64	.77

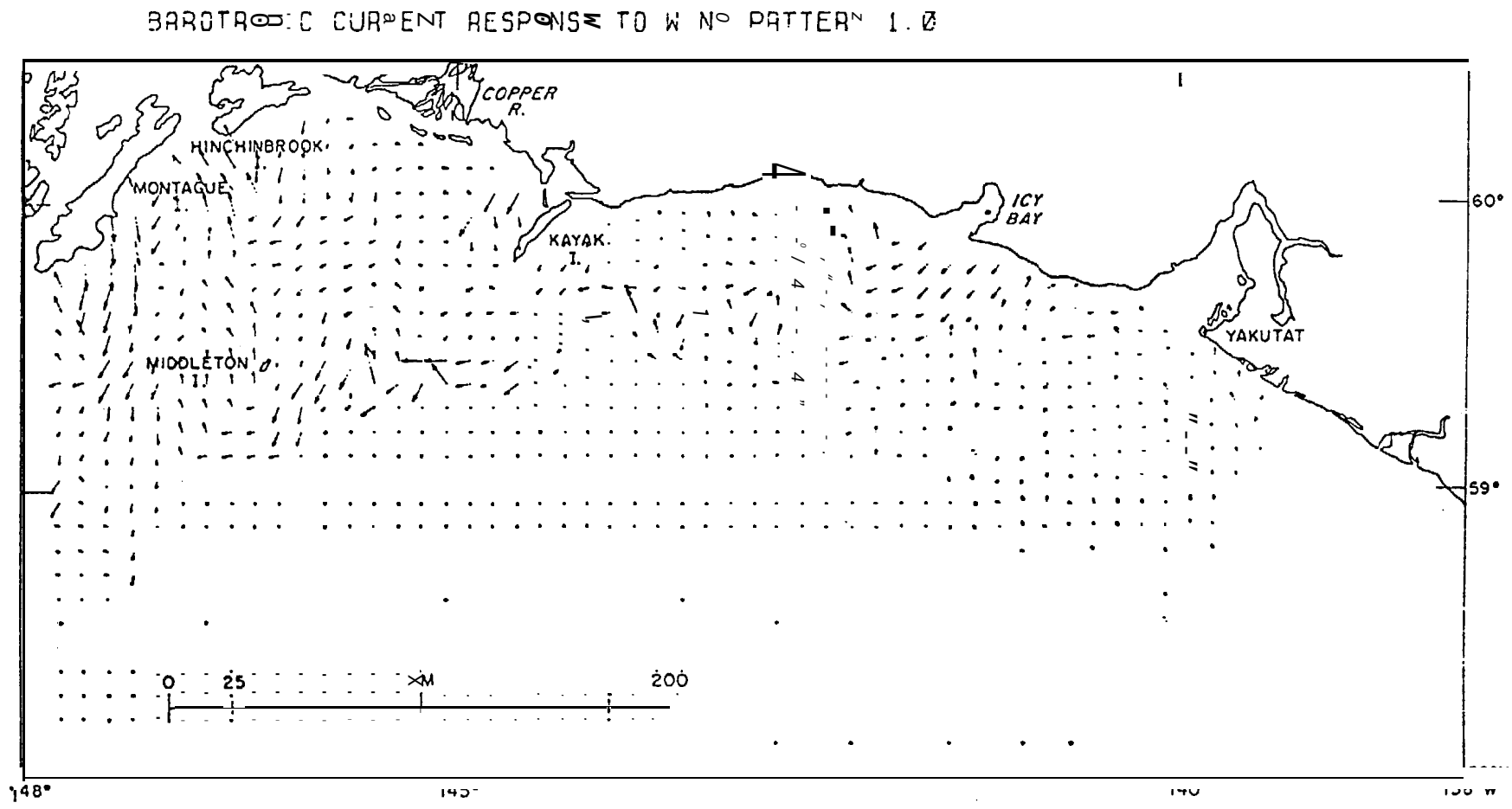

Figure 3-9. Composite wind set-up response for Northeast Gulf of Alaska weather type 1.0.

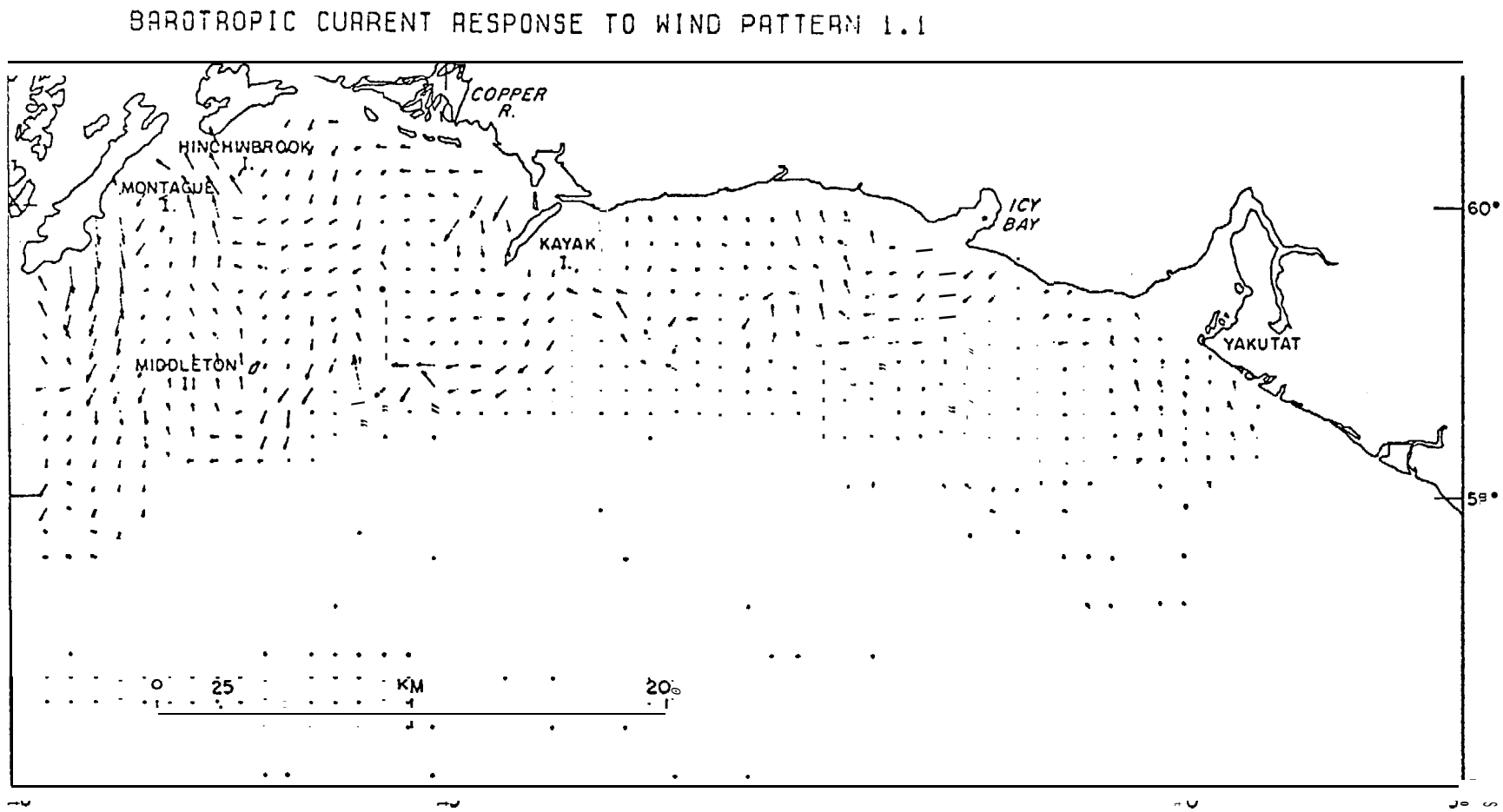

Figure 3.10. Composite wind set-up response for Northeast Gulf of Alaska weather type 1.1.

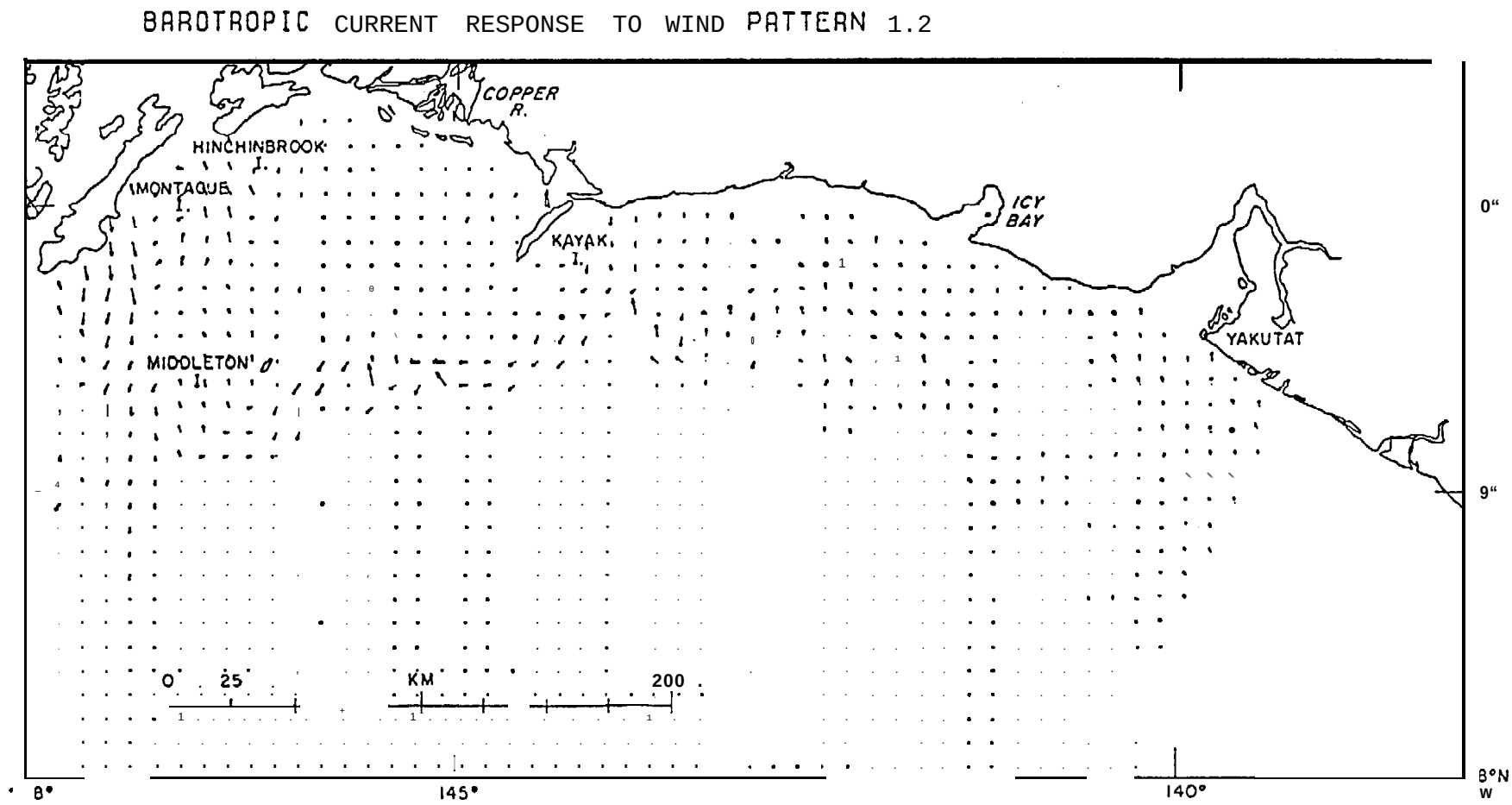

Figure 3-11. Composite wind set-up response for Northeast Gulf of Alaska weather type 1.2.

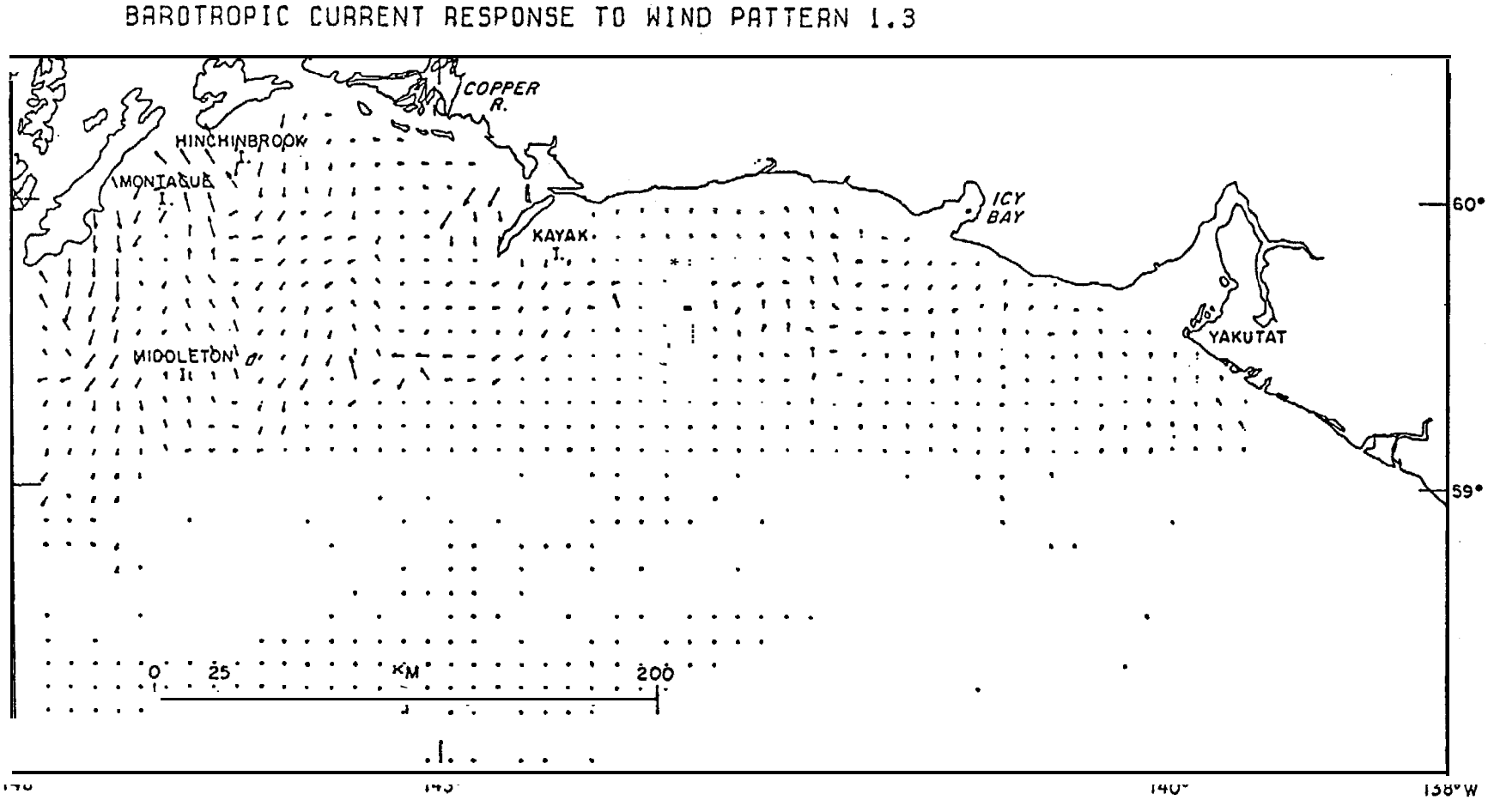

Figure 3-12. Composite wind set-up response for Northeast Gulf of Alaska weather type 1.3.

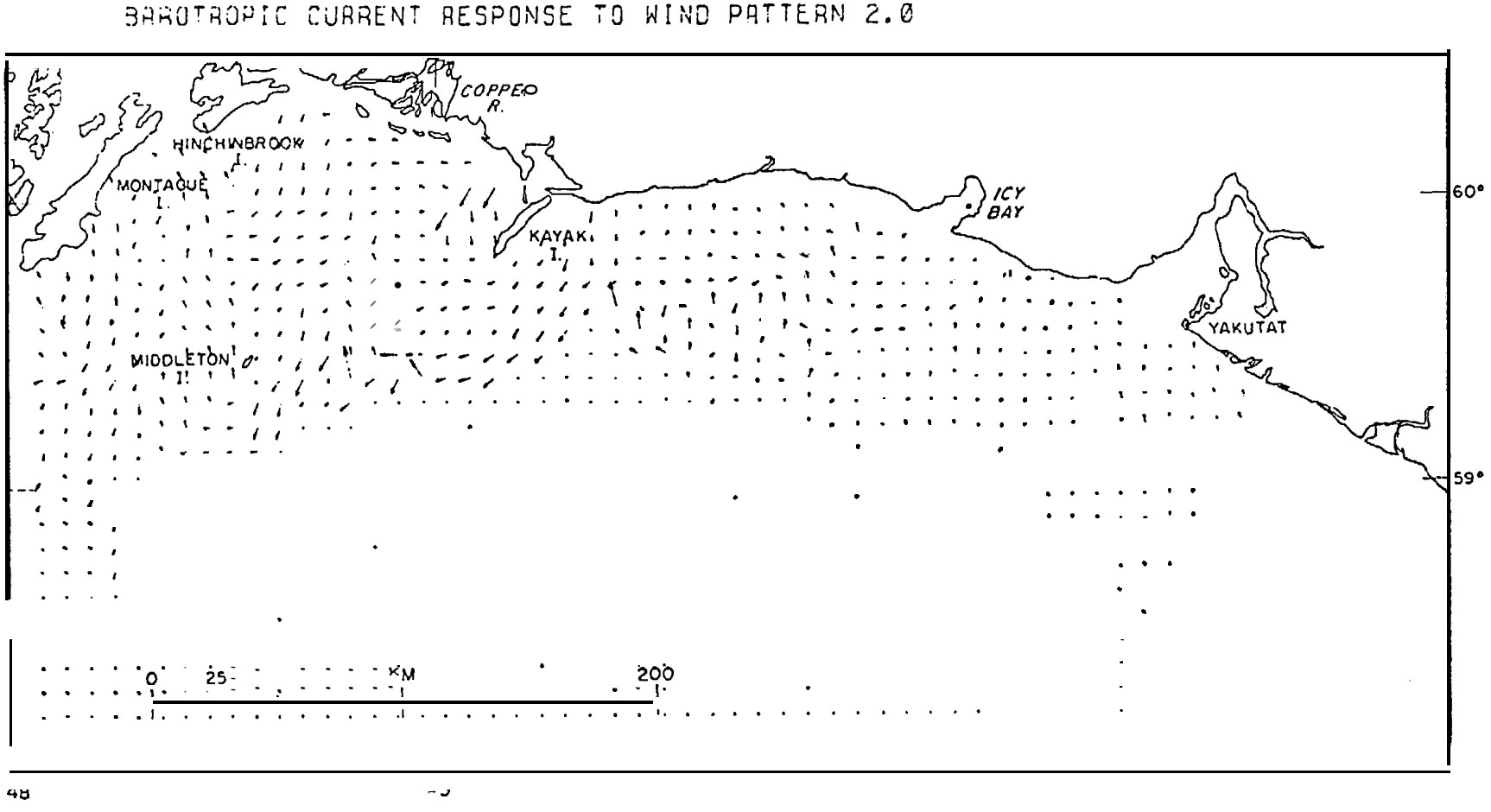

Figure 3-13. Composite wind set-up response for Northeast Gulf of Alaska weather type 2.0.

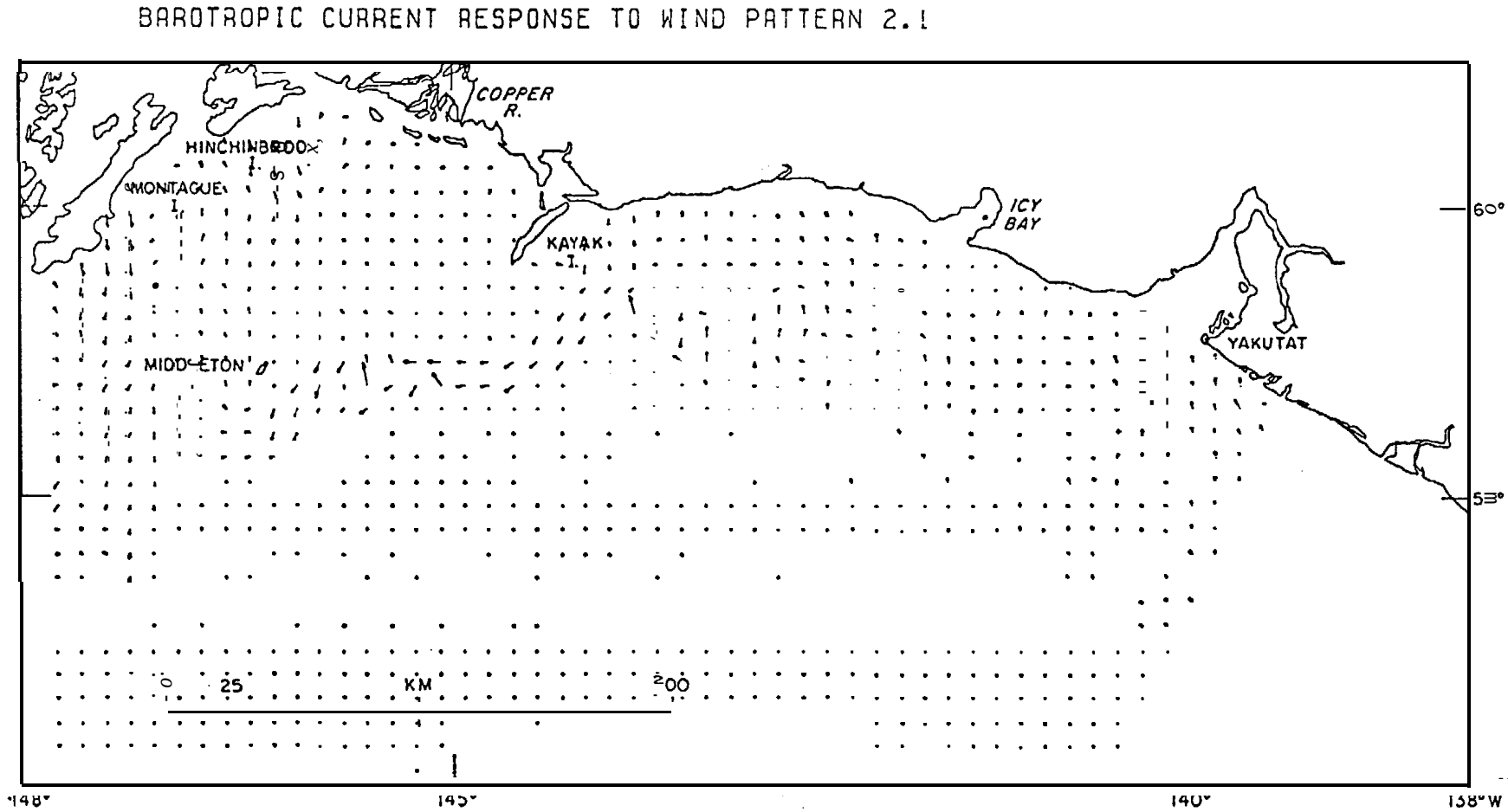

Figure 3-14. Composite wind set-up response for Northeast Gulf of Alaska weather type 2.1.

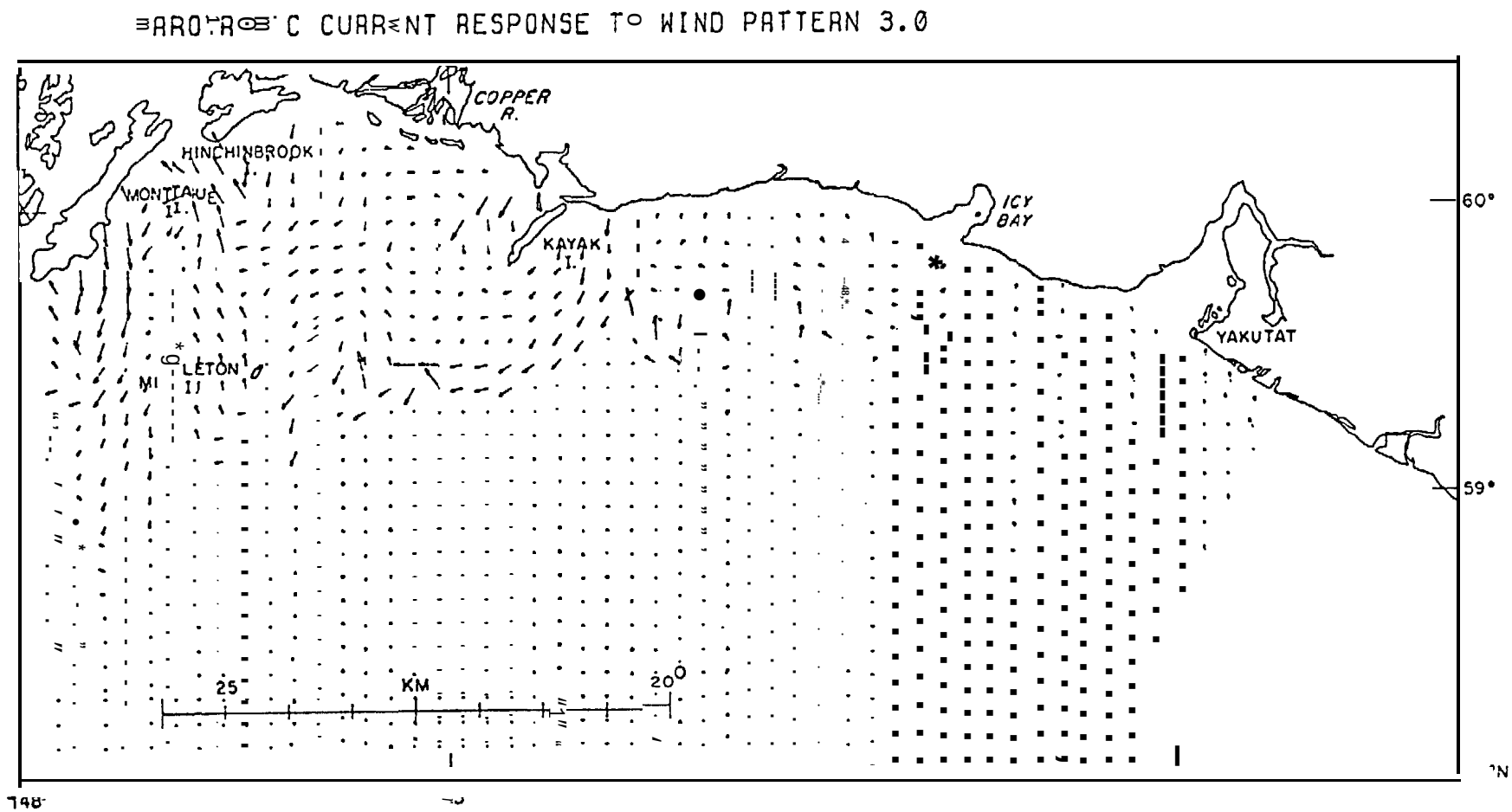

Figure 3-15. Composite wind set-up response for Northeast Gulf of Alaska weather type 3.0.

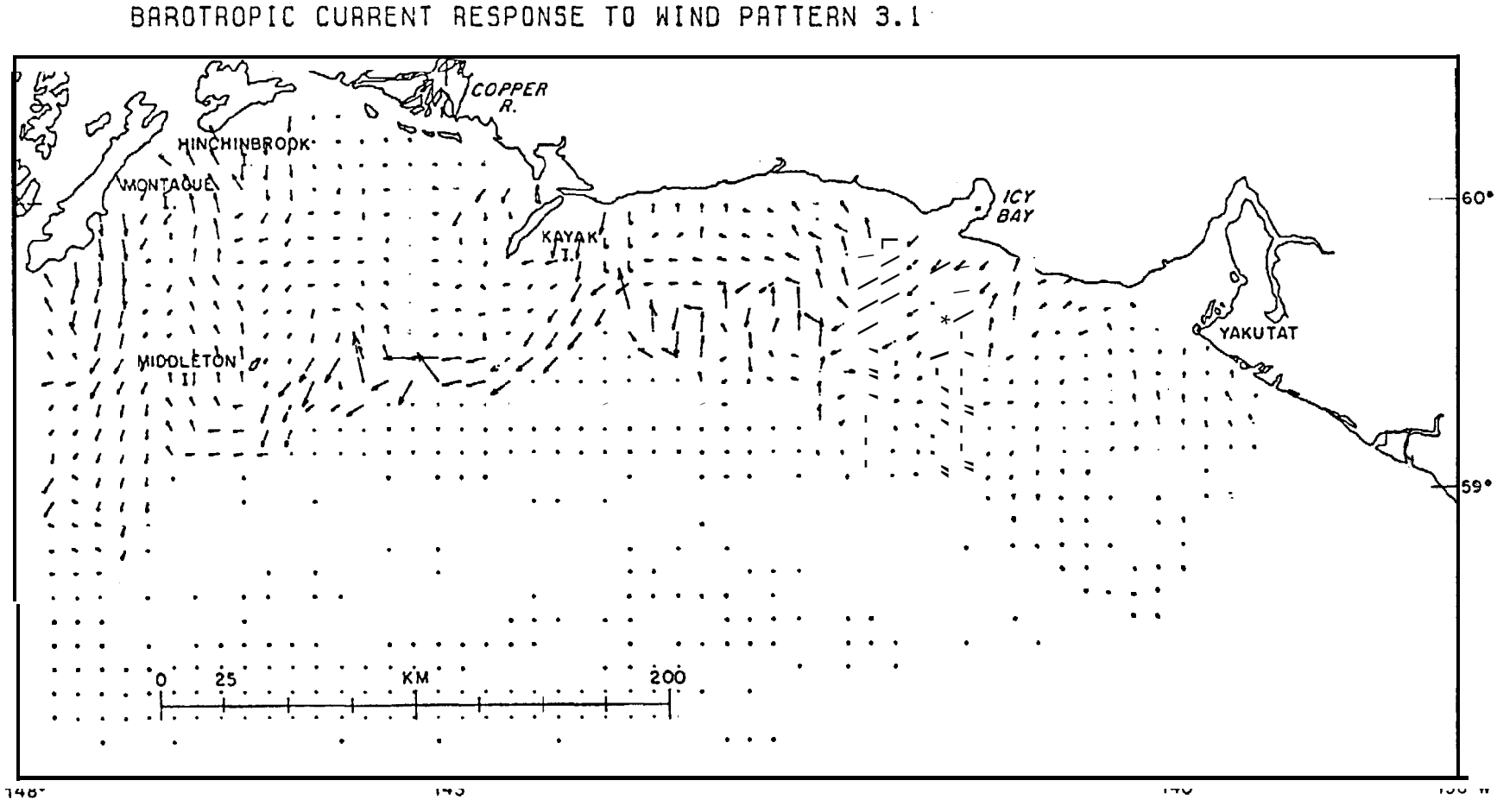

Figure 3-16. Composite wind set-up response for Northeast Gulf of Alaska weather type 3.1.

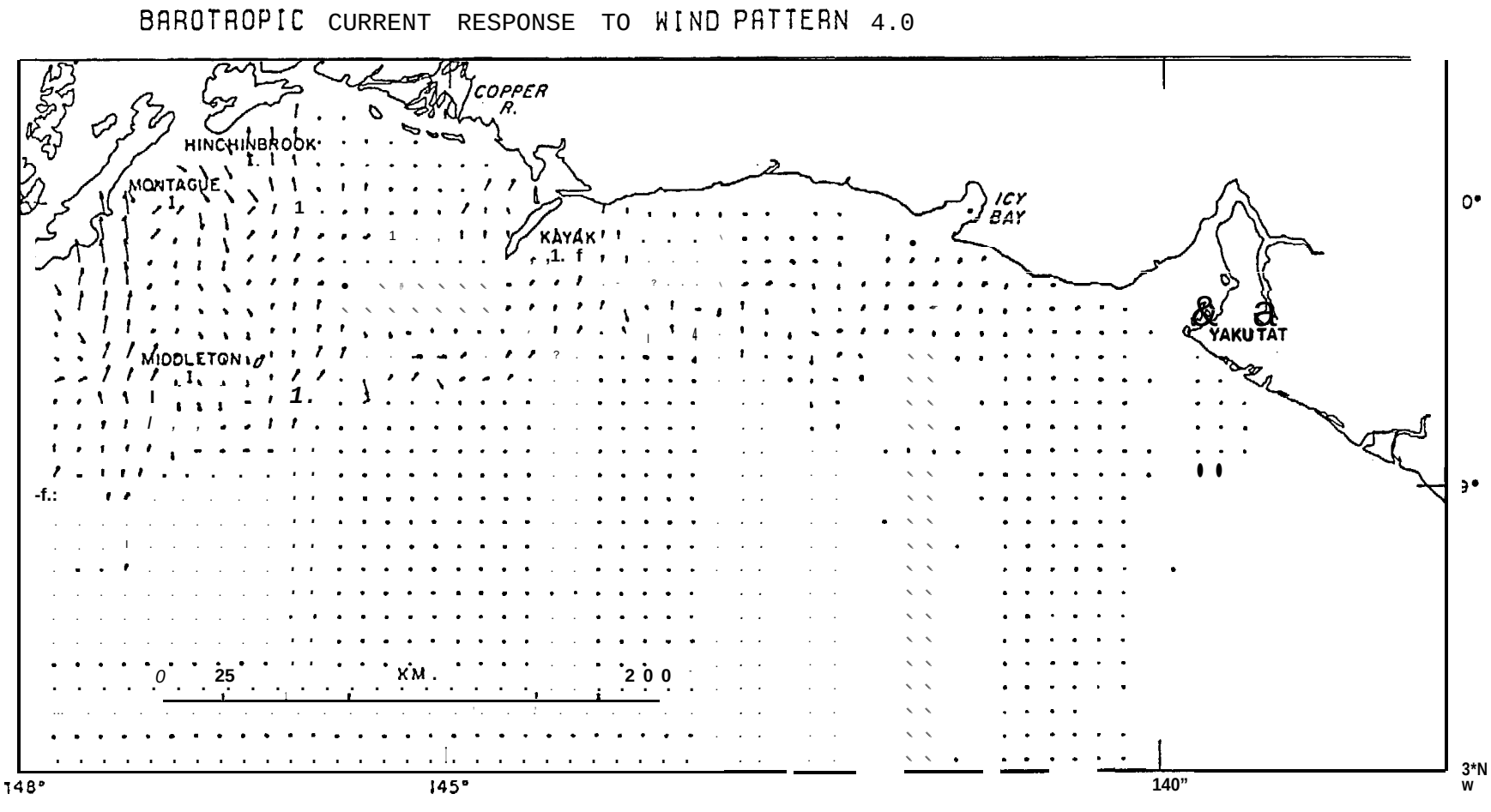

Figure 3-17. Composite wind set-up response for Northeast Gulf of Alaska weather type 4.0.

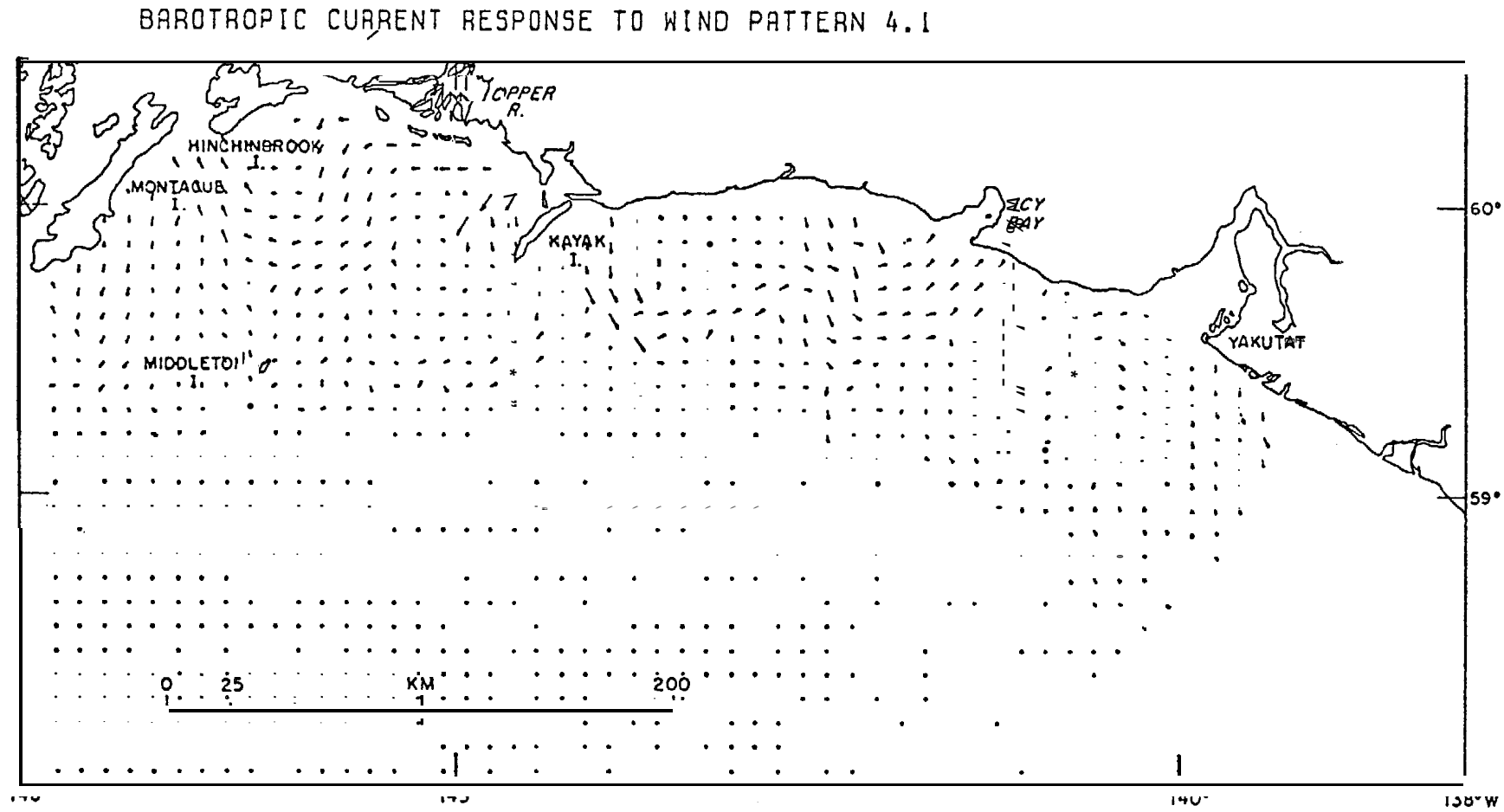

Figure 3-18. Composite wind set-up response for Nort east Gulf of Alaska weather type 4.1.

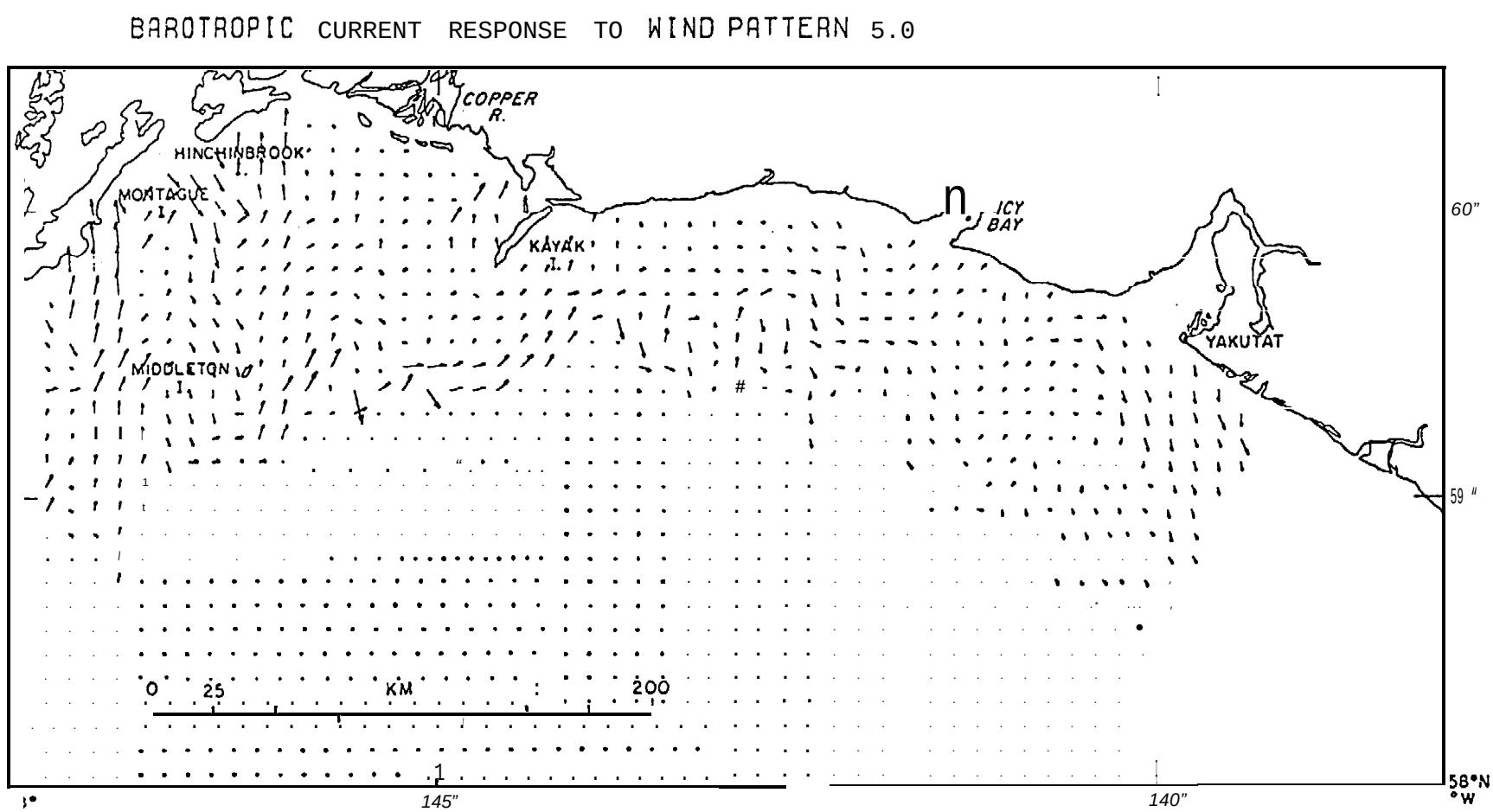

Figure 3-19. Composite wind set-up response for Northeast Gulf of Alaska weather type 5.0.

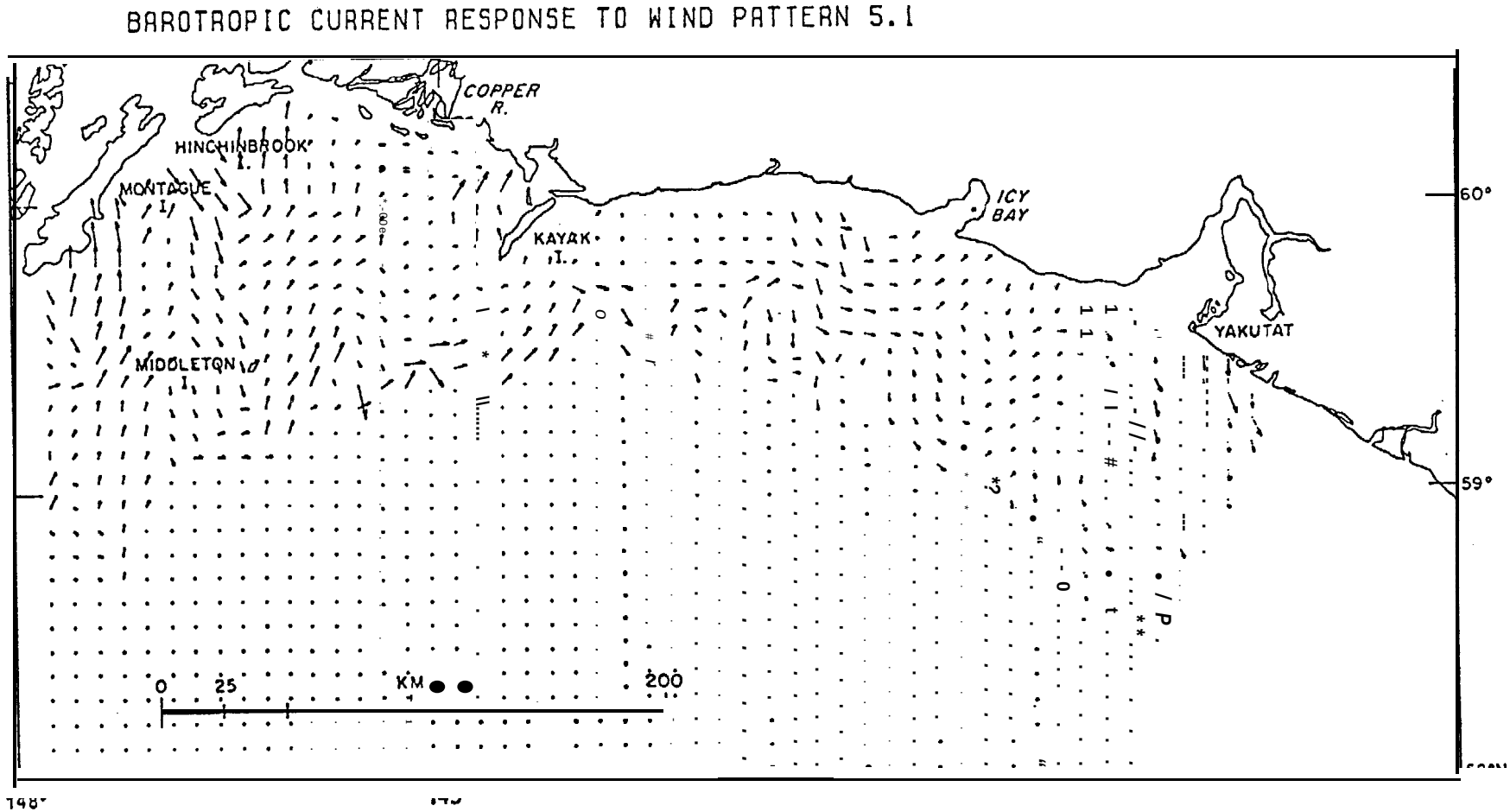

Figure 3-20. Composite wind set-up response for Northeast Gulf of Alaska weather type 5.1.

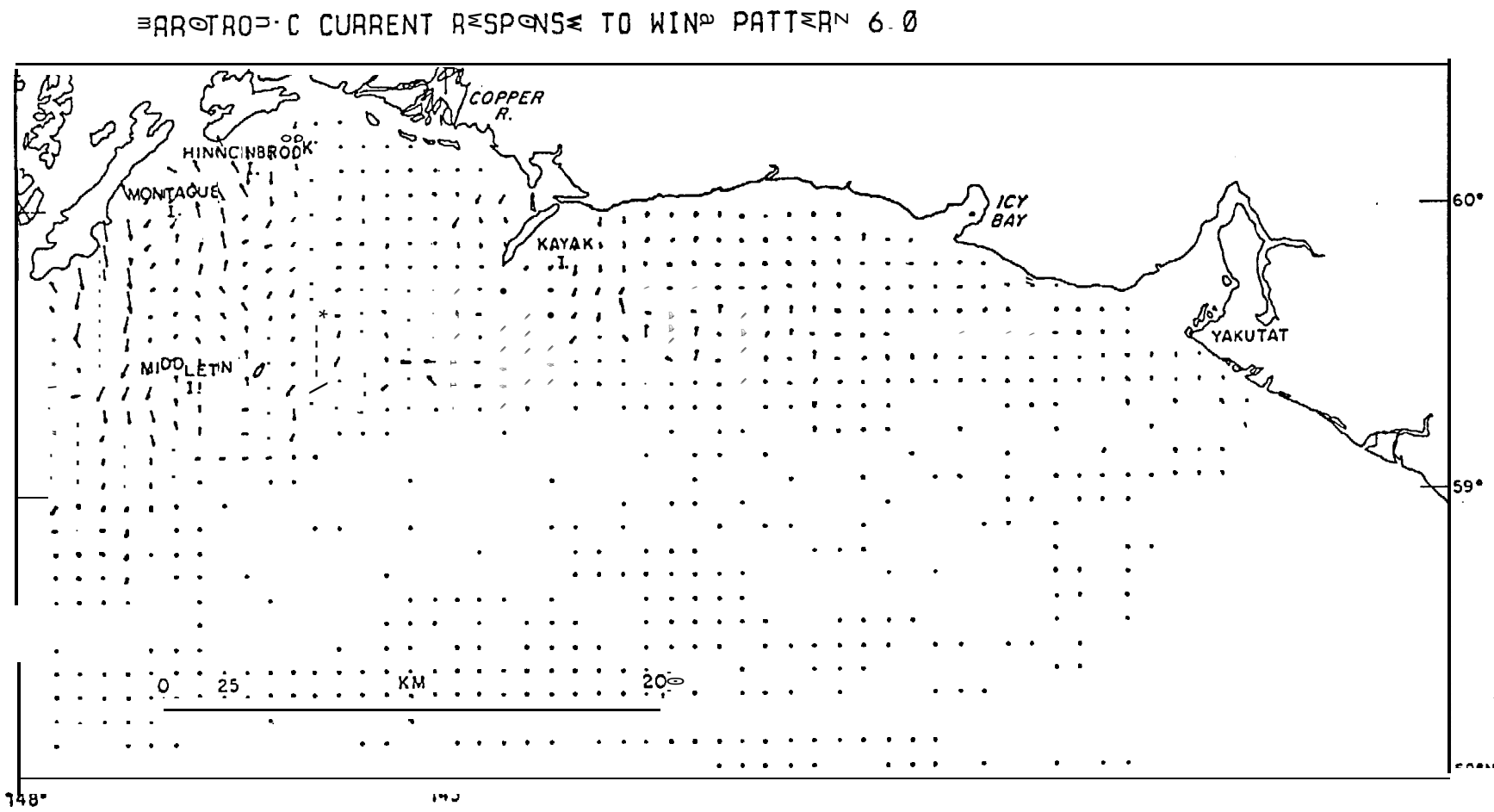

Figure 3-21. Composite Wind set-up for Northeast Gulf of Alaska weather type 6.0.

is similar to the first, except that the wind pattern is displaced to the west, causing a subsequent reduction of the currents in the eastern part of the region. The third current pattern in response to wind pattern (1.2), an eastward displacement of the low, shows significantly reduced flow over much of the area, since the coastal winds are directed more nearly perpendicular to the coast over the study area. The fourth pattern for the Gulf of Alaska low positioned to the extreme west (figure 3-12 - wind pattern 1.3) shows even more pronounced reduction of the currents in the eastern portion of the region.

Figures (3-13) and (3-14) show the current response to wind patterns (2.0) and (2.1), corresponding to an Aleutian low. The first of these is similar to (3-12), showing again a reduction of currents over the eastern half of the NEGOA shelf region. Figure (3-14)(for the summer case) shows continuation of flow along the shelf break, but significantly weaker flows over the shelf proper, with particularly quiescent conditions off of the Copper River region.

Figures (3-15) and (3-16) give the current response to wind patterns (3.0) and (3.1), which represent a high pressure situated over the Yukon, with the second including a katabatic outbreak in the winds over the Icy Bay and Copper River regions. Comparing the two current patterns clearly shows the results of these intense coastal winds. The first shows what might be considered the normal westward drift for the region. The second shows significantly increased flow over the eastern shelf region and along the shelf break, but a reduction of currents off the Copper River, since the along-shore component of the wind (bathystrophic forcing) is actually reduced in this region.

Figures (3-17) and (3-18) show the response to wind patterns (4.0) and (4.1), which represent summer positions of inland lows over Alaska.

Both show a general reversal of the shelf circulation, with the first giving stronger currents in the western NEGOA region and the second more intense flow along the east portion between Kayak Island and Yakutat.

Figures (3-19) and (3-20) shows the response to two alternate positions of the east Pacific high represented by wind patterns (5.0) and (5.1). Both show nearly identical eastward flowing currents over the entire NEGOA shelf region. These appear to be nearly opposite to the flow given in figure (3-9).

The final current pattern shown in figure (3-21) is the response of the region to a stagnating low off of the Queen Charlotte Islands. This shows generally weak flow over the shelf, with moderate westward currents along the shelf break off of Kayak Island and along Montague Island.

Subject to the assumptions that are inherent in the original weather typing and in the bathystrophic development of hinge responses along the coast, the thirteen current patterns shown represent a complete set, which should be capable of describing all the possible wind responses to be expected for the NEGOA shelf region. More importantly these current patterns are directly related to regional wind forcing, which in turn is related to large scale pressure maps. Such maps have been available for a long period of time so that reliable climatologies can be developed. Using these to key a sequence of current patterns, it becomes possible for the first time to develop regional “current climatologies" directly linked to the forcing and meteorological data base.

3.4 Density Driven Response

The density driven response to the NEGOA region will be given by the solution to equation (3-3). Input data for a density response current pattern must come from a mapping of the internal density field. This

data is collected on standard hydrographic cruises. A number of hydrographic studies have been carried out for the NEGOA region, and at this time seven independent sets are available which have a sufficient number of stations to cover the area. These data sets cover the following periods:

July, 1974

February, 1975

June, 1975 S

June, 1975 A

October, 1975

February, 1976

April, 1976

Once again it should be reiterated that the solution to equation (3-3) yields a minimum barotropic mode which is in reality a minimum bathymetric interaction mode consistent with the model dynamics, density distribution and bathymetry. In terms of a more classical approach this gives the dynamic height of the sea surface, assuming that the region has a terrain following level of no motion. As a practical matter for stations beyond the shelf, a level of no motion is assumed at 1200 meters. Subject to these conditions the density driven response patterns for the above data sets are shown in figures (3-22) through (3-28). Once again the vector arrows have been transformed from the triangular finite element grid to a regular cartesian grid for ease in computer storage and graphic representation. It should also be noted that these patterns are not of arbitrary magnitude, but give absolute velocities related to the shear induced by the baroclinic fields.

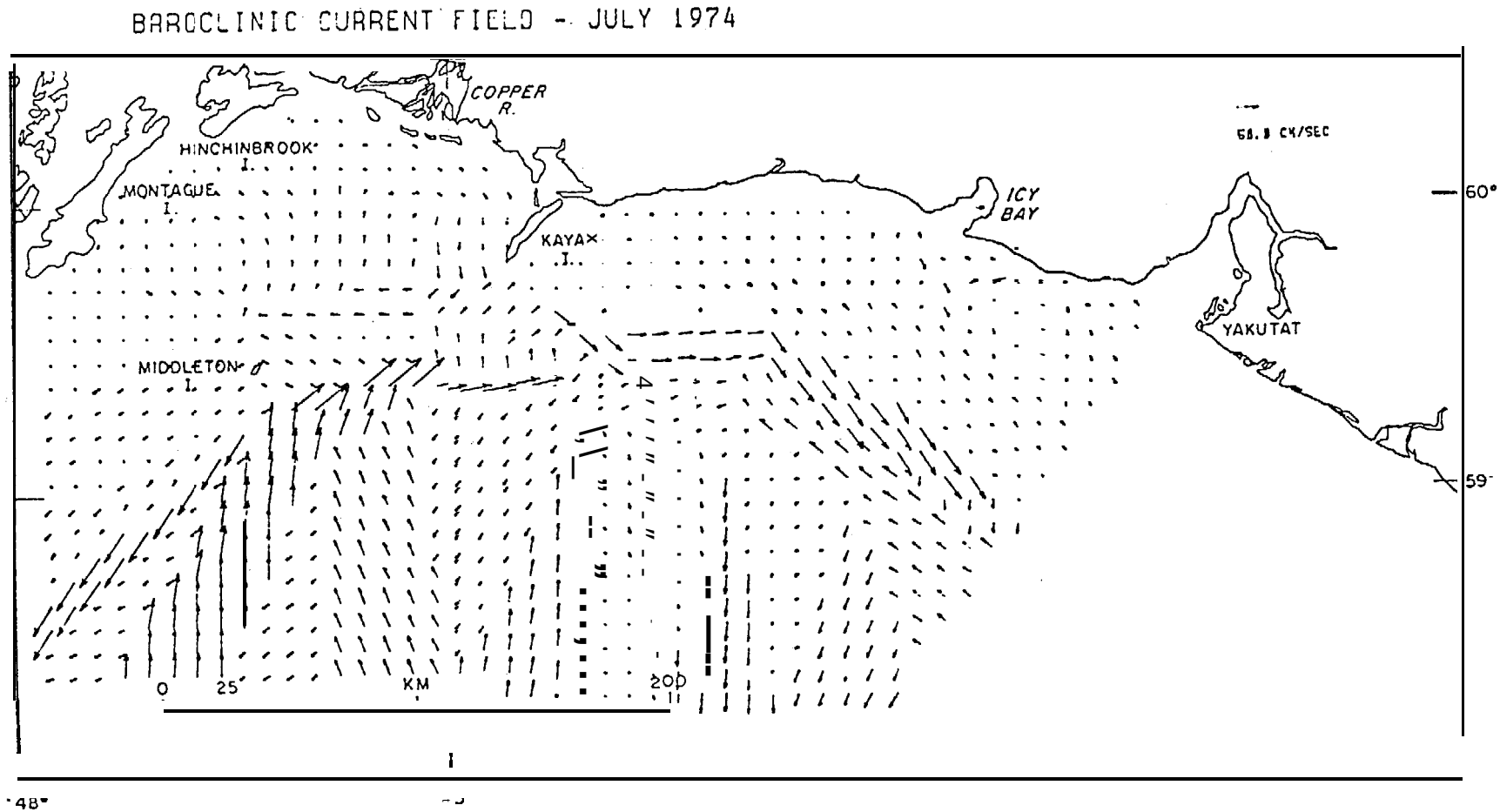

Figure 3-22. Density driven response currents for the Northeast Gulf of Alaska from data collected in July 1974.

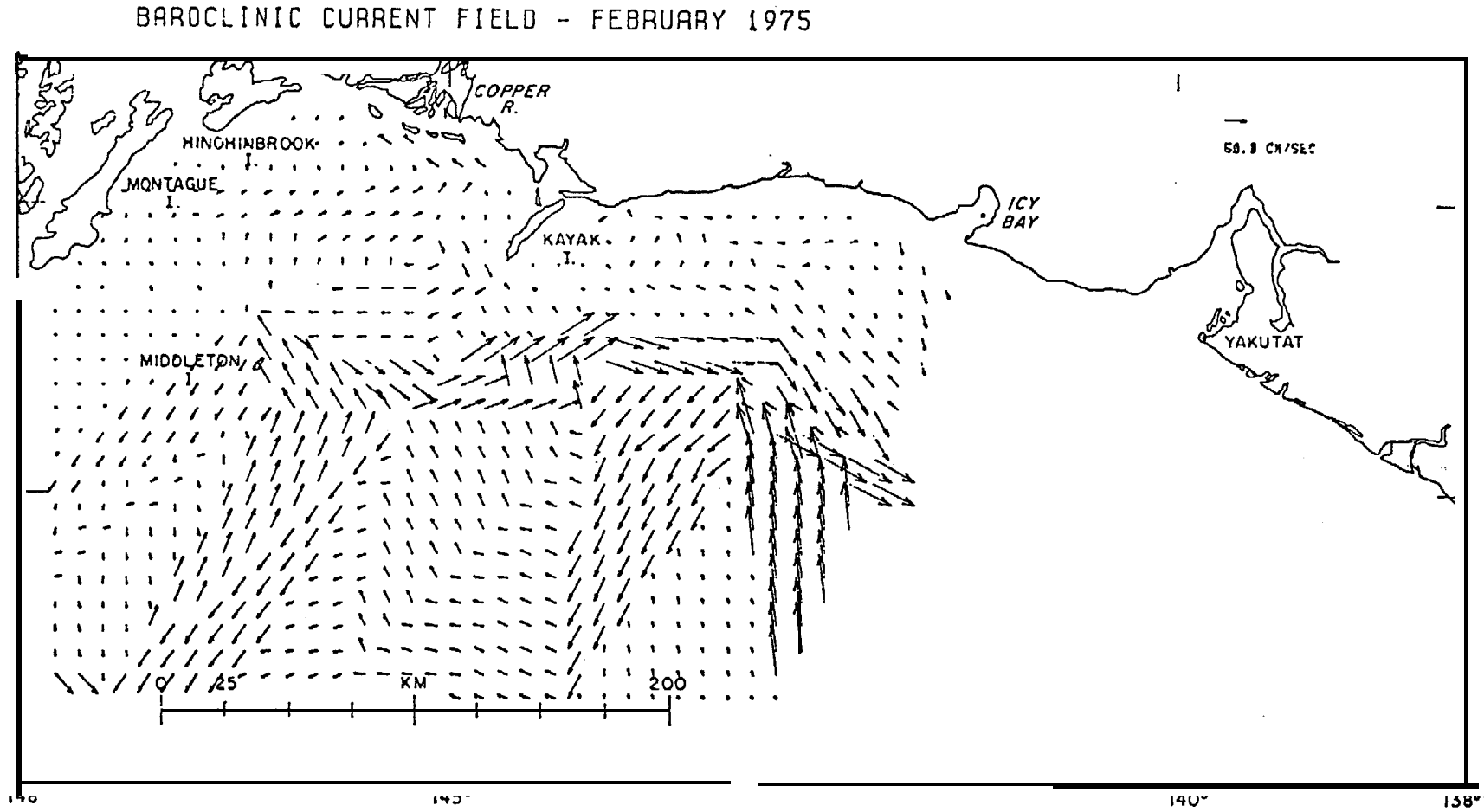

Figure 3-23. Density driven response currents for the Northeast Gulf of Alaska from data collected in February 1975.

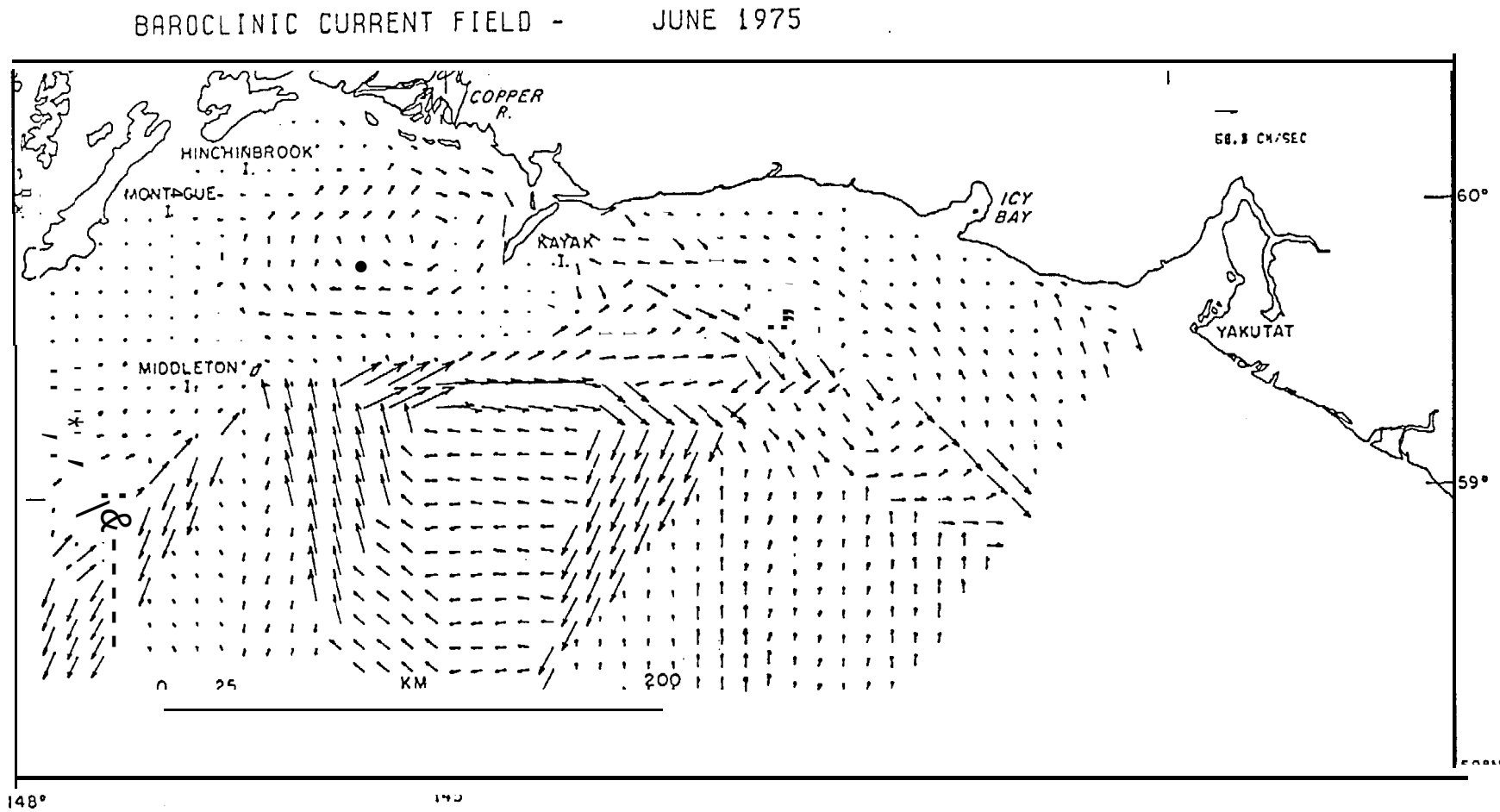

Figure 3-24. Density driven response currents for the Northeast Gulf of Alaska from data collected in June 1975 (NOAA Ship Surveyor).

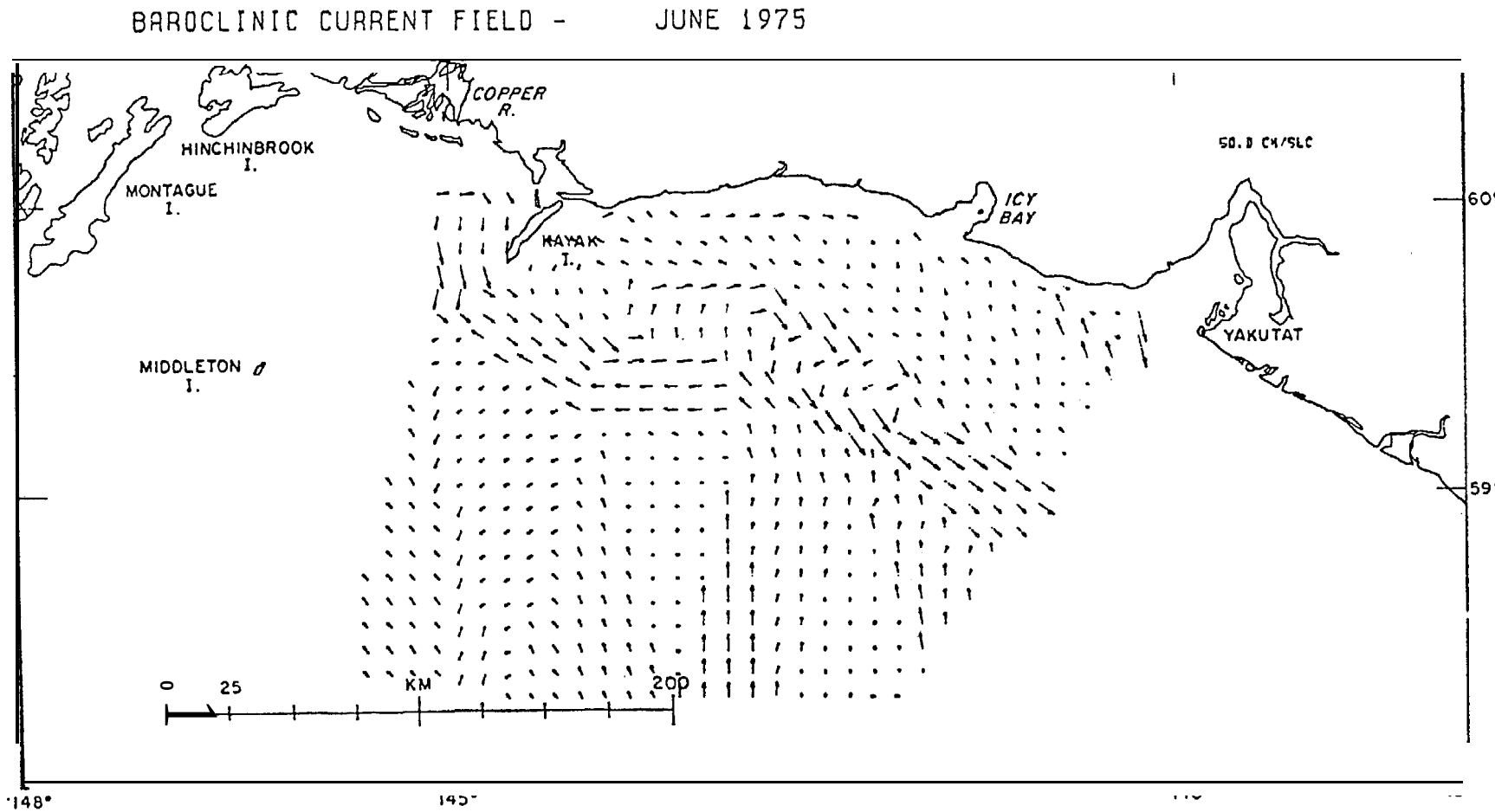

Figure 3-25. Density driven response currents for the Northeast Gulf of Alaska from data collected in June 1975 (R/V Acona).

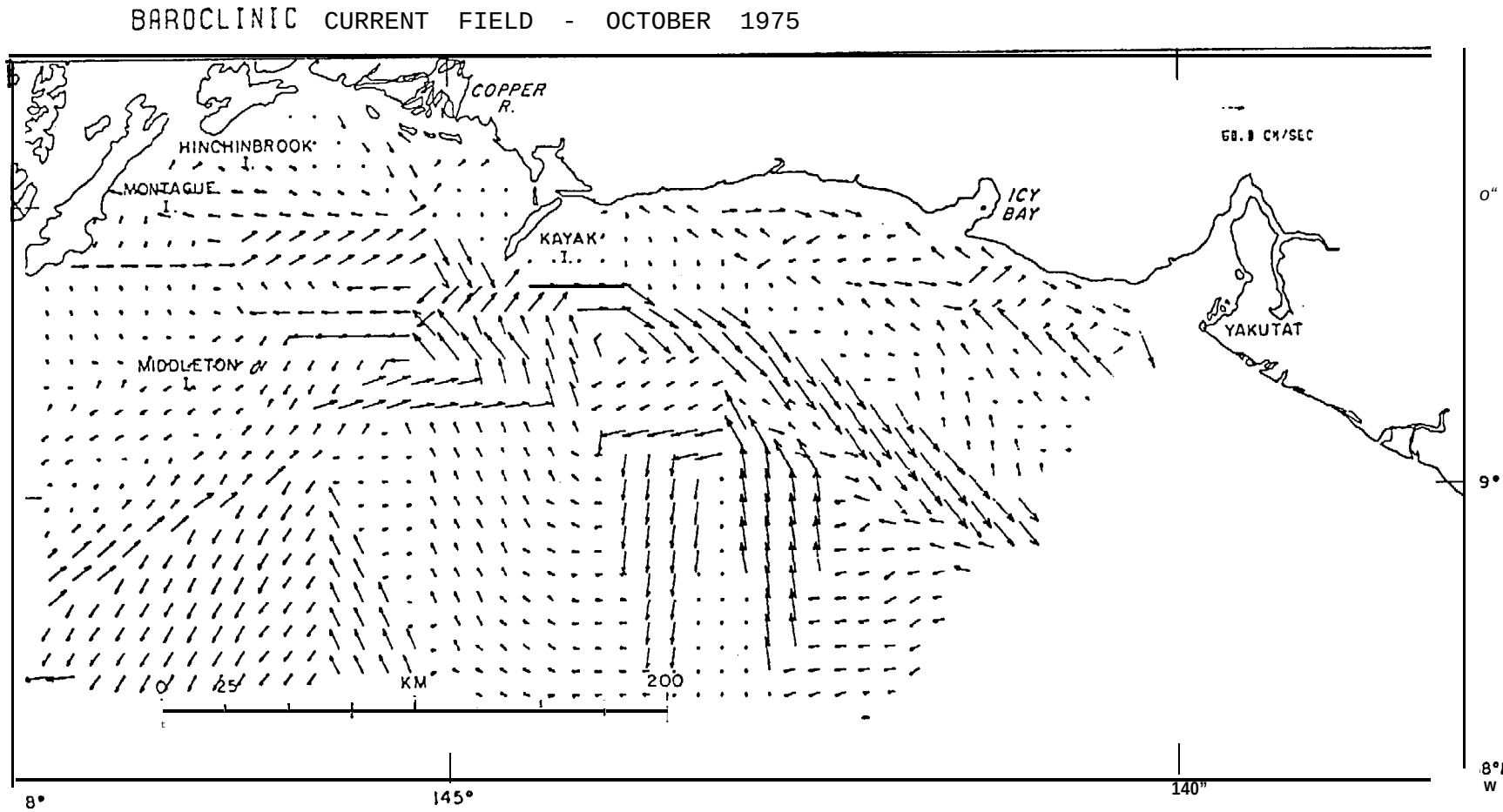

Figure 3-26. Density driven response currents for the Northeast Gulf of Alaska from data collected in October 1975.

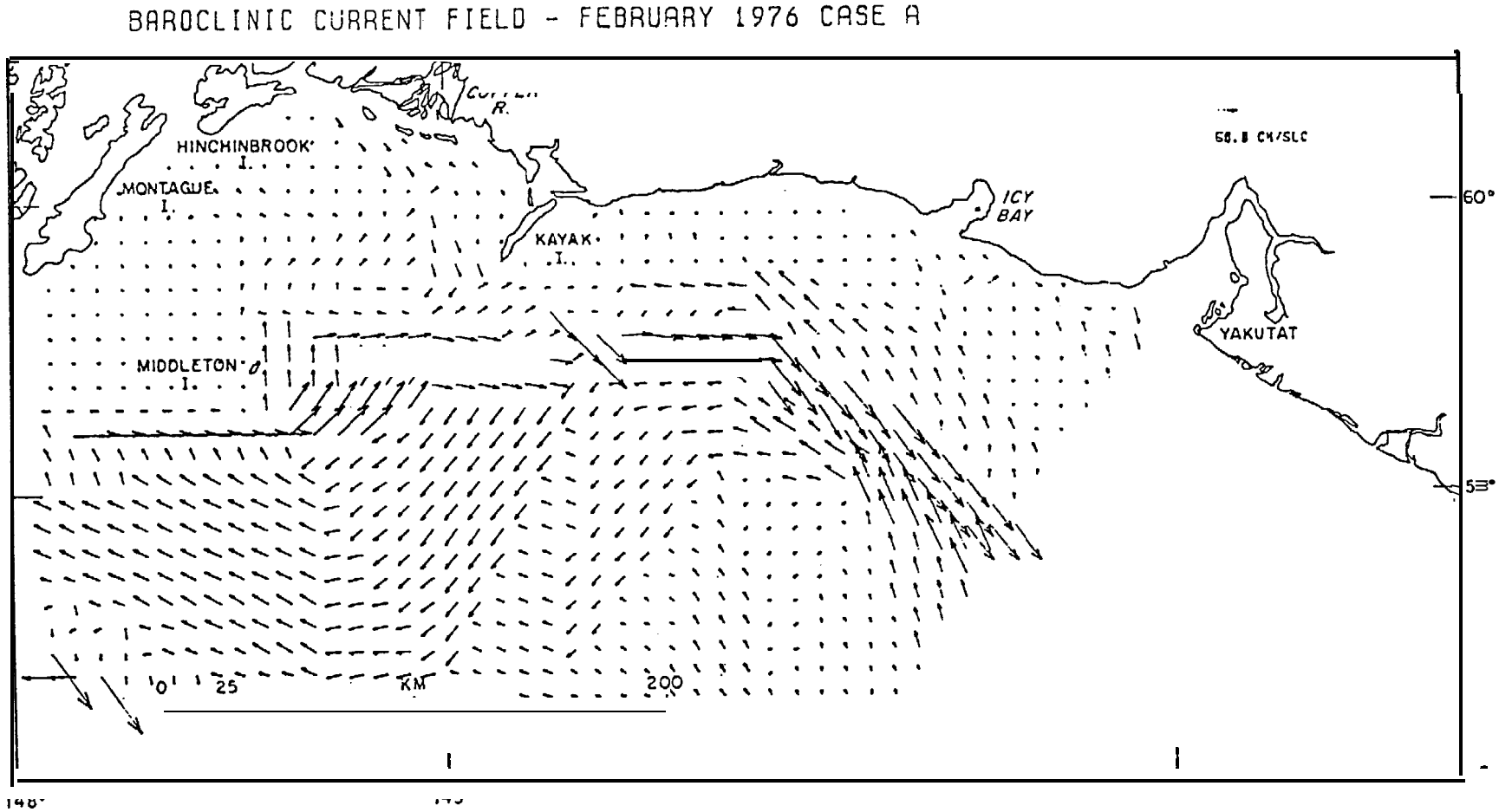

Figure 3-27. Density driven response currents for the Northeast Gulf of Alaska from data collected in February 1976.

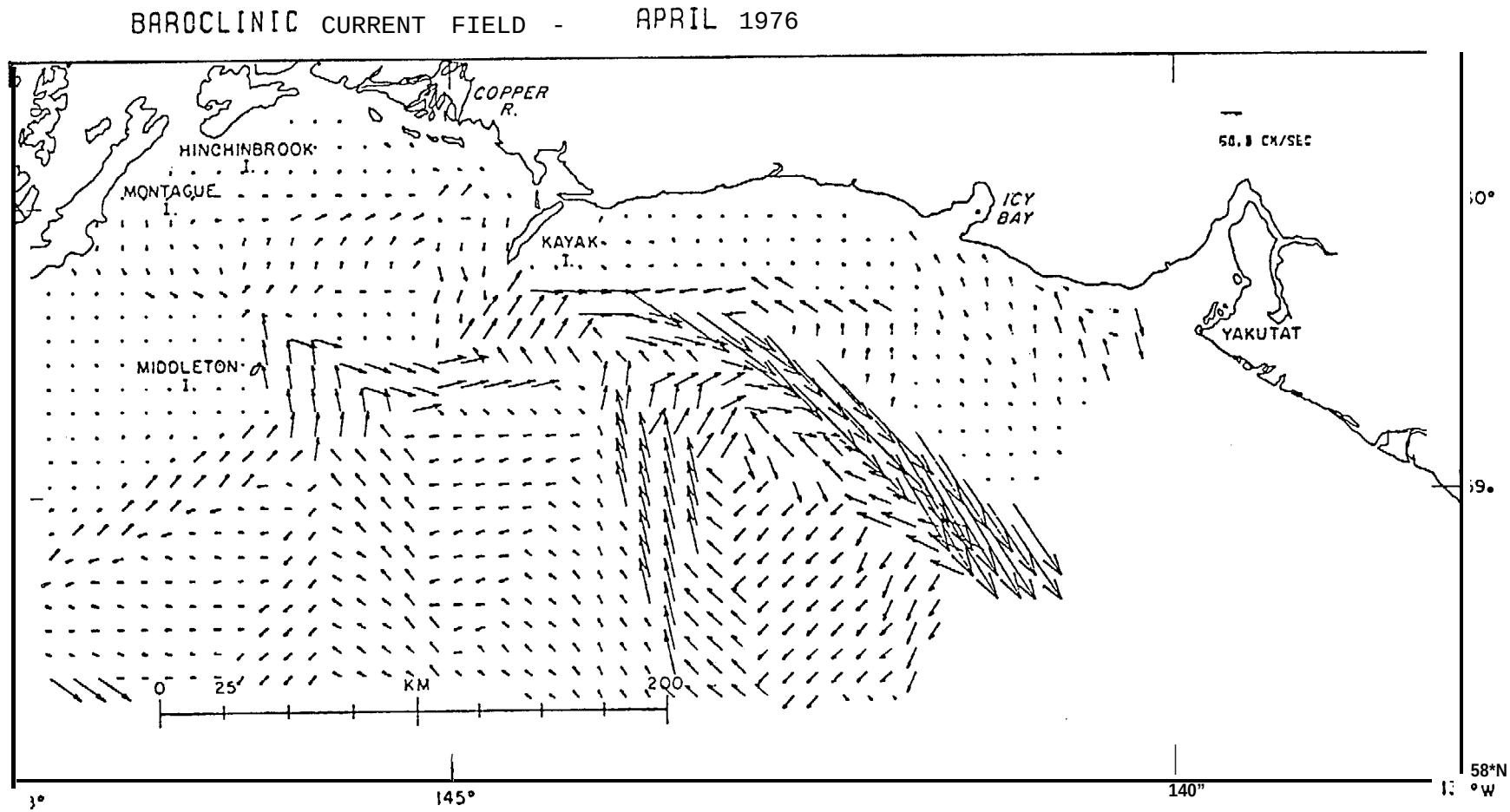

Figure 3-28. Density driven response currents for the Northeast Gulf of Alaska from data collected in April 1976.

An examination of the density driven response patterns reveals several immediate points. The first of these is that on the shelf proper the currents are considerably smaller than the ones seen off of the shelf. As a second point the off-shelf currents appear to be associated with large-scale (>200 km) eddies that are present in all the data sets. It is significant to note that although the position of these mesoscale baroclinic eddies varies from one cruise to the next, they are always present to some extent.

In an attempt to discuss the density driven response patterns in a systematic order, the on-shelf and off-shelf flow will be discussed separately.

Concentrating first on the on-shelf patterns, figure (3-22) indicates the density driven response for July, 1974. On the shelf (d < 100 fa.) the currents are generally weak (< 10 cm/see) with little organized flow except for an anticyclonic gyre to the west of Kayak Island and a westward flowing current NE of Middleton Island. There is also evidence of a slightly weaker cyclonic gyre NNW of Middleton Island, but it is less clear. The gyre or eddy behind Kayak Island has been discussed previously (Galt, 1976) and compared to other observational evidence.

Figure (3-23) shows the density driven response for data collected in February, 1975. On the shelf the currents are generally somewhat more energetic than during the previous summer. The anticyclonic gyre to the west of Kayak Island is still evident along with a westward flowing current along the coast off of the Copper River. There is also a generally consistent westward flow along the outer edge of the shelf which moves at about 40 cm/sec.

Figure (3-24) shows the density driven response for data collected

in June, 1975. In this case the gyre west of Kayak Island is particularly well developed with speeds of nearly a knot. In addition it appears that offshore the eddy S and SW of Kayak Island has moved into the region where the shelf narrows, and a fairly strong coastal current to the west is evident. As in the previous summer the southern extreme of the gyre west of Kayak Island appears to border on a westward flow to the NE of Middleton Island.

Figure (3-25) is particularly interesting in that it shows the density driven response from a partial field that was collected on a second cruise in June, 1975, approximately a week after the one shown in figure (3-24). Several significant changes are evident. First of all the currents south and east of Kayak Island have been deformed. Secondly, the large offshore gyre south of Kayak Island does not appear to have been sampled by the station spacing.

Figure (3-26) shows the density driven response currents for data collected in October, 1975. This appears to be an unusual pattern. Flow on the shelf is relatively energetic with bands of eastward flow particularly along the coast west of Icy Bay and east of the southern end of Montague Island. There is an indication of anticyclonic flow to the WSW of Kayak Island but the pattern is considerably deformed compared to previous realizations of this feature.

Figure (3-27) shows the density driven response for data collected in February, 1976. Once again this indicates the development of an anti-cyclonic gyre west of Kayak Island. Interestingly, just south of Kayak Island the flow is eastward as in the second June, 1975 pattern. Southeast of Icy Bay along the outer edge of the shelf (100 fa. contour) relatively strong NW flow is seen. The offshore pattern SE of Middleton Island

is clearly seen to penetrate onto the shelf.

Figure (3-28) shows the density driven response for April, 1976. West of Kayak Island the anticyclonic flow pattern is evident with a weaker cyclonic flow to the east of Montague Island. Once again it appears that the offshore circulation penetrates onto the shelf to the SE of Middleton Island and the SE of Kayak Island.

It is now necessary to focus attention on the offshore segments of the density driven current patterns. In doing this it is obvious from figures (3-22) through (3-28) that the sampling scale offshore is too coarse to accurately resolve the mesoscale eddies that are present. In addition the predicted currents are often large, with speeds in excess of two knots. For this deep region the model results are just what would be obtained from classical dynamic height calculations, and as such a more common presentation is the sea surface elevation contours. These are shown in figures (3-29) through (3-35) for the seven data sets previously considered. From the surface elevation contours the eddy nature of the patterns is more clearly seen, with an offshore length scale of approximately 200 km. The questions concerning origin and initial movement of these mesoscale features are of obvious oceanographic interest, but will not be addressed in the present study. It is enough to point out that they seem to be common for the Gulf of Alaska bight region and are an ubiquitous feature in the data.

A more pressing question concerning these mesoscale eddies is how they interact with the continental slope and shelf break area. Since the object of the present study is the NEGOA shelf region, it is this dynamic exchange and current description that are needed.

To address the eddy-slope interaction problem it is useful to first consider a baroclinicly balanced, symmetric, anticyclonic gyre moving

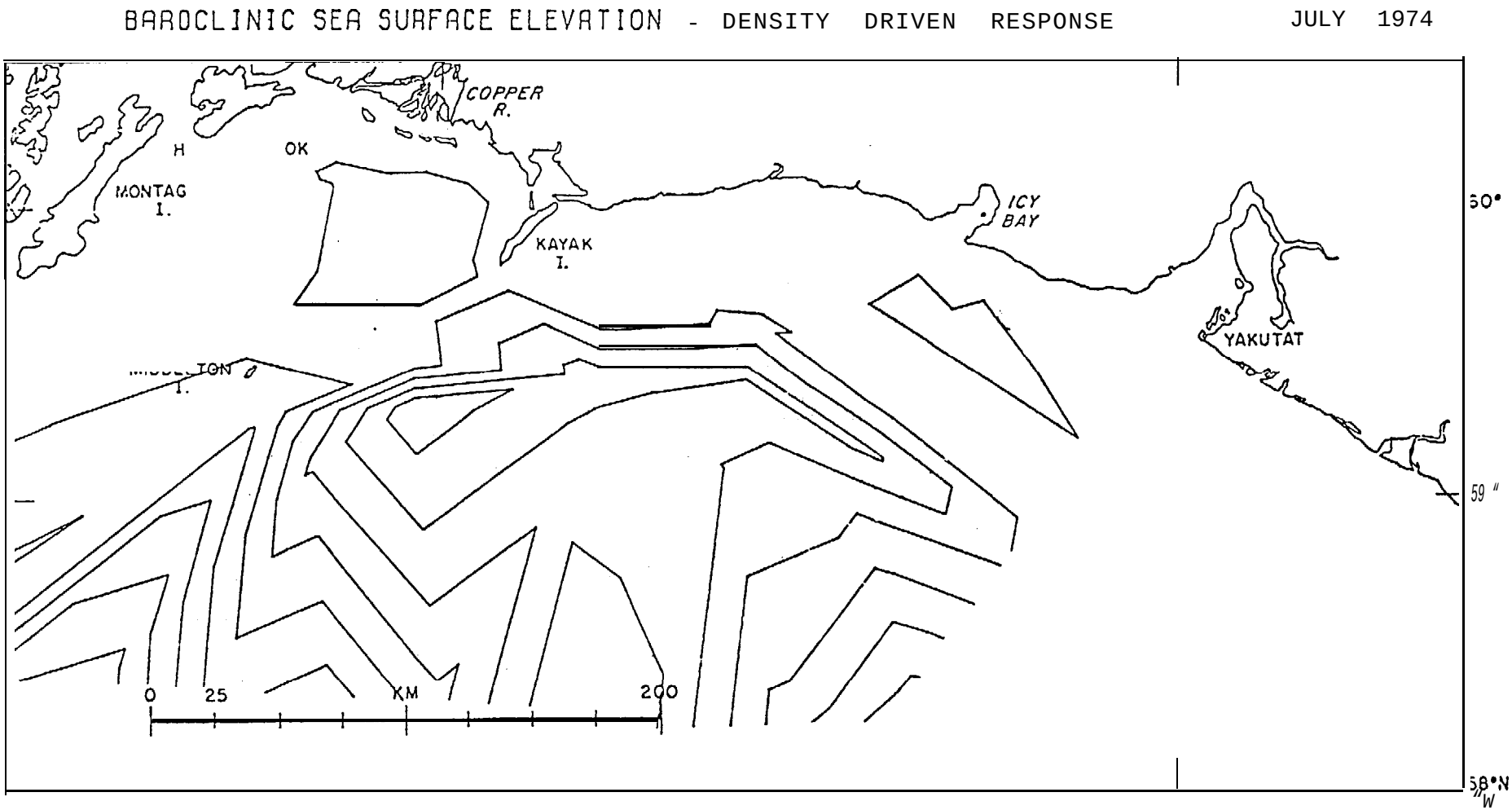

Figure 3-29. Sea surface elevation contours for Northeast Gulf of Alaska from data collected in June 1974. Contour interval is 4 cm/sec.

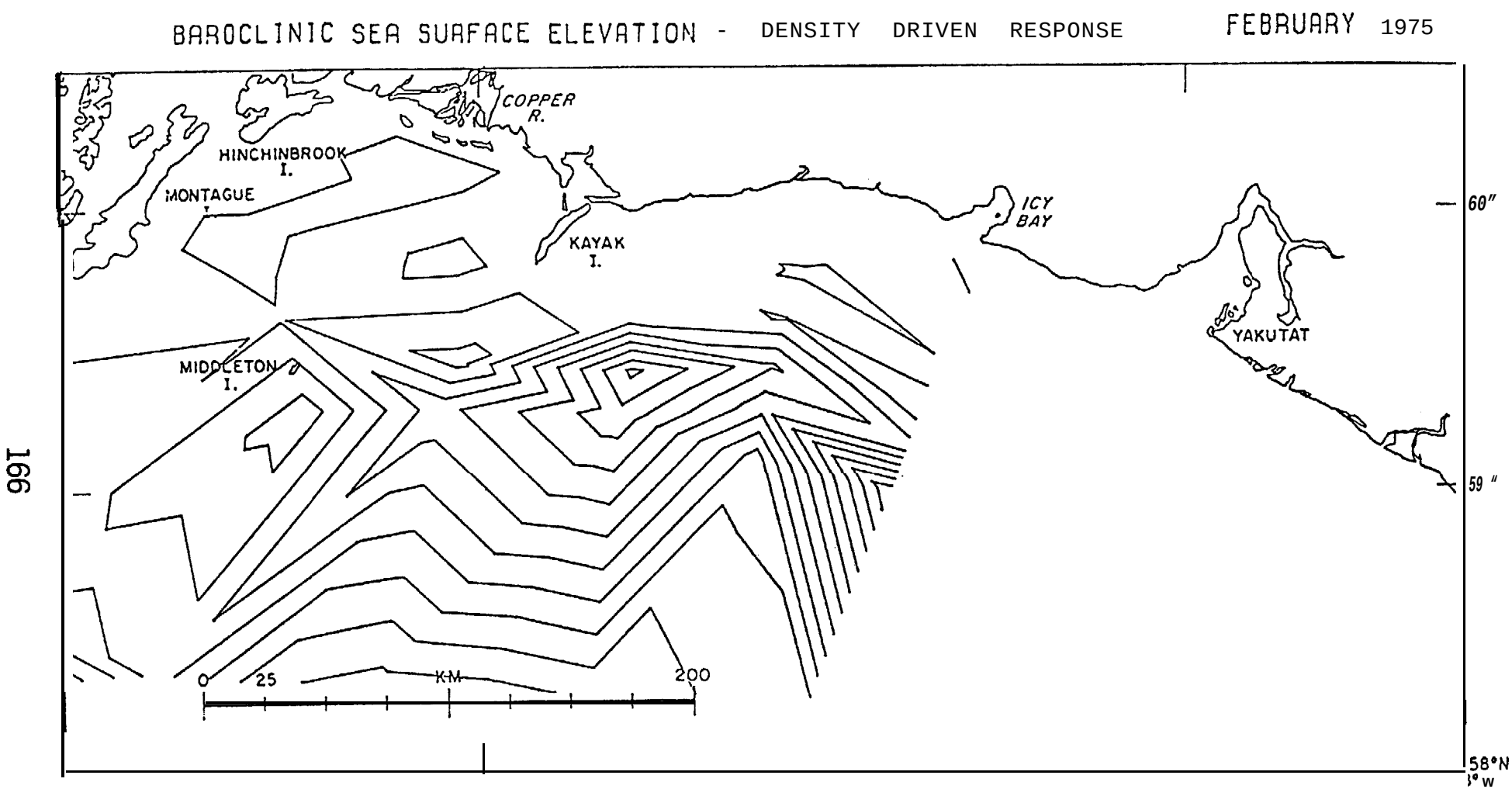

Figure 3-30. Sea surface elevation contours for Northeast Gulf of Alaska from data collected in February 1975. Contour interval is 4 cm/sec.

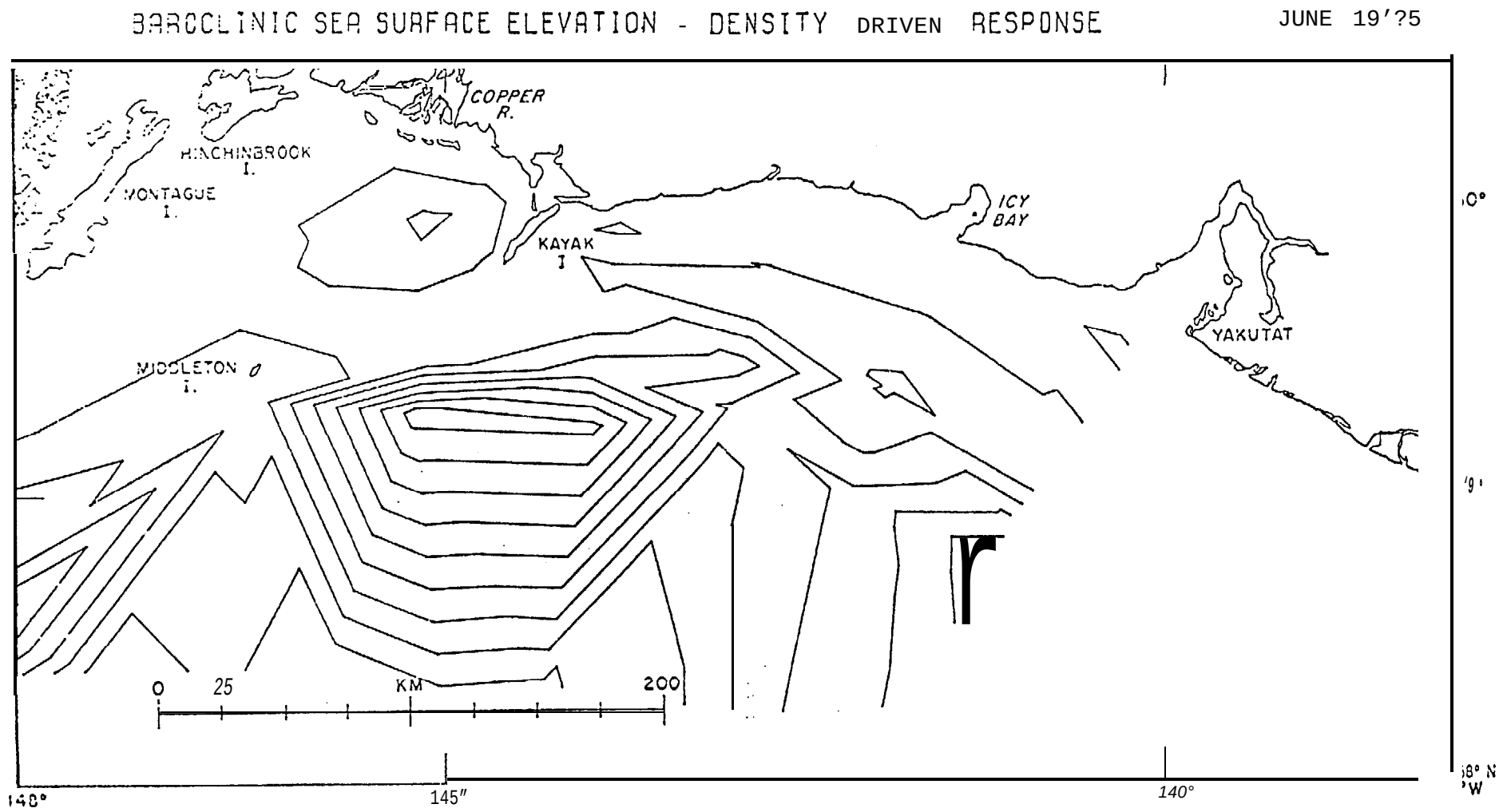

Figure 3-31. Sea surface elevation contours for Northeast Gulf of Alaska from data collected in June 1975 (NOAA Ship Surveyor). Contour interval is 4 cm/sec.

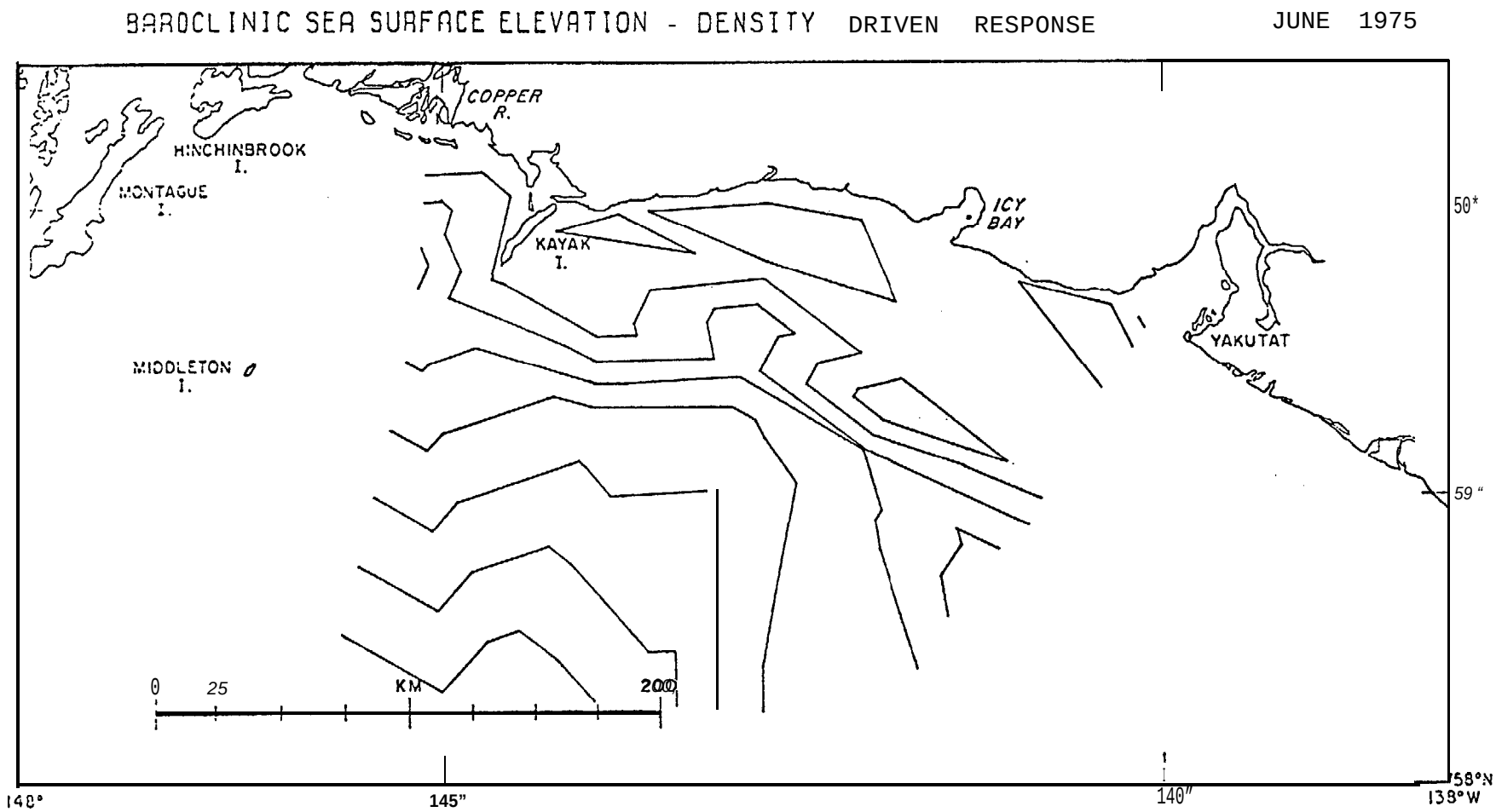

Figure 3-32. Sea surface elevation contours for Northeast Gulf of Alaska from data collected in June 1975 (R/V Acona). Contour interval is 4 cm/sec.

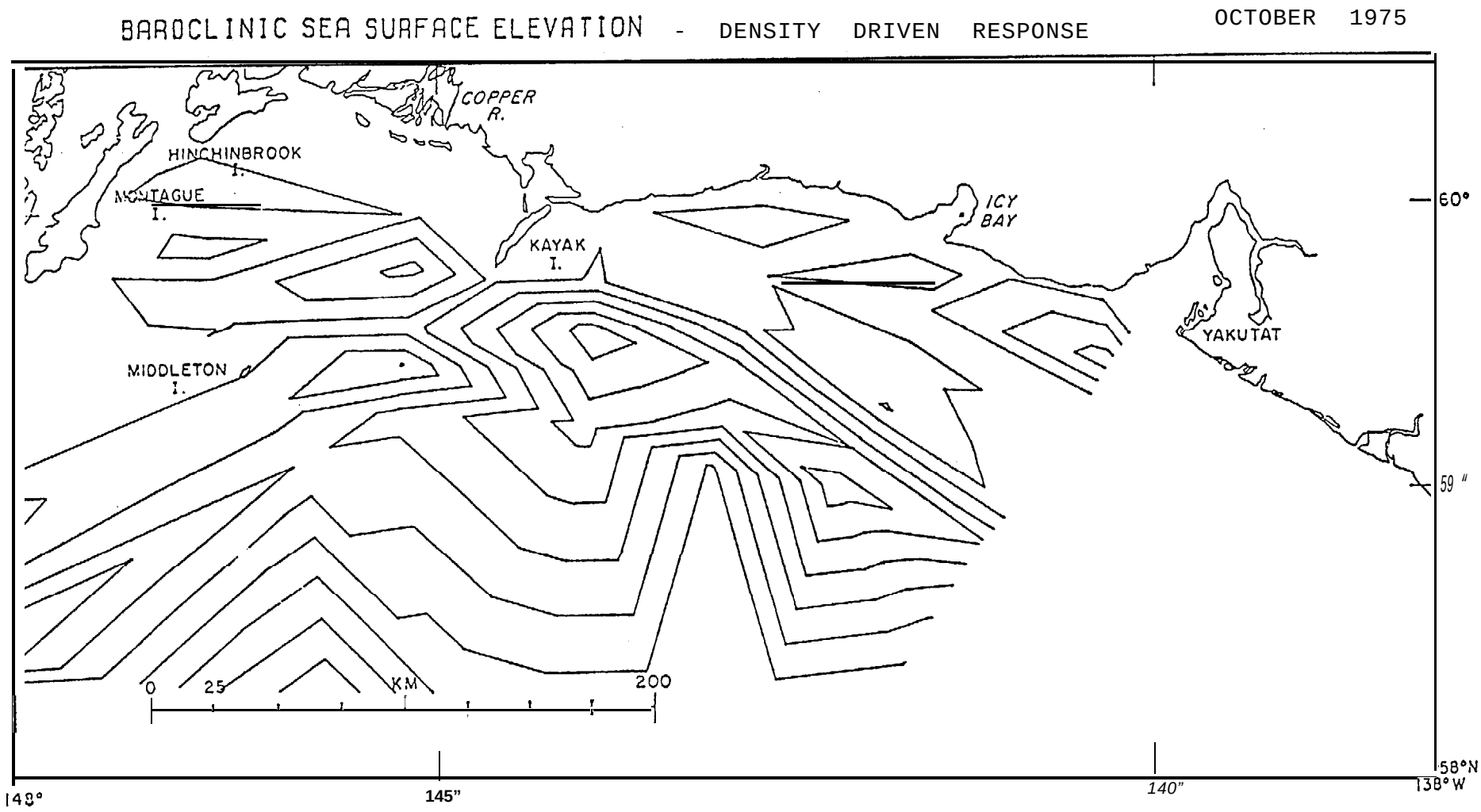

Figure 3-33. Sea surface elevation contours for Northeast Gulf of Alaska from data collected in October 1975. Contour interval is 4 cm/sec.

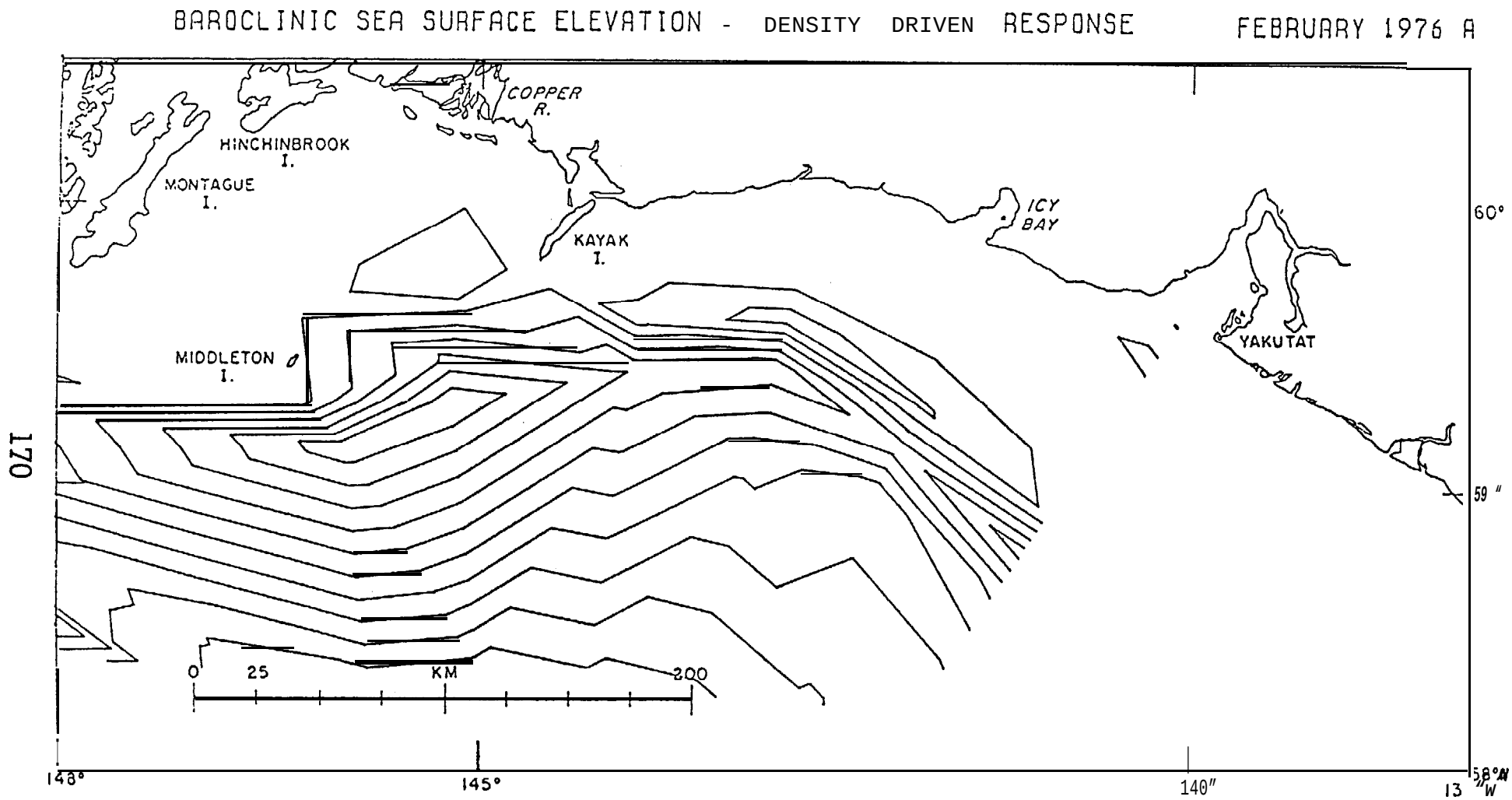

Figure 3-34. Sea surface elevation contours for Northeast Gulf of Alaska from data collected in February 1976. Contour interval is 4 cm/sec.

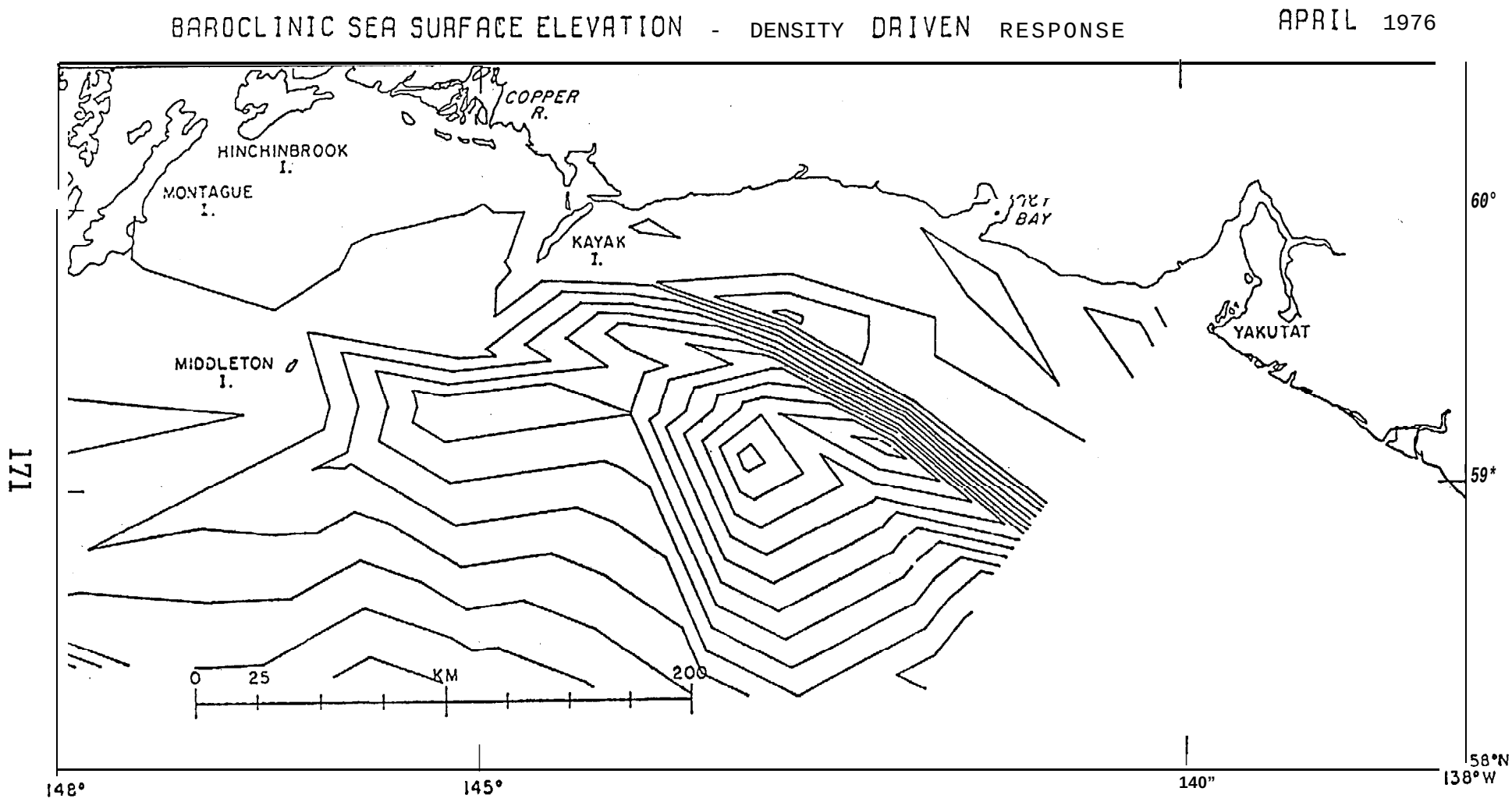

Figure 3-35. Sea surface elevation contours for Northeast Gulf of Alaska from data collected in April 1976. Contour interval is 4 cm/sec.

from deep water towards the slope (figure 3-36). As the gyre first encounters the bottom influence, pressure variations will be induced along the isobaths that the gyre is crossing. In particular, the center of its path will show higher pressure along any particular isobath than off to either the right or left. Under these conditions a careful examination of the $J(\alpha, d)$ term in equation (3-3) shows that the area to the left of the center line of the eddy must develop additional negative circulation, while the area to the right must compensate with the development of positive circulation. Putting these results together, the qualitative pattern must be deformed as is shown in figure (3-36). It is interesting to note that similar flow-bathymetry interactions have been described by Csanady (1978) under somewhat different initial conditions and referred to as arrested barotropic waves.

A close examination of figures (3-29) through (3-35) reveals that many of the eddies present appear to be compressed along the continental slope and show the characteristic extension to the east that is suggested in figure (3-36).

Offshore of the NEGOA shelf region mesoscale eddies commonly occur in deep water. As they encounter the continental slope they are dynamically modified through the action of the joint baroclinic - bathymetric term in the vorticity balance. When this happens, the onshore edge of the eddy is significantly compressed with a subsequent intensification of the currents. As this develops, a characteristic flattened loop pattern appears, which in extreme cases will appear as a banded pattern. This is a region where potentially strong currents may be expected over the shelf and shelf break region. From the NEGOA data it appears that these eddy related shelf edge currents do extend over the shelf break, at least in certain areas - in particular, SE of Middleton Island, SE of Kayak Island and SW of Icy Bay. The prediction, in even a statistical

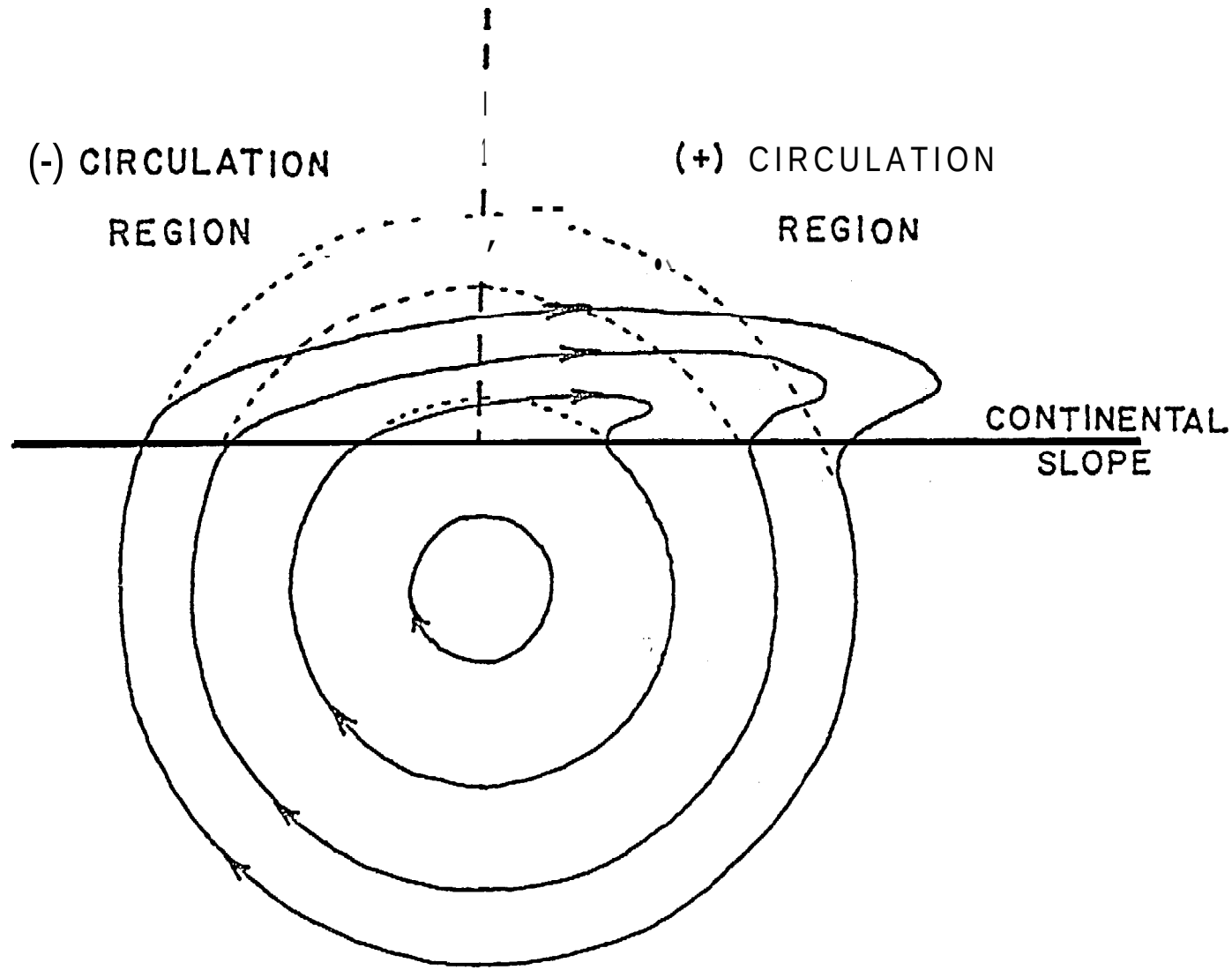

Figure 3-36. Representation of a deepwater mesoscale eddy and its deformation as it dynamically interacts with the continental slope.

sense, of these current patterns must be coupled to a more complete understanding of the distribution and movement of these offshore mesoscale eddies.

3.5 Composite Current Patterns

The total currents for the Northeast Gulf of Alaska will be represented by a simple linear superposition of the wind response component and the density driven response. How these are combined and what sequences are chosen to represent particular climatological periods depends on keying strategies which will be the subject of other NEGOA studies. The important point to be made here is that given the model dynamics, bathystrophic wind set-up, weather types and specific density fields, the totality of all possible, consistent current patterns is represented by the patterns shown here.

3.6 REFERENCES

Bakun, A. (1973): Coastal upwelling indices: West coast of North America. NOAA Tech. Report, NMFS SSRF - 671, 103 pp.

Beardsley, Robert C. and Bradford Butman (1974): Circulation on the New England continental shelf: Response to strong winter storms, Geophy. Res. Letters 1 (4), pp 181-184.

Csanady, G.T. (1978): Arrested Topographic Wave, J. Phy. Oc. 8(l), pp 47-62.

Favorite, F., A.J. Dodimeand and K. Nasu, (1976): Oceanography of the Sub-arctic Pacific region, 1960-71. Bull. Int. N. Pac. Fish. Comm., 33, 187 pp.

Galt, J.A. (1975): Development of a simplified diagnostic model for the interpretation of oceanographic data, NOAA Tech. Report ERL 339-PMEL 25 NOAA, U.S. Department of Commerce, Wash. DC, 36 pp.

Galt, J.A. (1976): Circulation studies on the Alaskan continental shelf off the Copper River, NOAA, U.S. Department of Commerce, Wash. DC, 46 pp.

Galt, J.A. and Thomas C. Royer (1975): Physical oceanography and dynamics of the NE Gulf of Alaska .Proceedings of the Symposium on Science, Resources and Technology in the Gulf of Alaska, Oct. 16-17, 1975, AINA

Galt, J.A., and Glen Watabayashi (1978): The linear decomposition of a diagnostic shelf circulation model and discussion of alternate boundary condition formulations, NOAA/ERL/PMEL (Draft Tech. Report),

Harm, Greg (1978): Diagnostic Model of Water and Oxygen Transport in the New York Bight. NOAA professional paper - Oxygen Depletion and Associated Mass Mortality in the NYB, 1976. Editor, R.L. Swanson.

Hayes, S.P. (1979): Variability of currents and bottom pressure across the continental shelf in the Northeast Gulf of Alaska, Journal Phy. Oc. (in press).

Hayes, S.P. and J.D. Schumacher (1976): Description of wind, current and bottom pressure variations on the continental shelf in the Northeast Gulf of Alaska, from February to May, 1975. JGR 81 (36), pp 6411-6419.

Hsueh, Y. and Chich Yuan Peng (1978): A diagnostic model of continental shelf circulation. JGR 83(C6), pp 3033-3041.

Overland, J.E. and Thomas R. Hiester (1978): A Synoptic Climatology for Surface Winds Along the Southern Coast of Alaska. NOAA/ERL/PMEL, Tech. Report (draft).

Pedlosky, J. (1974): Longshore currents, upwelling and bottom topography, Jour. Phy. Oc. 4(2), pp 214-226.

Putnins, P. (1966): Studies on the Meteorology of Alaska, Environmental Data Service, Silver Spring, MD, 90 pp.

Reynolds, R. Michael, Thomas R. Hiester and S.A. Macklin (1978): Coastal meteorology of the Gulf of Alaska, Icy Bay to Yakutat Bay, PMEL/ERL/NOAA, Tech. Report (in press).

Royer, T.C. (1975): Seasonal variations of waters in the northern Gulf of Alaska, DSR 22, pp 403-416.

Royer, T.C. (1978): On the effect of precipitation and runoff on coastal circulation in the Gulf of Alaska, J.P.O. (in press).

Royer, T.C., Donald V. Hansen and David J. Pashinski (1978): Coastal flow in the Gulf of Alaska as observed by dynamic topography and drogued drift buoys, (draft manuscript).

Watabayashi, G. and J.A. Galt (1978): A finite element solution technique for a diagnostic shelf circulation model. NOAA/ERL/PMEL Tech. Report (in review).

Welander, Pierre (1956): Wind action on a shallow sea: some generalization of Ekman's theory. Tellus 9(l), pp 45-52.

4. Development of the Environmental Library

4.1 Introduction

The oil spill trajectory model was designed for the implementation of a batch mode program on the ERL-owned CDC 6600 in Boulder, Colorado. The disk space associated with this machine is partitioned into user areas on a public disk pack. The trajectory model and graphics elements were written and are stored in one user area and the data package was assembled and is stored in another area. The separation of these functions allows the model to remain relatively independent of region. By dedicating a user area to environmental data endemic to a given region such as NEGOA, standardized procedures and file names can be used without confusion caused by duplicity of file names or by storage limitations.

In addition to the role as storage bin, the data library acts as an interface between sundry data sources and the program. Thus the library must contain routines necessary to convert both field data from the meteorological grids and the diagnostic model, and time series data from current meter records and anemometer records into formats palatable to the trajectory model . Conversions required such details as fitting area data to proper grids, making hourly averages on time series, and compacting real formatted velocity pairs into integer words to reduce core requirements. The library also contains programs to plot vectors of field data and stick plots of time series used in the verification and interpretation of model results.

4.2 Model Design and Data Structure

The Boulder computer system has a number of attributes which influenced the model design and concomitant data structure requirements. These at-

tributes deserve consideration because future users may wish to modify the design to effectively utilize a different computing system or size of data set,

A major consideration in the model construction is the management of large numbers of words of data. For the NEGOA prototype model runs we needed; a) thirteen wind patterns (u and v) on a 40 x 20 grid; b) thirteen barotropic current patterns (u and v) on a 60 x 30 grid; c} two baroclinic current patterns (u and v) on the same grid; d) two current meter and two anemometer records (u and v) for ideally 90 days, 24 per day; and e) two pattern sequences for 90 days and twice per day. These sum to approximately 92,000 decimal words of data. Th:e standard available core at Boulder is 256,000 octal or approximately 89,000 decimal words, Since the number of words is over the normal machine limit and since we must also allow for program core and other space requirements, we cannot load the entire data set at once in this format. Thus we must consider some alternatives.

In some systems, random access disk files could be used with a simple look-up algorithm added to the model program. This method would avoid loading the pattern data into core more than a few words at a time. 1/0 requirements would increase only moderately since random access reads are usually efficient. The Boulder facility does not have a random access capability so we are constrained to sequentially accessed files.

The costing algorithms on many machines are based on per second useage of the various systems resources including CPU time and 1/0 time. The Boulder system has relatively low I/O time limits and costs are high for 1/0 because the system runs near saturation. These factors eliminate the possibility of manipulating sequential files through repeated FORTRAN reads and rewinds at Boulder.

Another possibility for dealing with the mass of data is to reduce the size of the data set. There are a couple of alternatives. One is to reduce the number of words required to run the model by only loading those sets actually employed for a given model run. This was considered unacceptable since it meant reassembling the data set for every run, a cumbersome and error inducing exercise at best. A second alternative is to reduce the number of words required by simply packing the data. An asset of a CDC computer is it's word size; an integer word can have up to ten characters. We took advantage of this by packing the two velocity components into one integer word for each grid point of the field data and time step of the series. The core requirements were approximately halved which brought the program well within machine core limits. The disadvantage of this method is that the data must be unpacked as needed for each calculation. The method we chose was straightforward (described in the following section) and moderately quick (total model CP compilation is-3.5 seconds plus on the order of 20. seconds execution time per trajectory run, exclusive of plotting),. Other packing algorithms may be more efficient, but not others were explored since this one worked so well.

4.3 Interface Programs

Because every source seems to introduce its own problems, the number of interface programs appears to be proportional to the number of different types of data that are to be used. The routines presently available are described in this section and are abstracted in Table 4.1. The name of the procedure file which runs the program follows the program name in parentheses. The data files they call or create are summarized in Table 4.2,

The diagnostic model output includes surface u,v pairs and three vertex numbers for each triangle, and for each vertex number the location is given in a km based scaling system. The program REGRID (RUNGRID) decodes the position of the vertices into latitude and longitude. Then it maps u and v onto a regular grid by finding which triangle contains each point and assigning the associated triangle u and v to the regular grid point. If no data exists for a given grid point, then -999. is the value given u and v. No smoothing or interpolating is done. The output records contain I, J, U, V, and the triangle number and have the format (1X,2I5,2F10.3,I5). The output files are named either BOCnnmm for baroclinic runs where nn is year and mm is month, or RHINGEn for the barotropic single hinge cases where n is the case number.

The wind fields are recorded as wind speed and direction. The program MODWIND (RUNMOD) copies the case number and title for the wind case and then computes u and v at each grid point. If no data exists for a given grid point then 999. is the value given u and v. The output contains first a record with the case number and title with the format (1X,F3.1,6X,7A10), then the remaining records contain I, J, U, V and a sequence number and the format is (1 X,2I5,2F10.3,I5). The output files are named WINDnn, where nn is the case number multiplied by ten.

The program SUMGRID (RUNSMGD) needs to be implemented to make the summed barotropic fields described in section 3. The inputs are the barotropic single hinge cases RHINGEn. The coefficients are supplied by means of a data statement which must be offered for each summed field run. The output is in exactly the same format as REGRID output. The output files are called BWPnn where nn is the case number without the decimal point of the corresponding wind field.

It is important to verify the velocity fields before trying to make trajectory calculations, so a routine called PLOTVEC (RUNPLOT) was written to draw vectors on the same scale background as the trajectories. This routine can use any of the field data files as input since they are all formatted the same (BOCmmnn, RHINGEn, BWPnn, and WINDnn). The operating requirements are two-fold. The sense switches in the data statement at the beginning of the program must be properly set for either the current or wind case. Instructions for this are located in comment cards adjacent to the data statement. Also the title must be entered in a data statement. For the current runs the title must be supplied and for the wind runs the title must be set to blanks. The output of these runs are CALCOMP type plot commands. Examples of these plots can be seen in sections 2 and 3,

The final effort for preparing the field data for the trajectory model is the packing of the u, v pairs into integer words. This is accomplished by REPACK (RUNPACK). Each velocity component is rounded to the nearest tenth, multiplied by ten, fixed as an integer and added to a positive increment. This increment is chosen so that the entire set of numbers will be positive. Then both the integer versions of u and v are written into one word by multiplying the u value by twice the increment and adding the v value. As an example, for the NEGOA currents we used an increment of 5000, so the effect was to take UU.u and VV.v and make 5UUu5VVv an eight digit integer word. For the winds we used an increment of 500 so we made six digit words. If u and v were -999., then -999 was stored in

the integer word. The output records were written 1018 for the currents and 1016 for the winds. Instructions for setting the sense switches for either the current or wind case are located in comment cards at the beginning of the program. The output files are called WNDnn for the wind cases, and CURmmnn for the baroclinic currents, and CURnn for the barotropic currents. The thirteen NEGOA wind files were appended through a systems routine into one file called WINDXY for the trajectory model read. The order of the cases is just the numerical order of the pattern numbers. Similarly, the thirteen barotropic current files and the two baroclinic current files were appended into one file called CURRXY in the numerical order of the case numbers for the barotropic fields, followed by the chronological order for the baroclinic fields.

The next major undertaking is the treatment of the time series data. The program MAKECUR (RUNCUR) reads data from current meter tapes supplied by the Coastal Physics group from PMEL, averages the data automatically over every hour (not a running mean) and writes records containing date, time, u, v and a counter with the format (1X,A10,A5,2F8.3,I5). The output file names are CURnnl where nnl is the current meter station number.

The routine CONVOL (RUNCVL) makes running averages of any specified length on time series data. It calls files like CURnnl and writes files like FCRnnl with the same format.

The program STICK (RUNSTIK) makes stick plots of current time series data. It can attach either CURnnl or FCRnnl type files and outputs CALCOMP type plot commands. Examples of these plots can be seen in section 2. This program requires a reasonable effort on the operator's part and some prior knowledge of the data set, since the titles and date cutoffs need to be present at the beginning of the routine.

Following a similar sequence of preparation as with the pattern data,

we are now ready to pack the current meter data. Program PACKET (RUNPKCM) stores the u, v pairs as a single integer word in the same method as discussed in program REPACK. The output of PACKET is written on CURMnn, where nn is an abbreviated current meter label. The format of the output is 818.

The Middleton Island wind data came from a card deck supplied by the Institute of Marine Sciences (T, Royer). The card image file was given the name MIDISX. Program RDMISIS (LOADAT), converts from speed and direction to u and v, linearly interprets between data points to fill in gaps in the record, and packs the u, v pairs into single integer words. The output is written in 1216 on the file called WMIlkm, where k is the beginning month, l is the ending month, and m is the year, as in 197m. The integer sequence of wind patterns was appended to the end of WMklm and was stored in 3012 format.

The remaining function of the library is to help with the interpretation of the trajectory model results. A second version of the stick plot routine, STICK2 (RUNSTK2), was written to plot up time series like output from the trajectory model. The output file contains records of u, v pairs of the following quantities: the observed current at some station; the observed winds at Middleton Island, the baroclinic current at the spill, the total simulated current at the spill, and the total simulated wind at the spill. These records are written in 10F8.3 format. STICK2 reads these for one trajectory sequence and outputs CALCOMP type plot commands. This version of the stick plot routine is much more automatic than the other, since titles are consistent from run to run and the time axis progresses as hours since the beginning of the spill instead of being fixed to some particular dates. Examples of this type of plot can be seen in section 6.

4.4 Selection of the Prototype NEGOA Model Runs

The two study choices for NEGOA are July-August 1974 for a summer case and February-March 1975 for a winter case. Weather pattern maps were available from January 1974 through December 1975. The maps for 1976 have been ordered but were not available for weather typing for this report. The Middleton Island wind data is available for 24 May 1972 through 31 January 1977. CTD data for running the baroclinic cases of the diagnostic model were available for the following dates: July, 1974; February, 1975; June, 1975; October, 1975; February, 1976; and April, 1976. The latter three of these cases were not completed in time to be considered for the trajectory calculations because of difficulties experienced in obtaining the data sets. These problems have been detailed in previous reports.

The availability of CTD data limited our trajectory cases to three possible choices: summer 1974, winter 1975, and summer 1975. Current meter station 60A chronologically coincided well with the July 1974 CTD data set. Current meter station 62B fit well with the February 1975 CTD data set. Current meters 62C and 64 came before the June 1975 CTD data set and 62D came after. Thus the two best choices are February-March 1975 and July-August 1974. It should be noted that these cases are not representative of all possible winters and all possible summers. They are two particular seasonal cases and, as such, only represent the conditions in their own years.

TABLE 4,1
INTERFACE PROGRAM FILE DIRECTORY

File Name (Procedure File Name)	Description	Input File(s)	Output File(s)
REGRID (RUNGRID)	Finds u,v on rectangular grid from diagnostic triangular mesh	(Diagnostic model output files)	- BOCnnmm - RHINGEn
MODWIND (RUNMOD.)	Converts speed and direction to u,v for wind field	TYPEnn (card images)	- WINDnn
SUMGRID (RUNSMGD)	Sums single hinge diagnostic fields according to wind case	RHINGEn	- BWPnn
PLOTVEC (RUNPLOT)	Plots vector field over scaled area	WINDnn BOCmmnn BWPnn RHINGEn	- (plot files)
REPACK (RUNPACK)	Packs field data from real u,v pairs into single integer words	WINDnn BOCmmnn BWPnn	- WNDnn - CURnnmm - CURnn
MAKECUR (RUNCUR)	Chooses current meter data from tape and makes hourly averages	(Data tapes from Coastal Physics)	- CURnnl
CONVOL (RUNCVL)	Makes running averages on time series data	CURnnl	- FCRnnl
STICK (RUNSTIK)	Makes stick plots from time series data	FCRnnl CURnnl	- (plot files)
PACKET (RUNPKCM)	Packs current meter data from real u,v pairs into single integer words	CURnnl	- CURMnn
RDMIDIS (LOADAT)	Fills gaps in wind record and packs data from real u,v pairs into single integer words	MIDISX (card images)	- WMklm
STICK2 (RUNSTK2)	Makes stick plots of model data output	VELSTnn	- (plot files)

TABLE 4.2
DATA FILE TYPE DIRECTORY

File Name	Description	Format
RHINGEn	Diagnostic model barotropic field based on hinge numbered n. (I, J,U,V, ITRI)	(1X,2I5,2F10.3 ,I5)
BOCnnmm	Diagnostic model baroclinic field based on CTD casts taken MONTH mm, YEAR nn (I, J,U,V, ITRI)	(1 X,2I5,2 F10.3,I5)
BWPnn	Diagnostic model barotropic field based on RHINGEn files due to wind case nn (I, J, U,V, ICOUNT)	(1 X,215,2 F10.3I5)
WINDnn	Meteorological field data for case nn (I, J,U,V, ICOUNT)	(1 X,2I5,2 F10.3,I5)
WNDnn	Meteorological field data for case nn (W(I,J))	(10I6)
CURnn	Barotropic current field data for case nn (V(I,J))	(1018)
CURnnmm	Baroclinic current field data for case nnmm (V(I,J))	(10I8)
CURnnl	Current meter data from station nnl (DATE,TIME,U,V,ICOUNT)	(1X, A10,A5,2F8.3,I5)
FCRnnl	Filtered current meter data from station nnl (DATE, TIME, U,V, ICOUNT)	(1 X, A10,A5,2F8.3 ,I5)
CURMnn	Packed current meter data (V(t))	(8I8)
WMI1km	Packed wind series from Middleton Island (V(t))	(12I6)
VELSTnn	Model output for plotting time series (U1,V1 ,U2,V2,U3,V3,U4, V4,U5,V5) (see text for description)	(10 F8.3)

TABLE 4.3
AVAILABLE DATA SOURCES

Date	Weather Pattern Maps	Middleton Island Wind Data	CTD Data for Diagnostic Model Runs	Current Meter Records
1/74	*	*(24 May 1972)		
2	*	*		
3	*	*		
4	*	*		
5	*	*		
6	*	*		60A *
7	*	*		*
8	*	*		61 *
9	*	*		*
10	*	*		62A *
11	*	*		
12	*	*		
1/75	*	*	*	*
2	*	*		62B *
3	*	*		*
4	*	*		64 *
5	*	*		62C
6	*	*	*	
7	*	*		
8	*	*		62D *
9	*	*		
10	*	*	*	
11	*	*		
12	*	* (31 January 1977)		

5. Time Series Simulation and Validation

The model elements up to this point include arrays of wind and current velocities and a time series that sequences the wind and current patterns. The wind and current velocity arrays were derived using both physical insight and numerical models. In the case of the diagnostic model, for example, physical insight was used to simplify the dynamics of the modeled system. This simplification resulted in a set of equations that was amenable both to linearization and numerical solution. Both facets of this dynamical simplification were exploited in the solution technique. The wind field, in a similar fashion, was initially analyzed numerically using highly approximate formulas incorporating very simple dynamics, It was then modified using both experimental observations and the results of numerical studies of wind impinging on an idealized coastline. Finally, the sequence of wind patterns was determined by a variety of means, including some simple statistical methods, an examination of the surface wind observations from Middleton Island and EB33 and consideration of regional influences on the large scale baric patterns.

The idea underlying all this work was that the resultant product was to be used to calculate oil spill trajectories. Because of this goal, we considered both the requirement that the wind and current velocities be specified over space and the requirement that the temporal variability of these fields be modeled. In our judgement, the elements discussed up to this point represent the limit of state-of-the-art, deterministic techniques for achieving these goals. It now remains to be shown whether the model elements do, in fact, resemble the physical world. And, as a related task, we need to characterize statistically those departures between the model and the real world. These departures will both qualify the trajectory

results and identify the main priorities for subsequent work.

Because the principal dynamical omission in the current model was the acceleration term, and because the wind pattern typing was based on the idea of persistence, which is an obvious approximation, it is natural to consider the departure of actual time series observations from the modeled time series. It would be most desirable to do this at a variety of locations within the region, thereby providing a spatial dimension to the time series departures. However, we were limited in this study by the availability of wind and current observations. As we pointed out in the library section, the summer case includes "one station each of wind and current measurements, and the winter case includes two anemometer stations and one current meter station (both seasons, of course, also include complementary hydrographic measurements). This is hardly an overwhelming empirical" basis on which to judge the model elements. Further, these data are not independent of the model results as the winds, at least, were used in the weather typing. Thus, we are limited to characterizing the model departure at single points in the region, and these characterizations are not easily analyzed statistically due to the interplay of data and the selection of model parameters.

Figure 2-5 through 2-7 showed the average wind velocity (a vector quantity) for Middleton Island and EB33 as sorted by pattern type. The Middleton Island data, Figures 2-5 and 2-6, readily suggest that the directional specification for the wind patterns is very good for the majority of cases at Middleton Island. We have not calculated the statistical confidence limits for this direction parameter. This is due in part to the fact that the direction statistic is of a complicated functional form. More important than this functional complexity, however, are the facts that the time series data is not a sequence of independent values, but rather it exhibits correlations over considerable time lags; and the fact that this data was considered

in the pattern selection. These make analysis difficult. However; it is our subjective judgement that the correspondence shown in Figures 2-5 and 2-6 is not simply fortuitous. We believe it reflects a firm linkage between the model and the real world.

The EB33 data, on the other hand, is not so supportive of this assertion, Figure 2-7. However, even here we can see some tendency in the angular departures for the wind field to be flattened along the axis of the coast. The fact that the perturbations exhibit a pattern of this type is suggestive that the model is related to the observations, but that some unknown factor has entered the problem. There is no simple explanation for the phenomena, but further study may reveal the cause of this deviation. It might be a simple artifact in the sea surface pressure field, or it might represent some complex meteorological phenomena; both avenues should be explored. In the meantime we believe that this result simply implies our patterns are slightly off and not that the typing procedure is in question.

It is generally accepted that the higher frequency perturbation in the wind will be proportional to some longer time average of the wind. In the case at hand, the good correspondence in average wind direction shown in Figures 2-5 and 2-6 suggests that we might decompose the hourly perturbations into components lying along the pattern vector and normal to it. If the pattern changes, then we can consider a decomposition along a series of direction pairs that evolve linearly from the initial pattern direction to the subsequent pattern direction. If we then assume that the perturbations are nearly independent over several hours, it is possible to estimate the pattern amplitudes at the beginning and end of the transition using centered wind velocity averages at the time of the pattern measurement. With these assumptions, it is possible to attempt to further decompose

the variance associated with the sorted wind categories based on the amplitude and direction properties. This decomposition is illustrated in Figure 5-1.

The hypothesis underlying this decomposition is that the wind is composed of both a low frequency component that is measured by the sea surface pressure maps, and a higher frequency component that is superimposed on the fundamental flow. This higher frequency component should exhibit low time-wise correlation if our amplitude estimating technique is to be valid.

A simple test of this hypothesis was performed. The variances of the along and normal-to perturbations measured as in Figure 5-1 are shown plotted against the low frequency wind amplitude in Figures 5-2 and 5-3. Both summer and winter cases are shown. Notice that no dependency is suggested for the summer case, but that a strong dependency appears in the winter case. We suspect that the summer case variance is a measure of the intrinsic variability associated with the measurement technique. It might, for example, be associated with high frequency aliasing of the anemometer record. The winter case variance, however, is seen to grow with pattern strength. This variance may well be due to important meteorological phenomena that are of too small a scale to be resolved in the analysis underlying the sea level pressure maps.

We also examined the covariance between these perturbation components and found them to be uncorrelated. The principal axis of the perturbation was, therefore, in the normal direction (since this had the larger variance in both spring and summer) and the minor axis lay in the direction of the smoothly rotating wind pattern vector.

We know from Figures 2-5 and 2-6 that the average of the normal perturbation must be nearly zero for each of the wind patterns at Middleton Island.

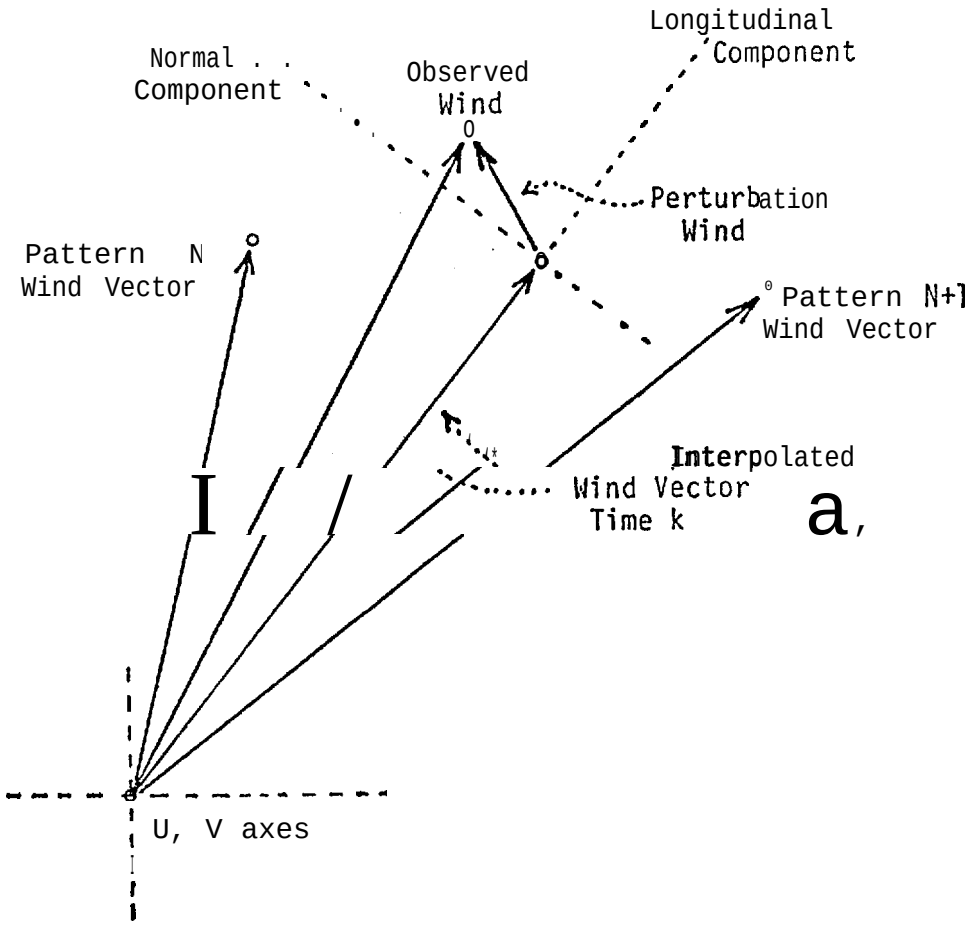

Figure 5-1. Vector plot of relationship between model predicted winds, measured winds and wind perturbation.

Figure 5-2. Variance of the Longitudinal Wind Velocity Perturbations.

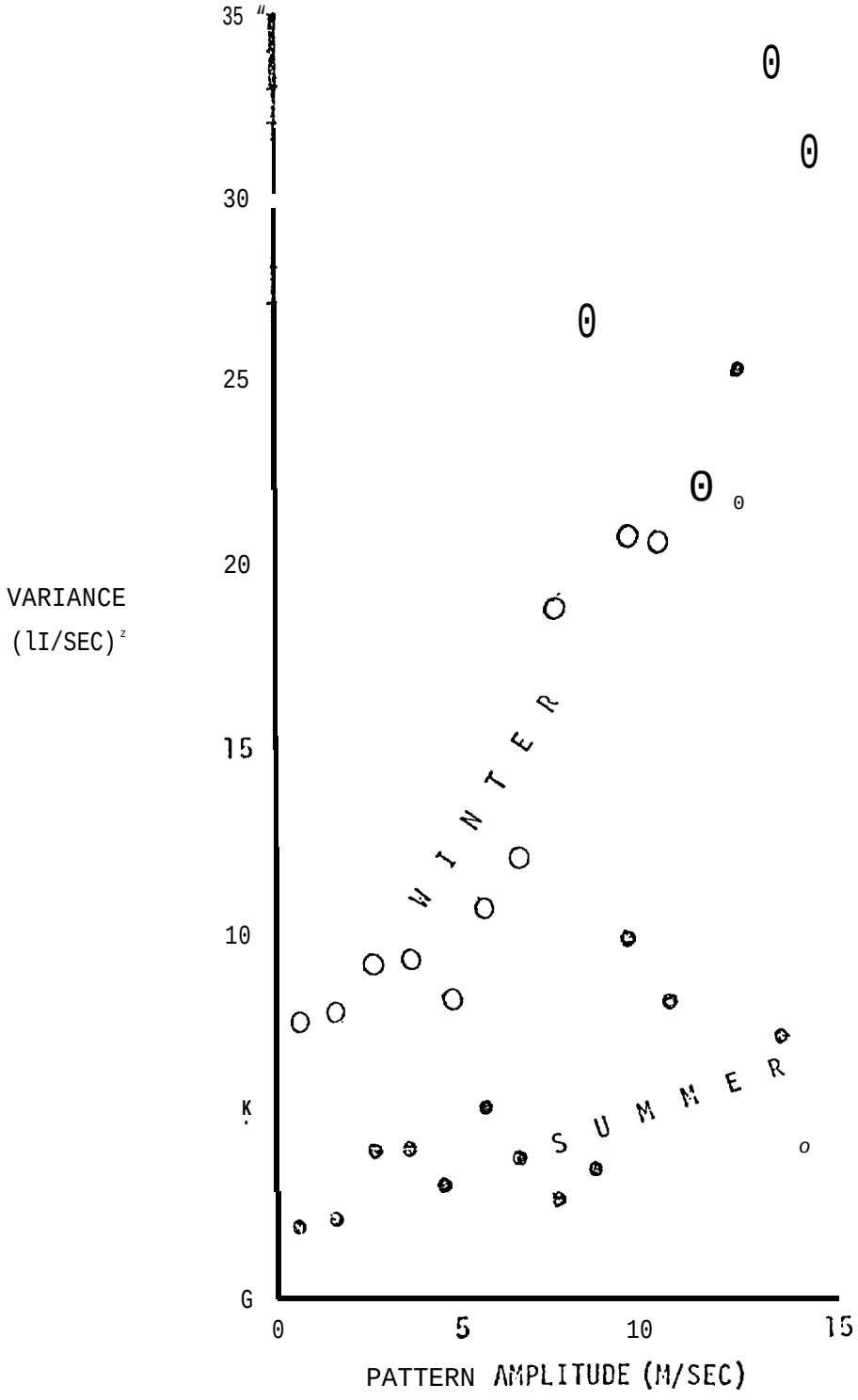

Figure 5-3. Variance of the Transverse Mind Velocity Perturbation.

If they exhibited a nonzero average of large magnitude, the vector averages would not lie in the vicinity of the pattern direction. The existence of large non-zero averages may be considered evidence of bias in the wind field patterns. Figure 5-4 shows the average of the along and normal-to perturbations as a function of low frequency wind amplitude. The summer case shows no important bias over the range of wind speeds studied. The winter case, however, suggests that the pattern vectors are rotated too far to the right by 5° or 10° at wind speeds of around 10 m/see. Again, a statistical interpretation of this result -is very difficult. We have sketched the 1σ confidence intervals assuming the data is independent. In fact, the zones should be larger. Nevertheless., the strong pattern shown in the figure leads us to believe that this result is significant, and it therefore merits further study.

We also examined the time-correlation of the along and normal-to perturbations. The correlations of the dimensional perturbation velocity components were very similar to those found in first order autoregressive processes. Typical time scales were on the order of 2½ hours for the along components and 3.8 to 4.8 hours (summer and winter respectively) for the transverse component. When these perturbations were normalized by dividing by the pattern amplitude, the new variate showed almost no correlation over lags of one hour.

These observations suggest several things. First, the wind model can be considered a useful analog of the real surface wind. It is a practical solution to the problem even though we know it has imperfections. The data from EB33, for example, showed that the model may have errors in the specification of the wind direction that range from near zero to as high as 45°, with a typical estimate being 10^{o} to 15°. Errors of this type are

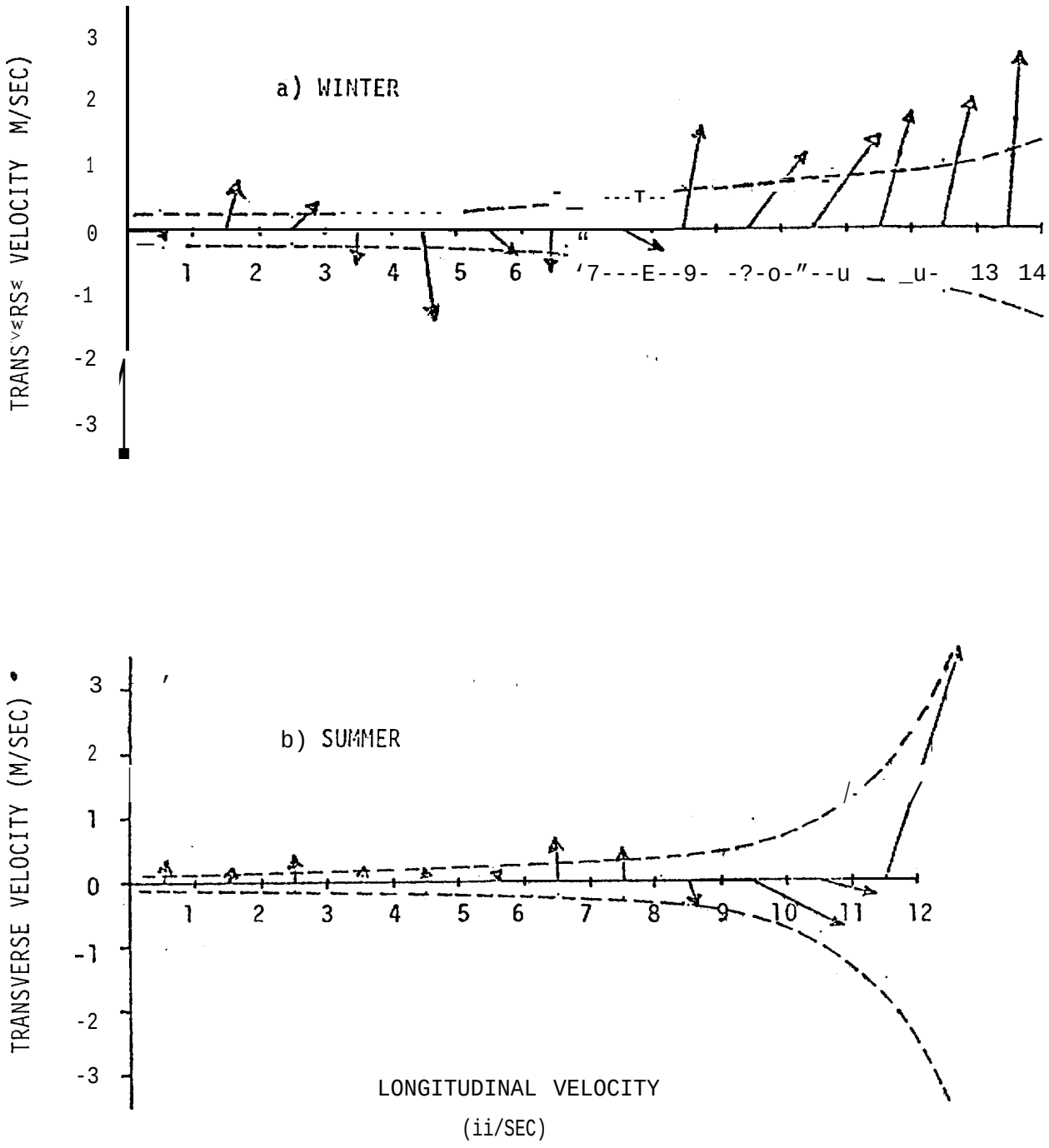

Figure 5-4. Observational Bias in the Wind Perturbation as a Function of Pattern Amplitude.

probably a function of position in the region., These nominal, and in principle correctable errors are to be compared with the much larger errors that would accompany a uniform direction model such as those used in past trajectory studies.

It is also apparent that a large portion of the wind velocity's variance can be explained by transitions between wind patterns. Further, the remaining variance can be explained in terms of longitudinal and transverse components with magnitudes that are proportional to the wind pattern strength in winter, and constant in summer. If this decomposition can be substantiated using other data sets in the NEGOA region, it presents the important possibility that the wind field could be completely synthesized using just the sea surface pressure maps. This would open the door to a true climatological analysis since the requisite pressure map data is available for very long periods of time,

We have not examined the relative amplitude information contained in the wind patterns. This analysis will require several simultaneous time series coupled with a more thorough understanding of the velocity perturbation problem including its spatial dependencies. It is a logical follow-on to the present study.

The current model was also examined. The important questions were whether the decomposition into barotropic and baroclinic geostrophic modes was justified; whether the assumption that the time variability was simply linked to the applied stress pattern; and whether these perturbations were well modeled by the transitions of barotropic modes.

Although our data base is rather limited, it appears that the decomposition into a baroclinic (and minimum barotropic) mode was a useful simplification. Figure 5-5 shows the long term, vector average current at stations 60 and 62B for the summer and winter seasons respectively. This

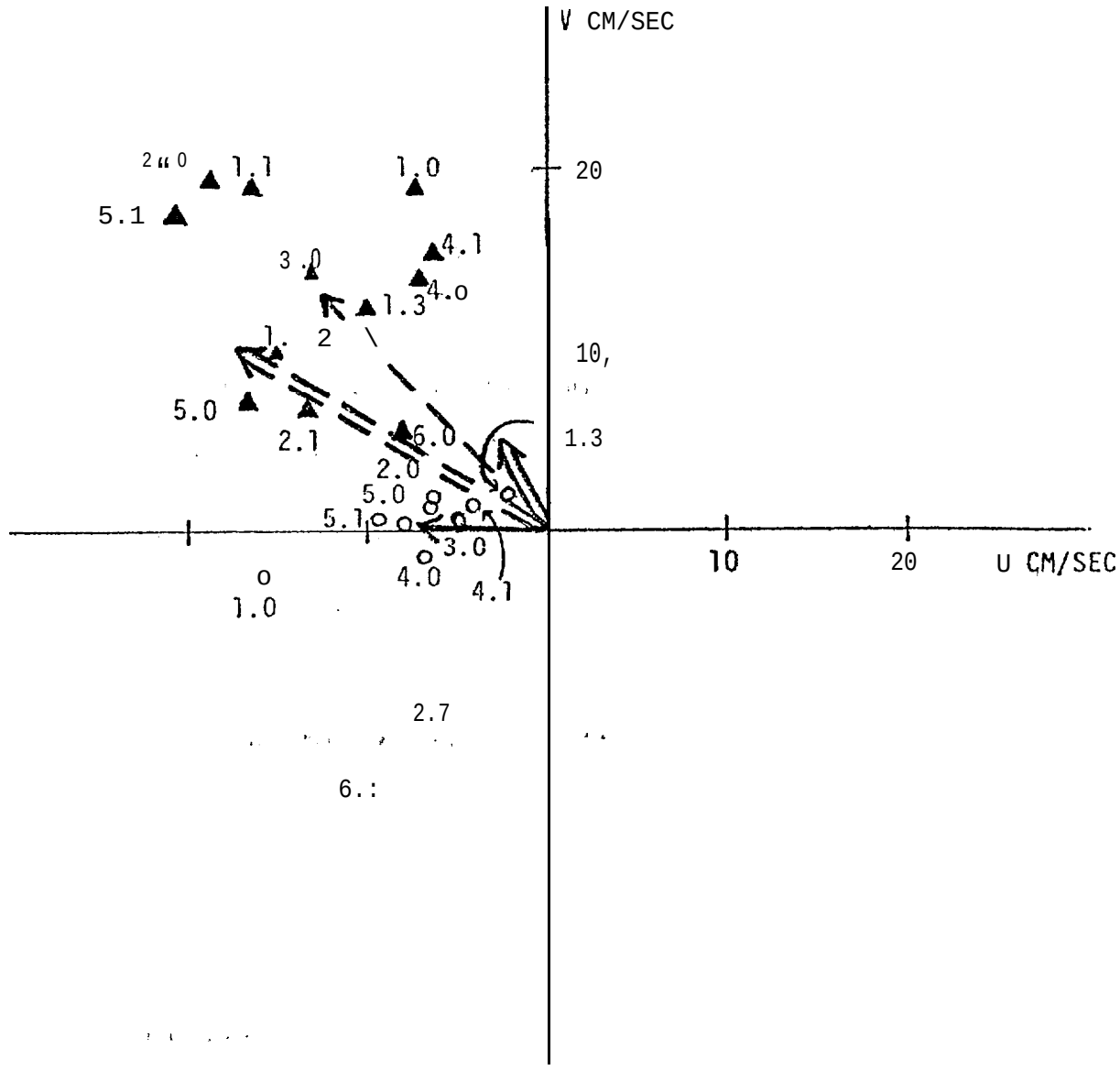

Figure 5-5. Comparison of observed currents by pattern type for winter station 62 (A) and summer station 60 (O). Single line and double line vectors represent the mean observed current and the barocli nic component respectively; dashed for winter, solid for summer.

long term average should correspond to the baroclinic mode under the assumptions that the density field is reasonably constant over the period in question and that the average, wind-driven barotropic component is nearly zero. This long term average current is also shown in Figure 5-5. It is readily seen in Figure 5-5 that the baroclinic current exhibits some angular error, with respect to the long term average current in both cases, with the most pronounced error occurring at Station 60, which is in the Copper River gyre. The error in direction at Station 60 might be associated either with the coarse resolution provided off the Copper River gyre by the hydrographic stations, or it might represent some net contribution from the wind-driven barotropic modes. Despite this angular error, however, we can see that the magnitudes of the baroclinic velocities are approximately correct for both cases. It is our judgement that these results are in sufficient agreement to warrant preliminary acceptance of the decomposition techniques.

The second question was whether the current perturbations could be usefully sorted based on the weather pattern. Figure 5-5 also addresses this question. It shows the average observed currents sorted by pattern type. The standard deviations for these averages were typically on the order of 1 to 3 cm/sec assuming the samples were independent. Correcting this range upwards to account for the probable correlation between samples, we find that the analysis does not support grouping of current observations by weather patterns, since all the groups are close to the overall mean current vector. We have also performed an analysis in which the currents lagged the wind patterns and found a similar lack of support for the simple wind-driven hypothesis. We believe this is caused by strong high frequency oscillations in the data associated with tidal motions, shelf waves, and other phenomena not considered in our model formulation.

Because the sorting by pattern type was not successful, it is premature to compare the individual barotropic current modes with the current meter observations sorted by weather type. A logical follow on to the present work would be to examine the filtered data to see both if it could be usefully sorted by pattern type and if the residual exhibits properties like those predicted by the barotropic modes.

For the purposes of the trajectory model it appears that we can reasonably expect the baroclinic currents to be well modeled. The remainder is best treated as a stochastic residual, It is not realistic to expect this residual to be constant over the spatial domain, Bottom topography and other effects will undoubtedly channel and amplify the perturbations. As an approximate, but theoretically somewhat justifiable approach, we therefore will use the barotropic response to scale and direct the perturbations. The exact algorithm is discussed in the following chapter.

6. Trajectories

In physical terms, the trajectory model is composed of several FORTRAN programs and a variety of data sets that depict the spatial and temporal variability of the wind and current. The main trajectory program, AMCTRAJ (Appendix G), calculates the boundary location of an oil spill given wind and current time series, wind and current patterns, and starting date and locations. The output from this program is then converted to graphical plots of the trajectories using the program PICTUR and loadsets specific to our plotting equipment. An auxillary output is also avialable from AMCTRAJ which can be used to generate the stick plots of the wind and current time series as seen at the wind and current stations and at the simulated spill.

The principal considerations for the design of the program AMCTRAJ were the storage requirements for the extensive spatial fields of the wind and current. Approximately 46,000 words were required for storage in the program. These problems were discussed above in the description of the environmental libraries. The numerical algorithm that uses these fields to calculate a simulated oil spill trajectory is relatively simple and will be described below. This functional portion of the program required a relatively small amount of core, about 24,000 CDC words.

The important conceptual function of the trajectory model is that it implements a number of hypotheses by which we synthesize the available environmental information into a simulated oil spill trajectory. Although the hypotheses relating to our description of the environment have been discussed separately in the various sections above, it is useful to reiterate them here.

1. We have assumed that the surface wind field can be related to large scale synoptic sea level pressure maps. The calculation of the surface wind field was done using accepted procedures, but it has not been verified for NEGOA with independent data, although preliminary results suggest reasonable correspondence. These maps are our only data incorporating both spatial and temporal variability.

2. We have assumed that the sea level pressure maps exhibit characteristic features with sufficient regularity that they can be approximated with a small set of generic patterns. Our preliminary analysis indicates that this assumption is probably acceptable.

3. We have assumed that the current field can be completely decomposed into barotropic and baroclinic geostrophic components. We explicitly neglect tidal and inertial currents, consigning all such currents to simulation via a scaled and rotated perturbation term.

4, We assume the baroclinic current field is constant throughout the simulation period. This is probably a rather weak assumption because there is much evidence suggesting the presence of transient mesoscale eddies along the shelf break.

5. We assume that the barotropic modes are established instantaneously and without lag in response to surface stress applied by the large scale wind pattern. We further assume that the magnitude of these currents will be proportional to the square of the surface wind speed (i.e., proportional to surface stress).

Within this heirarchy of assumptions, it appears that the wind related assumptions are the least suspect in so far as they appear to yield realistic wind behavior. The current assumptions, on the other hand, appear to be rather crude. Not surprisingly, perhaps, the baroclinic current appears

to be the best modeled current component. It fits the long term average current fairly well at stations 60 and 62B. This baroclinic component incorporates data from the quasi-synoptic hydrographic measurements in the region and so in a sense it is analogous to the derivation of the wind field from the surface level pressure. This is to say that the baroclinic current is based on a lot of data that can be combined in a dynamically consistent model. The barotropic current, however, had no directly measured input term, but was in fact calculated from the derived wind fields for the hypothesized generic wind field patterns. Being twice removed from actual data, it is not surprising that it was poorly substantiated by the current meter records.

Because of the poor state of our measurements of currents in the region, these hypotheses should not be judged solely on the basis of how wall they fit our very limited data. Hypotheses, in fact, are constructed mainly for the purpose of reducing the data required, and so any data-poor study must rely heavily upon assumptions in the form of hypotheses. The question then becomes whether the hypothesis was sufficiently simple to allow future verification and whether there was any theoretical basis for the hypothesis that might endow it with intrinsic credibility. In the case at hand, the assumption of non-inertial dynamics does allow the theoretical decomposition of the current problem into baroclinic and barotropic portions. There is good reason to suggest that these geostrophic components are important in the net transport problem. Further, the assumption is subject to easy validation given more extensive current meter records than those examined here. Thus, the assumption provides a practical first step towards grappling with the larger problems.

In addition to hypotheses regarding the synthesis of the environmental data, the model is also dependent upon an hypothesized oil transport equation.

It is beyond the scope of this report to detail the uncertainties we presently face regarding the mechanisms responsible for oil spill transport on the ocean. However, it should be pointed out that there is neither a substantial theoretical basis for the oil-on-water problem, nor is there a data base of sufficient size to suggest an empirical basis. In these circumstances we have simply assumed that the velocity of the oil will be given by the vector sum of the current velocity and three percent of the wind velocity. This is a formulation that is generally accepted and which has some empirical evidence to support it.

Figure 6,1 shows the method used to synthesize the local wind velocity. The surface wind fields were utilized to provide the relative magnitude and the direction of the local wind. The. absolute magnitude of the local wind was obtained from the time series data by comparing the twelve hourly centered average of the time series data to the wind field magnitude at the anemometer station. The factor formed from the ratio of these numbers was then applied to the local wind velocity. Thus, if the wind field showed a wind velocity of 12 m/see to the NW at the local coordinate, and if the nominal wind speed at the anemometer location was 10 m/see whereas the twelve hourly average was 5 m/see in the time series data, the wind field would be scaled by (5 ÷ 10), resulting in a modeled wind of 6 m/see to the NW at the local coordinate.

Hourly perturbations were then added to the scaled wind field velocity to simulate the higher frequency changes. These perturbations were calculated by first determining the differences between the hourly time series velocity and the scaled wind field velocity at the anemometer location. This perturbation was then resolved into components lying along and normal to the vector of the wind field velocity. These components were then scaled by the ratio

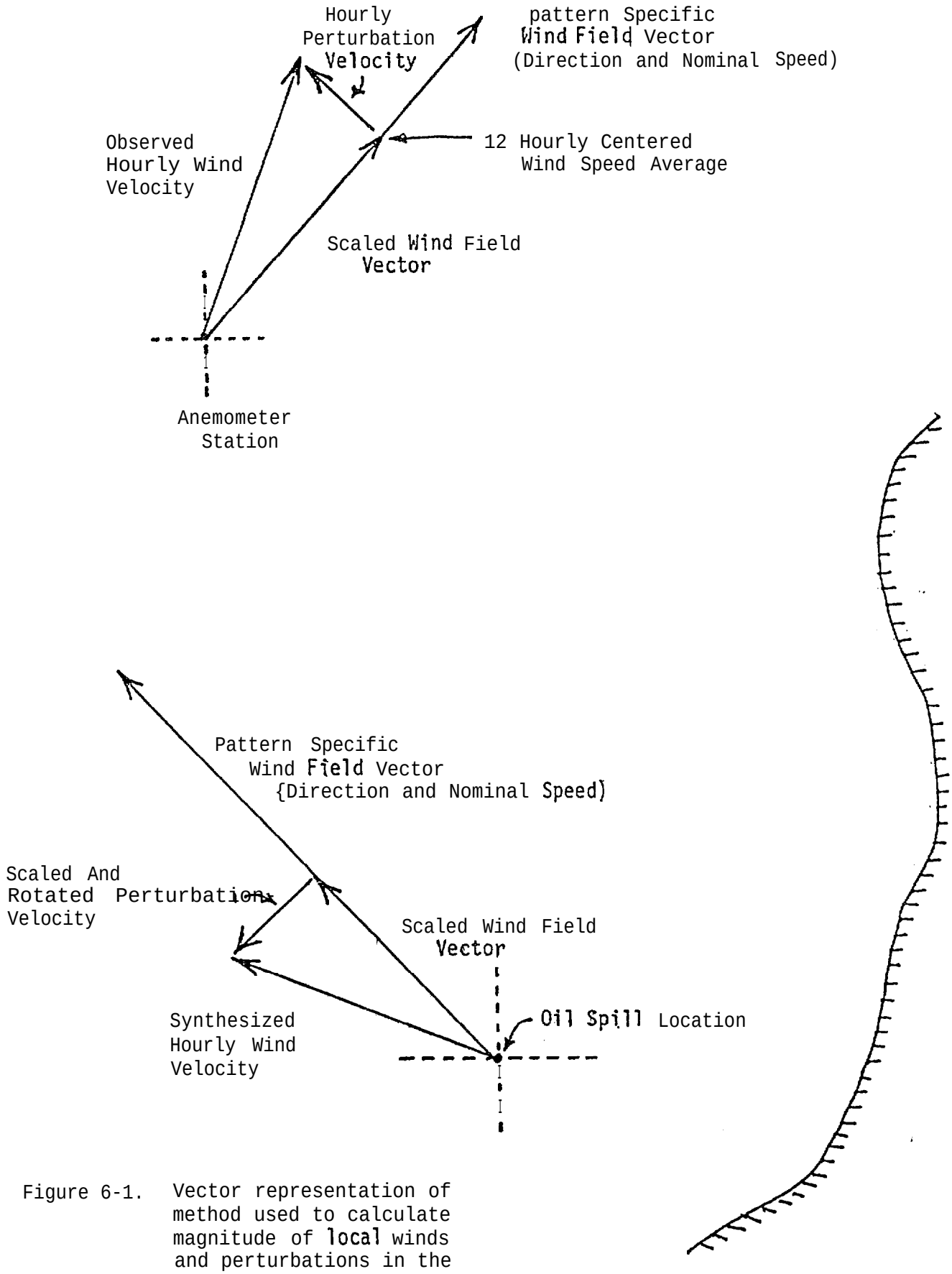

Figure 6-1. Vector representation of method used to calculate magnitude of local winds and perturbations in the wind field.

of the wind field speed at the local position and the wind field speed at the anemometer.' Finally, the perturbations were then added in the along and normal to direction relative to the local wind velocity. Thus in the example above a perturbation of 1 m/see lying to the left perpendicular of the wind field velocity at the anemometer station would be scaled by (12 ÷ 10) and added to the local velocity in the left perpendicular direction. In this case, the direction of the perturbation is towards the SW since the field velocity was to the NW, and the amplitude would be 1.2 m/see.

Figure 6-2 shows the technique used to synthesize the current velocity. This technique was related to that used for the winds. However, under the assumption of geostrophic motion, the dynamical balance governing the currents will require the perturbations to nearly follow the bottom topography. Although this quasi-steady 'assumption will not be valid for high frequency motions, we felt it plausible to require that the perturbations be oriented with respect to the axis of the barotropic current velocity. Therefore, the baroclinic component is first subtracted from the observed (hourly) current at the current meter location. A perturbation velocity is then determined by subtracting the barotropic current component from the residual. This perturbation is then resolved into along and left perpendicular components relative to the barotropic current direction. These perturbations are then added to the local barotropic current in coordinates rotated to coincide with the local barotropic direction. The barotropic current is scaled by the square of 'the wind field strength. The perturbation components are scaled by the ratio of the local barotropic current to the barotropic current at the current meter location. Thus periods of strong winds in the time series data will induce strong barotropic motion and locations with low relative barotropic current velocities will have correspondingly small current perturbations.

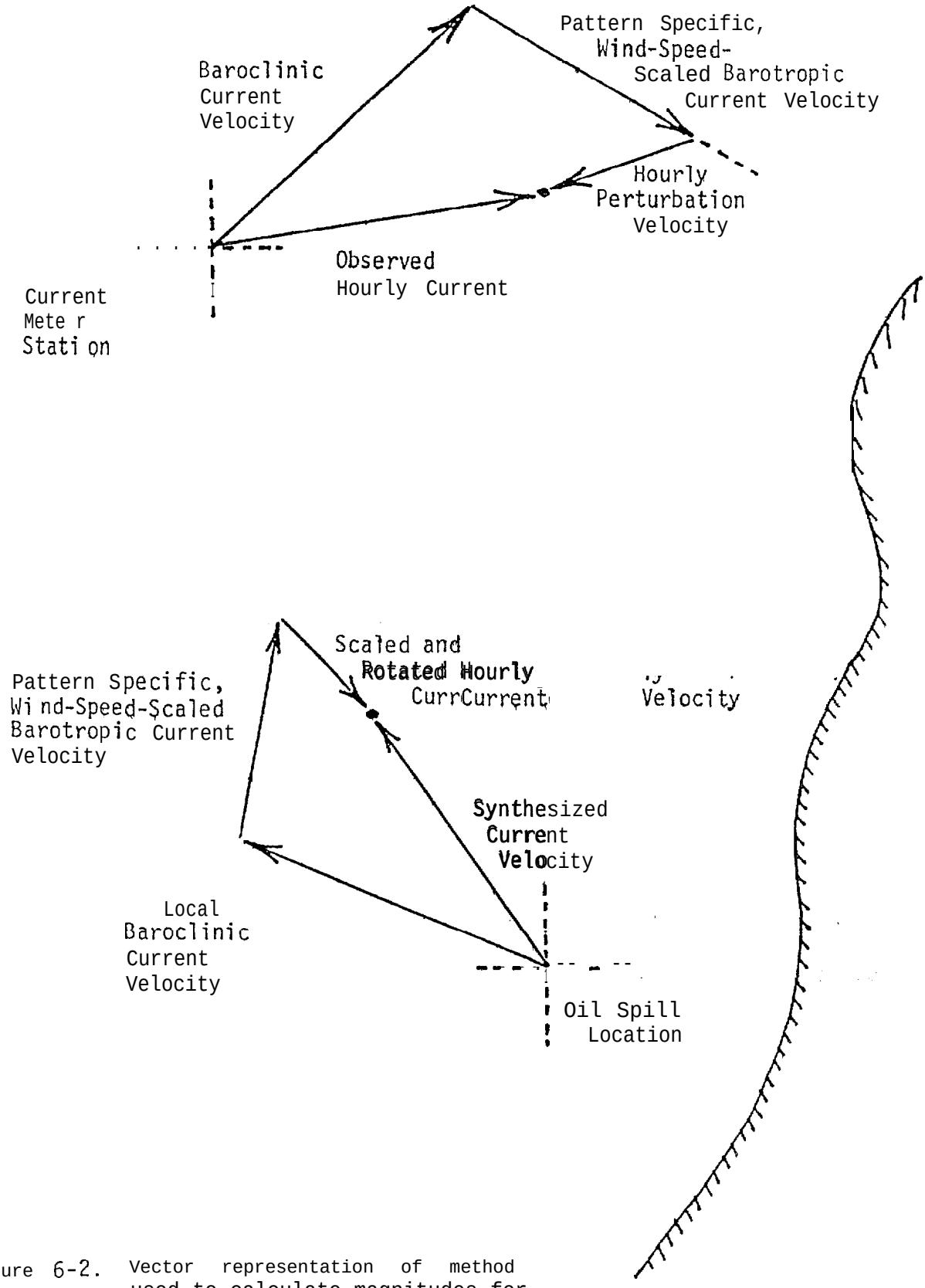

Figure 6-2. Vector representation of method used to calculate magnitudes for local wind-set-up currents and cumulative current perturbation velocities.

It should be noted that the perturbation incorporated into the wind set-up current mode is a measure of the cumulative errors that are seen in the entire current prediction process. Errors in the current meters, wind field typing errors, errors in the bathystrophic assumption, errors associated with the baroclinic current resolution and errors induced by the model dynamics are all lumped at this point. In this sense the perturbations are a measure of the total system errors and should not be associated with the single barotropic wind-set mode.

The combined model is now available to carry out trajectory analysis for the NEGOA region. For purposes of this demonstration seven release sites have been chosen (figure 6-3). A summer period of July and August, 1974 and a winter period of February and March, 1975 are investigated. At each site a release is hypothesized every five days and the trajectory is continued until it either exits the model or exhausts the two month study period.

The summer period will be considered first. The baroclinic data for this period was collected in July, 1974 and is described in section three of this report. This component of the flow is dominated by the mesoscale currents induced by eddies along the continental slope. On the shelf proper the baroclinic currents are generally weak, but the anticyclonic gyre to the west of Kayak Island is evident, The winds for the period are usually weak with types 4 and 5 present throughout the record. The perturbations in the currents are obtained from NEGOA current station 60 which is located just off shore from the Copper River. It is useful to note that this is an area where the predicted currents are quite weak and variable. Since these observations will determine the scale and relative directional stability of the predicted currents throughout the model we can expect that the choice of this current meter as a keying station will lead to a relatively

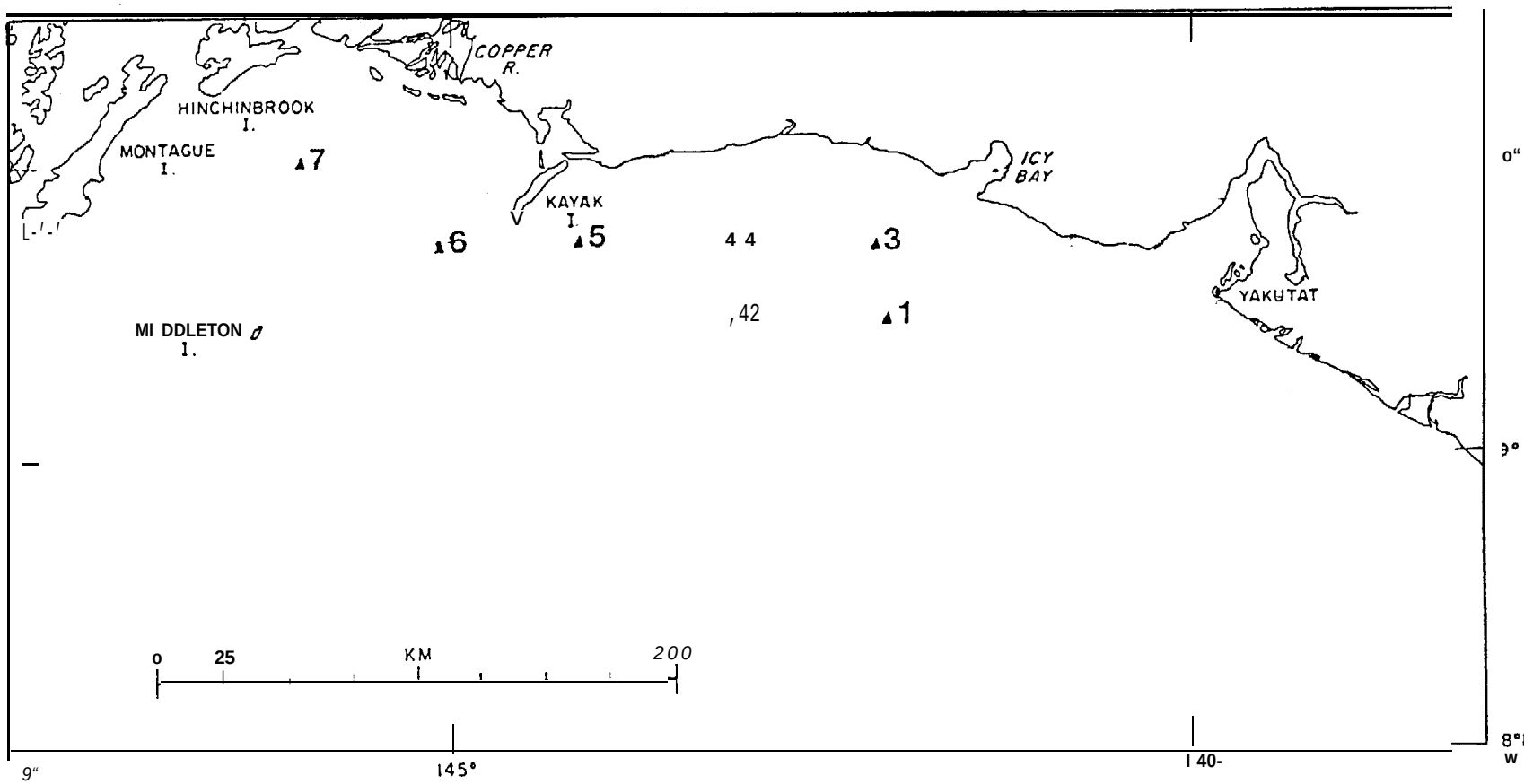

Figure 6-3. Chart of release sites for NEGOA trajectory studies.

high level of uncertainty. This will be reflected in the trajectories as increased scatter. In retrospect, current station 60 would not be considered an optimal choice and had model results been available prior to deployment alternate locations should have been considered. Despite the problem of this station placement it should be clear that the model results will still be correct within the context of the formulation and accurately represent the uncertainty inherent in the input data.

The trajectories from release location one are shown in figure 6-4. This release point is located on the outer continental shelf southwest of Icy Bay. From this point the trajectories are seen to move towards shore with a potential threat to about 150 km of the coastline. Over this region of shelf both winds and currents are weak and hundreds of hours are typical for transit times to shore.

Trajectory releases from site two are shown in figure 6-5. This location is in the vicinity of the continental slope mid-way between Icy Bay and Kayak Island. These trajectories show a quite different behavior than was seen in releases from site one. They are immediately under the influence of the relatively strong baroclinic current that is due to an offshore eddy interacting with the continental slope. This "carries them rapidly to the southwest. Under the influence of onshore winds most of them are eventually moved out of the current onto the shelf, where many are seen to move in a clockwise arch following the deep valley that cuts across the shelf southwest of Yakutat. This example also shows several interesting exceptions. Two trajectories move quickly onto the shelf and progress more or less directly onshore. Two other trajectories are seen to move out of the southwesterly baroclinic current in an offshore direction and their movement is then dominated by the offshore baroclinic circulation.

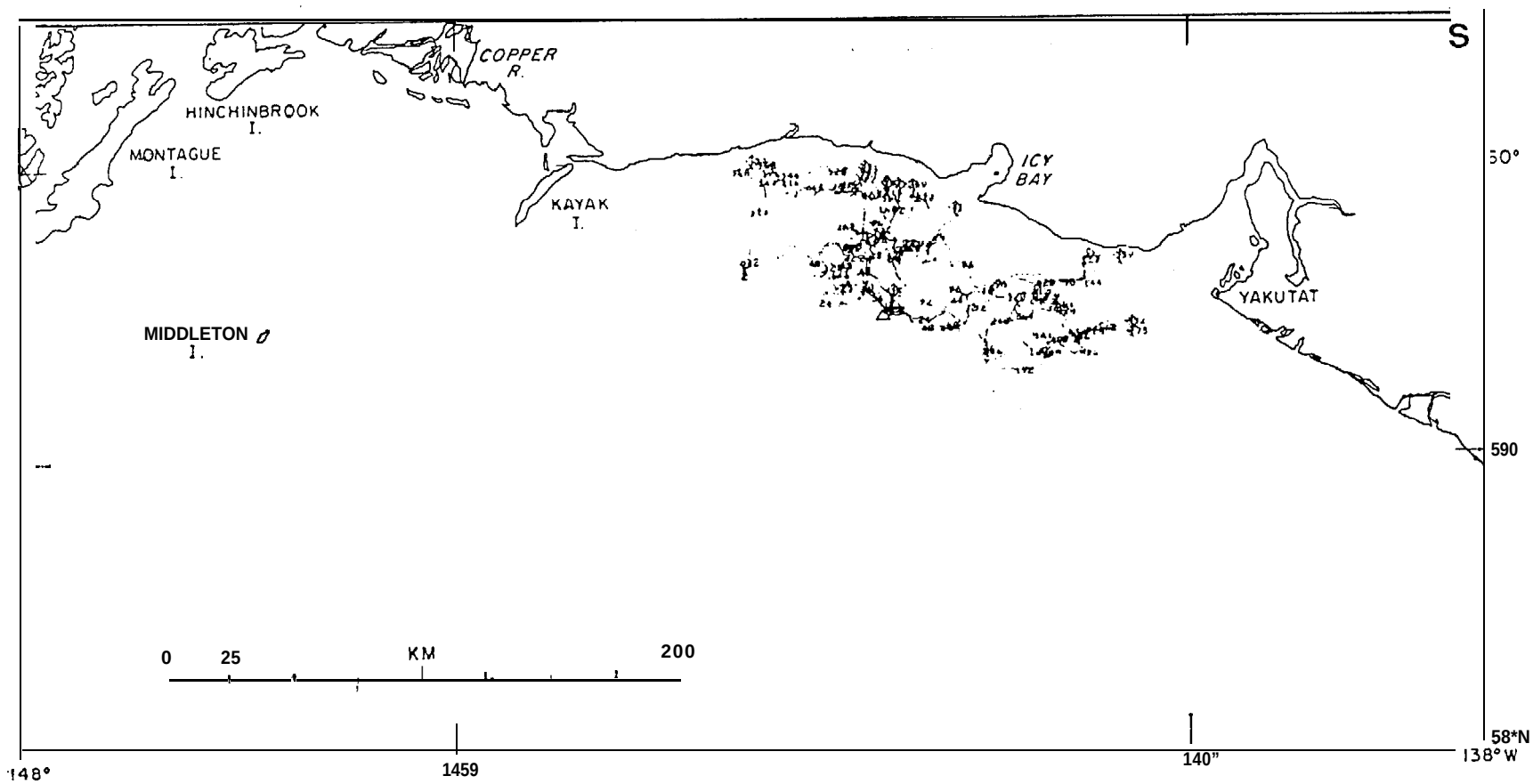

Figure 6-4. Surer trajector es of releases from site one.

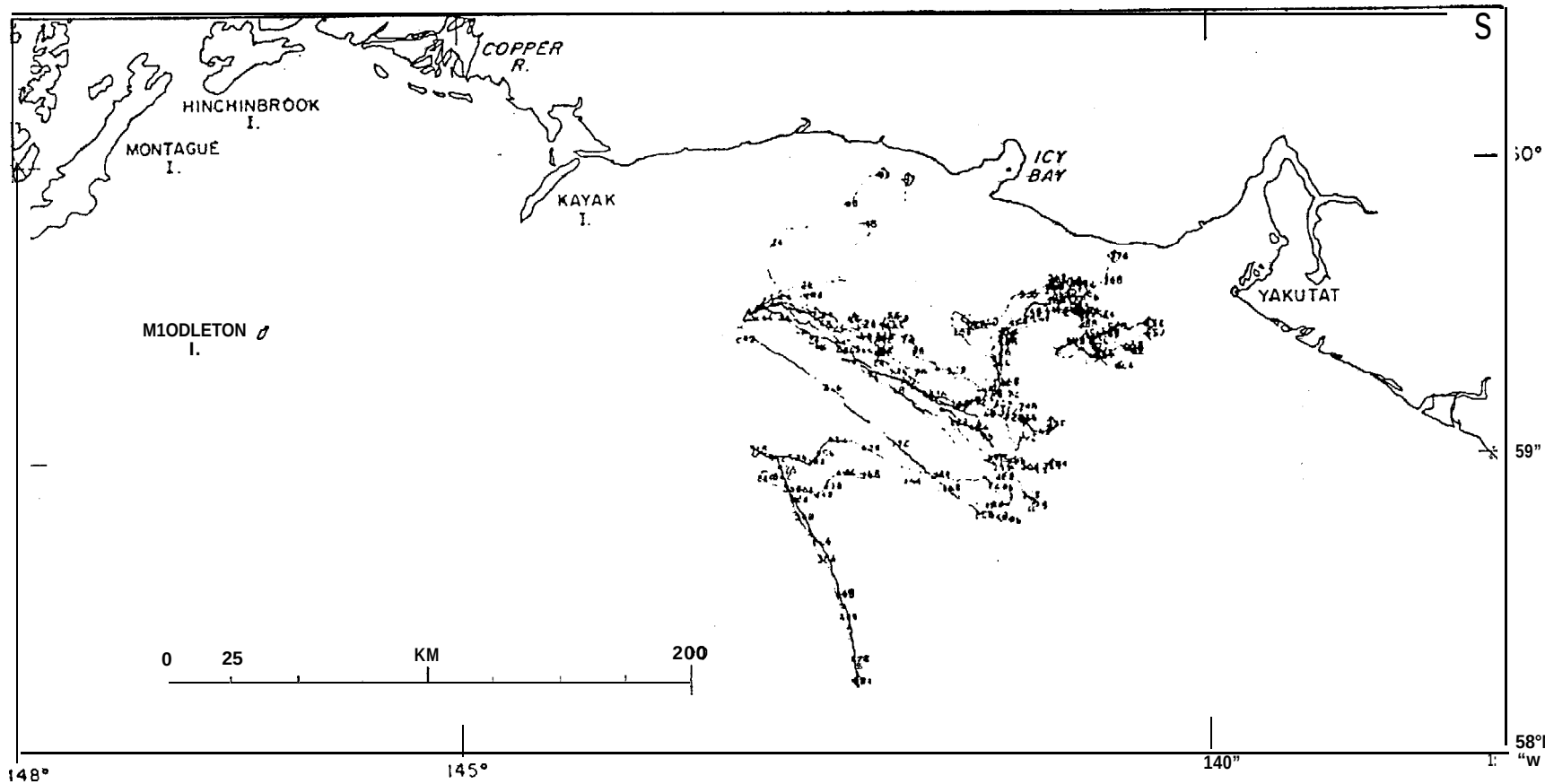

Figure 6-5. Summer trajectories of releases from site two.

It is interesting to note that a satellite tracked drogue released from the spill of the ARGO MERCHANT seemed to follow a similar sort of dynamic path associated with a baroclinic Gulf Stream eddy.

Release site three is on the shelf southwest of Icy Bay. Trajectories leading from this point are shown in figure 6-6 and for the most part move directly towards the coast with the exception of a couple that move towards the east, apparently dominated by weather types 5.0 and 5.1.

Release site four is on the shelf mid-way between. Icy Bay and Kayak Island. Trajectories from this location are shown in figure 6-7. This is a region of complex bathymetry and although the trajectories generally lead north and northwest wide variations are seen both in pathways and transit times.

Release site five is on the shelf southeast of Kayak Island. Trajectories from this site are shown in figure 6-8. Most of the trajectories tend towards the coast, but this is once again a complex area where the shelf is quite narrow. Some of the trajectories are seen to lead offshore and come under the influence of the baroclinic currents along the continental slope, traveling nearly two hundred kilometers before being blown out of the stream back onto the shelf.

Release site six is southwest of Kayak Island and the trajectories from this point are seen in figure 6-9. From these the anticyclonic gyre west of Kayak Island is seen to dominate the pathways with most of the trajectories showing long residence times and eventually moving towards the Copper River region. A secondary area where these trajectories tend to concentrate is towards the northwest and Hinchinbrook and Montague Islands. One trajectory diverges from the pattern and is seen to move east for about three days eventually going ashore halfway to Icy Bay.

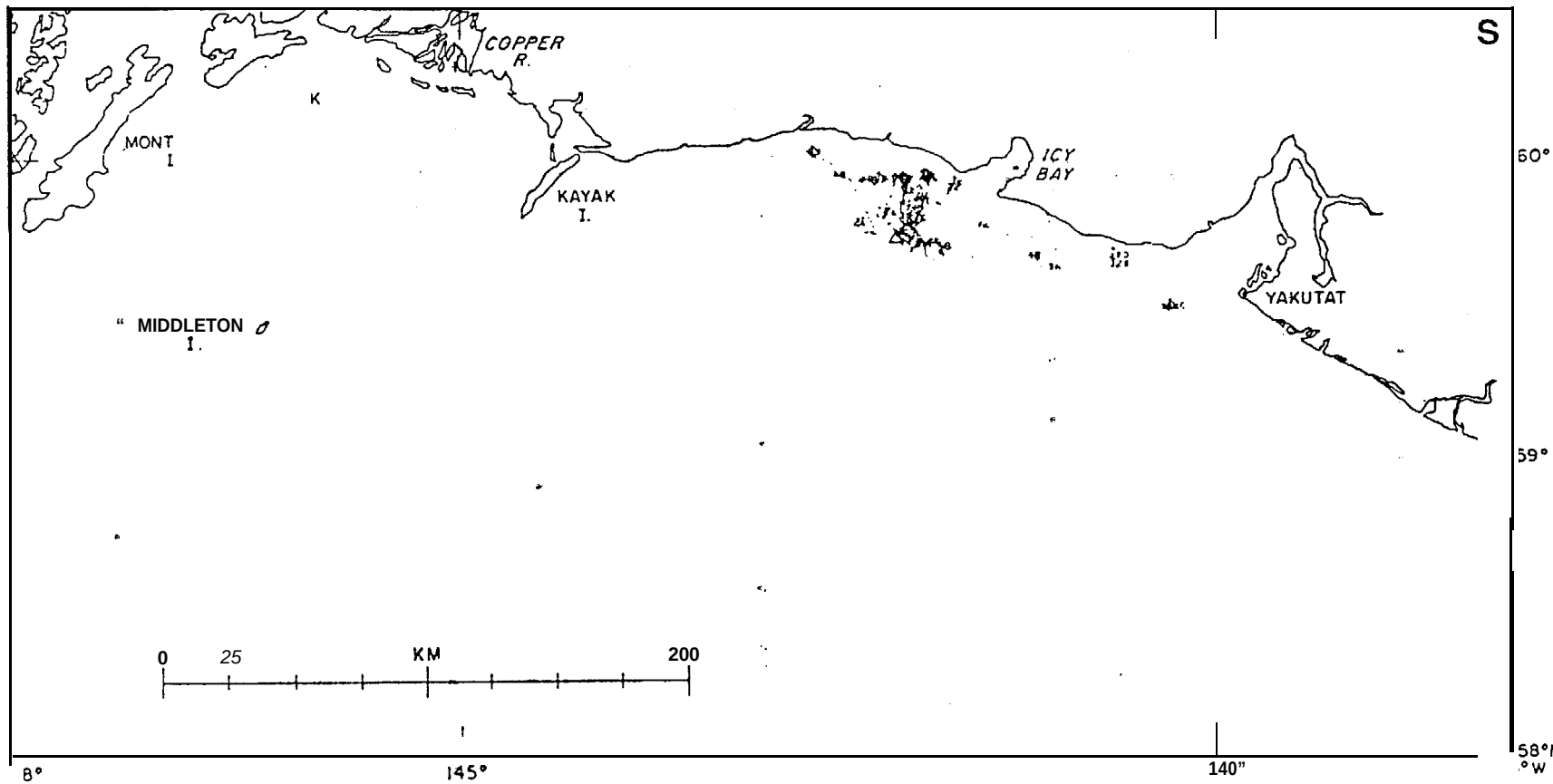

Figure 6-6. Summer trajectories of releases from site three.

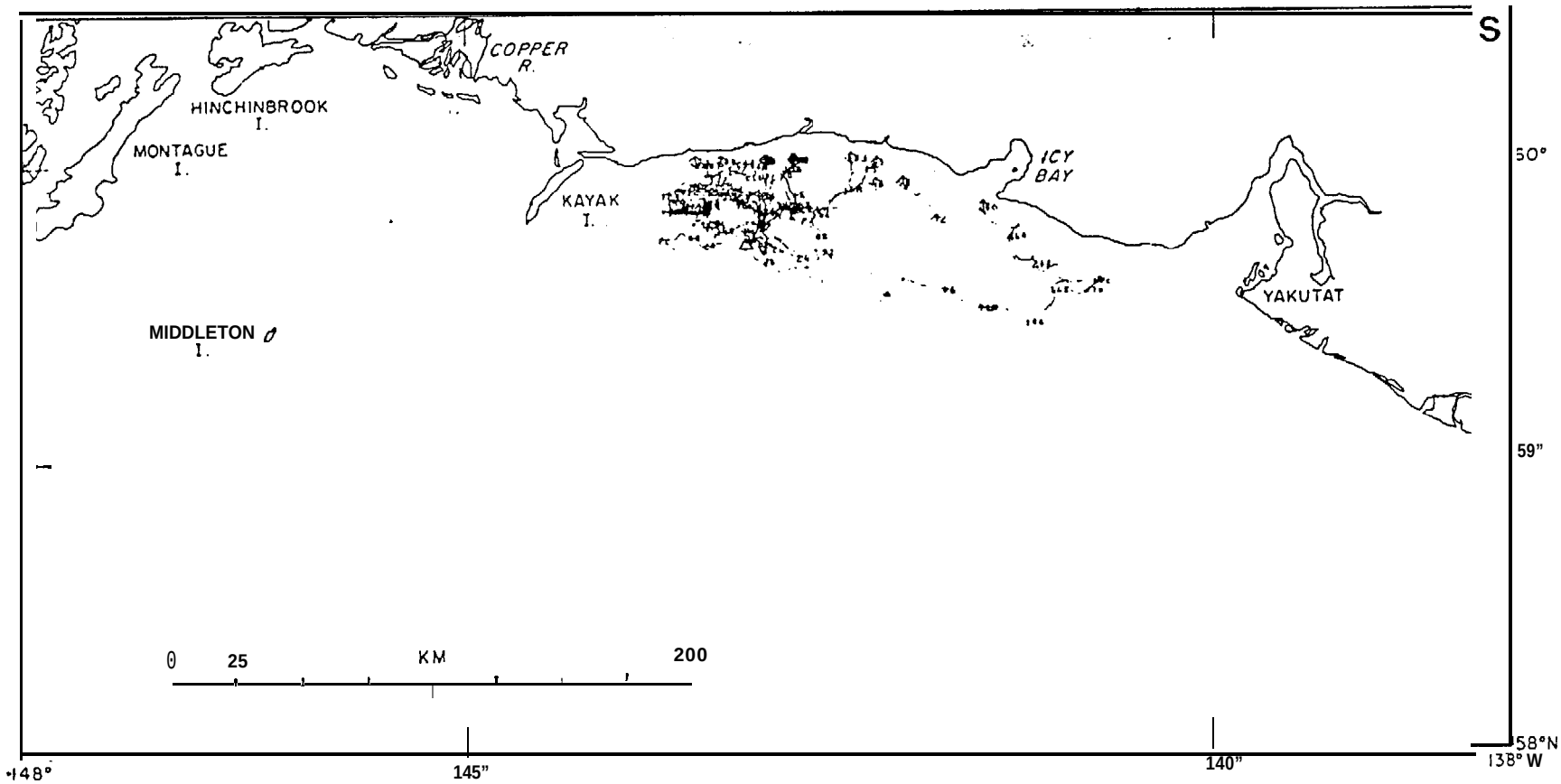

Figure 6-7. Summer trajectories of releases from site four.

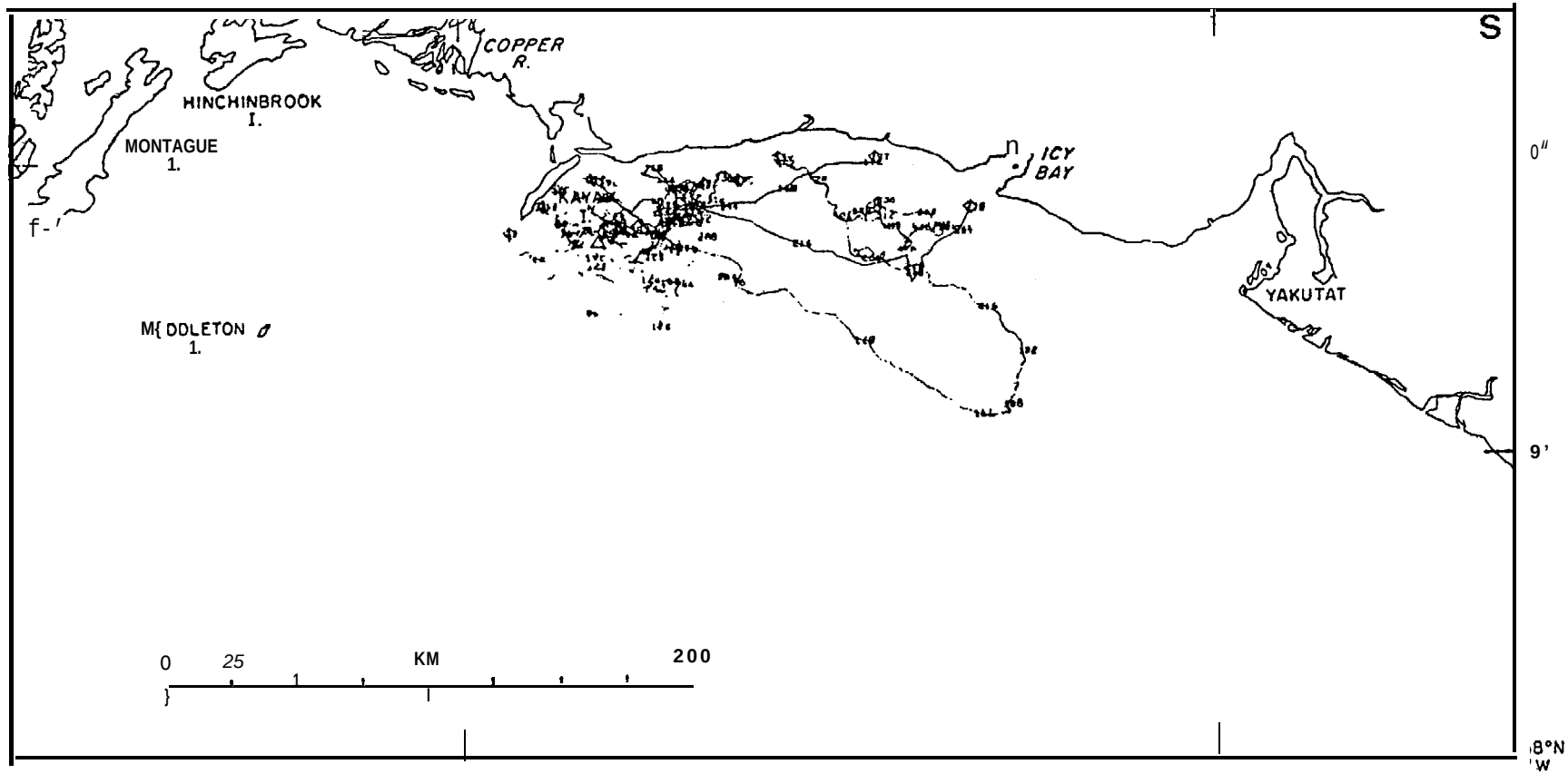

. Figure 6-8. Summer trajectories of releases from site five.

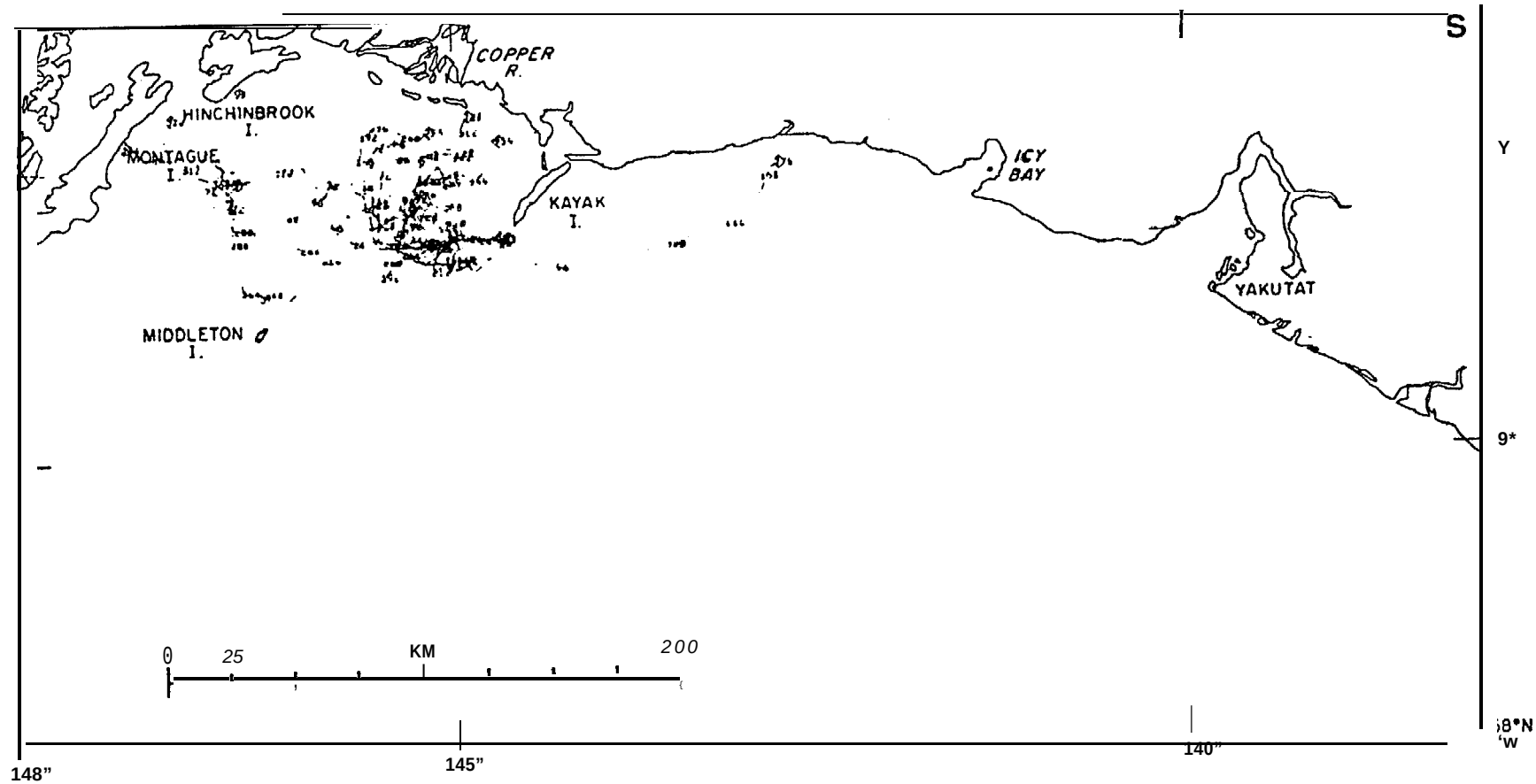

Figure 6-9. Summer trajectories of releases from site six.

Trajectories from the last release site (seven) are shown in figure 6-10. This location is in the region known as Tarr Bank and is situated southeast of Hinchinbrook Island. Releases from this point move onshore and potentially threaten a long section of coast from the Copper River to Montague Island.

A second series of releases were considered for each of the above locations under conditions appropriate for the following winter. The climate types that represented the February and March 1975 period showed proportionately more 1, 2 and 6 patterns corresponding to oceanic lows in various positions. These in turn lead to dominant westerly flow predicted in the wind set-up modes over the shelf. The winds at Middleton Island that were used to scale the model were more energetic than for the previous summer and as a result predicted displacements were generally more rapid. The density data used to describe the baroclinic mode were obtained in February 1975. The field shows strong flows along the continental slope associated with mesoscale eddies offshore. The anticyclonic eddy to the west of Kayak Island is well developed and a generally westward drift is seen along the outer edge of the shelf. This data set does not extend to the east beyond Icy Bay and this sets the limit of the overall model domain. The current meter station used to scale the residual currents was at station 62B which was located near the edge of the shelf southwest of Icy Bay in a region of large bathymetric gradients. This was once again not an optimal choice for a current meter reference station. In this case the predicted currents were significant, but its location near the edge of the shelf put it in an area of strong baroclinic activity and the response to set-up modes was not very sensitive to alternate patterns since it showed strong evidence of bathymetric constraints. Once again the use of this current meter station

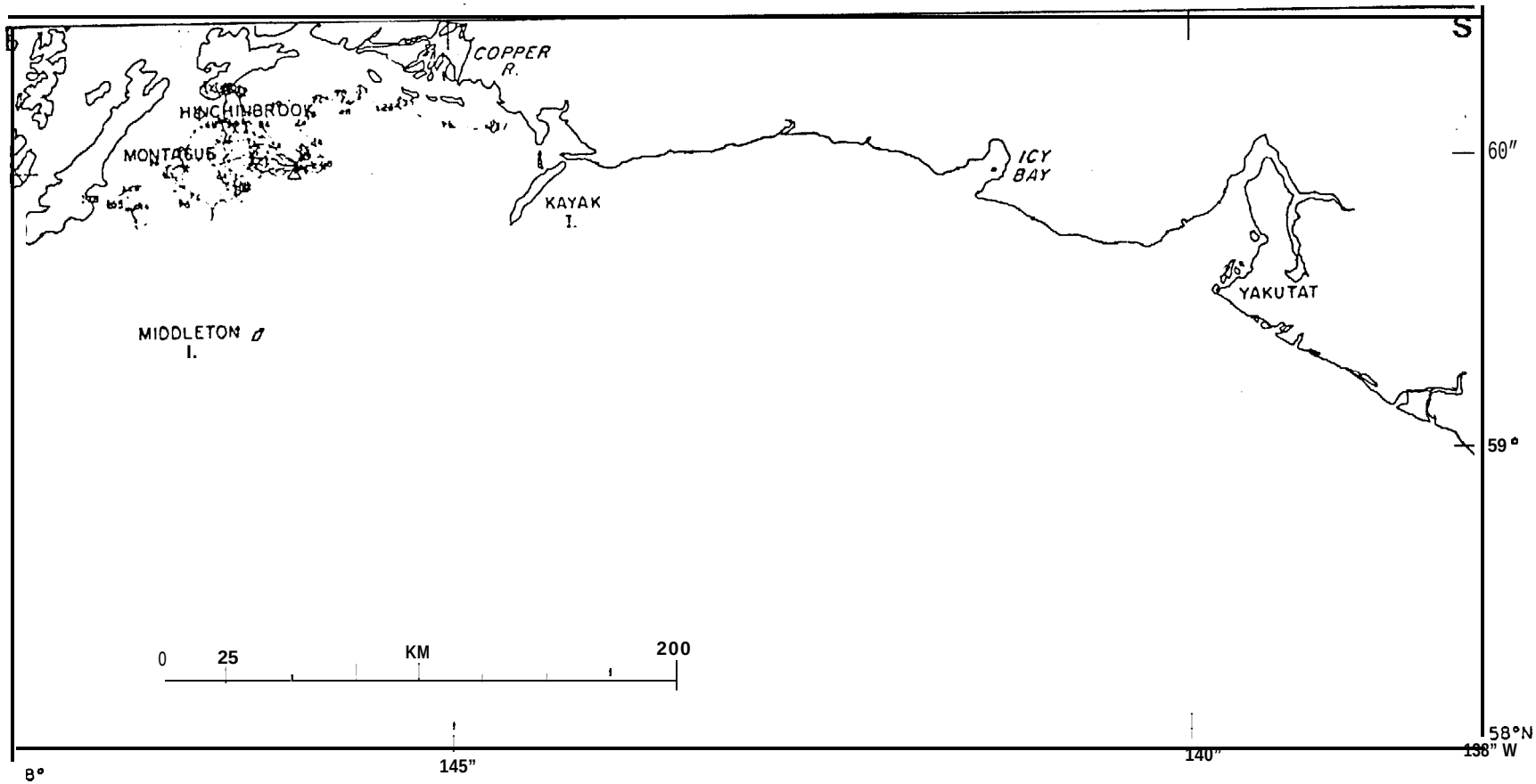

Figure 6-10. Summer trajectories of releases from site seven.

location for scaling the modeled current residual will be correctly represented by a higher level of uncertainty in the trajectories.

Trajectories released from site one are shown in figure 6-11. The majority of these are seen to move northwest across the shelf, although several come under the influence of the offshore eddy south-southwest of Kayak Island. This release site appears to threaten a large section of coast in both summer and winter examples.

Releases from site two are shown in figure 6-12. As before, this location is strongly influenced by the baroclinic currents along the slope and lead to initial displacements to the east. Trajectories that move north out of this current under the influence of the wind appear to establish a northerly movement trending towards the coast. Interestingly, one trajectory pathway escapes south of the gyre located over the slope and reverses the apparent trend by consistently moving out to sea.

Trajectories released from site three southwest of Icy Bay are shown in figure 6-13. The majority of these move onshore covering a seventy kilometer front along the coast. Three exceptions are seen to move offshore where they are clearly influenced by baroclinic flow. Two of the three stay in the current band flowing west along the outer edge of the shelf and end up at Kayak Island. The third track moves even farther offshore and is carried southeast by the continental slope eddy.

Trajectories from site four are shown in figure 6-14. This location shows a wide scatter (recall that it is a region of complex bathymetry) with all but one of the trajectories trending north and west threatening a wide section of coastline. As with site three, one trajectory leads offshore and comes under the influence of the continental slope baroclinic gyre.

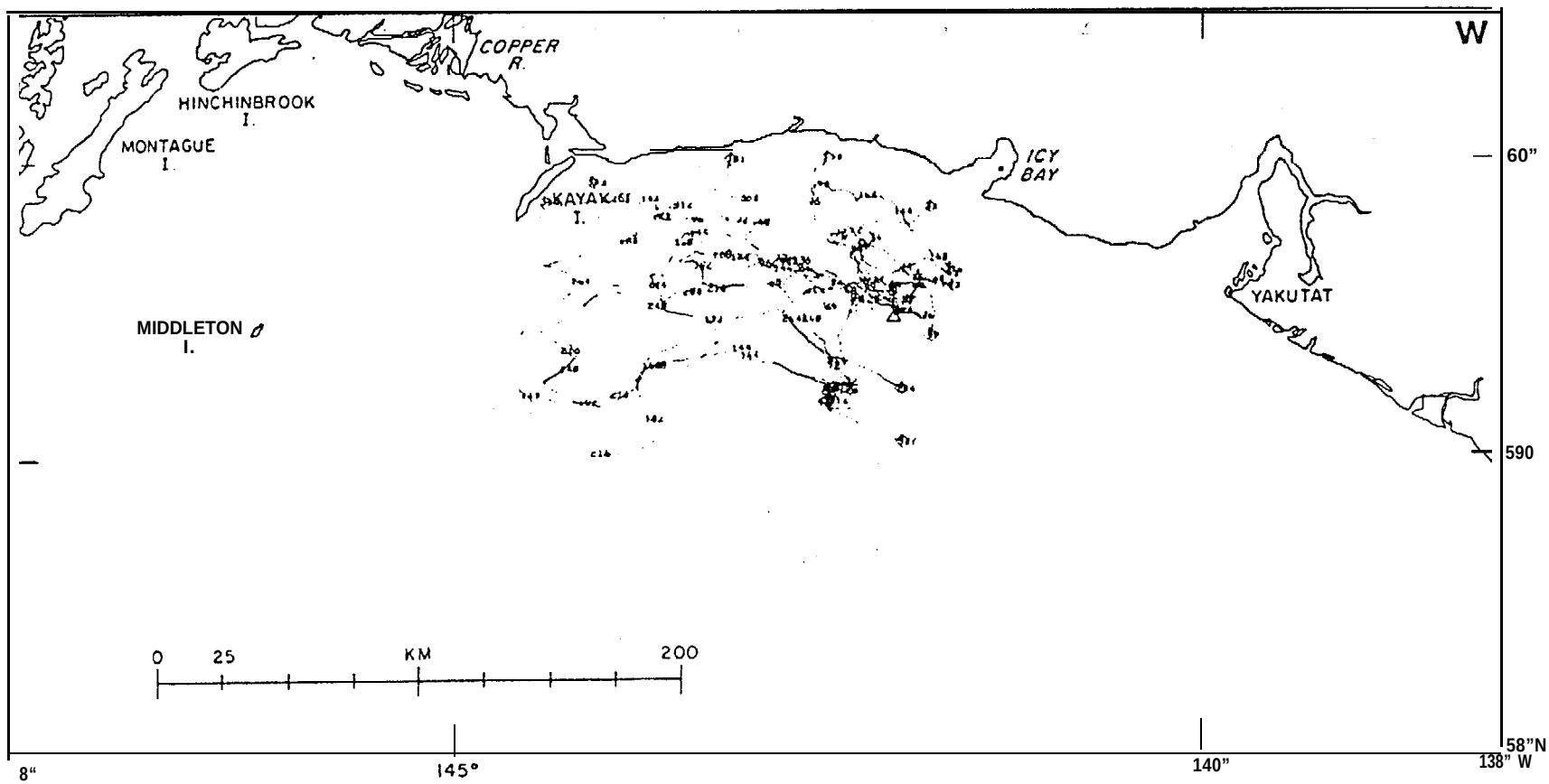

Figure 6-11. Winter trajectories of releases from site one.

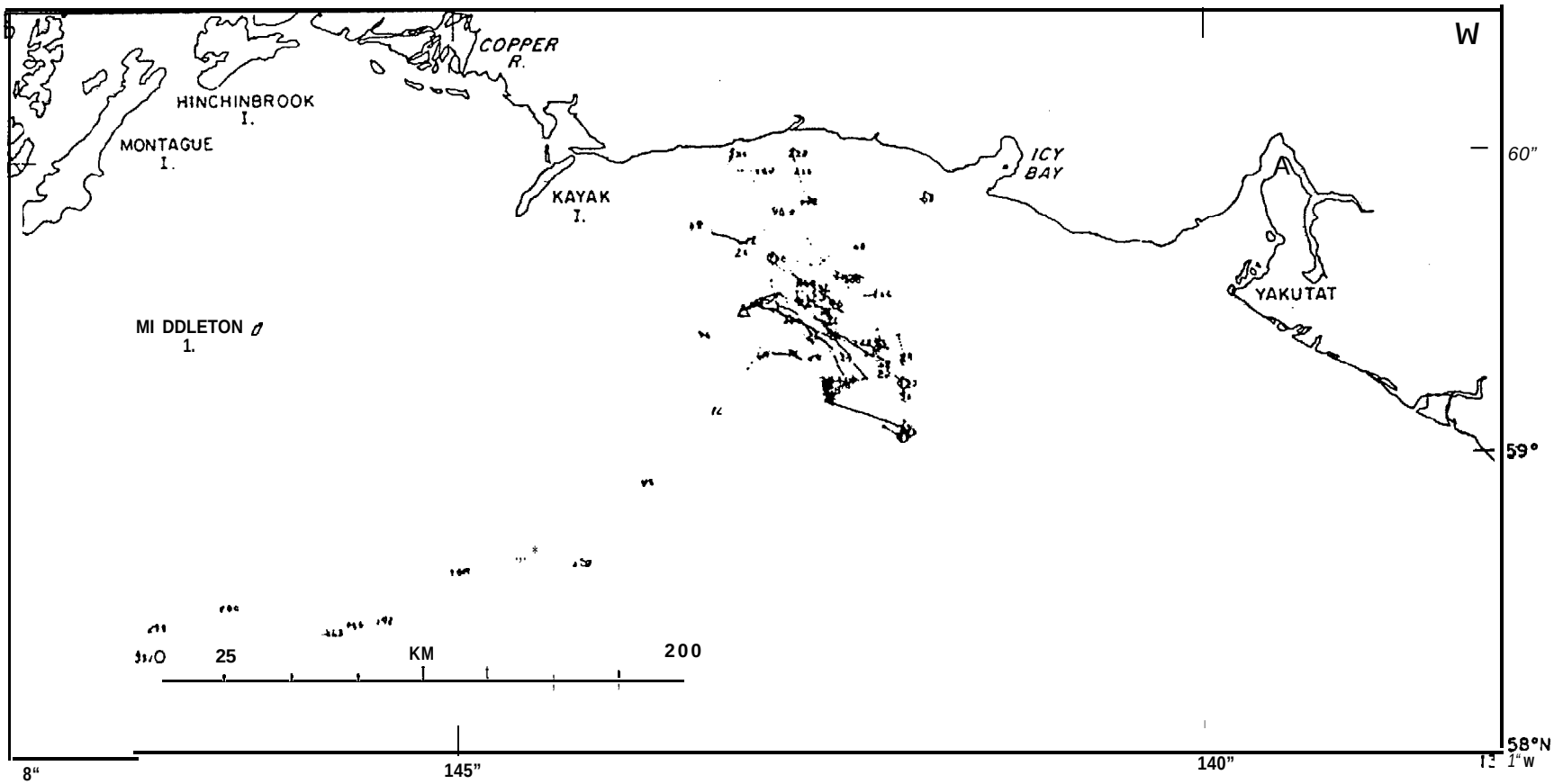

Figure 6-12. Winter trajectories of releases from site two.

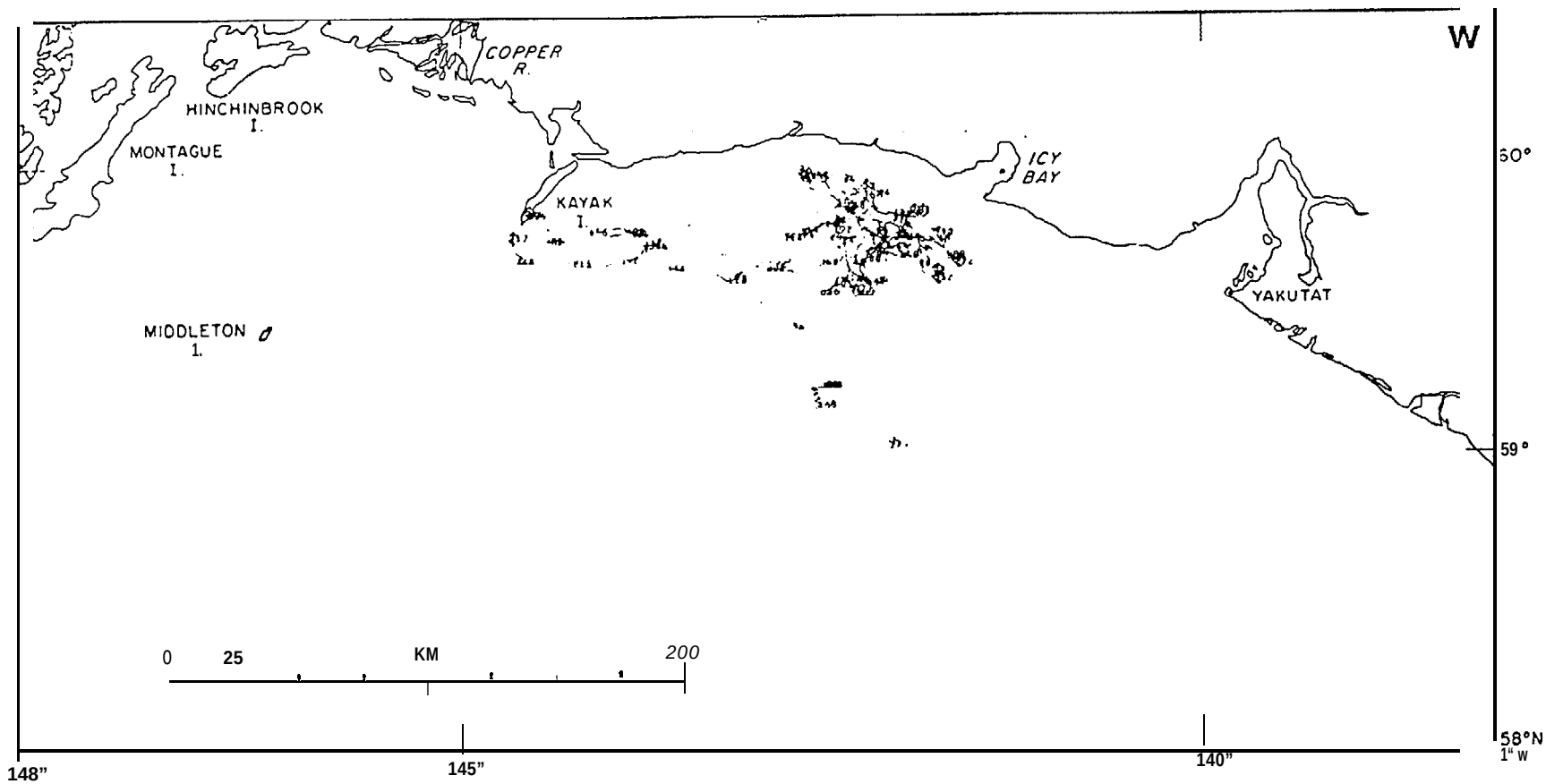

Figure 6-13. Winter trajectories of releases from site three.

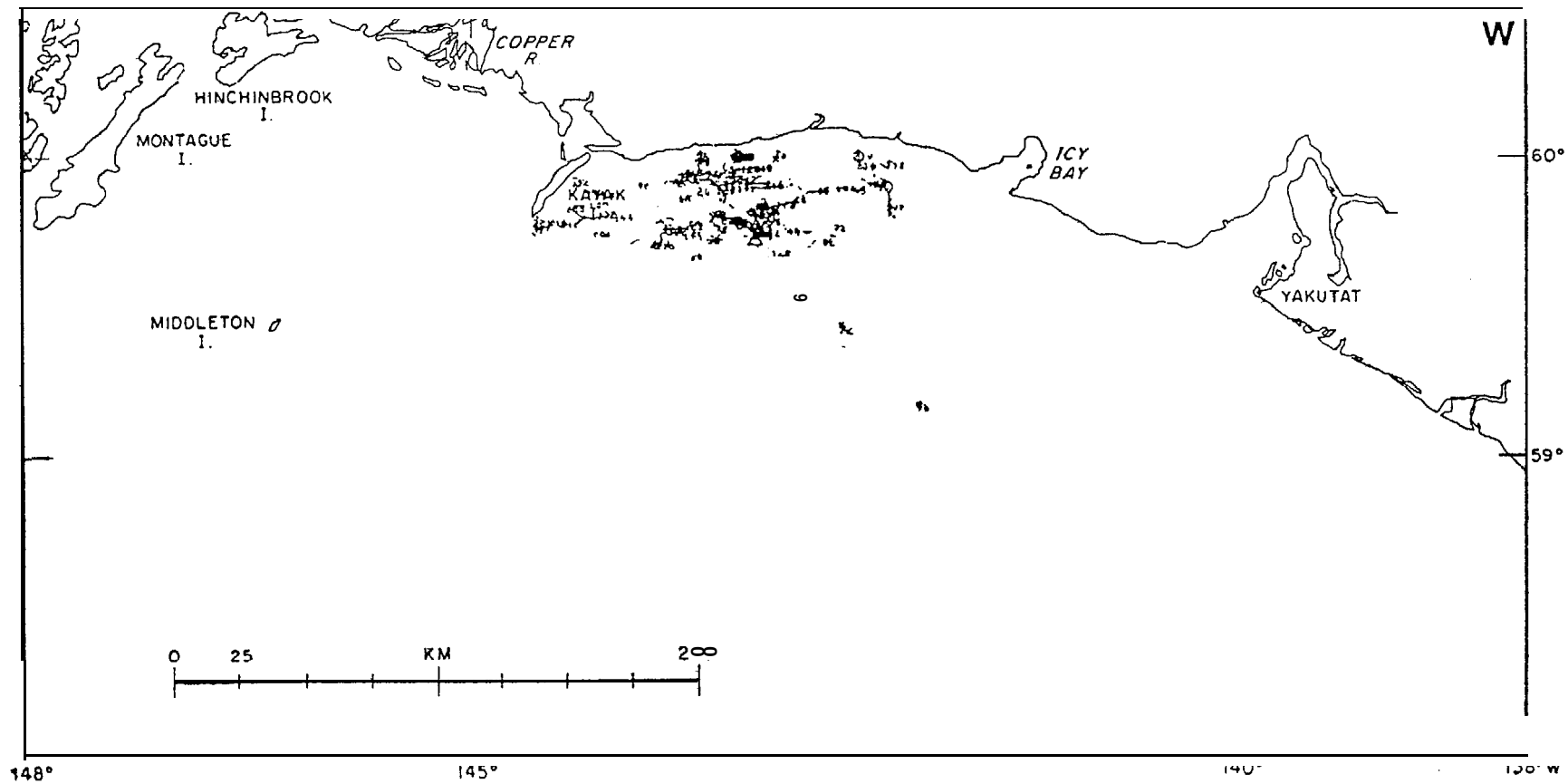

Figure 6- 4. Winter trajectories of releases from s te four.

The releases from site five southwest of Kayak Island are shown in figure 6-15. Most of these move north impacting the southeast coast of Kayak Island. Two exceptions are seen. The first of these moves offshore and follows the now familiar, but still minority drift to the southwest under the influence of baroclinic currents. Another pathway is seen to move southwest, round Kayak Island, and eventually end up at the Copper River.

Trajectories from site six are shown in figure 6-16 and show a wide scatter, but appear to fall into several classes. The majority appear to be trapped in the gyre circulation west of Kayak Island and eventually end on the west coast of Kayak Island and along the Copper River delta. A second class moves west north of Middleton Island and then northwest towards Hinchinbrook Island, A subclass of the pathways that initially move west appear to travel south in the vicinity of Middleton Island and then move east or west subject to influence of the shelf edge baroclinic currents:

Releases from site seven are shown in figure 6-17. From this location the majority of the tracks move northwest towards Hinchinbrook Island and the entrance to Prince Williams Sound.

Thus far this analysis has concentrated on collections of spills from various locations with comments being confined to general characteristics. The dynamic decomposition of the model and component reconstruction make it possible to examine trajectories in much more detail. The individual displacements associated with direct wind drift, baroclinic currents and wind set-up plus residual currents can each be monitored throughout the calculations. To demonstrate this five individual trajectories from the summer and winter periods are examined in detail. First, considering the July and August 1974 period, two trajectories have been selected from release

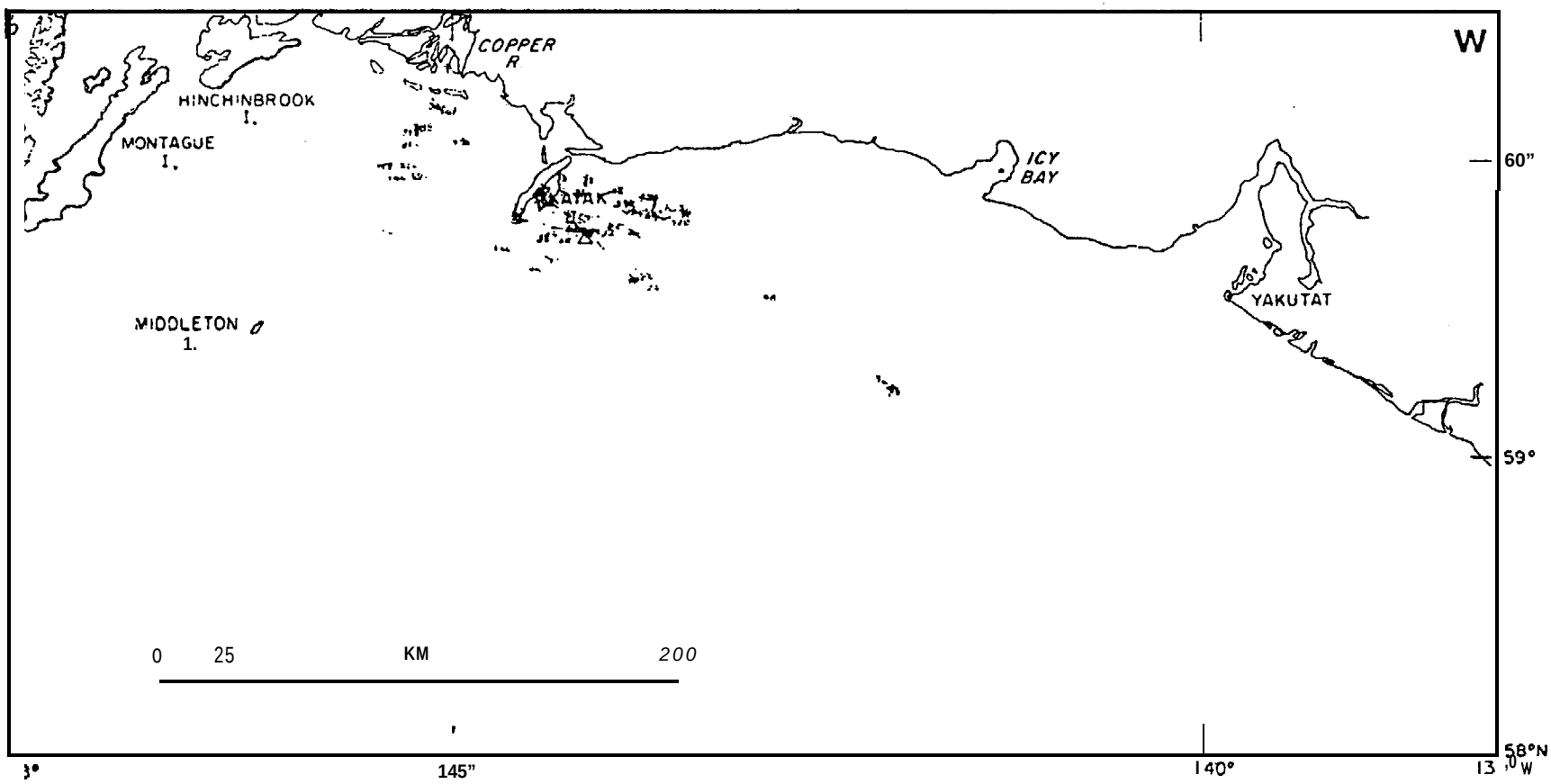

Figure 6-15. Winter trajectories of releases from site five.

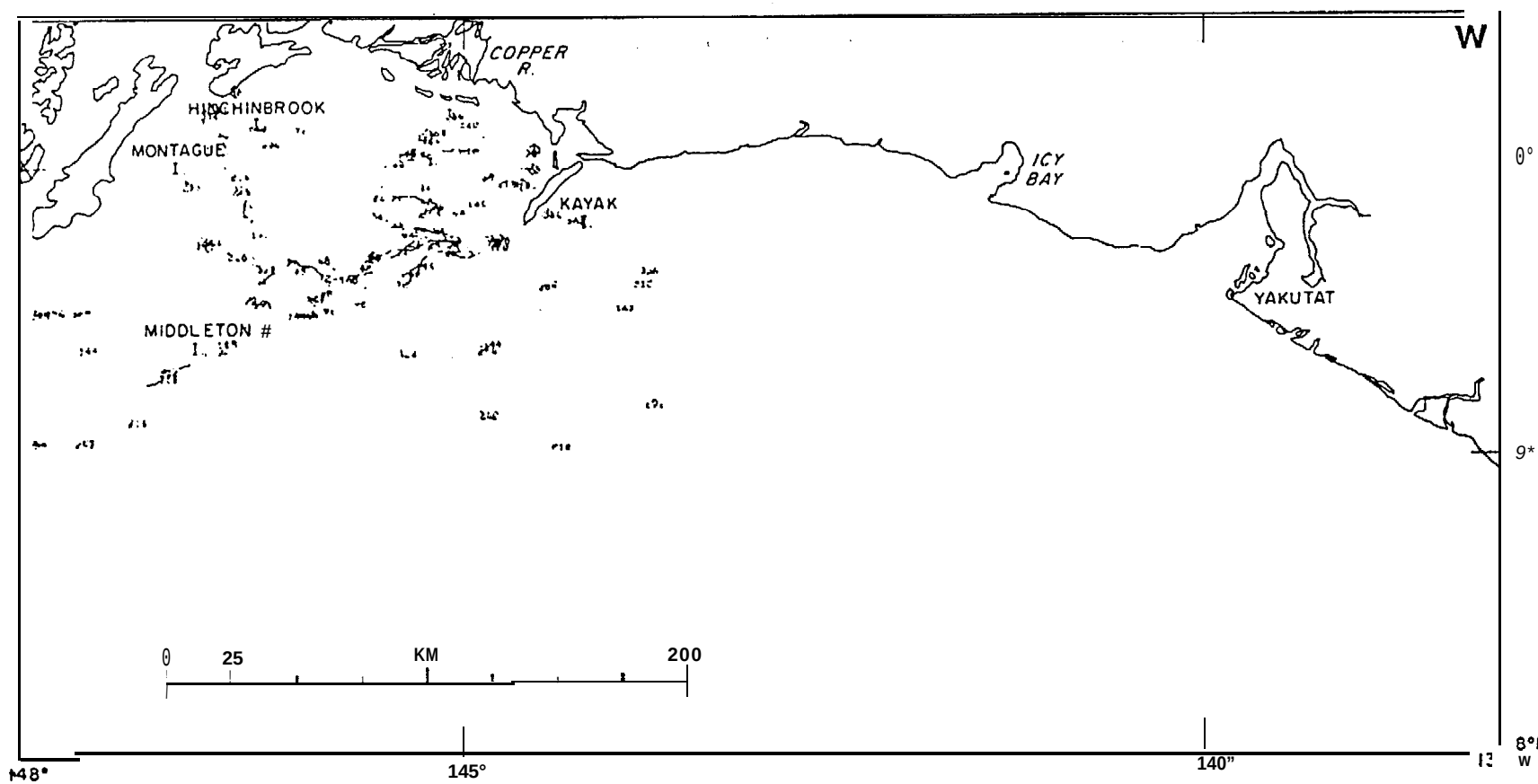

Figure 6-16. Winter trajectories of releases from site six.

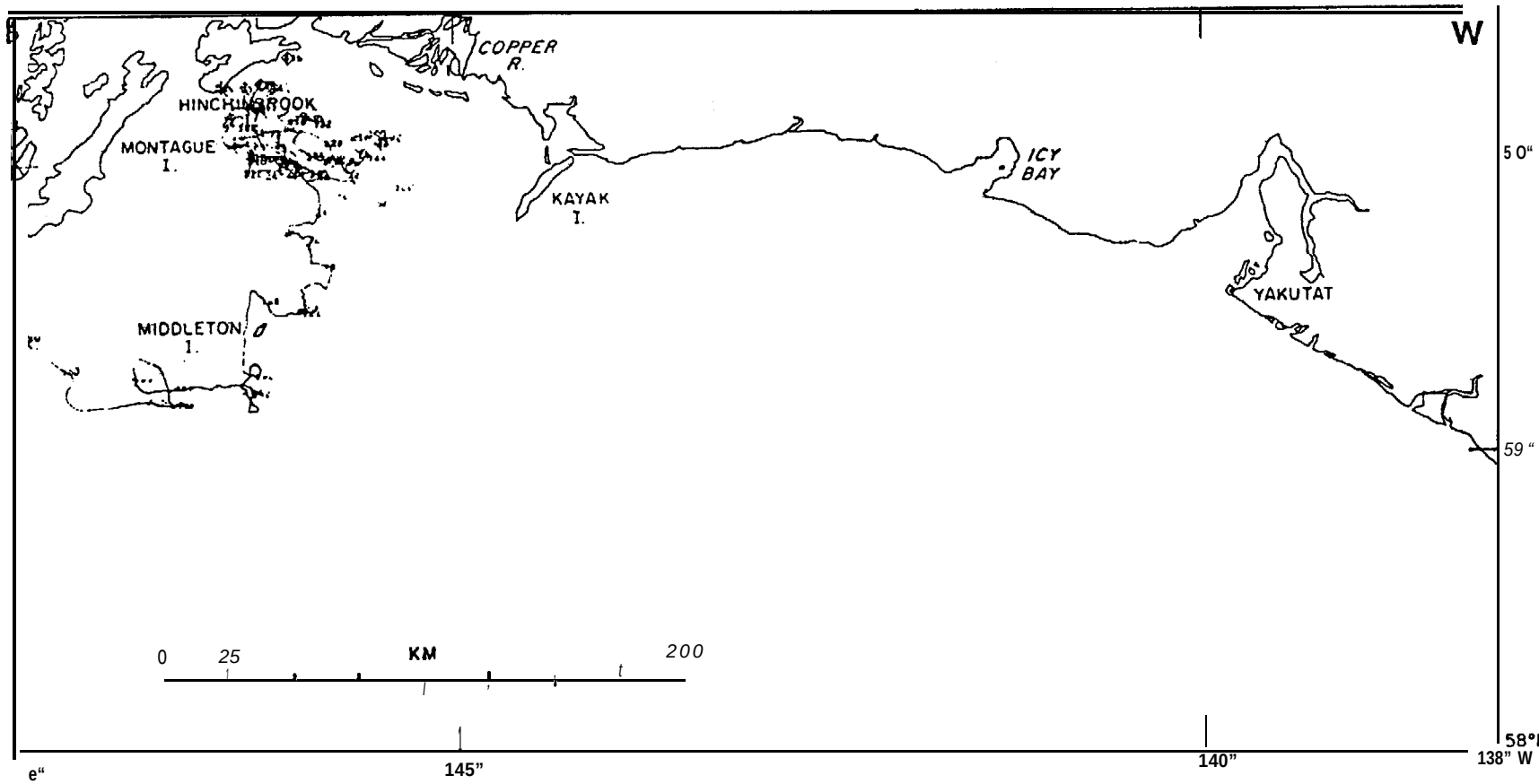

Figure 6-17. Winter trajectories of releases from site seven.

site two (figure 6-18) and three trajectories have been selected from release site six (figure 6-19).

Trajectory s1 is seen to move generally northwest from spill" site two . The specific components responsible for this motion are shown in figure 6-20. This particular track was initiated on the 16th of August. Figure 6-20 shows five different time series vector stick plots. The first two represent the observed currents and winds that are used to scale the . pattern and current residual. The last three time series vector stick plots represent the conditions as predicted from the model within the Lagrangian frame of reference following the path of the trajectory. The first two keying stations are basically Eulerian data.. Many trajectory estimates in the past have been based on progressive vector diagrams derived from "such data. These clearly will not reflect the appropriate pattern information; that is, progressive vector diagrams can't represent trajectories unless the fields have no spatial derivatives. The next three plots indicate the spatial pattern information incorporated into the model. These plots can be thought of as data collected from a drifting platform, collecting wind, current and density data. Also included are the uncertainties suggested by a comparison of model predictions and observational data at the location of the current keying station. This analysis shows that the direct wind forcing and baroclinic currents did not contribute significantly to the movement of this trajectory. The total simulated current was clearly responsible fcr this trajectory's movement.

The second summer trajectory (s2) selected for study was initiated on the 17th of July. The components responsible for this trajectory are shown in figure 6-21. Initially (up to about 150 hours) the baroclinic currents dominate the movement and the trajectory trends southeast. From about 200 to 300 hours the total current moves the path south out of the

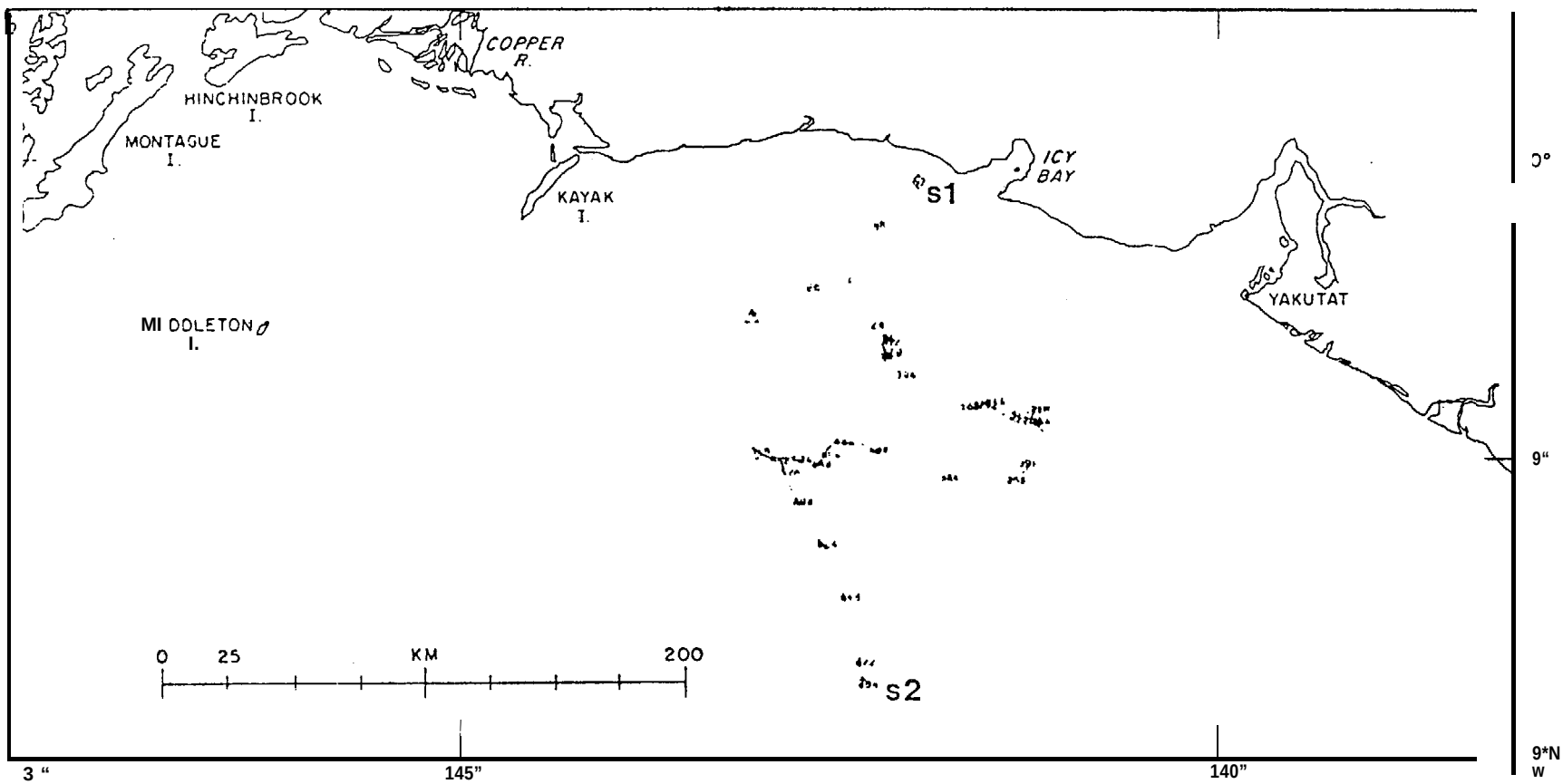

Figure 6-18. Individual summer trajectories s1 and s2 of releases from site two.

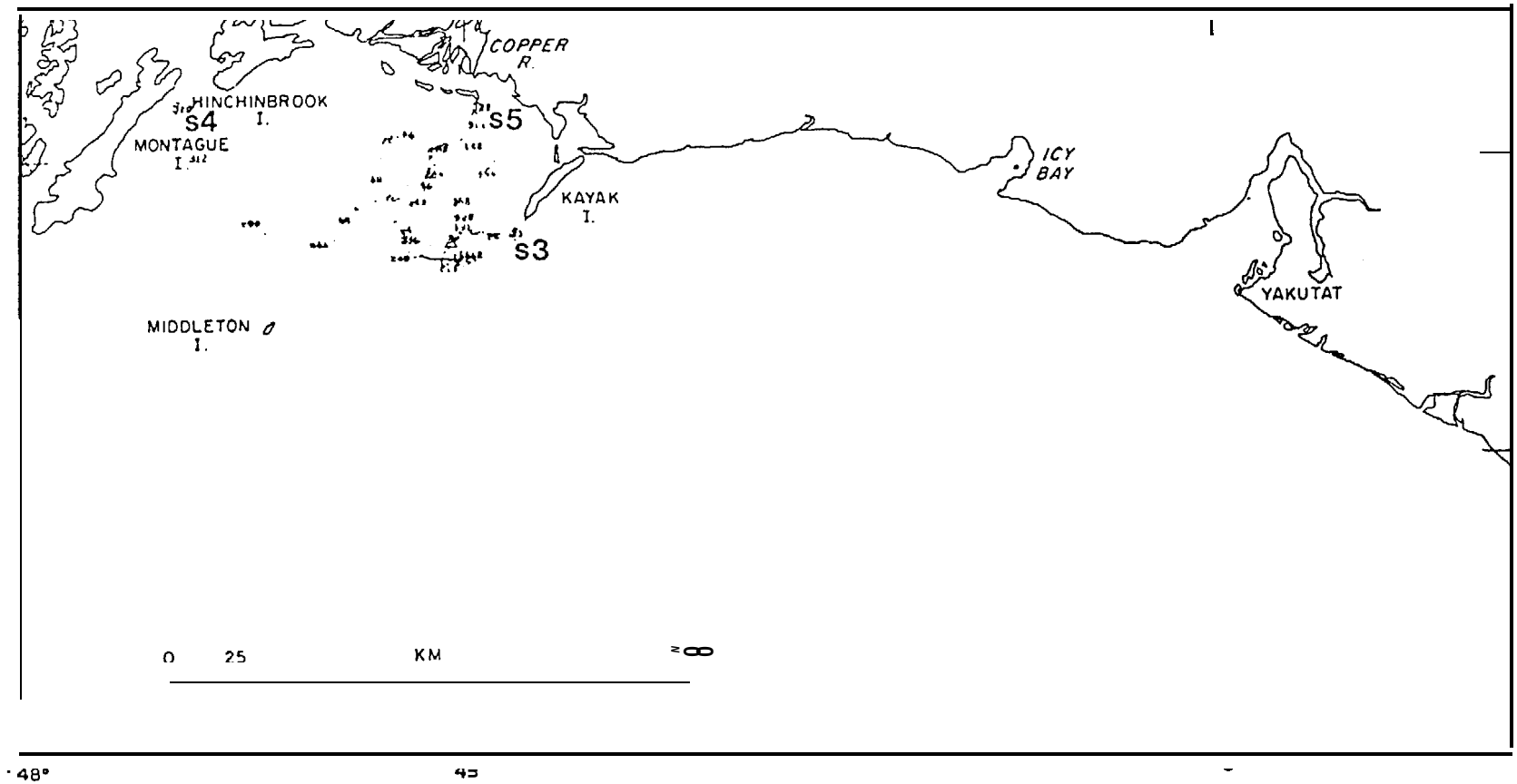

Figure 6-19. Individual trajectories s3, s4, and s5 of releases from site two.

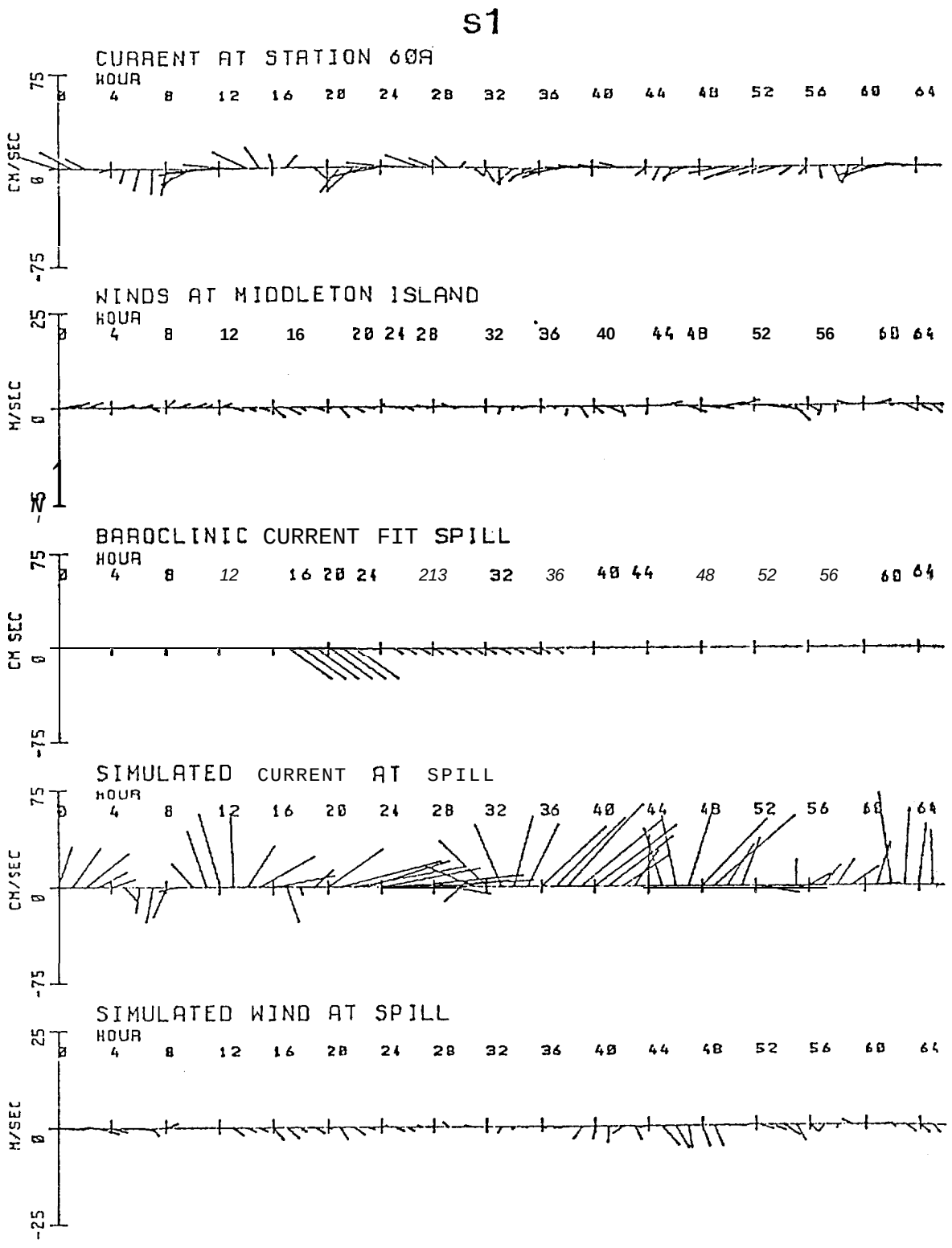

Figure 6-20. Detailed analysis of trajectory s1.

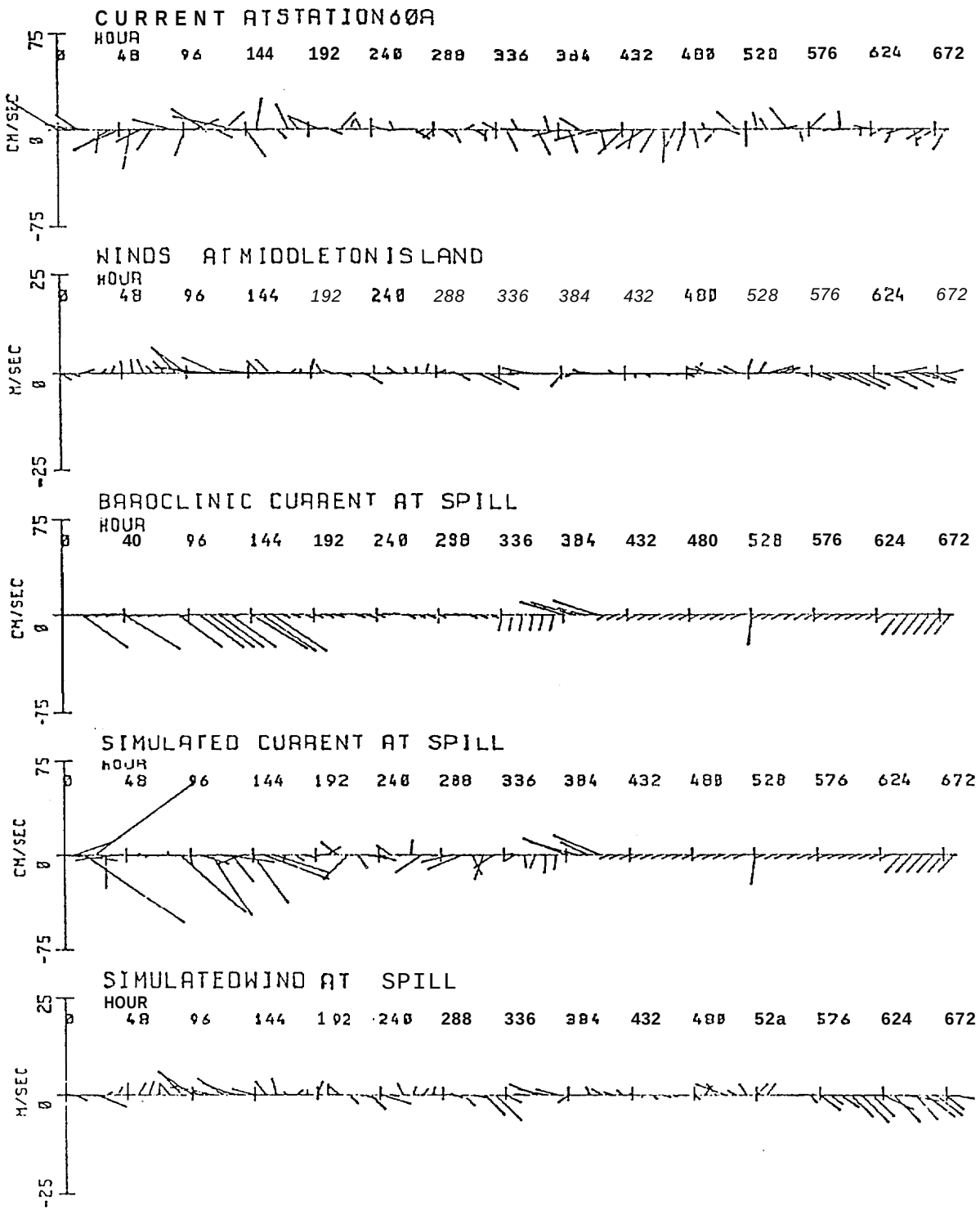

Figure 6-21. Detailed analysis of trajectory s2.

dominant slope current. After 300 hours baroclinic currents are again seen to dominate the movement (the trajectory is beyond the shelf edge and influence of the hinge set-up modes]. Towards the end of this case study, after 480 hours the general winds increase and are seen to result in a significant southeasterly component to the trajectory movement.

The third summer study (s3) is of a short trajectory released from site six on the 7th of July. This trajectory leads quickly to the west, towards Kayak Island. The results of this analysis are shown in figure 6-22. The baroclinic currents for this trajectory are consistently to the south representing part of the gyre to the west of Kayak Island. This is countered by hinge set-up flow to the north such that the total currents have a steady easterly component. The wind drift is never dominant, but steadily to the east. The net result of these factors is a direct path to the east.

The fourth summer trajectory to be studied (s4) was released from site six on the 22nd of July. The results of this analysis are seen in figure 6-23. For the entire 300 plus hours of this drift the direct wind contribution was small. For the first 130 hours this trajectory is within the Kayak Island gyre pattern with the movement first north then east and finally south. After about 144 hours the path has lead back nearly to its original position. At this point several strong southerly excursions carry the path out of the gyre to the westerly flowing region. After 200 hours the currents carry the trajectory steadily west and finally north, encountering quite strong currents in the vicinity of the sea valley leading in towards Hinchinbrook just before it goes ashore.

The last summer trajectory (s5) investigated left site six on the 6th of August and the results of this analysis are shown in figure 6-24.

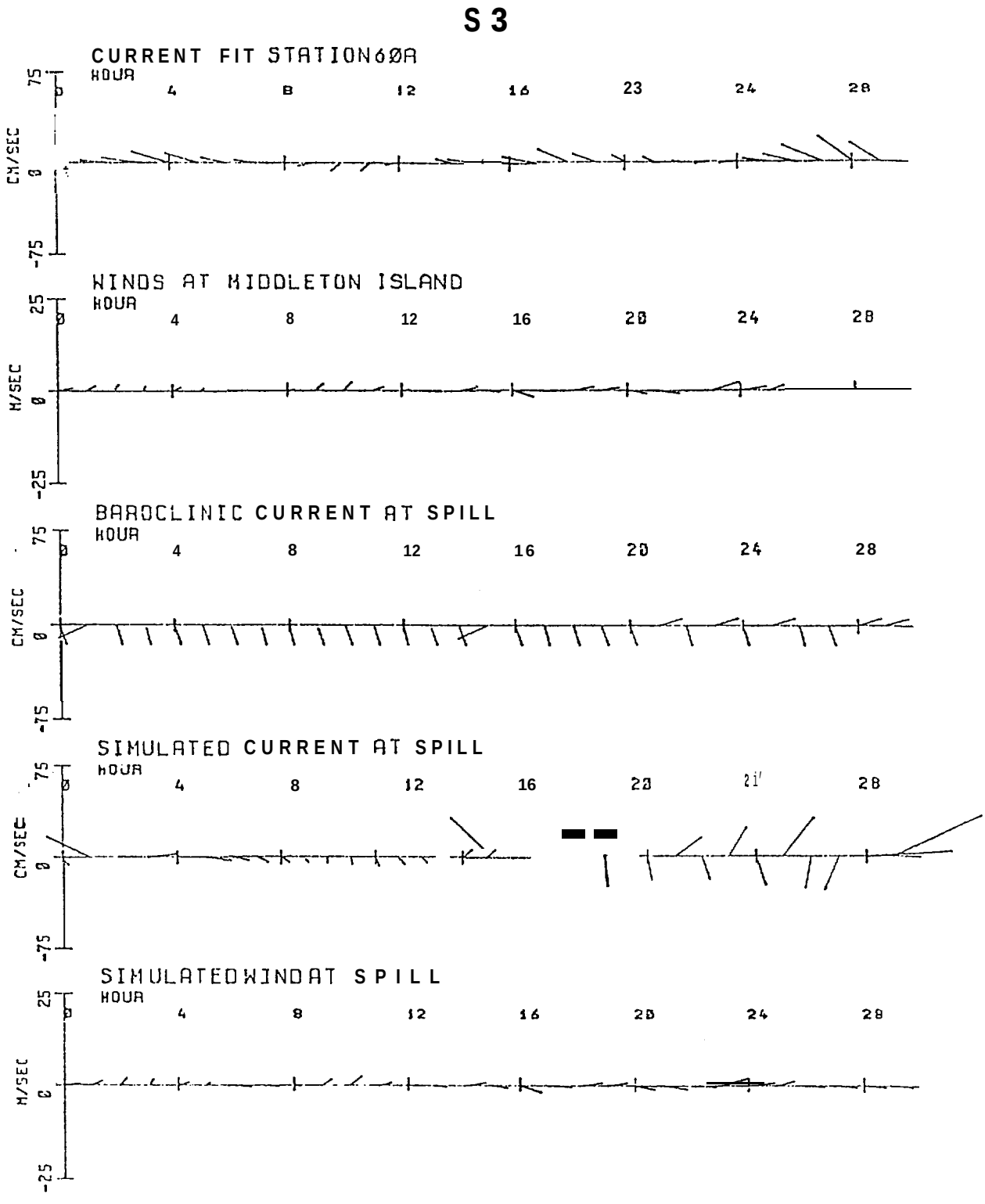

Figure 6-22. Detailed analysis of trajectory s3.

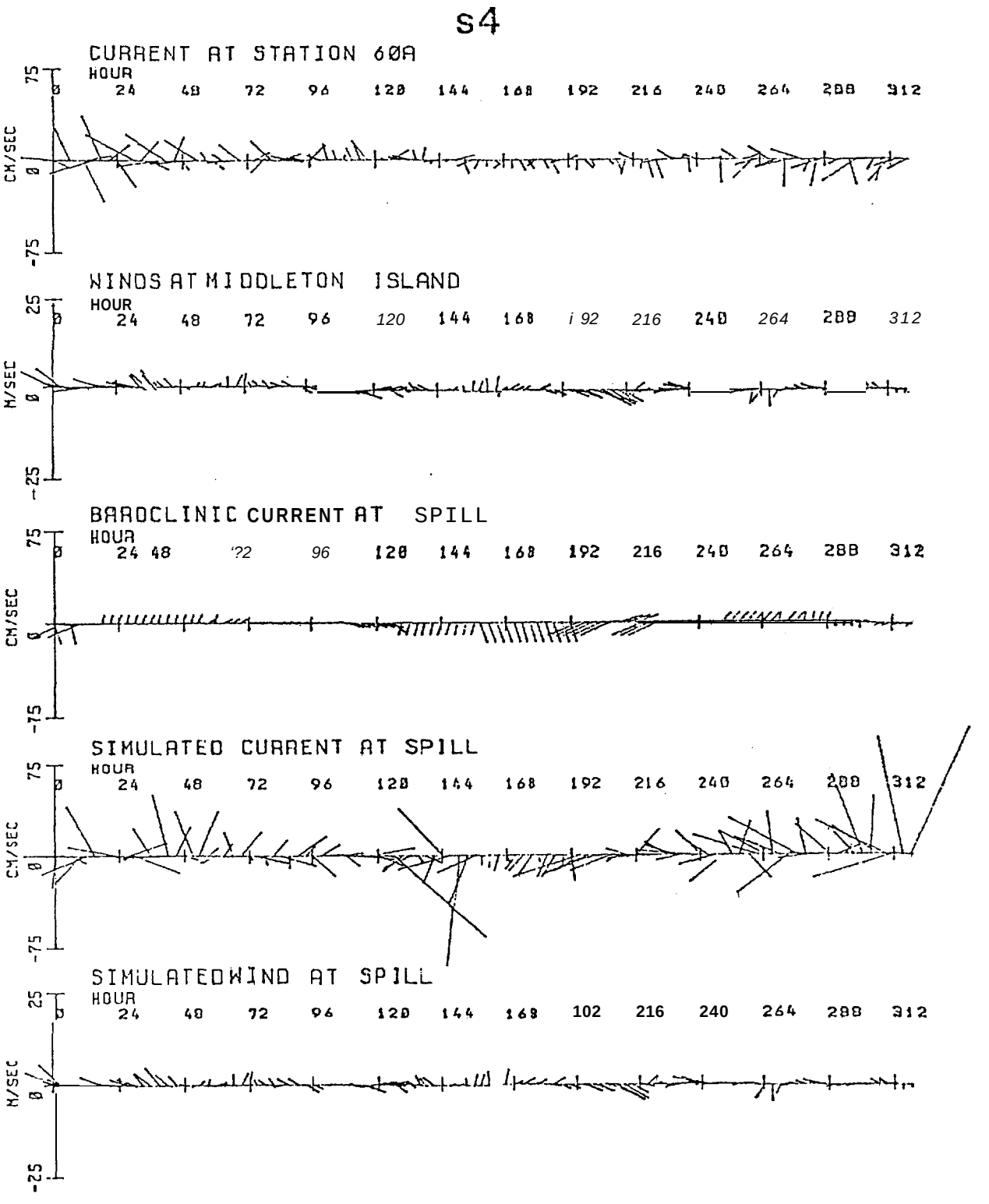

Figure 6-23. Detailed analysis of trajectory s4.

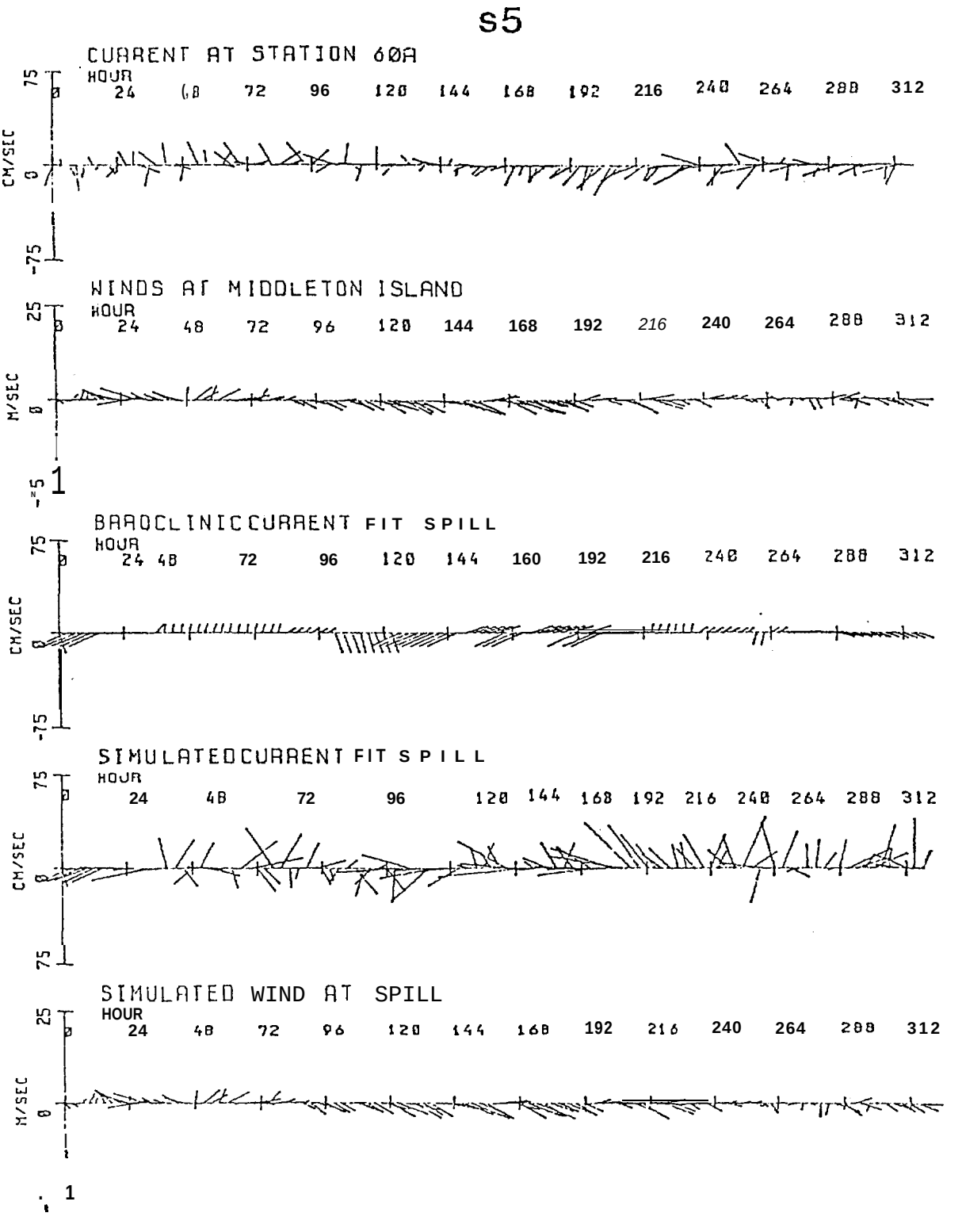

Figure 6-24. Detailed analysis of trajectory s5.

Once again the direct wind contribution is small although it is steadily to the east and slightly south. The currents (both baroclinic and total) show evidence of the Kayak Island gyre, moving north for about 100 hours, south for another 60 and then more or less steadily north till the path leads ashore near the Copper River. Like the last example, this trajectory leads back to its point of origin, but did not receive a short southerly push necessary to escape the gyre circulation.

Of the five winter trajectories studied in detail three originated from site five southeast of Kayak Island (figure 6-25) and two originated from site seven (figure 6-26).

The first winter trajectory (wI) left site five on the 2nd of February and proceeded rapidly (about 2 km per hour) to the east-southeast. The results of this analysis are shown in figure 6-27. During the first 18 hours the currents carried the path strongly to the south under the influence of weather type 6.0. This was able to move the trajectory into the area where baroclinic currents along the continental slope dominate the movement, as can be seen from the currents after about 20 hours. The winds, although never really a major factor, pick up after about 20 hours and remain in the same general direction as the currents contributing to the large overall drift.

The second winter trajectory (w2) left site five on the 27th of February and is quite different from the case considered above (figure 6-28). The first three days both the currents and winds are seen to carry the path to the east with the currents adding a slight northerly component. This carries the trajectory onto a shelf region where barcclinic currents are continually weak. Up until about 220 hours the path wanders around with the winds and currents often counter to each other. At around 230 hours a stronq wind event is seen to develop local winds in excess of 20

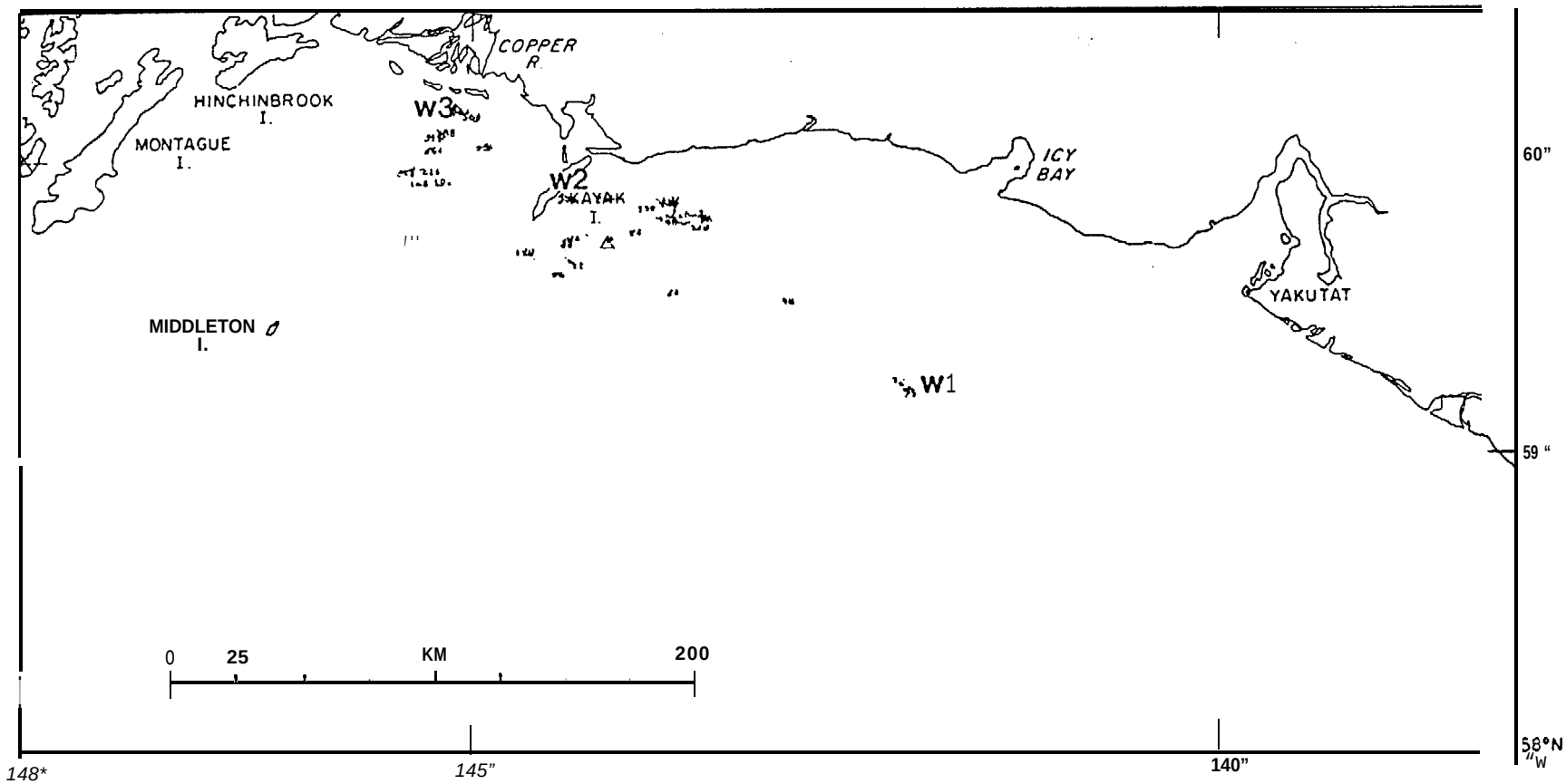

Figure 6-25. Individual winter trajectories w1, w2, and w3 of releases from site five.

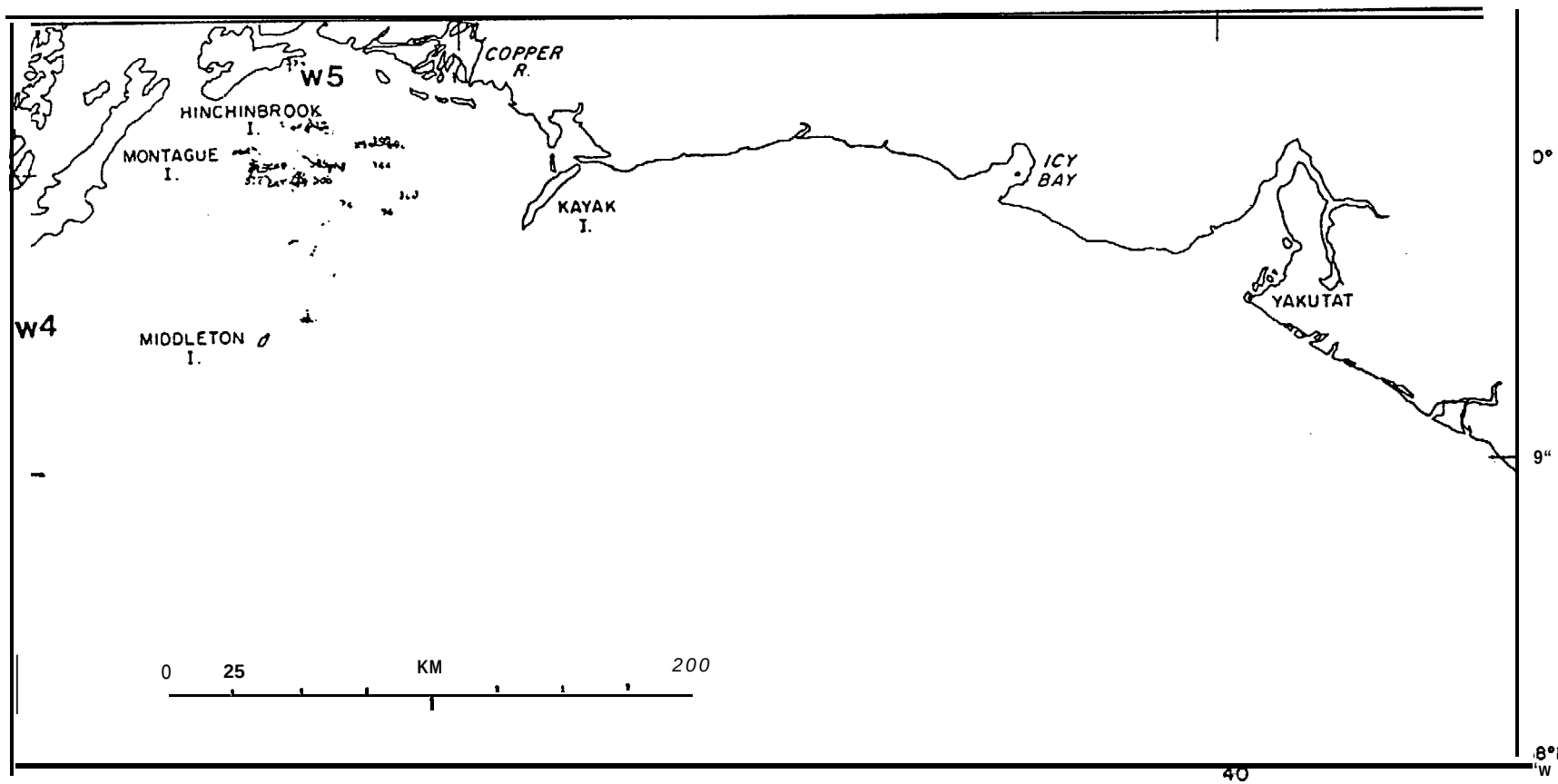

Figure 6-26. Individual winter trajectories w4 and w5 of releases from site seven.

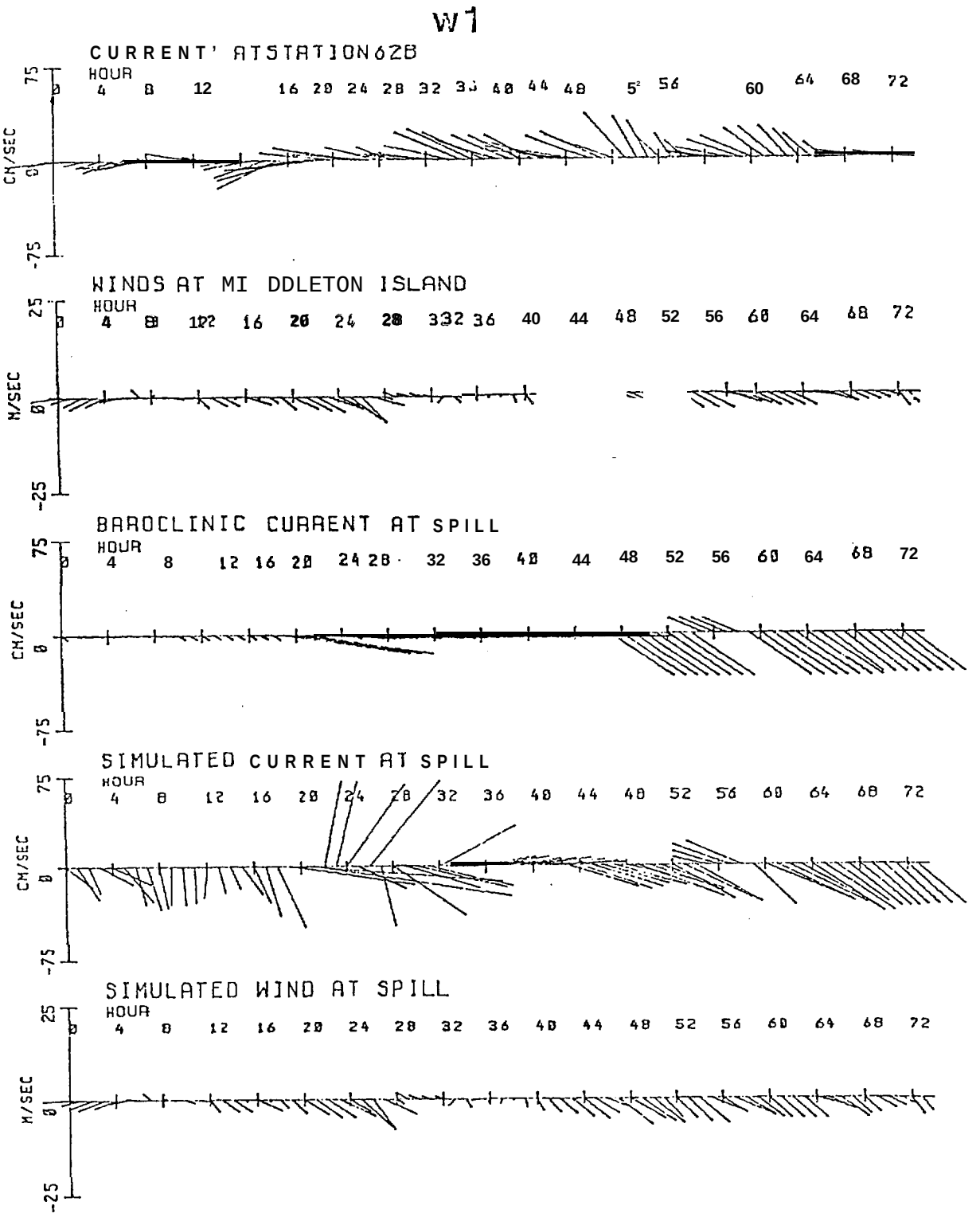

Figure 6-27. Detailed analysis of trajectory w1.

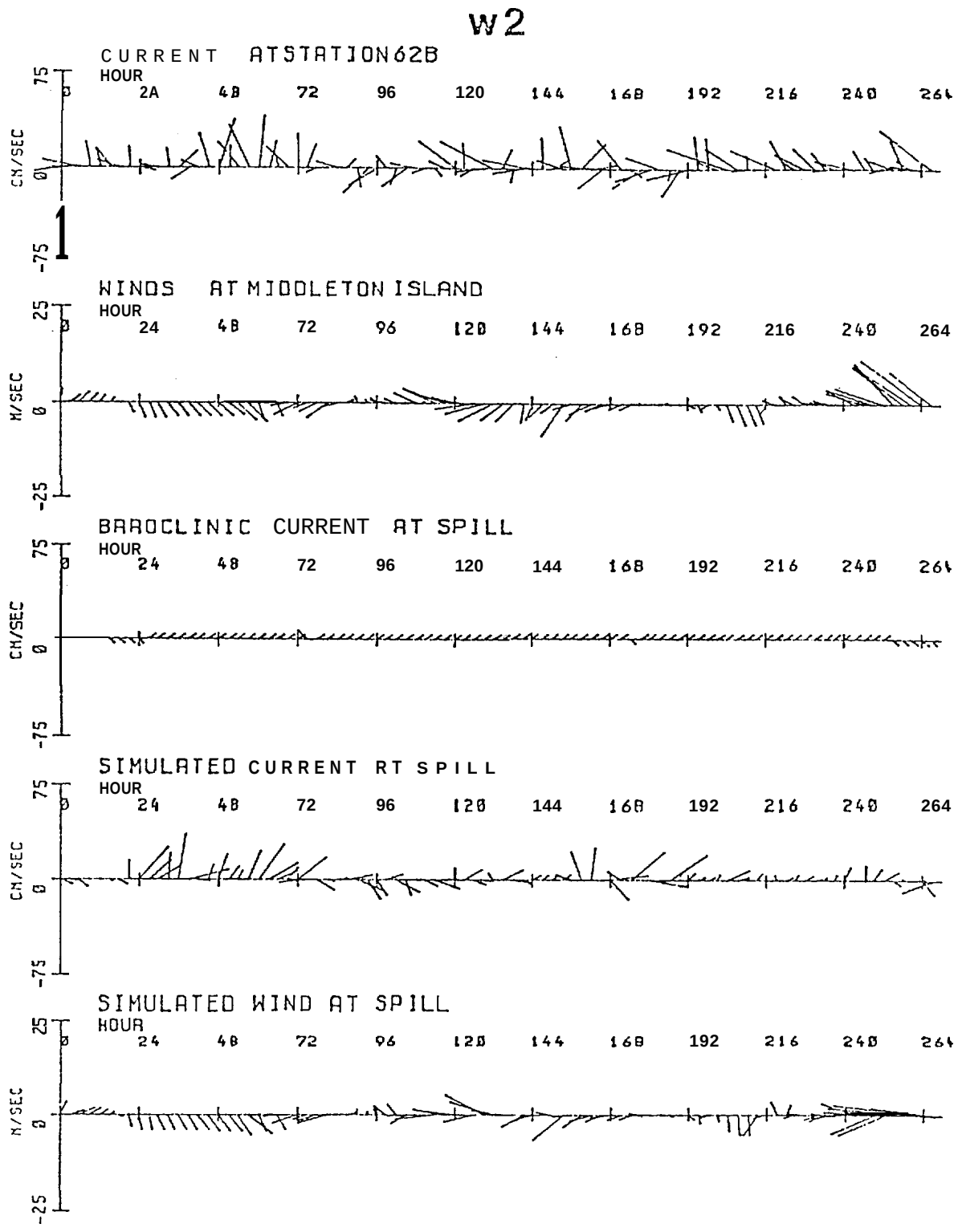

Figure 6-28. Detailed analysis of trajectory w2.

m/see driving the trajectory westward into Kayak Island.

The third trajectory studied from the winter data (w3) left site five on March 4th. The results of this investigation are seen in figure 6-29 and show an interesting series of exchanges between dominant processes. For the first 24 hours the wind kicks the path off to the west. On the third day the total current advects to the south. From 72 to 110 hours the baroclinic and wind currents are mostly at odds resulting in a slow movement to the northwest. About hour 120 a strong wind event sends the trajectory off to the west. After hour 150 the winds and currents, although strong, are pretty much balancing each other and the net drift is north as indicated by the baroclinic currents.

These last three trajectories, all from site five, indicate the significance of early movements and their role in moving the trajectory into different advective regimes.

The fourth winter trajectory to be studied (w4) in detail left site seven on the 2nd of February (figure 6-30). For the first 100 hours the winds, although not as strong as the currents, are more persistent and lead to a net southerly drift. After about 120 hours the baroclinic currents are relatively large and influence the overall currents. Their influence is particularly evident in the direction reversal seen north of Middleton Is-land (figure 6-26). From 200 hours onward the wind and currents are highly variable and a number of loops and meanders are seen in the trajectory.

The last trajectory studied (w5) was released from site seven on the 4th of March and the results are shown in figure 6-31. For the entire duration of this trajectory the baroclinic currents are small. For approximately 300 hours the currents and winds are both large, but often counter each other and the trajectory oscillates east and west. After about 300 hours both develop northerly components and the resultant path quickly moves north to hit the coast on Hinchinbrook Island.

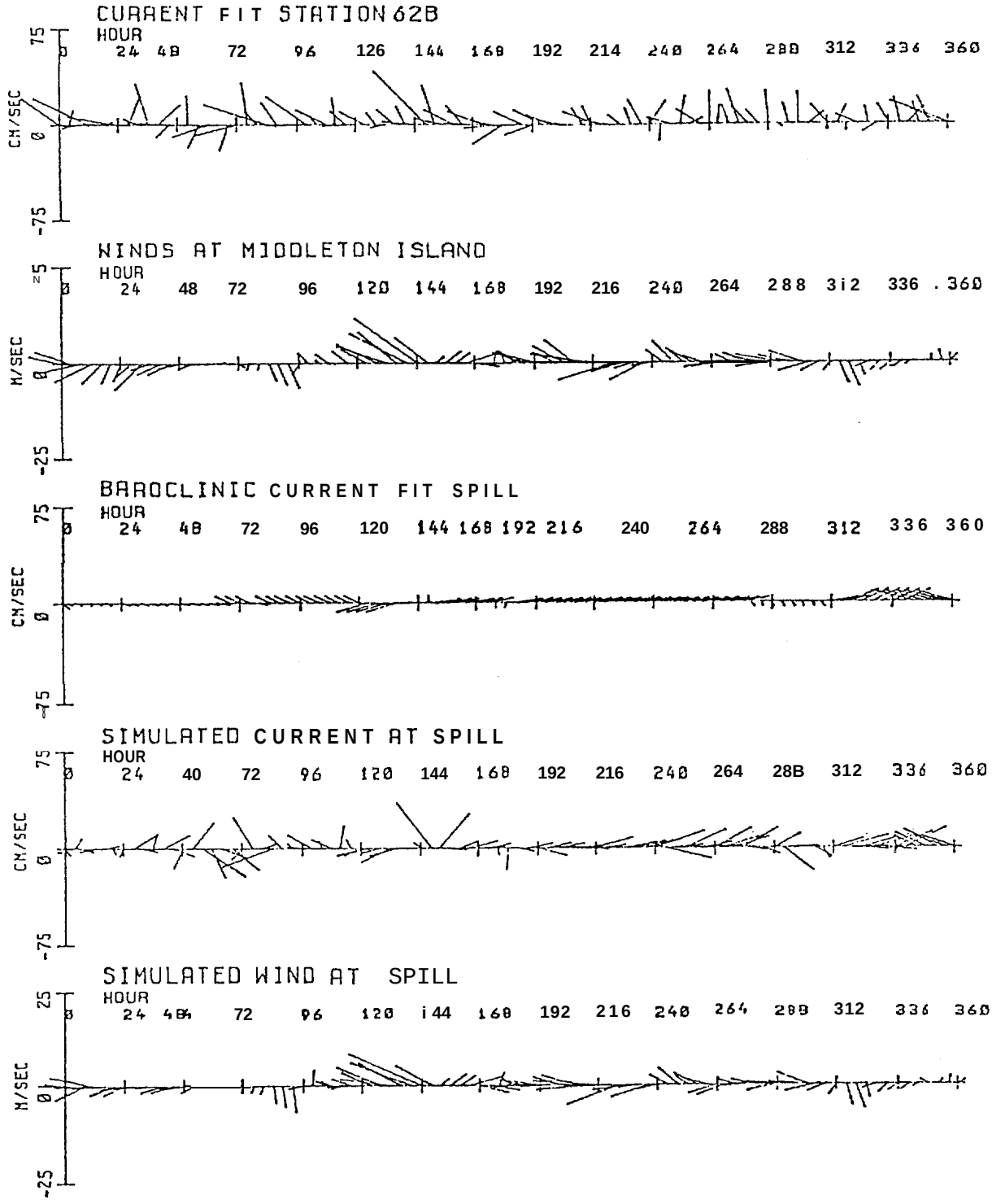

Figure 6-29. Detailed analysis of trajectory w3.

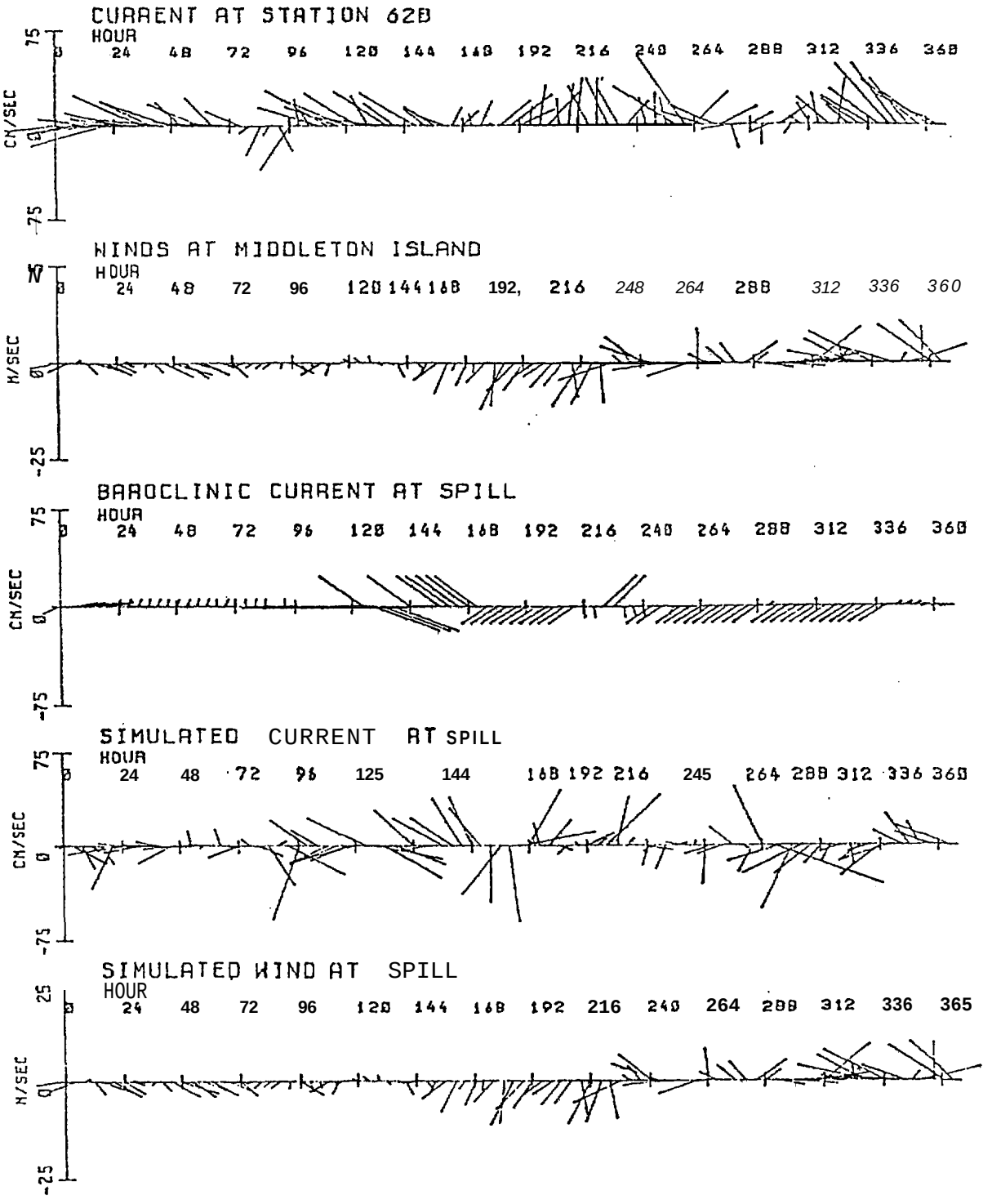

Figure 6-30. Detailed analysis of trajectory w4.

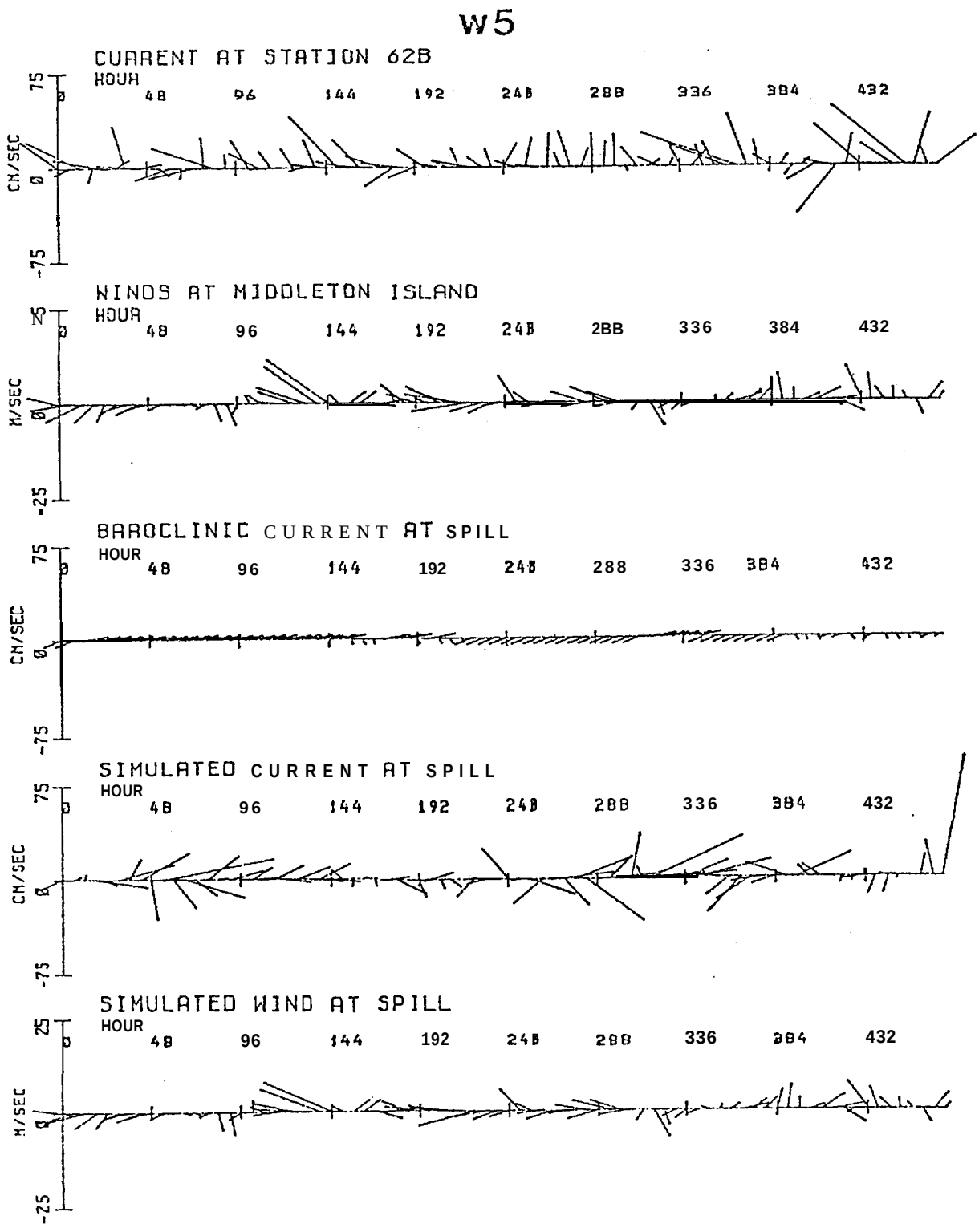

Figure 6-31. Detailed analysis of trajectory w5.

In this section a demonstration of trajectory analysis techniques has been presented using NEGOA data. In this the model synthesized the results of the components described in the earlier chapters of this report. The integration and graphic presentation of all the component segments as well as a detailed analysis of selected trajectories is documented in a representative presentation.

7. Conclusions

A comprehensive trajectory model has been developed for NEGOA with the following features:

The model includes three elements - surface wind drift, barotropic currents (wind driven) and baroclinic currents (density driven}, The elements form a physically consistent set with approximately the same level of sophistication in each component. The formulation explicitly couples wind and current variations as suggested by observational shelf studies.

Synoptic meteorological data drive a set of local wind fields and the barotropic component of a diagnostic model of coastal currents. The set of local wind and current fields are chosen to represent the observed range of atmospheric variability. The data set for the baroclinic component of the diagnostic model is the available hydrographic survey data.

The linear decomposition of the diagnostic model into density and wind driven components makes it possible to identify the regional response associated with each of the forcing mechanisms.

The Green's function solution for the barotropic current response for NEGOA is complete for any arbitrary wind field. The diagnostic model need not be run on a case by case basis for the barotropic component in future trajectory calculations.

A method for treating the uncertainty in the input data to trajectory calculations is included. The difference between a current meter record and the cumulative model response is treated as a residual. The residual is applied throughout the field, scaled by the ratio of the barotropic response at each location to the response at the current meter. The result represents a dispersive element in the family of trajectories which accounts for both unresolved high frequencies in the current field and cumulative model uncertainty.

The input to the trajectory calculations are the available long time series of sea level pressure charts and, at present, a surface current meter and anemometer time series. The possibility exists to remove the dependence on the current meter and anemometer through a stochastic treatment of residuals.

This report has presented sample trajectory calculations for July-August 1974 and February-March 1975. It does not include the climatological assessment of spill possibilities in NEGOA. Such

an assessment may now be undertaken based upon available data.

Conclusions about current circulation in NEGOA which have been derived from RU#140 to date are:

Baroclinic response, particularly the encroachment of mesoscale eddies, dominates the currents at the shelf break.

In general, surface wind drift and barotropic response dominate currents on the shelf.

The major exception is the baroclinic gyre behind Kayak Island, which occurs in 6 of 7 density data sets.

The results of the diagnostic model infer that the coherence length scale of currents on the shelf is on the order of 30 km, the diffusive scale, and is order 300 km at the shelf break, controlled by conservation of potential vorticity along isobaths.

To measure currents in NEGOA certain locations are much more desireable than others, relative to their horizontal coherence, magnitude and variability.

Dispersion of trajectories is quite large and bimodal. Temporal variation of wind plays an important role as well as the spatial variations of the relative magnitude of wind driven and density driven drift.